Hall, Fenella T.H. (2011) Mathematical models for class-D amplifiers. PhD thesis, University of Nottingham.

Mathematical Models for
Class-D Amplifiers

Fenella T. H. Hall, MMath.

Thesis submitted to The University of Nottingham
for the degree of Doctor of Philosophy

July 2011

Abstract

We here analyse a number of class-D amplifier topologies. Class-D amplifiers operate by converting an audio input signal into a high-frequency square wave output, whose lower-frequency components can accurately reproduce the input. Their high power efficiency and potential for low distortion makes them suitable for use in a wide variety of electronic devices. By calculating the outputs from a classical class-D design implementing different sampling schemes we demonstrate that a more recent method, called the Fourier transform/Poisson resummation method, has many advantages over the double Fourier series method, which is the traditional technique employed for this analysis. We thereby show that when natural sampling is used the input signal is reproduced exactly in the low-frequency part of the output, with no distortion. Although this is a known result, our calculations present the method and notation that we later develop.

The classical class-D design is prone to noise, and therefore negative feedback is often included in the circuit. Subsequently we incorporate the Fourier transform/Poisson resummation method into a formalised and succinct analysis of a first-order negative feedback amplifier. Using perturbation expansions we derive the audio-frequency part of the output, demonstrating that negative feedback introduces undesirable distortion. Here we reveal the next order terms in the output compared with previous work, giving further insight into the nonlinear distortion. We then further extend the analysis to examine two more complex negative feedback topologies, namely a second-order and a derivative negative feedback design. Modelling each of these amplifiers presents an increased challenge due to the differences in their respective circuit designs, and in addition, for the derivative negative feedback amplifier we must consider scaling regimes based on the relative magnitudes of the frequencies involved. For both designs we establish novel expressions for the output, including the most significant distortion terms.

Acknowledgements

Contents

Introduction

Audio amplifiers are used increasingly in our everyday lives. In many of their applications efficiency is highly desirable to reduce power consumption. This is important not only from an environmental and cost perspective, but also to maximise battery life on portable devices.

Traditional audio amplifiers can achieve efficiencies only in the region of 65-70%, whereas class-D amplifiers can achieve over 90% efficiency [1, 2]. Their high power efficiency, and because less energy is dissipated as heat so there is no need for a large heat sink, means they are suited for use in very small devices, or those where a long battery life is essential, e.g. mobiles, laptops, hearing aids and MP3 players, as well as home sound systems.

The key feature of class-D amplifiers that provides such high efficiency is that they are switching amplifiers. This means that their output is a high-frequency square wave that alternates between two voltages. We will see later how such a square wave is able to reproduce a (clearly non-square-wave) audio signal in the amplifier output.

While efficiency is desirable, it is also vital that the amplifier output has low distortion. Theoretically a classical class-D amplifier is able to reproduce an input signal with no distortion at all. It has long been known that this is the case if a sinusoidal signal is input [3], and has been shown more recently for a general input signal [4]. Class-D amplifiers have been implemented commercially only since the transistors required to manufacture them became readily available in the early 1990s [5].

We first explain in §1.1 why it is useful for a class-D amplifier to have a square wave output and how the square wave output is created. We also consider how such a square wave output can reproduce an audio signal. Then, in §1.2 we discuss research into class-D amplifiers and modifications to the classical design, and also consider how the square wave output of the amplifier can be analysed. Finally in §1.3 we set out the
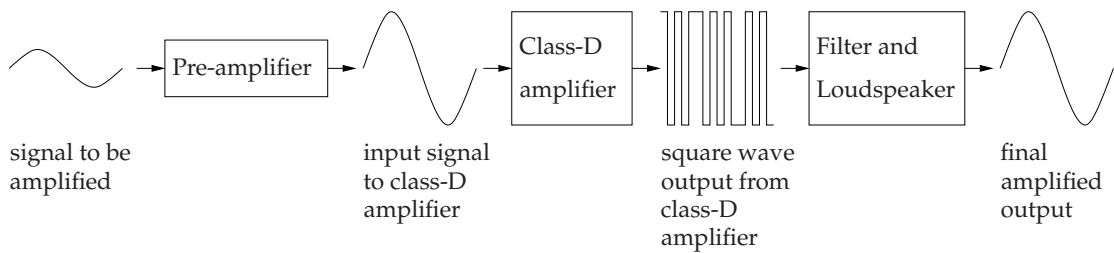
Figure 1.1: How class-D amplifiers are used in the output stage.

structure of thesis.

1.1 A square wave is crucial

Counter-intuitive though it may seem, the square wave output from class-D amplifiers can reproduce a sound free from distortion, and in a highly efficient manner. A high-frequency square wave is the most efficient output, much more efficient than a slowly-varying output signal where a lot of energy would be dissipated as heat.

In order to understand how the square wave output from the amplifier provides low distortion, it is important to examine how the amplifier is used. Class-D amplifiers are used in the output stage (see figure 1.1). A pre-amplifier first increases the amplitude of the low-amplitude analogue audio signal. The signal, now at the required amplitude for playback, then passes through a class-D amplifier, which converts the signal into a more efficient form (a square wave) for playback. The square wave then passes through a filter and a loudspeaker, which plays the final output signal in its amplified form.

Therefore, rather than to increase amplitude, the aim of a class-D amplifier is to convert the input signal into a square wave that represents the input signal. To do this, a class-D amplifier creates a square wave whose width varies according to the input signal, via a process called pulse width modulation (PWM). The way this process is carried out is important because after filtering, the output should ideally equal the signal input to the class-D amplifier.

A wide variety of techniques of PWM exist and we discuss these in more detail in chapter 2. Here we look at the process of PWM in general terms.

When PWM is used, a relatively low-frequency input signal is compared with a carrier wave of much higher frequency to create a high-frequency square wave that switches between voltages $+V$ and $-V$. The widths of the pulses in this resulting
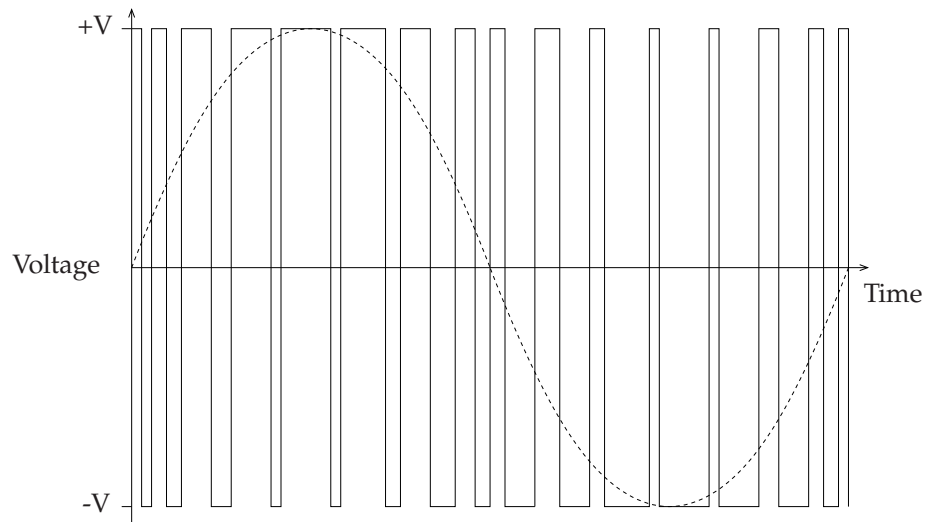
Figure 1.2: Schematic diagram showing a square wave output (solid line) produced by PWM of a sinusoidal input signal (dashed line). In practice, the frequency of the square wave is typically $100 - 250$ times higher than that of the input signal.

square wave depend on the input signal, as depicted in figure 1.2. Thus the pulse width modulated square wave is composed of low-frequency components related to the input signal, and high-frequency components related to the carrier wave. The square wave is then passed through a filter where the high-frequency components are attenuated, while the low-frequency components are allowed to pass through relatively unchanged. These low-frequency components constitute the final output, which is as close to the original input signal as possible.

The duty cycle of this square wave is defined as the ratio between the length of time the wave is at $+V$ and the period of the carrier wave. An ideal square wave, which is at $+V$ for half of the period and $-V$ for the remaining half, has a 50% duty cycle. Therefore we see that when PWM is used it is the duty cycle of the square wave output which varies according to the input signal.

It is not immediately obvious how the pulse width modulated square wave output relates to the input signal. We can understand it in two ways. Firstly, if we take an average of the square wave over a time interval that is long compared with the period of the square wave but short compared with the period of the input signal, we obtain an approximation to the input signal over that time. Secondly, if we consider the Fourier transform of the modulated square wave, it consists of high-frequency components due to the carrier wave and low-frequency components due to the input signal.

In choosing the frequency of the carrier wave, there are several points to consider. When the input signal is compared with the carrier wave to produce the square wave

output, the input signal is sampled, i.e. values of the input signal are "picked out". For the output to represent the input signal, the sample must contain all of the important information of the original input signal. If we take a very large number of samples clearly it would be easy to do this, but the components of the amplifier cannot perform at very high frequencies. However, if we take too few samples, the function produced may be indistinguishable from another sampled signal. For instance, if we sample $\sin 3x$ every $\frac{\pi}{2}$ the result is exactly the same as if we had sampled $-\sin x$, and similarly samples of $\sin 2x$ look the same as a zero signal. These are known as aliasing errors. Thus there is a balance between choosing a carrier wave with high enough frequency to avoid aliasing errors, but low enough frequency that the amplifier components operate correctly. In addition, the carrier wave frequency must be high enough for the resulting high-frequency components of the square wave output to be distinct from the low-frequency components related to the input signal, so that the high-frequency components can be filtered out. The typical frequency ranges are 80-250kHz for the carrier wave [1], and 20Hz-20kHz for the input signal [6].

We have discussed in general terms how the signal input to a class-D amplifier can be reproduced from its square wave output with no distortion, thus enabling class-D amplifiers to be used in a highly efficient output stage with no distortion. In chapter 2 we will present a quantitative analysis showing that the output can be distortion free. In the next section we consider class-D amplifier designs and how they can be analysed.

1.2 Class-D amplifier designs and methods of analysis

Here we review class-D amplifier designs before considering the methods that exist to analyse the outputs from the different designs.

The classical class-D amplifier design is known to reproduce the input signal exactly in the low-frequency part of the output with no distortion [1, 7]. However, this simple design is susceptible to noise, for example due to non-ideal components, or variation in the carrier wave [8]. For this reason, negative feedback is often implemented in class-D designs. Negative feedback allows the output to be "fed back" into the circuit, in order to achieve a final output that is closer to the input signal. While negative feedback reduces noise in the circuit, it does however introduce distortion [7]. This is investigated in more detail in chapter 3. Many designs exist that aim to reduce the distortion inherent in negative feedback amplifiers, and we analyse two such designs in chapters 4 and 5.

In order to examine the differences between amplifier designs, as well as the differ-

ences between the many diverse PWM processes, we need to analyse the pulse width modulated square wave that is created by each. To do this we must determine the switching times, which are the times at which the square wave switches. For the classical class-D design, the switching times of the square wave are defined by simple equations. For class-D designs with negative feedback, more effort is required to find the switching times. Regardless of how the square wave is created (by whichever amplifier or PWM process), once we know the switching times, in fact the mathematical analysis is very similar.

The main difficulty in analysing a pulse width modulated square wave is that the square wave switches down and up within the period prescribed by the carrier wave, but the times at which the switching occur are determined by the input signal. Thus, even for a periodic or quasiperiodic input signal, the square wave output is only quasiperiodic.

The earliest and most commonly used method for analysing pulse width modulated square waves is the double Fourier series method, first put forward by Bennett [9] and later developed by Black [3]. This approach is sometimes referred to as Black's double wall method. Using this method it is possible to write the output as a double Fourier series, thus allowing a comparison of the Fourier components of the output from one amplifier design or modulation process with those from another. However, the method is limited to a sinusoidal input signal, the techniques used are complex and major adjustments are required to analyse different modulation processes.

Several newer procedures exist that avoid the double Fourier series method, [4, 10], and while they can be used to confirm the results of [3], these are still not straightforward to implement or adaptable to different modulation processes.

However, Cox and Creagh [11] present a method (that we will refer to as the Fourier transform/Poisson resummation method) that we believe offers considerable advantages over previous ones. It is much simpler and so is quicker to execute, and can be modified easily to accommodate a variety of modulation schemes. In chapter 2 we will demonstrate both the double Fourier series method and the Fourier transform/Poisson resummation method, and establish the advantages of the latter method.

In this section, we have identified several amplifier designs that we will investigate in detail in later chapters, and considered the methods we will use to do so.

1.3 Thesis structure

The structure of the thesis is as follows.

In chapter 2 we investigate classical class-D amplifiers. To analyse the pulse width modulated square wave output we discuss the double Fourier series method and the Fourier transform/Poisson resummation method, introduced briefly above, in more detail. We reproduce the outputs from two commonly used PWM schemes using both methods, in order to show the advantages of the Fourier transform/Poisson resummation method. In the second part of the chapter we further illustrate the Fourier transform/Poisson resummation method, using it to calculate and compare the outputs resulting from a number of different types of PWM, including Δ-compensation uniform sampling.

As we outlined above, the output from classical class-D designs is affected by noise, and negative feedback is often introduced to counter this problem. In chapter 3 we investigate the standard class-D design with negative feedback, termed a first-order negative feedback amplifier. The approach we use to analyse the design is a more formalised version of that in [7]. We first model the amplifier design using a system of nonlinear difference equations. Then we use perturbation expansions, based on a small parameter that is the ratio of the input signal frequency to the carrier wave frequency, to solve these to find the switching times of the square wave. We incorporate the Fourier transform/Poisson resummation method in the latter stages of the analysis to determine the final output.

Although negative feedback reduces noise in the output, unfortunately it also introduces distortion. In chapters 4 and 5 we extend the method used in chapter 3 to more complex designs with negative feedback, which aim to reduce the distortion produced by negative feedback. In chapter 4 we investigate a second-order negative feedback amplifier, and in chapter 5 we investigate a derivative negative feedback amplifier. By thoroughly modelling these designs analytically, which to our knowledge has not been presented before, we aim to determine whether these designs improve upon the first-order negative feedback design, and whether it is possible to improve their distortion performance further. Moreover, our objective is to demonstrate the potential of our method of analysis for investigating more complex negative feedback class-D amplifier topologies.

In chapter 6 we review the main conclusions of the thesis, and consider potential future work.

Methods for analysing class-D amplifiers

2.1 Introduction

RECALL that class-D amplifiers are switching amplifiers. The output from such an amplifier is a square wave, created by a process called pulse width modulation (PWM), whose duty cycle varies according to the signal input to the amplifier. The square wave output is then filtered so that the final amplifier output comprises only low-frequency components related to the input signal. Class-D amplifiers are used in a highly-efficient output stage after pre-amplification, and so the aim is not to increase the amplitude of the input signal, but for the filtered output to resemble the input signal as closely as possible (as discussed in chapter 1). It is well known that for a classical class-D amplifier the input signal can be reproduced exactly in the theoretical output (see, for example [3, 4]).

In order to investigate class-D amplifiers, it is therefore essential to analyse the square wave output produced by PWM. However, it is not straightforward to achieve this because, even for a periodic or quasiperiodic input, the output is only quasiperiodic. As we discussed in chapter 1, several methods of PWM analysis exist. The aim of this chapter is to model the classical class-D design, and in doing so we review two methods of PWM analysis.

We begin in §2.2, by introducing some of the many different PWM processes that can be used to create the square wave output. In §2.3, we calculate the pulse width modulated output from a classical class-D amplifier, and show that the input signal can be reproduced exactly in the theoretical output. We demonstrate two different methods of calculating this output, in order to highlight the advantages of the second

method. The first method we implement is the double Fourier series method [3], which is the most commonly used. However, the approach is unnecessarily complex and it is circuitous, though possible, to extend the method to more advanced modulation schemes [12, 13]. The second method we execute is the Fourier transform/Poisson resummation method [11], which is simpler and can be adapted easily to investigate other modulation schemes.

In §2.4 we use the Fourier transform/Poisson resummation method to analyse the outputs resulting from a range of PWM schemes, one of which is equivalent to Δ-compensation uniform sampling [14]. Although largely these are known results, the analysis demonstrates the relative simplicity and adaptability of the Fourier transform/Poisson resummation method compared with the double Fourier series method.

2.2   Sampling and modulation processes

Many different methods of sampling (how discrete values of the input signal are chosen in order to calculate the switching times of the square wave) and pulse width modulation (how the switching times of the square wave are defined) exist. The outputs resulting from each method have distinct properties. We discuss two common types of sampling and two modulation techniques, and describe how the output is produced in each case. We use the superscript $*$ to denote dimensional variables.

Natural sampling and regular sampling (which is sometimes referred to as uniform sampling) are two commonly used methods of sampling. We now show how these methods can be implemented to create a pulse width modulated square wave output, $g^*(t^*)$, that alternates between $+V$ and $-V$. The switching times of $g^*(t^*)$ are determined by the intersection of the input signal $s^*(t^*)$ with a high-frequency carrier wave $v^*(t^*)$ of period T and (angular) frequency $\omega_c^* = \frac{2\pi}{T}$. The carrier wave can be defined in different ways, according to the type of modulation required, as we shall see below.

We assume that $|s^*(t^*)| \leq V$ for all t^*. We can use either natural sampling or regular sampling to determine the switching times. When natural sampling is used, the switching occurs when $s^*(t^*) + v^*(t^*) = 0$. When regular sampling is used, the input signal is sampled at a fixed time in each carrier wave period, and the switching occurs when this sample equals minus the carrier wave. For example, if the input signal is sampled at the beginning of each carrier wave period, when $t^* = nT$, the switching occurs at a time t^* later in that carrier wave period when $s^*(nT) + v^*(t^*) = 0$.

It is possible to use either single-edge or double-edge modulation. When single-

edge modulation is used, only one edge of the square wave output is determined by the input signal, the other edge occurs at a fixed time. The leading edge of the square wave is defined as the one that switches from $-V$ to $+V$, and the trailing edge is defined as the one that switches from $+V$ to $-V$. Since we may fix either one edge or the other, there are two types of single-edge modulation. If leading-edge modulation is used, the leading edge is determined by the input signal and the trailing edge remains fixed. If trailing-edge modulation is used, the trailing edge is determined by the input signal and the leading edge remains fixed. For single-edge modulation the carrier wave is a sawtooth wave with period T, where for leading-edge modulation it is defined to be

$$v^*(t^*) = -V + \frac{2V}{T}(t^* - nT) \text{ for } nT < t^* < (n+1)T, \tag{2.2.1}$$

and for trailing-edge modulation it is defined to be

$$v^*(t^*) = V - \frac{2V}{T}(t^* - nT) \text{ for } nT < t^* < (n+1)T,$$

the negative of that for leading-edge modulation. Figure 2.1 shows how $g^*(t^*)$ is produced by leading-edge modulation for both natural and regular sampling.

When double-edge modulation is used, both edges of the output are determined by the input signal. In contrast to single-edge modulation, the carrier wave for double-edge modulation is a triangular wave of period T. Double-edge modulation can be either symmetric or asymmetric. If it is symmetric, both edges are determined by one sample of the input signal. For example, if we use symmetric regular sampling, the input signal is sampled at the beginning of the carrier wave period and the switching occurs when $s^*(nT) + v^*(t^*) = 0$, i.e. twice in each carrier wave period because the carrier wave is triangular. If double-edge modulation is asymmetric, each edge is determined by a different sample of the input signal. For example, if we use asymmetric regular sampling, the input signal is sampled at the beginning and halfway through each carrier period. The switching then occurs when $s^*(nT) + v^*(t^*) = 0$ for $nT \le t^* < nT + \frac{T}{2}$ and $s^*\left(\left(n + \frac{1}{2}\right)T\right) + v^*(t^*) = 0$ for $nT + \frac{T}{2} \le t^* < (n+1)T$.

Natural and regular sampling have been investigated extensively, and it is well-documented that natural sampling produces less distortion than regular sampling. This has been shown for a general input signal [4], and has also been verified for particular input signals, [15–19]. In §2.3 we will demonstrate this (via both the double Fourier series method and the Fourier transform/Poisson resummation method) by calculating the output from a classical class-D amplifier when natural sampling is used, and then when regular sampling is used.
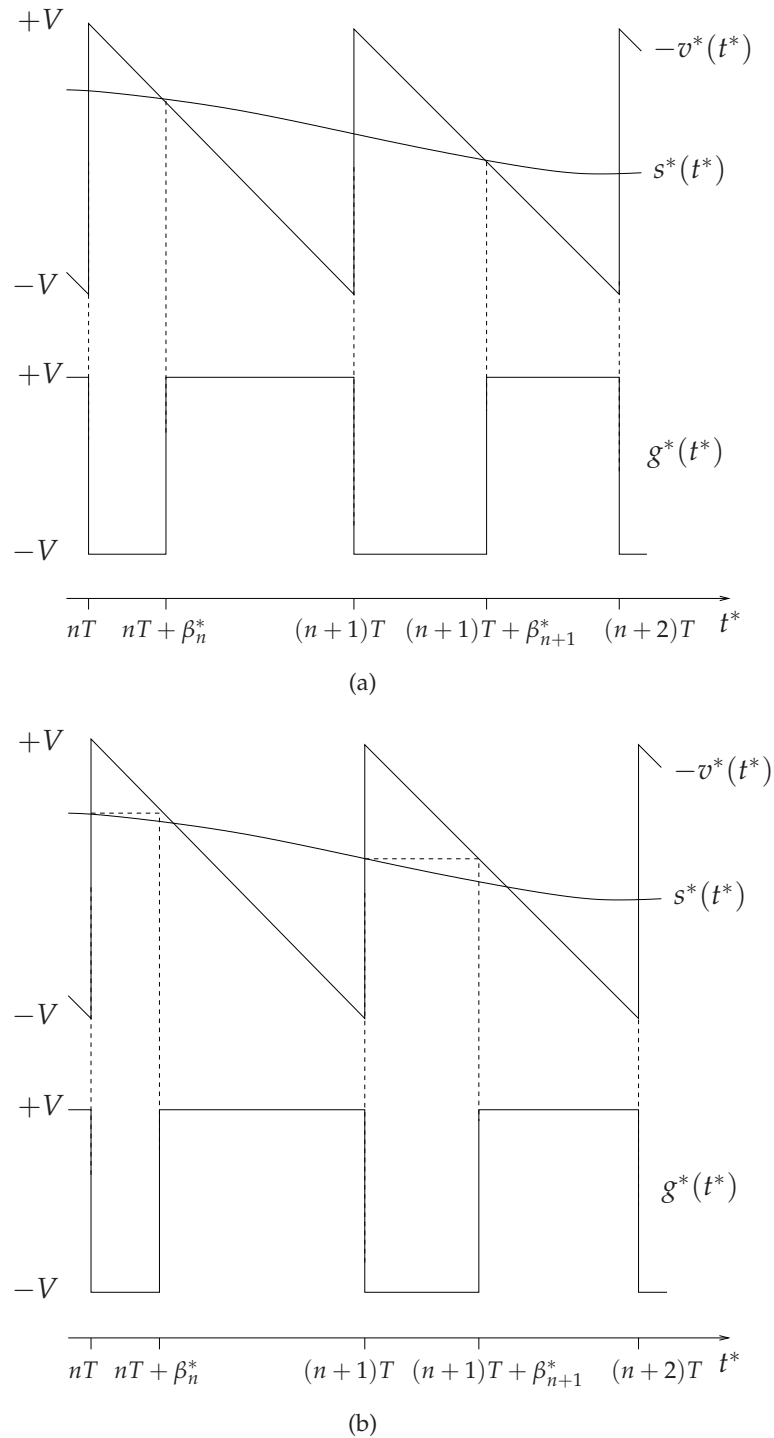
Figure 2.1: Diagrams to show (a) natural sampling, and (b) regular sampling, leading-edge modulation. In each diagram the switching times $t^* = nT + \beta_n^*$ of the leading edges of the square wave output $g^*(t^*)$ are determined by the intersections of either (in the case of natural sampling) the input signal $s^*(t^*)$ or (in the case of regular sampling) the sample $s^*(nT)$ of the input signal, with minus the carrier wave, $-v^*(t^*)$. The trailing edges of the square wave output are fixed at $t^* = nT$.
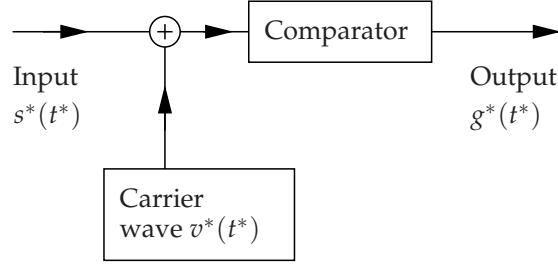
Figure 2.2: Schematic diagram representing the classical class-D amplifier design.

2.3 Analysis of a classical class-D amplifier

We model a classical class-D amplifier, as depicted in figure 2.2. The input signal $s^*(t^*)$ is first added to a carrier wave $v^*(t^*)$. The resulting voltage, $s^*(t^*) + v^*(t^*)$, is fed into a comparator that produces a square wave output, $g^*(t^*)$, defined by

$$g^*(t^*) = \begin{cases} -V & \text{for } s^*(t^*) + v^*(t^*) < 0 \\ +V & \text{for } s^*(t^*) + v^*(t^*) > 0. \end{cases} \tag{2.3.1}$$

Note that we will investigate this classical class-D amplifier design for a sinusoidal input signal, defined to be

$$s^*(t^*) = s_0 V \sin \omega_a^* t^*, \tag{2.3.2}$$

where s_0 is a constant and ω_a^* is the frequency of the input signal.

For illustrative purposes we consider only leading-edge modulation in this section, purely for simplicity. This means that only the edge of the square wave output $g^*(t^*)$ that switches from $-V$ to $+V$ is determined by the input signal; the edge that switches from $+V$ to $-V$ is fixed in time. We could in principle similarly consider the output resulting from any other form of PWM (discussed in §2.2), but shall not do so here.

The carrier wave is therefore a sawtooth wave defined by (2.2.1), and we apply natural and regular sampling as depicted in figure 2.1. The square wave $g^*(t^*)$ switches from $-V$ to $+V$ at times $t^* = nT + \beta_n^*$ and from $+V$ to $-V$ at times $t^* = nT$, and therefore we may write

$$g^*(t^*) = \begin{cases} -V & \text{for } nT < t^* < nT + \beta_n^* \\ +V & \text{for } nT + \beta_n^* < t^* < (n+1)T. \end{cases} \tag{2.3.3}$$

Note that we have given two expressions for $g^*(t^*)$, i.e. (2.3.1) and (2.3.3). These are not contradictory: (2.3.1) gives the conditions for $g^*(t^*)$ to switch in terms of $s^*(t^*)$ and $v^*(t^*)$, while (2.3.3) then defines the switching times.

We now nondimensionalise the model set out above. Because the model for a classical class-D amplifier is relatively simple, this step is admittedly not necessary here.

However, it is a useful step in simplifying our models for the more complicated negative feedback amplifier designs in chapters 3-5, and so for consistency we will also nondimensionalise here. We nondimensionalise using the voltage scale V, the maximum amplitude of the square wave output $g^*(t^*)$, and the time scale T, the period of the carrier wave $v^*(t^*)$, and use unstarred equivalents of the starred variables to denote the nondimensional variables. Thus

$$s(t) = \frac{s^*(t^*)}{V}, g(t) = \frac{g^*(t^*)}{V}, v(t) = \frac{v^*(t^*)}{V}, t = \frac{t^*}{T}, \omega_c = \omega_c^* T, \omega_a = \omega_a^* T.$$

With reference to the dimensional definitions (2.2.1)-(2.3.3) the nondimensional $g(t)$, $s(t)$, $v(t)$ and the switching times are now defined by

$$g(t) = \begin{cases} -1 & \text{for } s(t) + v(t) < 0 \\ +1 & \text{for } s(t) + v(t) > 0, \end{cases} \tag{2.3.4}$$

$$s(t) = s_0 \sin \omega_a t, \tag{2.3.5}$$

$$v(t) = -1 + 2(t - n) \text{ for } n < t < n + 1, \tag{2.3.6}$$

$$g(t) = \begin{cases} -1 & \text{for } n < t < n + \beta_n \\ +1 & \text{for } n + \beta_n < t < n + 1. \end{cases} \tag{2.3.7}$$

Note that the nondimensional carrier wave $v(t)$ has period 1 and frequency $\omega_c = 2\pi$.

Figure 2.3 is a dimensionless version of figure 2.1, showing how the square wave output is created by natural sampling and by regular sampling. Since we are investigating leading-edge modulation, the trailing edge of the square wave is fixed at $t = n$, whilst the position $t = n + \beta_n$ of the leading edge varies according to the input signal. When natural sampling is used, the leading-edge switching occurs when $s(t) + v(t) = 0$. Thus for natural sampling we have

$$\beta_n = \frac{1}{2}(1 - s(n + \beta_n)). \tag{2.3.8}$$

When regular sampling is used, the input signal is sampled at the beginning of each carrier wave period, $t = n$. The leading-edge switching occurs when $s(n) + v(t) = 0$. Thus for regular sampling we have

$$\beta_n = \frac{1}{2}(1 - s(n)). \tag{2.3.9}$$

We can see immediately that there is a significant difference between the switching times for natural and regular sampling: β_n is defined implicitly for natural sampling but explicitly for regular sampling. This difference means that the method used to analyse the square wave output produced by natural sampling needs to be altered to investigate that produced by regular sampling.
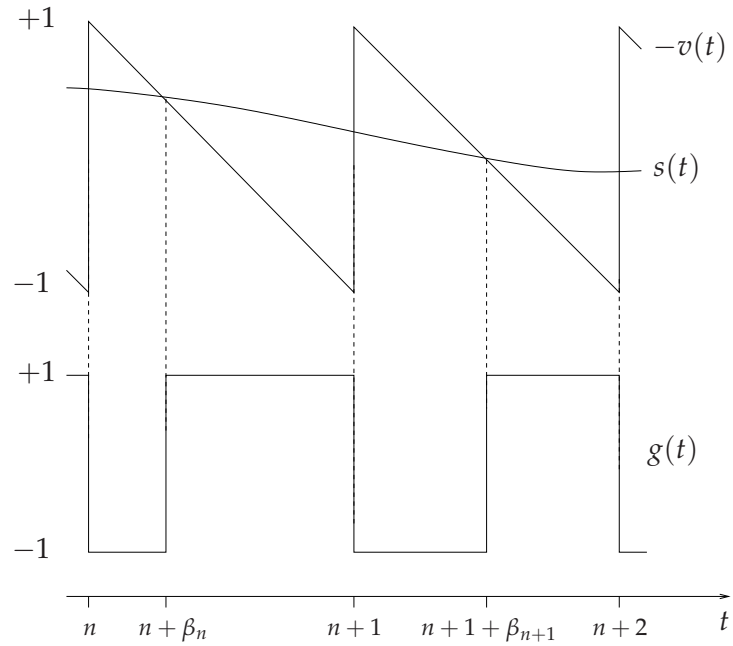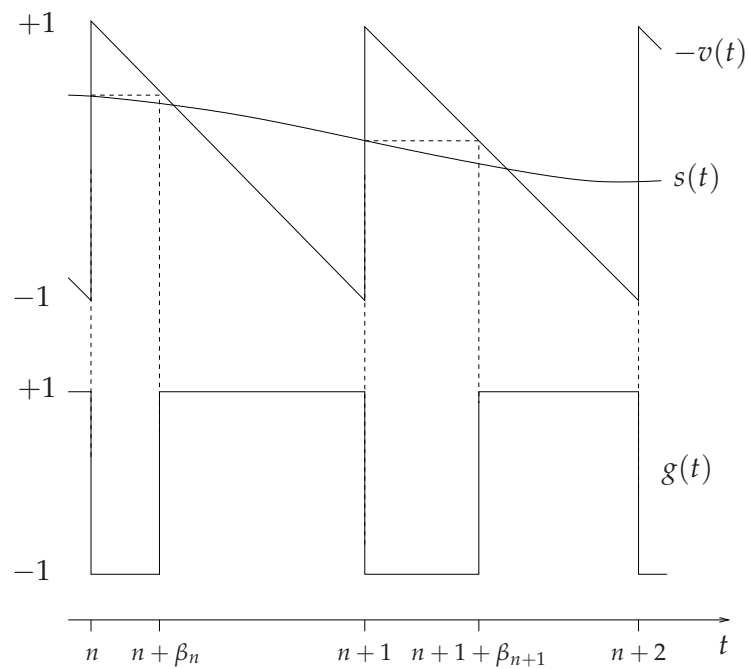
Figure 2.3: Diagrams to show (a) natural sampling, and (b) regular sampling, leading-edge modulation in terms of the dimensionless variables. In each diagram the switching times $t = n + \beta_n$ of the leading edges of the square wave output $g(t)$ are determined by the intersections of either (in the case of natural sampling) the input signal $s(t)$ or (in the case of regular sampling) the sample $s(n)$ of the input signal, with minus the carrier wave, $-v(t)$. The trailing edges of the square wave output are fixed at $t = n$.

13

The outputs resulting from these two types of sampling will be calculated in §2.3, and their characteristics will be compared in §2.3.3. However, there is a simple comparison we can make here. We define the short-time average of a function to be its average over the carrier wave period,

$$\langle g(t) \rangle = \int_n^{n+1} g(t)\, dt, \tag{2.3.10}$$

and thus, from (2.3.7), for leading-edge modulation we find that the short-time average of $g(t)$ over the nth period is

$$\langle g(t) \rangle = 1 - 2\beta_n.$$

In addition, we define the long-time average of a function to be its average over infinitely many carrier wave periods. Computing the short-time average over the nth period for natural sampling we therefore obtain

$$\langle g(t) \rangle = s(n + \beta_n),$$

and for regular sampling,

$$\langle g(t) \rangle = s(n).$$

From these short-time averages we can deduce that, while we expect the output to be dominated by the input signal for both types of sampling, the output for regular sampling will be delayed by on average half a carrier wave period (since the long-time average of β_n is $\frac{1}{2}$) compared to that for natural sampling.

The nondimensional model for a classical class-D amplifier is given by the system of equations (2.3.4)-(2.3.7), where the leading-edge switching times of the square wave output are defined by (2.3.8) for natural sampling and (2.3.9) for regular sampling. The square wave output comprises components related to the input signal as well as higher-frequency components related to the carrier wave. In order to understand how such an amplifier can reproduce the input signal exactly in the low-frequency components of its output, we must manipulate the expression for the square wave output into a form that clearly shows its components.

In the next section we analyse the square wave output $g(t)$ via two different methods, with the aim of highlighting the advantages of the second method. Thus in §2.3.1 we calculate the outputs resulting from natural sampling and then regular sampling via the double Fourier series method. This method involves introducing two separate timescales relating to the carrier wave frequency and the input signal frequency. Then, in §2.3.2, we recalculate the outputs from both sampling schemes via the Fourier

transform/Poisson resummation method and show that it offers several advantages compared with the double Fourier series method. The main difference between the methods is that the Fourier transform/Poisson resummation method does not introduce the two separate timescales. In addition, the Fourier transform/Poisson resummation method uses the Poisson resummation formula to bypass some of the lengthy steps involved in the double Fourier series method.

2.3.1 Double Fourier series method

Here we implement the double Fourier series method to investigate the outputs from a classical class-D amplifier when natural sampling or when regular sampling is used to create the square wave output. The method exploits the double periodicity of the output by defining two variables that vary on the two timescales involved.

The method was originally used by Bennett [9] to analyse a half wave rectifier (a device that transmits zero voltage when the applied input voltage is negative, and transmits a voltage proportional to the input voltage when the input is positive). Bennett investigated a half wave rectifier with two applied frequencies, meaning that the input voltage is a function of two separate frequencies. Bennett realised that the output is in fact doubly periodic and was then able to write the output as a double Fourier series.

Later, Black [3] developed this method for use in PWM. In realising that the pulse width modulated output is periodic in both the timescale $2\pi/\omega_c$, where ω_c is the carrier wave frequency, as well as $2\pi/\omega_a$, where ω_a is the frequency of the input signal, Black was able to write the output as a double Fourier series, and thus analyse the components. This method was only applied to natural sampling initially, but was later adapted to regular sampling by Bowes [20].

We use this method first to examine the output when natural sampling is used to determine the switching times of the square wave, and then to examine the output when regular sampling is used instead. We compare the results from each.

2.3.1.1 Natural sampling

In this section we analyse the output resulting from leading-edge natural sampling modulation of a sinusoidal input signal using the double Fourier series method.

First we note that the square wave $g(t)$ defined by (2.3.7) varies on two timescales: it alternates between $+1$ and -1 according to ω_c, the frequency of the carrier wave;

and the width of the pulses varies according to the frequency of the input signal, ω_a. Because we have nondimensionalised, ω_c is now equal to 2π. As we wish to find the double Fourier series of the output, it makes sense to define two new variables

$$x = \omega_c t, \tag{2.3.11}$$

$$y = \omega_a t, \tag{2.3.12}$$

and rewrite the output in terms of these. We note that writing y in terms of x gives $y = \frac{\omega_a}{\omega_c} x$. We now formulate a generalised version of the problem in terms of the independent variables x and y to find the general output $g(x, y)$. We will later find the particular solution along the line $y = \frac{\omega_a}{\omega_c} x$, which gives the output $g(t)$ that we desire.

In terms of x and y, (2.3.8), which defines the leading-edge switching times β_n becomes

$$\beta_n = \frac{1}{2}(1 - s_0 \sin y). \tag{2.3.13}$$

We now write the inequalities in (2.3.7), which defines $g(t)$, in terms of the new variables and obtain

$$g(x, y) = \begin{cases} -1 & \text{for } 2\pi n < x < 2\pi n + \pi(1 - s_0 \sin y) \\ +1 & \text{for } 2\pi n + \pi(1 - s_0 \sin y) < x < 2\pi(n+1), \end{cases} \tag{2.3.14}$$

which is represented in figure 2.4. The shaded regions depict where the output is -1 and the unshaded regions depict where the output is $+1$. These regions are bounded by the lines $x = 2\pi n$ and $x = 2\pi n + \pi(1 - s_0 \sin y)$. Time increases along the line $y = \frac{\omega_a}{\omega_c} x$, which specifies the particular solution we are interested in. The points where the edges of the shaded regions intersect with the line $y = \frac{\omega_a}{\omega_c} x$ are the switching times ($t = 0, \beta_0, 1, 1 + \beta_1$ are shown in the diagram). It is now easy to see from the diagram that the output $g(x, y)$ is doubly 2π-periodic. It is 2π-periodic in x since increments of n are multiplied by 2π. The output is also 2π-periodic in y since $\sin y$ is 2π-periodic in y. It is also worth noting that from the diagram we can see that if the gradient of the line $y = \frac{\omega_a}{\omega_c} x$ is shallower ($\omega_c \gg \omega_a$) then it will intersect with the lines $x = 2\pi n$ and $x = 2\pi n + \pi(1 - s_0 \sin y)$ more times in any given period in y. This corresponds to more frequent sampling of the input signal.

The general output (2.3.14) is now in a form from which we can more easily find the double Fourier series. We therefore write $g(x, y)$ as a double Fourier series

$$g(x, y) = \sum_{m,n=-\infty}^{\infty} G_{m,n} e^{inx + imy},$$

where

$$G_{m,n} = \frac{1}{4\pi^2} \int_0^{2\pi} \int_0^{2\pi} g(x, y) e^{-i(nx + my)} \, dx \, dy. \tag{2.3.15}$$
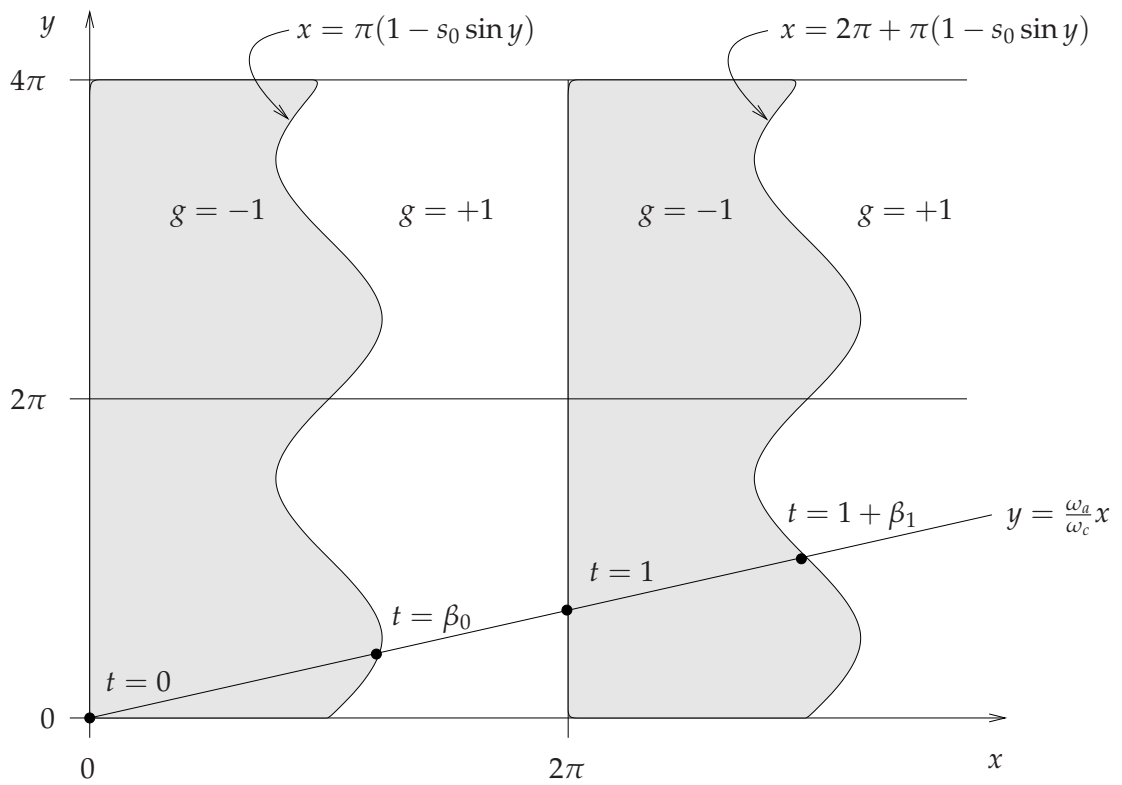
Figure 2.4: The output $g(x, y)$, shown over two periods in x, resulting from natural sampling of a sinusoidal input signal. The line $y = \frac{\omega_a}{\omega_c} x$ specifies the particular solution we are interested in.

Since we integrate the general output $g(x, y)$ over only one period in x and y, we require (2.3.14) only for the zeroth period in x and we integrate as follows

$$
\begin{aligned}
G_{m,n} &= \frac{1}{4\pi^2} \int_0^{2\pi} e^{-imy} \left\{ -\int_0^{\pi(1-s_0 \sin y)} e^{-inx} \, dx + \int_{\pi(1-s_0 \sin y)}^{2\pi} e^{-inx} \, dx \right\} dy \\
&= \frac{1}{2\pi^2 in} \int_0^{2\pi} e^{-imy} \left\{ e^{-\pi in} e^{\pi in s_0 \sin y} - 1 \right\} dy,
\end{aligned}
\tag{2.3.16}
$$

provided $n \neq 0$. If $m \neq 0$ as well we find

$$
\begin{aligned}
G_{m,n} &= \frac{(-1)^n}{2\pi^2 in} \int_0^{2\pi} e^{-imy} e^{\pi in s_0 \sin y} \, dy \\
&= \frac{(-1)^n}{\pi in} J_m(\pi n s_0),
\end{aligned}
\tag{2.3.17}
$$

where in the last step we use

$$
J_m(z) = \frac{1}{2\pi} \int_0^{2\pi} e^{-imy} e^{iz \sin y} \, dy,
\tag{2.3.18}
$$

a property of Bessel functions adapted from [21]. Note that we assumed both $m, n \neq 0$ to get this result, so to find all of the Fourier coefficients we need to calculate the integral when m and/or n are equal to zero.

We first take the case $n = 0$ for any m. From (2.3.15) the coefficients are

$$
\begin{aligned}
G_{m,0} &= \frac{1}{4\pi^2} \int_0^{2\pi} \int_0^{2\pi} g(x, y) e^{-imy} \, dx \, dy \\
&= \frac{s_0}{2\pi} \int_0^{2\pi} e^{-imy} \sin y \, dy \\
&= \frac{s_0}{4\pi i} \int_0^{2\pi} e^{i(1-m)y} - e^{-i(1+m)y} \, dy.
\end{aligned}
\tag{2.3.19}
$$

This integral is zero except when $m = \pm 1$. Thus the only two nonzero coefficients when $n = 0$ are

$$
\begin{aligned}
G_{1,0} &= \frac{s_0}{2i}, \\
G_{-1,0} &= -\frac{s_0}{2i}.
\end{aligned}
$$

In the general output $g(x, y)$ these two coefficients correspond to the component $s_0 \sin y$. Thus we see that the input signal is reproduced exactly in the output from the classical class-D amplifier when natural sampling is used.

Secondly we take the case $m = 0, n \neq 0$. From (2.3.16) the coefficients are

$$
\begin{aligned}
G_{0,n} &= \frac{1}{2\pi^2 in} \int_0^{2\pi} (-1)^n e^{\pi in s_0 \sin y} - 1 \, dy \\
&= \frac{(-1)^n J_0(n\pi s_0) - 1}{\pi in},
\end{aligned}
\tag{2.3.20}
$$

where we have used (2.3.18) with $m = 0$ in the last step.

We have now found all of the Fourier coefficients and hence the general output $g(x, y)$ is

$$g(x, y) = s_0 \sin y + \sum_{n=-\infty}^{\infty}{}' \frac{[(-1)^n J_0(\pi n s_0) - 1]}{\pi i n} e^{inx} + \sum_{m=-\infty}^{\infty}{}' \sum_{n=-\infty}^{\infty}{}' \frac{(-1)^n J_m(\pi n s_0)}{\pi i n} e^{i(nx+my)},$$

where $\sum_n'$ means omitting the term $n = 0$, and $\sum_m'$ means omitting the term $m = 0$. Reverting to the original single variable t we find the output $g(t)$ is

$$g(t) = s_0 \sin \omega_a t - \sum_{m=-\infty}^{\infty} \sum_{n=-\infty}^{\infty}{}' \frac{[\delta_{m0} - (-1)^n J_m(\pi n s_0)]}{\pi i n} e^{i\omega_{mn} t}, \qquad (2.3.21)$$

where

$$\omega_{mn} = n\omega_c + m\omega_a, \qquad (2.3.22)$$

and where

$$\delta_{m0} = \begin{cases} 1 & \text{for } m = 0 \\ 0 & \text{otherwise.} \end{cases} \qquad (2.3.23)$$

If we convert this result back to dimensional terms, it is in agreement with [4]. It is clear from this result that the only component in the low-frequency part of the output ($n = 0$) is exactly the input signal. Outside of the low-frequency range, i.e. for $n \neq 0$, there are additional components in the output. These high-frequency components are filtered out of the final amplifier output by a low-pass filter, and so the final output contains only the low-frequency component. Thus we see that when natural sampling is used to create the square wave output, the amplifier output is exactly the input signal, as desired.

We now examine the output from a classical class-D amplifier when the square wave output is created by regular sampling. We again utilise the double Fourier series method, though an alteration to the technique used above for natural sampling is required to accommodate the different switching times.

2.3.1.2 Regular sampling

In this section we find the output resulting from leading-edge regular sampling modulation of a sinusoidal input signal using the double Fourier series method. The approach is the same as that for natural sampling above except that the leading-edge switching times β_n are now defined explicitly rather than implicitly, and so an additional change of variables is needed, as will become apparent.

As in §2.3.1.1 we begin by defining the new variables x and y, given by (2.3.11) and (2.3.12) respectively. However, we notice that β_n depends on $s(n)$ rather than $s(t)$ since we are using regular sampling rather than natural sampling. Thus it makes sense to define a new set of variables X and Y, where

$$X = x, \tag{2.3.24}$$
$$Y = y - \frac{\omega_a}{\omega_c}(X - 2\pi n), \tag{2.3.25}$$

where

$$n = (X - X \bmod 2\pi)/(2\pi). \tag{2.3.26}$$

Note that in (2.3.25) if we write X and y in terms of t, we simply have $Y = 2\pi n \frac{\omega_a}{\omega_c} = \omega_a n$. We now formulate a generalised version of the problem in terms of the independent variables X and Y to find the general output $G(X, Y)$, which we define by

$$G(X, Y) = g\left(x = X, y = Y + \frac{\omega_a}{\omega_c}(X - 2\pi n)\right).$$

We will later find the particular solution along the line $Y = \omega_a n$, which gives the output $g(t)$ that we desire.

We can now write the equation for the switching times (2.3.9) in terms of our new variables,

$$\beta_n = \frac{1}{2}(1 - s_0 \sin Y).$$

Thus in terms of the new variables the generalised form of the output (2.3.7) is

$$G(X, Y) = \begin{cases} -1 & \text{for } 2\pi n < X < 2\pi n + \pi(1 - s_0 \sin Y) \\ +1 & \text{for } 2\pi n + \pi(1 - s_0 \sin Y) < X < 2\pi(n+1), \end{cases} \tag{2.3.27}$$

which is shown in figure 2.5. Figure 2.4, which shows the output for natural sampling, is very similar. The general output $g(x, y)$ for natural sampling (2.3.14) is in an equivalent form to $G(X, Y)$ here. The differences are only that we have made a change of variables from x,y to X,Y, and therefore the switching times are now determined by the intersection of the lines $X = 2\pi n$ and $X = 2\pi n + \pi(1 - s_0 \sin Y)$ with the piecewise constant line $Y = 2\pi n \frac{\omega_a}{\omega_c}$. We notice that if we increase ω_c, the constant $2\pi n \frac{\omega_a}{\omega_c}$ is smaller and this corresponds to more frequent sampling of the input signal.

The general output $G(X, Y)$ is doubly 2π-periodic and thus we wish to write the output as a double Fourier series. However, we want to obtain the final output in the form $g(t) = \sum_{m,n} G_{m,n} e^{i\omega_{mn} t}$, so that we can compare the results with those for natural
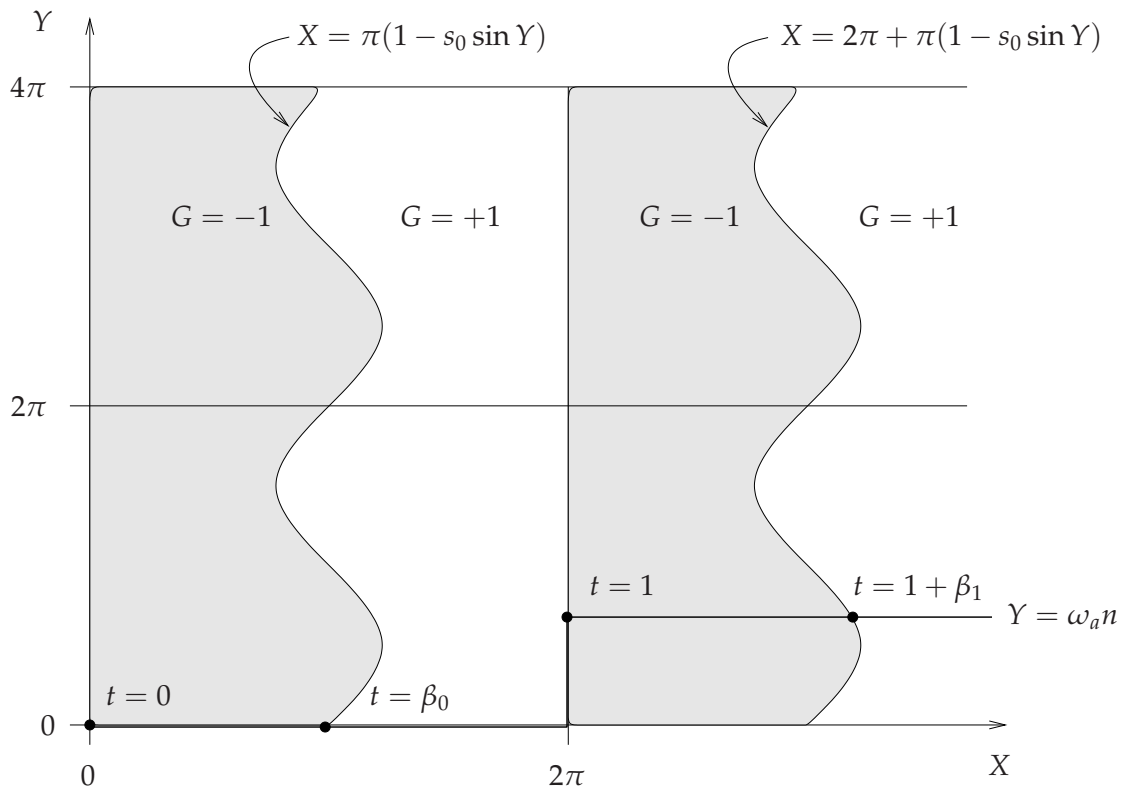
Figure 2.5: The output $G(X, Y)$, shown over two periods in X, resulting from regular sampling of a sinusoidal input signal. The line $Y = \omega_a n$ represents the particular solution we are interested in.

(a) (b) (c)
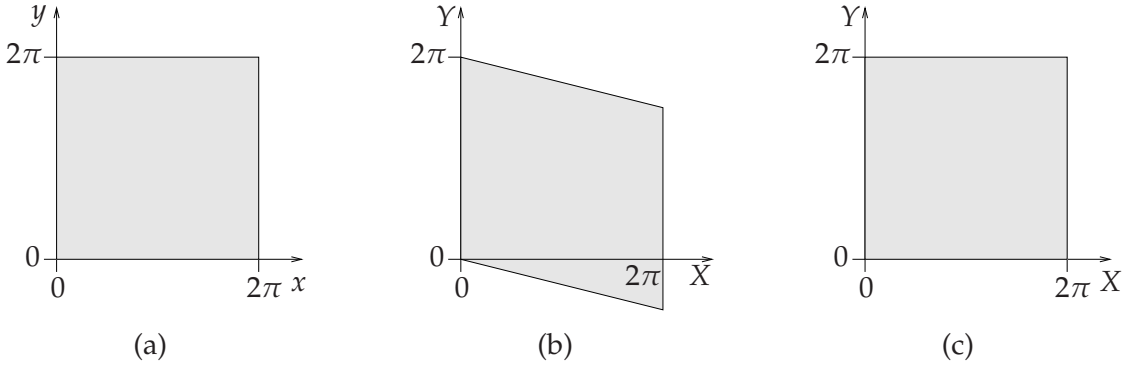
Figure 2.6: Diagram showing the domain of integration (a) in x,y, (b) transformed into X,Y, and (c) an equivalent domain in X,Y.

sampling. Therefore we start by writing the double Fourier series of $G(X,Y)$ in terms of x and y rather than X and Y,

$$g(x,y) = \sum_{m,n=-\infty}^{\infty} G_{m,n} e^{inx+imy},$$

where

$$G_{m,n} = \frac{1}{4\pi^2} \int_0^{2\pi} \int_0^{2\pi} g(x,y) e^{-i(nx+my)} \, dx \, dy, \tag{2.3.28}$$

and then to compute the integral in (2.3.28), we change the variables of integration to X and Y,

$$G_{m,n} = \frac{1}{4\pi^2} \int_0^{2\pi} \int_0^{2\pi} G(X,Y) e^{-i((n+m\frac{\omega_a}{\omega_c})X+mY)} \, dX \, dY. \tag{2.3.29}$$

Notice that we are able to keep the domain of integration the same (see figure 2.6). Initially in x,y the domain is a square. Since $X = x$, the limits for X are still $X = 0$ and $X = 2\pi$. From these limits on X, and the definition of n, (2.3.26), we must have $n = 0$, and thus from (2.3.25), the limits $y = 0$ and $y = 2\pi$ become respectively

$$Y = -\frac{\omega_a}{\omega_c}X,$$
$$Y = 2\pi - \frac{\omega_a}{\omega_c}X,$$

so the region becomes a parallelogram, as depicted in figure 2.6(b). Since $G(X,Y)$ is 2π-periodic in Y, integrating over the parallelogram will give the same answer as integrating over the simpler square domain shown in figure 2.6(c).

We now compute the integral in (2.3.29). If we let $p = n + m\frac{\omega_a}{\omega_c}$ in (2.3.29) we find

$$G_{m,n} = \frac{1}{4\pi^2} \int_0^{2\pi} \int_0^{2\pi} G(X,Y) e^{-i(pX+mY)} \, dX \, dY,$$

which is the same as (2.3.15) for natural sampling except $g(x, y)$, x, y and n are replaced by $G(X, Y)$, X, Y and p respectively. Since the function $g(x, y)$ for natural sampling, given by (2.3.14), is equivalent to $G(X, Y)$ here, with X and Y replaced with x and y, we can use the results from natural sampling to find those for regular sampling. Hence from (2.3.17) we find for $m \neq 0$, $p \neq 0$,

$$G_{m,n} = \frac{(-1)^p}{\pi i p} J_m(\pi p s_0),$$

which in terms of m and n is

$$G_{m,n} = \frac{2(-1)^n e^{-im\omega_a/2} J_m(\omega_{mn} s_0/2)}{i\omega_{mn}},$$

for $m \neq 0$, $\omega_{mn} \neq 0$.

We now consider the coefficients when m and/or p are zero. First, when $p = 0$, from (2.3.19), the coefficients are zero except when $m = \pm 1$. However, in this case since $p = 0$ we must have $n = \pm\frac{\omega_a}{\omega_c}$ which is not an integer. Thus the coefficients are zero in this case. Secondly, for $m = 0$, $p \neq 0$ we have from (2.3.20),

$$G_{0,n} = \frac{(-1)^n J_0(\pi p s_0) - 1}{\pi i p},$$

which in terms of m and n is

$$G_{0,n} = \frac{2(-1)^n J_0(\omega_{mn} s_0/2) - 1}{i\omega_{mn} s_0}.$$

Combining these results and returning to our original variable t we obtain the specific solution we require, the output for regular sampling,

$$g(t) = \sum_{m,n=-\infty}^{\infty} G_{m,n} e^{i\omega_{mn} t}, \tag{2.3.30}$$

where ω_{mn} is defined by (2.3.22),

$$G_{m,n} = \begin{cases} 0 & \text{for } \omega_{mn} = 0 \\ \dfrac{2[(-1)^n e^{-im\omega_a/2} J_m(\omega_{mn} s_0/2) - \delta_{m0}]}{i\omega_{mn}} & \text{for } \omega_{mn} \neq 0, \end{cases}$$

and δ_{m0} is defined by (2.3.23). If we convert this back to dimensional terms, this result is in agreement with [4]. From (2.3.30) we can see immediately that in contrast to natural sampling, there are many components in the low-frequency part of the output (where $n = 0$) and thus distortion has been introduced. We will analyse this regular sampling output and compare it with that for natural sampling in §2.3.3.

We have now found the outputs resulting from natural and regular sampling via the double Fourier series method. When natural sampling is used, the low-frequency

part of the output is exactly the input signal, but when regular sampling is used there is distortion in this low-frequency part. However, the double Fourier series method is not simple, and a lot of additional effort is needed to analyse regular sampling. In next section we repeat the calculations of the outputs resulting from natural and regular sampling, but implement the Fourier transform/Poisson resummation method instead, aiming to show that it has many advantages over the double Fourier series method.

2.3.2 Fourier transform/Poisson resummation method

We now calculate the outputs from a classical class-D amplifier resulting from natural and regular sampling, as in §2.3.1, but use the Fourier transform/Poisson resummation method to find the output. Obviously we aim to show that the results for natural sampling agree for both methods and the results for regular sampling agree for both methods. In repeating the calculation here via the Fourier transform/Poisson resummation method we aim to illustrate the considerable advantages this method has over the double Fourier series method. Whereas the double Fourier series method used above involves defining the problem in terms of two separate timescales, this method avoids this cumbersome step, instead relying on the Poisson resummation formula, see for example [22],

$$\sum_{n=-\infty}^{\infty} h(n) = \sum_{n=-\infty}^{\infty} \int_{-\infty}^{\infty} e^{2\pi i n \tau} h(\tau) \, d\tau. \tag{2.3.31}$$

We use the Fourier transform/Poisson resummation method first in §2.3.2.1 to examine the output when natural sampling is used to determine the switching times of the square wave, and then in §2.3.2.2 to examine the output when regular sampling is used instead. We compare the results for each sampling scheme with the corresponding results derived using the double Fourier series method.

2.3.2.1 Natural sampling

We now repeat the calculation of the output from a classical class-D amplifier resulting from leading-edge natural sampling modulation of a sinusoidal input signal that we carried out in §2.3.1, but now use Fourier transform/Poisson resummation method rather than the double Fourier series method.

We first write the output (2.3.7) in a form that will simplify the calculation,

$$g(t) = 1 - 2 \sum_{n=-\infty}^{\infty} \chi(t; n, n + \beta_n), \tag{2.3.32}$$

where the "top hat" function χ is defined by

$$\chi(t; t_1, t_2) = \begin{cases} 1 & \text{for } t_1 < t < t_2 \\ 0 & \text{otherwise.} \end{cases} \tag{2.3.33}$$

The switching times β_n are given by (2.3.8) with $t = n + \beta_n$,

$$\beta_n = \frac{1}{2}(1 - s(n + \beta_n)). \tag{2.3.34}$$

Note that if we were to consider trailing-edge or double-edge modulation, instead of the leading-edge modulation we look at here, we would write the trailing-edge switching times as $t = n + \alpha_n$, where the definition of α_n would depend on the type of PWM. To illustrate how this method can be applied to any type of PWM, we therefore consider the trailing-edge switching times to occur at $t = n + \alpha_n$, but define $\alpha_n = 0$.

The first step in finding the output is to apply the Poisson resummation formula to the sum in (2.3.32). To do this we first define τ to be a continuous version of the discrete n. We now write the switching times in terms of τ. We define the generalised switching time functions $\alpha(\tau)$ such that $\alpha(n) = 0$, and $\beta(\tau)$ such that $\beta(n) = \beta_n$. Therefore, by definition, $g(t)$ switches to -1 at $t = \tau + \alpha(\tau)$, and to $+1$ at $t = \tau + \beta(\tau)$. With these definitions, we find

$$\alpha(\tau) = 0, \tag{2.3.35}$$
$$\beta(\tau) = \frac{1}{2}(1 - s(\tau + \beta(\tau))), \tag{2.3.36}$$

where we have used (2.3.34) to determine $\beta(\tau)$.

We now apply the Poisson resummation formula (2.3.31) to (2.3.32) to give

$$g(t) = 1 - 2 \sum_{n=-\infty}^{\infty} \int_{-\infty}^{\infty} e^{2\pi i n \tau} \chi(t; \tau + \alpha(\tau), \tau + \beta(\tau)) \, d\tau. \tag{2.3.37}$$

Note that the "top hat" function is nonzero for $\tau + \alpha(\tau) < t < \tau + \beta(\tau)$, but in order to compute the integral in this expression, we must find the limits on τ rather than t. We therefore define the times at which $g(t)$ switches to -1 to be $\tau = A(t)$, equivalent to the times $t = \tau + \alpha(\tau)$, where $A(t)$ is a function to be found. Similarly we define the times at which $g(t)$ switches to $+1$ to be $\tau = B(t)$, equivalent to the times $t = \tau + \beta(\tau)$, where $B(t)$ is a function to be found. With reference to figure 2.7 we note that if we write the "top hat" function in terms of τ it is now nonzero for $B(t) < \tau < A(t)$.

We need to determine $A(t)$, which gives the times τ at which $g(t)$ switches to -1. At these times, $t = \tau + \alpha(\tau)$ where $\alpha(\tau)$ is given by (2.3.35), and thus $\tau = t$. Since $t = \tau + \alpha(\tau)$ is equivalent to $\tau = A(t)$, we must have that

$$A(t) = t. \tag{2.3.38}$$
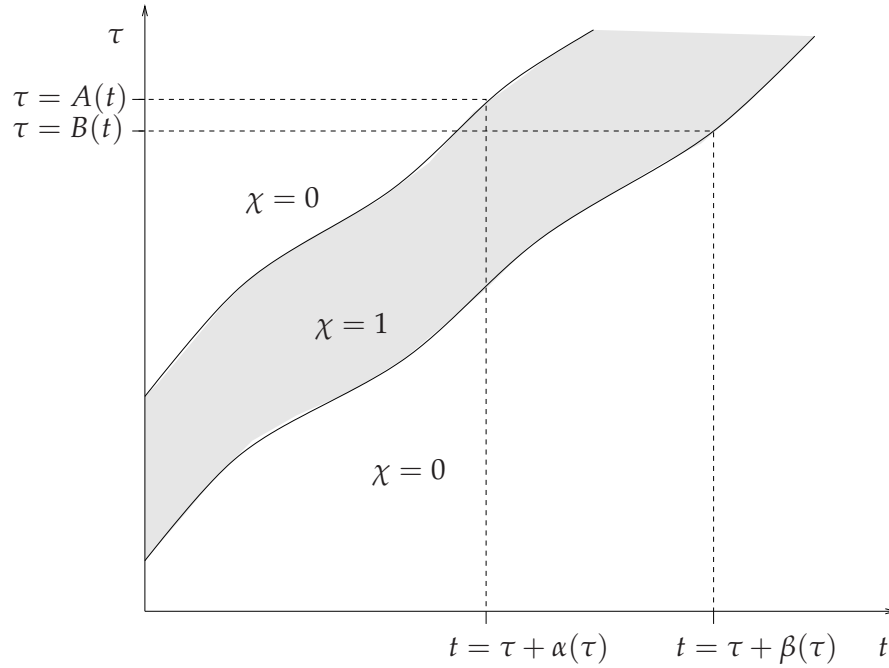
Figure 2.7: Diagram showing the relationship between t and τ.

We now determine $B(t)$ in the same way. The times τ at which $g(t)$ switches to $+1$ are given by $B(t)$. Since at these times $t = \tau + \beta(\tau)$ we must have from (2.3.36)

$$t = \tau + \frac{1}{2}(1 - s(t)),$$

and by rearranging to find τ we obtain

$$B(t) = t - \frac{1}{2}(1 - s(t)). \tag{2.3.39}$$

Both equations defining the switching times are now explicit. Originally, the switching times were defined by $t = \tau + \alpha(\tau)$ and $t = \tau + \beta(\tau)$, where $\alpha(\tau)$ and $\beta(\tau)$ are given by (2.3.35) and (2.3.36) respectively, and where (2.3.36) is implicit. Now, the switching times are defined by $\tau = A(t)$ and $\tau = B(t)$, where the functions $A(t)$ and $B(t)$ are given by (2.3.38) and (2.3.39) respectively, and where both are explicit.

We can now easily find the output. Writing the "top hat" function in terms of the limits on τ, (2.3.37) becomes

$$\begin{aligned}
g(t) &= 1 - 2 \sum_{n=-\infty}^{\infty} \int_{-\infty}^{\infty} e^{2\pi i n \tau} \chi(\tau; B(t), A(t)) \, d\tau \\
&= 1 - 2 \sum_{n=-\infty}^{\infty} \int_{B(t)}^{A(t)} e^{2\pi i n \tau} \, d\tau,
\end{aligned}$$

since the "top hat" function is nonzero only for $B(t) < \tau < A(t)$. We split the summation into two parts: the first part containing only the terms resulting from $n = 0$; the

second containing all terms except those resulting from $n = 0$,

$$g(t) = 1 - 2 \int_{B(t)}^{A(t)} d\tau - 2 \sum_{n=-\infty}^{\infty}{}' \int_{B(t)}^{A(t)} e^{2\pi i n \tau} \, d\tau,$$

where $\sum_n'$ means omitting the term $n = 0$. We integrate this and substitute for $A(t)$ and $B(t)$ from (2.3.38) and (2.3.39) producing

$$g(t) = s(t) - \sum_{n=-\infty}^{\infty}{}' \frac{e^{i n \omega_c t}}{\pi i n} \left(1 - (-1)^n e^{\pi i n s(t)} \right), \tag{2.3.40}$$

where $\omega_c = 2\pi$. An obvious advantage in using this method can be seen here: we are able to determine for a general input signal $s(t)$ that the low-frequency part of the output is exactly the input signal, in contrast to the double Fourier series method where we need to specify the input signal to ascertain this. This result can be achieved by another method [4], but the calculations are much more algebraically involved.

The output (2.3.40) is a formula valid for a general input $s(t)$. To make further progress we specify that the input signal is sinusoidal, defined by (2.3.5). We then apply the Jacobi-Anger Bessel function identity [23],

$$e^{i z \sin \theta} = \sum_{m=-\infty}^{\infty} J_m(z) e^{i m \theta}, \tag{2.3.41}$$

and obtain

$$g(t) = s_0 \sin \omega_a t - \sum_{n=-\infty}^{\infty}{}' \frac{e^{i n \omega_c t}}{\pi i n} \left(1 - (-1)^n \sum_{m=-\infty}^{\infty} J_m(\pi n s_0) \right).$$

Finally the output is determined to be

$$g(t) = s_0 \sin \omega_a t - \sum_{m=-\infty}^{\infty} \sum_{n=-\infty}^{\infty}{}' \frac{[\delta_{m0} - (-1)^n J_m(\pi n s_0)]}{\pi i n} e^{i \omega_{mn} t}, \tag{2.3.42}$$

where ω_{mn} is defined by (2.3.22) and δ_{m0} is defined by (2.3.23). As expected, this output agrees exactly with that found using the double Fourier series method, (2.3.21). The motivation to repeat the calculation using this method was to demonstrate the benefits of the Fourier transform/Poisson resummation method. We have not needed to introduce two separate timescales in this method, which greatly simplifies the calculation, and by using the Poisson resummation formula, the number of steps is greatly reduced. In addition to determining the output more quickly and simply, this method also allows us to establish for a general input signal that the input signal is reproduced exactly in the output.

In the next section we repeat the calculation of the output for regular sampling, which demonstrates further the advantages of using the Fourier transform/Poisson resummation method.

2.3.2.2 Regular sampling

We find the output from a classical class-D amplifier resulting from regular sampling leading-edge modulation of a sinusoidal input signal using the Fourier transform/Poisson resummation method as opposed to the double Fourier series method. This example again demonstrates the relative simplicity of the Fourier transform/Poisson resummation method.

The method for finding the output here is different from that for natural sampling. We first take the Fourier transform of the output, then apply the Poisson resummation formula, and finally invert the transform to obtain the output in the desired form. The reason for incorporating the Fourier transform into the method for regular sampling is that we need to use the equations for the switching times in their explicit form. The switching times for natural sampling are implicit, but those for regular sampling are explicit.

We start by writing the output (2.3.7) in a form that simplifies the following calculations. Because the first step is to take the Fourier transform, the simplest form for $g(t)$ here is

$$g(t) = \sum_{n=-\infty}^{\infty} \chi(t; n + \beta_n, n + 1) - \sum_{n=-\infty}^{\infty} \chi(t; n, n + \beta_n), \tag{2.3.43}$$

where the "top hat" function χ is defined by (2.3.33), and the switching times β_n are given by (2.3.9).

We define the following notation for the Fourier transform,

$$\hat{g}(\omega) = \int_{-\infty}^{\infty} g(t) e^{-i\omega t} \, dt, \tag{2.3.44}$$

and then take the Fourier transform of (2.3.43),

$$
\begin{aligned}
\hat{g}(\omega) &= \int_{-\infty}^{\infty} \sum_{n=-\infty}^{\infty} \chi(t; n + \beta_n, n + 1) e^{-i\omega t} \, dt - \int_{-\infty}^{\infty} \sum_{n=-\infty}^{\infty} \chi(t; n, n + \beta_n) e^{-i\omega t} \, dt \\
&= \sum_{n=-\infty}^{\infty} \left[\int_{n+\beta_n}^{n+1} e^{-i\omega t} \, dt - \int_{n}^{n+\beta_n} e^{-i\omega t} \, dt \right].
\end{aligned} \tag{2.3.45}
$$

We split this expression into two parts as we must consider the cases $\omega = 0$ and $\omega \neq 0$ separately. We will return to the zero-frequency component of the output later, but for now focus on the nonzero-frequency components, which are given by

$$\hat{g}(\omega) = \sum_{n=-\infty}^{\infty} \frac{2e^{-i\omega n}}{i\omega} \left[e^{-i\omega \beta_n} - 1 \right],$$

for $\omega \neq 0$. Using the definitions of β_n and $s(t)$, (2.3.9) and (2.3.5), we obtain

$$\hat{g}(\omega) = \sum_{n=-\infty}^{\infty} \frac{2e^{-i\omega n}}{i\omega} \left[e^{-i\omega(1 - s_0 \sin \omega_a n)/2} - 1 \right].$$

28

We use the Jacobi-Anger Bessel function identity (2.3.41) to obtain

$$\hat{g}(\omega) = \sum_{m,n=-\infty}^{\infty} \frac{2e^{-i\omega n}}{i\omega} \left[e^{-i\omega/2} J_m(\omega s_0/2) - \delta_{m0} \right],$$

and then apply the Poisson resummation formula (2.3.31) to find

$$\hat{g}(\omega) = \sum_{m,n=-\infty}^{\infty} \int_{-\infty}^{\infty} \frac{2e^{i(n\omega_c + m\omega_a - \omega)\tau}}{i\omega} \left[e^{-i\omega/2} J_m(\omega s_0/2) - \delta_{m0} \right] d\tau.$$

The integral in this expression is zero except when $\omega = \omega_{mn}$, where ω_{mn} is defined by (2.3.22). Thus we find

$$\hat{g}(\omega) = \sum_{m,n=-\infty}^{\infty} \int_{-\infty}^{\infty} \frac{2e^{i(\omega_{mn}-\omega)\tau}}{i\omega_{mn}} \left[e^{-i\omega_{mn}/2} J_m(\omega_{mn}s_0/2) - \delta_{m0} \right] d\tau \qquad (2.3.46)$$

for $\omega_{mn} \neq 0$. These nonzero-frequency components are now written directly as a Fourier transform. This will be simple to invert later to find the nonzero-frequency components of $g(t)$, but we first examine the zero-frequency component of $g(t)$.

We determine the zero-frequency component, $\hat{g}(0)$, by considering the short- and long-time averages (defined at the beginning of §2.3) of $g(t)$. The short-time average of $g(t)$ is

$$\begin{aligned} \langle g(t) \rangle &= 1 - 2\beta_n \\ &= s_0 \sin \omega_a n, \end{aligned}$$

and therefore the long-time average of $g(t)$ is zero. Thus $g(t)$ has no zero-frequency component, and so $\hat{g}(0) = 0$.

This conclusion can also be reached by computing $\hat{g}(0)$ directly, as follows. Considering (2.3.45) for $\omega = 0$ we find

$$\begin{aligned} \hat{g}(0) &= \sum_{n=-\infty}^{\infty} \left[\int_{n+\beta_n}^{n+1} dt - \int_{n}^{n+\beta_n} dt \right] \\ &= \sum_{n=-\infty}^{\infty} [1 - 2\beta_n] \\ &= \sum_{n=-\infty}^{\infty} s(n). \end{aligned}$$

Applying the Poisson resummation formula, and using the definition of the input signal, we find

$$\hat{g}(0) = \frac{s_0}{2i} \sum_{n=-\infty}^{\infty} \int_{-\infty}^{\infty} e^{2\pi i n \tau} (e^{i\omega_a \tau} - e^{-i\omega_a \tau}) \, d\tau.$$

This integral is only nonzero when $2\pi n \pm \omega_a = 0$. However, in this instance n would not be an integer, and so $\hat{g}(0) = 0$, as we concluded above.

29

By directly inverting the Fourier transform in (2.3.46), and since $g(t)$ has no zero-frequency component, we can now obtain the full output in the form we desire,

$$g(t) = \sum_{m,n=-\infty}^{\infty} G_{m,n} e^{i\omega_{mn}t}, \tag{2.3.47}$$

where ω_{mn} is defined by (2.3.22),

$$G_{m,n} = \begin{cases} 0 & \text{for } \omega_{mn} = 0 \\ \dfrac{2\left[(-1)^n e^{-im\omega_a/2} J_m\left(\omega_{mn} s_0/2\right) - \delta_{m0}\right]}{i\omega_{mn}} & \text{for } \omega_{mn} \neq 0, \end{cases}$$

and δ_{m0} is defined by (2.3.23). As expected, this output agrees exactly with that calculated via the double Fourier series method (2.3.30). Both the Fourier transform/Poisson resummation method used here, and the double Fourier series method require adaptation to analyse regular sampling. But by comparing the methods, we can see that the Fourier transform/Poisson resummation method is more easily adaptable to regular sampling. Instead of making multiple changes of variables as is necessary when using the double Fourier series method to analyse regular sampling, the only additional steps needed when using this method are to take the Fourier transform and later invert, which is much simpler and quicker. As for natural sampling, using the Poisson resummation formula here also simplifies the calculation.

2.3.3 Comparison of natural sampling and regular sampling outputs

We now compare the output we have calculated for natural sampling (given by (2.3.21) via the double Fourier series method, equal to (2.3.42) calculated via the Fourier transform/Poisson resummation method) with that for regular sampling (given by (2.3.30), equal to (2.3.47)).

In order to compare natural sampling with regular sampling, we write the natural sampling output in the form

$$g(t) = \sum_{m,n=-\infty}^{\infty} G_{m,n} e^{i\omega_{mn}t}, \tag{2.3.48}$$

where

$$G_{m,n} = \begin{cases} \frac{i}{2}s_0 & \text{for } n = 0, \ m = -1 \\ -\frac{i}{2}s_0 & \text{for } n = 0, \ m = 1 \\ 0 & \text{for } n = 0, \ m \neq \pm 1 \\ \dfrac{(-1)^n J_m(n\pi s_0) - \delta_{m0}}{\pi i n} & \text{for } n \neq 0. \end{cases}$$

The natural and regular sampling outputs are now in the same form, and so we can easily analyse the differences in the low-frequency part of the outputs (where $n = 0$)

by looking at the coefficients $G_{m,0}$. These coefficients determine the amplitudes of the harmonics (components whose frequency is a multiple of that of the input signal) in the low-frequency part of the outputs. As we noted before, the low-frequency natural sampling output is exactly the input signal, and we can now see from (2.3.48) that the two coefficients $G_{-1,0}$ and $G_{1,0}$ constitute this component.

To compare the component with frequency ω_a for the two sampling schemes we compute series expansions for $\omega_a \ll 1$ of the coefficients $G_{-1,0}$ and $G_{1,0}$ for regular sampling,

$$G_{-1,0} = \frac{i}{2}s_0 - \frac{s_0}{4}\omega_a + O(\omega_a^2), \tag{2.3.49}$$

$$G_{1,0} = -\frac{i}{2}s_0 - \frac{s_0}{4}\omega_a + O(\omega_a^2). \tag{2.3.50}$$

(Note that $\omega_a \ll 1$ is a sensible approximation to consider as it requires that the frequency of the input signal is much smaller than the carrier wave frequency, which is desirable as it results in a less distorted final output from the amplifier, as discussed in §1.1.) Therefore the component with frequency ω_a in the output is

$$
\begin{aligned}
G_{-1,0}e^{-i\omega_a t} + G_{1,0}e^{i\omega_a t} &= s_0 \sin \omega_a t - \frac{s_0 \omega_a}{2}\cos \omega_a t + O(\omega_a^2) \\
&= s_0 \sin\left(\omega_a\left(t - \frac{1}{2}\right)\right) + O(\omega_a^2).
\end{aligned}
$$

Thus we see that in contrast to natural sampling, regular sampling reproduces a delayed version of the input signal in the output, as predicted by the short-time averages of the outputs from the two sampling types, discussed at the beginning of §2.3. This delay by half a carrier wave period is due to the switching times β_n being determined by a sample of the input signal that is taken on average half a carrier wave period before the switching occurs. Because this delay is in practice so small (a typical carrier wave period is approximately 10 microseconds), it is imperceptible to the human ear.

Note that, since $J_{-m}(-z) = J_m(z)$, the coefficient $G_{-m,0}$ is the complex conjugate of $G_{m,0}$. Therefore to compare the remainder of the low-frequency part of the outputs for the two sampling schemes, we compute series expansions for $\omega_a \ll 1$ of only the coefficients $G_{m,0}$ for $m > 1$ for regular sampling,

$$G_{2,0} = \frac{i}{8}s_0^2 \omega_a + \frac{s_0^2}{8}\omega_a^2 + O(\omega_a^3), \tag{2.3.51}$$

$$G_{3,0} = -\frac{3i}{64}s_0^3 \omega_a^2 - \frac{9s_0^3}{128}\omega_a^3 + O(\omega_a^4), \tag{2.3.52}$$

$$G_{4,0} = \frac{i}{48}s_0^4 \omega_a^3 + \frac{s_0^4}{24}\omega_a^4 + O(\omega_a^5), \tag{2.3.53}$$

$$G_{5,0} = -\frac{125i}{12288}s_0^5 \omega_a^4 - \frac{625s_0^5}{24576}\omega_a^5 + O(\omega_a^6), \tag{2.3.54}$$

where we are interested in the largest distortion terms and so stop at $m = 5$. Thus for regular sampling the second harmonic ($m = 2$) is $O(\omega_a)$ and in general, $G_{m,0} = O(\omega_a^{m-1})$ for $m \geq 1$. These harmonics all contribute to the regular sampling output being a distorted version of the input signal.

An effective way to analyse the output resulting from a particular sampling scheme is to plot the spectrum, i.e. plot the magnitude of the amplitude of each coefficient $G_{m,n}$ in the output against its frequency ω. By plotting and comparing the spectra of different sampling schemes we can see clearly what the components of each output are, and their magnitudes, and so determine which sampling scheme produces the output with lower distortion.

The spectrum for regular sampling is plotted in figure 2.8 next to the spectrum for natural sampling. Note that to plot both spectra on the same graph we have shifted the spectrum for regular sampling to the right by 0.05, so that, for example, the black peak that appears at $\omega = 0.3$ is actually the peak that corresponds to $\omega = 0.25$.

We can see clearly in figure 2.8 that the only component in the low-frequency part of the natural sampling spectrum is exactly the input signal, whereas for regular sampling the input signal harmonics of the input signal appear in the low-frequency part of the output. These harmonics can be seen more clearly in figure 2.8(b) where we plot only the low-frequency part of the output. Thus comparing the low-frequency parts of the spectra for natural and regular sampling, it is obvious that the output resulting from regular sampling contains much more distortion than that from natural sampling, which contains no distortion.

Outside the low-frequency part of the spectrum, the outputs from both sampling schemes comprise peaks at multiples of the carrier wave frequency as well as lower amplitude peaks (called sidebands) concentrated around multiples of the carrier wave frequency. Note that we have chosen to plot the spectra up to $\omega = 16$ in figure 2.8 merely so that the low-frequency part of the spectra, as well as the peaks at $\omega = 2\pi$ and $\omega = 4\pi$ (i.e. at the carrier wave frequency and at twice the carrier wave frequency) and their corresponding sidebands, can be seen clearly. In addition there are peaks at, and sidebands around, all larger multiples of the carrier wave frequency, as can be determined from the natural and regular sampling output formulae. There are minor differences in the amplitudes of these peaks outside the low-frequency part of the spectrum for regular sampling compared with natural sampling, but these are irrelevant as they will be attenuated by a low-pass filter.
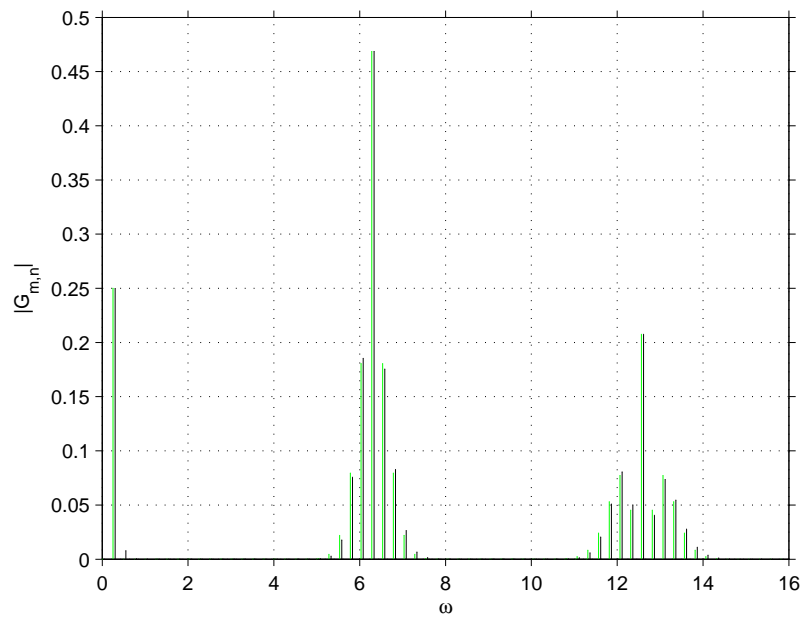
(a)
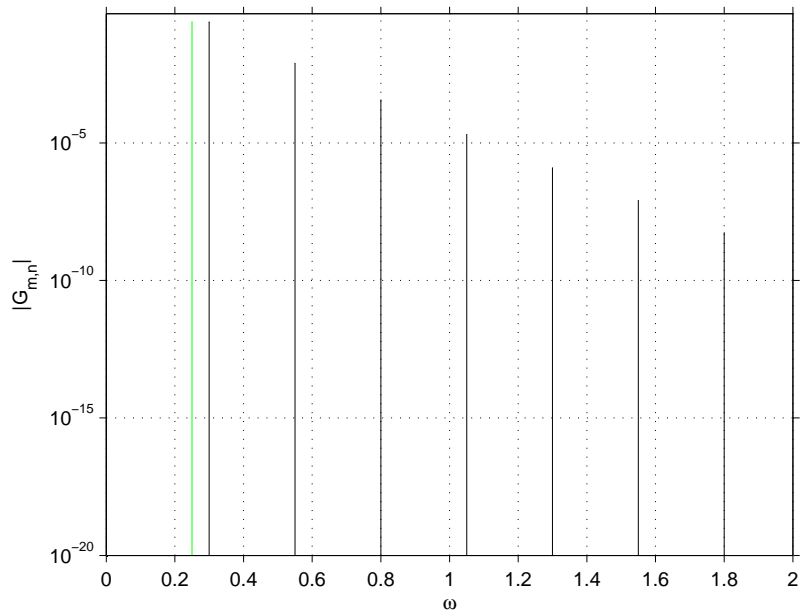
(b)

Figure 2.8: Natural sampling (in green) and regular sampling (in black, shifted to the right by 0.05) spectra resulting from leading-edge modulation of a sinusoidal input signal, $0.5 \sin 0.25t$. Figure (a) shows the full spectra, while figure (b) shows only the low-frequency parts of the spectra with a logarithmic scale on the vertical axis.

2.3.4   Discussion

We have determined the outputs from a classical class-D amplifier when a sinusoidal signal is input and leading-edge natural or regular sampling PWM is used to create the square wave output. For natural sampling, the input is reproduced exactly in the output, and there are no other terms in the low-frequency part of the output, and so the input signal can be reproduced with no distortion. For regular sampling, the input signal is reproduced with distortion and harmonics of the input signal appear in the low-frequency part of the output, and so the amplifier output is a distorted version of the input signal.

Although natural sampling provides better distortion performance than regular sampling, it is only suited to some applications. The equations for the natural sampling switching times are implicit, and so natural sampling is often used in analogue applications, but is difficult to implement digitally [16]. The equations for the regular sampling switching times are explicit and so this sampling scheme is commonly used in digital applications. This motivates us to investigate sampling schemes that aim to provide low distortion, like natural sampling, whilst being simple to use in digital applications, like regular sampling. We will consider several such sampling schemes in the next section.

We calculated the outputs for the two sampling schemes first using the commonly used double Fourier series method, and then repeated the calculations using the Fourier transform/Poisson resummation method, in order to illustrate the advantages of the latter method. If we compare the two methods for natural sampling, it is easy to see that the latter method is simpler and quicker to implement. Not needing to introduce two separate timescales to the problem and using the Poisson resummation formula shortens the calculation considerably. In addition, it is possible to demonstrate via the Fourier transform/Poisson resummation method for a general input signal that the low-frequency part of the output for natural sampling is exactly the input signal, which is not possible via the double Fourier series method.

Both methods require adaptation to examine the output resulting from regular sampling. However, using the double Fourier series method, an additional change of variables is required to solve the problem, making the method unnecessarily complex. The alteration to the Fourier transform/Poisson resummation method is to take the Fourier transform, which is simple to invert later. This change ensures that the equations for the switching times are used in their explicit form.

Each method requires separate consideration of particular frequency components,

though using the Fourier transform/Poisson resummation method this can be done quickly, especially in the natural sampling case.

The Fourier transform/Poisson resummation method has considerable advantages over the double Fourier series method. It is shorter and simpler to use, as well as being more easily adaptable to different sampling schemes. It enables easy comparisons between existing modulation and sampling techniques, as well as mathematical analysis of new or complex strategies that so far have not been tackled. In the following section we will implement this method to investigate a variety of sampling schemes, further showing that it is an adaptable method.

2.4 Analysis of sampling schemes via Fourier transform/Poisson resummation method

We established in the previous section that, to analyse the pulse width modulated square wave output from a class-D amplifier, the Fourier transform/Poisson resummation method is preferable to the double Fourier series method. Here we further demonstrate the simplicity and adaptability of the Fourier transform/Poisson resummation method by considering several sampling schemes that are complex to analyse using the double Fourier series method.

We also illustrated in the previous section the differences between natural and regular sampling, the most important being that, in the low-frequency part of the output, natural sampling reproduces the input signal exactly with no distortion, whilst regular sampling reproduces the input signal with distortion. Due to the implicit nature of the natural sampling switching times, natural sampling is used in analogue applications, while regular sampling is implemented in digital applications (in spite of the resulting harmonic distortion) because the regular sampling switching times are explicit. There is, therefore, motivation to look for a sampling scheme that provides low distortion, like natural sampling, but is also simple to use in digital applications, like regular sampling. Several schemes exist that aim to achieve this, and we discuss several of them now with a view to investigating some in more detail.

Direct sampling, presented by Kim and Ehsani [24], is a sampling scheme that aims to improve upon regular sampling. Contrary to Bowes discussion [25] of the method, the direct sampling method is distinct from other sampling techniques. While, as Bowes concludes, this sampling method produces a pulse width modulated square wave with "virtually identical" area to that produced by regular sampling, the square

wave is still slightly different and consequently the spectrum is different (compared with that for regular sampling, see for example [16]). However, there is very little to be gained in using this type of sampling. The output produced is no better than that from regular sampling even though it is more complex to implement practically, since direct sampling involves integrating the input signal over each carrier wave period. Thus we will not investigate this method further.

Mellor, Leigh and Cheetham [26] propose another sampling technique, called enhanced sampling. In this method, a transformed version $s_n(t)$ of the input signal $s(t)$ is sampled naturally, where

$$s_n(t) = s((1 - \epsilon)(t - n) + n) \text{ for } 0 \leq \epsilon \leq 1.$$

Notice that when $\epsilon = 1$ this process is equivalent to regular sampling, and when $\epsilon = 0$ it is equivalent to natural sampling. With the chosen value $\epsilon = 1/2$, the scheme aims to achieve the advantages of both natural and regular sampling. However, we believe it does not offer any advantage over natural or regular sampling for two reasons. Firstly, the scheme is not simple to implement digitally because the switching times are still implicit. Secondly, comparing spectra for enhanced and regular sampling, although the third harmonic is attenuated when enhanced sampling instead of regular sampling, the second harmonic, which is of larger amplitude than the third harmonic, is the same for enhanced and regular sampling. Therefore we do not consider this scheme in more detail.

Another novel sampling process is Δ-compensation uniform sampling, as put forward by Li, Gwee and Chang [14]. This method attempts to approximate natural sampling by using only samples at the beginning and end of the carrier wave period so that the process can be implemented digitally. Linear interpolation could be used to determine the switching times, but this is computationally expensive as it involves division. To avoid this, Li, Gwee and Chang present a different way of using the two samples to approximate the switching times, and find that the resulting output contains less distortion than regular sampling.

Δ-compensation uniform sampling is, however, derived unsystematically. We therefore start in §2.4.1 by looking at simple alterations to regular sampling that offer improvements in distortion performance. We consider three schemes that offer compounding improvements and find that the third scheme is equivalent to Δ-compensation uniform sampling. We analyse all three schemes using the Fourier transform/Poisson resummation method and plot the resulting spectra to compare our results.

2.4.1 Sampling schemes related to regular sampling

We analyse a range of sampling schemes that aim to emulate the low distortion of natural sampling but are less computationally expensive to implement digitally than natural sampling, as regular sampling is. Therefore our aim is to find a scheme that has less harmonic distortion than regular sampling, but uses samples of the input signal at fixed times in the carrier wave period. As the sampling schemes we investigate rely on samples of the input signal at fixed times, the switching times are explicit. Hence to examine the outputs resulting from these sampling schemes we use the Fourier transform/Poisson resummation method as demonstrated for regular sampling in §2.3.2.2.

As in §2.3 we consider leading-edge modulation, and thus the output $g(t)$ resulting from each sampling scheme is defined by (2.3.7), where the leading-edge switching times β_n will be defined differently for each scheme. As above we consider a sinusoidal input signal, $s(t) = s_0 \sin \omega_a t$. Note that our model is dimensionless, as in §2.3, and so voltages and times have been nondimensionalised using the voltage scale V and the time scale T respectively.

To determine whether each scheme is an improvement on regular sampling we calculate the output resulting from each scheme and plot each of their spectra next to the regular sampling spectrum, in the same way as we compared natural and regular sampling in §2.3.3. To analyse the differences in the low-frequency part of the outputs in more detail, we examine the amplitudes of the low-frequency harmonics in the outputs, again in the same way as in §2.3.3 where we consider series expansions of the harmonics for small ω_a. By investigating the sampling schemes that follow, we aim to obtain one with reduced harmonic distortion compared with the regular sampling output, i.e. one or more of the harmonics have smaller amplitude than the corresponding harmonic for regular sampling. Note that we focus on the low-frequency part of the output because higher-frequency components in the output will be attenuated by a low-pass filter, and so any small changes to the higher-frequency part of the spectrum are irrelevant.

2.4.1.1 Averaged two-sample scheme

As a first attempt to improve upon regular sampling, it proves useful to consider a scheme where we replace $s(n)$ by $\frac{s(n)+s(n+1)}{2}$ in the leading-edge switching times for regular sampling, (2.3.9). This doubles the number of samples of the input signal per carrier wave period used to create the square wave output, and so it seems likely that it will offer some improvement compared to regular sampling. By using samples at the

beginning and end of the carrier wave period it also introduces a symmetry into the scheme.

The leading-edge switching times β_n for this sampling method thus are given by

$$\beta_n = \frac{1}{2}\left(1 - \frac{s(n) + s(n+1)}{2}\right).$$

where $s(t)$ is sinusoidal, defined by (2.3.5). In order to calculate the output, it is beneficial to rewrite this equation with as few terms containing $\sin \omega_a n$ as possible. This simplifies the final output by reducing the number of sums of Bessel functions in the output. Thus we write the equation for the switching times in the form

$$\beta_n = \frac{1}{2}\left(1 - s_0 \cos\left(\frac{\omega_a}{2}\right) \sin\left(\omega_a n + \frac{\omega_a}{2}\right)\right).$$

We find the output resulting from this sampling scheme via the Fourier transform/Poisson resummation method, and thus obtain

$$g(t) = \sum_{m,n=-\infty}^{\infty} G_{m,n} e^{i\omega_{mn}t},$$

where

$$G_{m,n} = \begin{cases} 0 & \text{for } \omega_{mn} = 0 \\ \dfrac{2[(-1)^n J_m(\zeta_{m,n}) - \delta_{m0}]}{i\omega_{mn}} & \text{for } \omega_{mn} \neq 0, \end{cases}$$

ω_{mn} is defined by (2.3.22), and where

$$\zeta_{m,n} = \frac{\omega_{mn}s_0}{2} \cos\left(\frac{\omega_a}{2}\right).$$

To analyse the amplitudes of the low-frequency harmonics, we look at the series expansions of the coefficients $G_{m,0}$ for $1 \leq m \leq 5$ for $\omega_a \ll 1$,

$$G_{1,0} = -\frac{i}{2}s_0 + \frac{i}{64}s_0(s_0^2 + 4)\omega_a^2 + O(\omega_a^4),$$
$$G_{2,0} = \frac{i}{8}s_0^2\omega_a - \frac{i}{96}s_0^2(s_0^2 + 3)\omega_a^3 + O(\omega_a^5),$$
$$G_{3,0} = -\frac{3i}{64}s_0^3\omega_a^2 + \frac{9i}{4096}s_0^3(3s_0^2 + 8)\omega_a^4 + O(\omega_a^6),$$
$$G_{4,0} = \frac{i}{48}s_0^4\omega_a^3 - \frac{i}{480}s_0^4(2s_0^2 + 5)\omega_a^5 + O(\omega_a^7),$$
$$G_{5,0} = -\frac{125i}{12288}s_0^5\omega_a^4 + \frac{625i}{1179648}s_0^5(5s_0^2 + 12)\omega_a^6 + O(\omega_a^8).$$

If we compare these with the corresponding series expansions for regular sampling, (2.3.50)-(2.3.54), we see that the largest order terms in each harmonic are exactly the same and as such this method appears not to be any improvement on regular sampling.
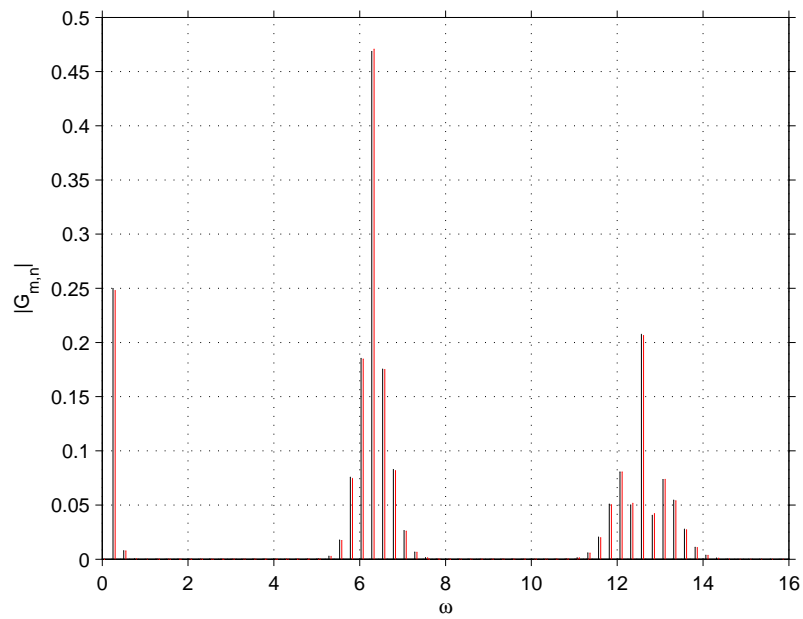
(a)
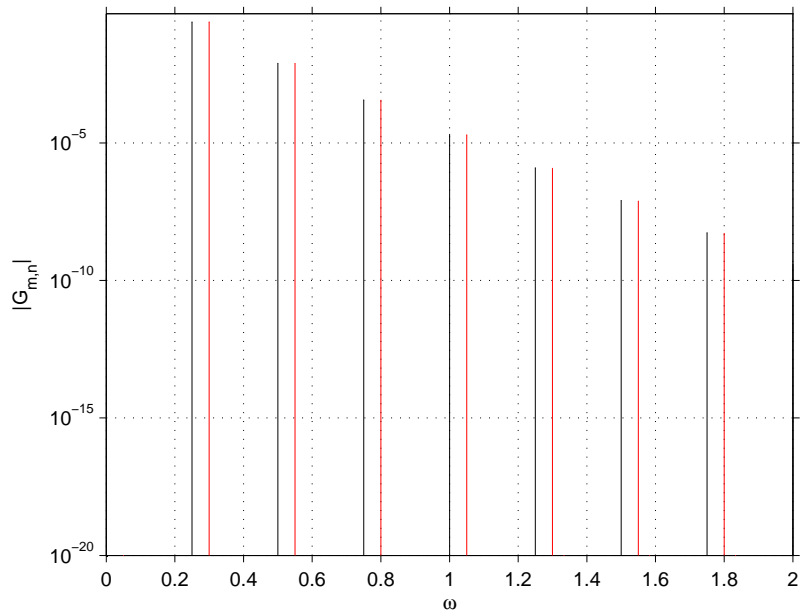
(b)

Figure 2.9: Regular sampling (in black) and averaged two-sample (in red, shifted to the right by 0.05) spectra resulting from leading-edge modulation of a sinusoidal input signal, $0.5 \sin 0.25t$. Figure (a) shows the full spectra, while figure (b) shows only the low-frequency parts of the spectra with a logarithmic scale on the vertical axis.

By plotting the spectra resulting from regular sampling next to that for the averaged two-sample scheme in figure 2.9, we confirm that the outputs are almost exactly the same.

However, this averaged two-sample scheme does introduce an odd/even pattern into the series expansions: odd harmonics (m odd) contain only even powers of ω_a, and even harmonics (m even) contain only odd powers of ω_a. If we are able to combine this sampling scheme with another we may obtain a scheme that results in reduced harmonic distortion. For example, if we combined this averaged two-sample scheme with one that removes the $O(\omega_a)$ term in $G_{2,0}$, then the coefficient $G_{2,0}$ in the resulting scheme would be of $O(\omega_a^3)$. We consider such a combination in §2.4.1.3, though first turn our attention to a scheme that removes the $O(\omega_a)$ term in $G_{2,0}$, thus reducing the amplitude of the second harmonic.

2.4.1.2 Two-sample three-term Taylor series scheme

We here examine a sampling scheme that offers a reduction in harmonic distortion compared to regular sampling. To obtain switching times for such a scheme we look for a way to approximate the natural sampling switching times, since we know that the output for natural sampling contains no harmonic distortion in the low-frequency part of the output.

To approximate the natural sampling switching times we start by expanding the natural sampling switching time equation, (2.3.8), as a Taylor series,

$$\beta_n = \frac{1}{2}\left[1 + s(n) + \beta_n \dot{s}(n) + \frac{\beta_n^2}{2!}\ddot{s}(n) + \ldots\right].$$

If we then assume $\dot{s}(n)$ is small, equivalent to assuming $\omega_a \ll 1$, we can make the approximation

$$\dot{s}(n) \approx s(n+1) - s(n).$$

Using this approximation and just the first three terms of the above Taylor series we obtain an approximation to the natural sampling switching time equation,

$$\beta_n = \frac{1}{2}\left[1 + s(n) + \beta_n[s(n+1) - s(n)]\right] + O(\omega_a^2).$$

Ignoring terms of $O(\omega_a^2)$ and smaller, and rearranging the above to find β_n we obtain

$$
\begin{aligned}
\beta_n &\approx \frac{1 - s(n)}{2 + s(n) - s(n+1)} \\
&\approx \frac{1}{2}[1 - s(n)]\left[1 - \frac{s(n+1) - s(n)}{2}\right] \\
&= \frac{1}{2}\left[1 - \frac{s(n+1) + s(n)}{2} + s(n)\frac{s(n+1) - s(n)}{2}\right],
\end{aligned}
\qquad (2.4.1)
$$

where we have used a binomial series expansion in the first step. The leading-edge switching times for this sampling scheme, which we will call the two-sample three-term Taylor series scheme, are thus defined by (2.4.1), and we now proceed to calculate the resulting output.

We first rewrite (2.4.1) in a form that will simplify the expression for the output, as we did in §2.4.1.1,

$$
\begin{aligned}
\beta_n &= \frac{1}{2}\left[1 - \frac{s_0^2}{2}\sin^2\left(\frac{\omega_a}{2}\right) - s_0\cos\left(\frac{\omega_a}{2}\right)\sin\left(\omega_a n + \frac{\omega_a}{2}\right)\right. \\
&\quad \left. + \frac{s_0^2}{2}\sin\left(\frac{\omega_a}{2}\right)\sin\left(2\omega_a n + \frac{\omega_a}{2}\right)\right],
\end{aligned}
$$

and then calculate the output via the Fourier transform/Poisson resummation method. We find the output to be

$$
g(t) = \sum_{m,n=-\infty}^{\infty} G_{m,n}e^{i\omega_{mn}t}, \tag{2.4.2}
$$

where

$$
G_{m,n} = \begin{cases} 0 & \text{for } \omega_{mn}=0 \\ \displaystyle\sum_{p=-\infty}^{\infty} \frac{2\left[(-1)^{n+p}e^{i\eta_{m,n,p}}J_{m-2p}(\zeta_{m,n})J_p(\theta_{m,n}) - \delta_{m0}\delta_{p0}\right]}{i\omega_{mn}} & \text{for } \omega_{mn}\neq 0, \end{cases}
$$

and where

$$
\begin{aligned}
\eta_{m,n,p} &= \frac{\omega_{mn}s_0^2}{4}\sin^2\left(\frac{\omega_a}{2}\right) - \frac{\omega_a p}{2}, \\
\theta_{m,n} &= \frac{\omega_{mn}s_0^2}{4}\sin\left(\frac{\omega_a}{2}\right).
\end{aligned}
$$

Again, to examine the amplitudes of the low-frequency harmonics, we compute the series expansions of the coefficients $G_{m,0}$ for $1 \leq m \leq 5$ for $\omega_a \ll 1$,

$$
\begin{aligned}
G_{1,0} &= -\frac{i}{2}s_0 + \frac{i}{64}s_0(4 - s_0^3)\omega_a^2 + O(\omega_a^3), \\
G_{2,0} &= \frac{s_0^2}{16}\omega_a^2 + \frac{i}{96}s_0^2(2s_0^2 - 1)\omega_a^3 + O(\omega_a^4), \\
G_{3,0} &= \frac{3i}{64}s_0^3\omega_a^2 + \frac{3}{64}s_0^3\omega_a^3 + O(\omega_a^4), \\
G_{4,0} &= \frac{5i}{192}s_0^4\omega_a^3 - \frac{s_0^4}{64}\omega_a^4 + O(\omega_a^5), \\
G_{5,0} &= \frac{25i}{4096}s_0^5\omega_a^4 - \frac{25}{6144}s_0^5\omega_a^5 + O(\omega_a^6).
\end{aligned}
$$

We compare these series expansions with those for regular sampling. The most important difference between them is that the second harmonic is only $O(\omega_a^2)$ here, but for

41

regular sampling it is $O(\omega_a)$. The other harmonics are of the same order as the equivalent regular sampling harmonics. These characteristics can be seen in figure 2.10 where we plot the spectra for regular sampling and the two-sample three-term Taylor series scheme.

We can see how the reduction in the second harmonic arises if we look at $G_{2,0}$ in more detail. We define

$$G_{2,0} = \sum_{p=-\infty}^{\infty} \mathcal{G}_p,$$

where

$$\mathcal{G}_p = \frac{(-1)^p e^{i\eta_{2,0,p}} J_{2-2p}\left(\zeta_{2,0}\right) J_p\left(\theta_{2,0}\right)}{i\omega_a}.$$

Using standard power series expansions and $J_k(z) \sim \frac{\left(\frac{z}{2}\right)^k}{k!}$ for k fixed, $k \neq -1, -2, -3, \ldots$ and $z \to 0$ we find that

$$\mathcal{G}_p = \begin{cases} O\left(\omega_a^{1+4|p|}\right) & \text{for } p \leq 0 \\ O\left(\omega_a^{1+4(p-1)}\right) & \text{for } p \geq 1, \end{cases}$$

and thus $p = 0$ and $p = 1$ contribute the largest terms to the sum $G_{2,0}$. If we look at series expansions for these two values of p separately,

$$\mathcal{G}_0 = -\frac{i}{8}s_0^2\omega_a + \frac{i}{96}s_0^2(3 + s_0^2)\omega_a^3 + O(\omega_a^4),$$

$$\mathcal{G}_1 = \frac{i}{8}s_0^2\omega_a + \frac{s_0^2}{16}\omega_a^2 - \frac{i}{96}s_0^2(2 + 3s_0^2)\omega_a^3 + O(\omega_a^4),$$

we see that the $O(\omega_a)$ terms cancel, leaving the $O(\omega_a^2)$ term from $p = 1$ as the largest term contributing to the sum $G_{2,0}$.

We note that in this scheme there is no odd/even pattern in the series expansions of the harmonics, as there is in the averaged two-sample scheme. In the averaged two-sample scheme we introduced a symmetry into the switching times by replacing $s(n)$ with $\frac{s(n)+s(n+1)}{2}$, and this resulted in an odd/even pattern in the series expansions of the harmonics. As we discussed at the end of §2.4.1.1, introducing such a symmetry to this sampling scheme may offer a further reduction in harmonic distortion, and we investigate this in the next section.

2.4.1.3 Averaged two-sample three-term Taylor series scheme

We believe that by introducing a symmetry into the switching times for the two-sample three-term Taylor series scheme, in the same way as we introduced a symmetry into the
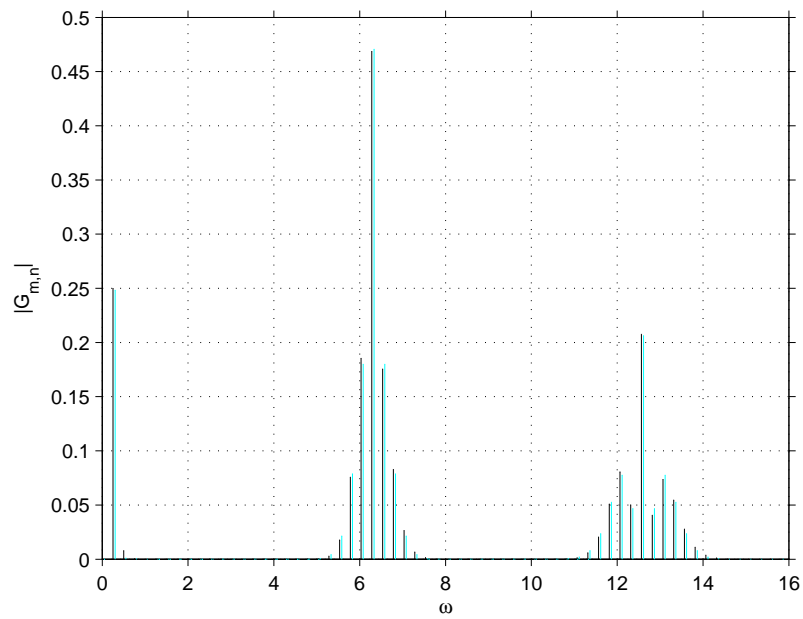
(a)
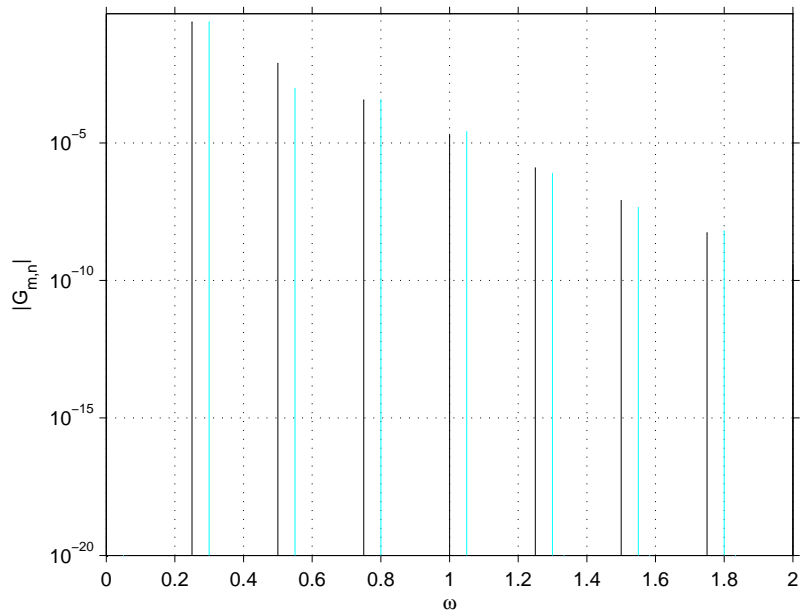
(b)

Figure 2.10: Regular sampling (in black) and two-sample three-term Taylor series (in cyan, shifted to the right by 0.05) spectra resulting from leading-edge modulation of a sinusoidal input signal, $0.5 \sin 0.25t$. Figure (a) shows the full spectra, while figure (b) shows only the low-frequency parts of the spectra with a logarithmic scale on the vertical axis.

regular sampling switching times in §2.4.1.1, it may be possible to improve upon the two-sample three-term Taylor series scheme used in the previous section. We therefore implement a sampling scheme that uses the two-sample three-term Taylor series switching times, (2.4.1), but with the $s(n)$ in the last term replaced by $\frac{s(n)+s(n+1)}{2}$, so that

$$\beta_n = \frac{1}{2}\left[1 - \frac{s(n+1)+s(n)}{2} + \frac{s(n)+s(n+1)}{2}\frac{s(n+1)-s(n)}{2}\right]. \qquad (2.4.3)$$

These are the leading-edge switching times for this sampling scheme, which we will call the averaged two-sample three-term Taylor series scheme, and we now determine the output created by this sampling scheme.

As for the previous two sampling schemes, we first rewrite the switching times (2.4.3) in a form that will simplify the expression for the output,

$$\beta_n = \frac{1}{2}\left[1 - s_0\cos\left(\frac{\omega_a}{2}\right)\sin\left(\omega_a n + \frac{\omega_a}{2}\right) + \frac{s_0^2}{4}\sin\left(\omega_a\right)\sin\left(2\omega_a n + \omega_a\right)\right].$$

We then calculate the output via the Fourier transform/Poisson resummation method and obtain

$$g(t) = \sum_{m,n=-\infty}^{\infty} G_{m,n}e^{i\omega_{mn}t}, \qquad (2.4.4)$$

where

$$G_{m,n} = \begin{cases} 0 & \text{for } \omega_{mn} = 0 \\ \displaystyle\sum_{p=-\infty}^{\infty} \frac{2[(-1)^{n-p}J_{m-2p}(\zeta_{m,n})J_p(\iota_{m,n}) - \delta_{m0}\delta_{p0}]}{i\omega_{mn}} & \text{for } \omega_{mn} \neq 0, \end{cases}$$

and where

$$\iota_{m,n} = \frac{\omega_{mn}s_0^2}{8}\sin\omega_a.$$

Comparing this output with that from the two-sample three-term Taylor series scheme, we see there are only subtle differences. Here, the term $e^{i\eta_{m,n,p}}$ multiplying the Bessel functions is missing, and the argument of the second Bessel function has changed from $\theta_{m,n}$ to $\iota_{m,n}$. Again, we analyse the amplitudes of the harmonics by computing the series expansions of the coefficients $G_{m,0}$ for $1 \leq m \leq 5$ for $\omega_a \ll 1$,

$$G_{1,0} = -\frac{i}{2}s_0 + \frac{i}{64}s_0(4 - s_0^2)\omega_a^2 + O(\omega_a^4),$$

$$G_{2,0} = \frac{i}{96}s_0^2(1 - 2s_0^2)\omega_a^3 + O(\omega_a^5),$$

$$G_{3,0} = \frac{3i}{64}s_0^3\omega_a^2 + O(\omega_a^4),$$

$$G_{4,0} = \frac{5i}{192}s_0^4\omega_a^3 + O(\omega_a^5),$$

$$G_{5,0} = \frac{25i}{4096}s_0^5\omega_a^4 + O(\omega_a^6).$$
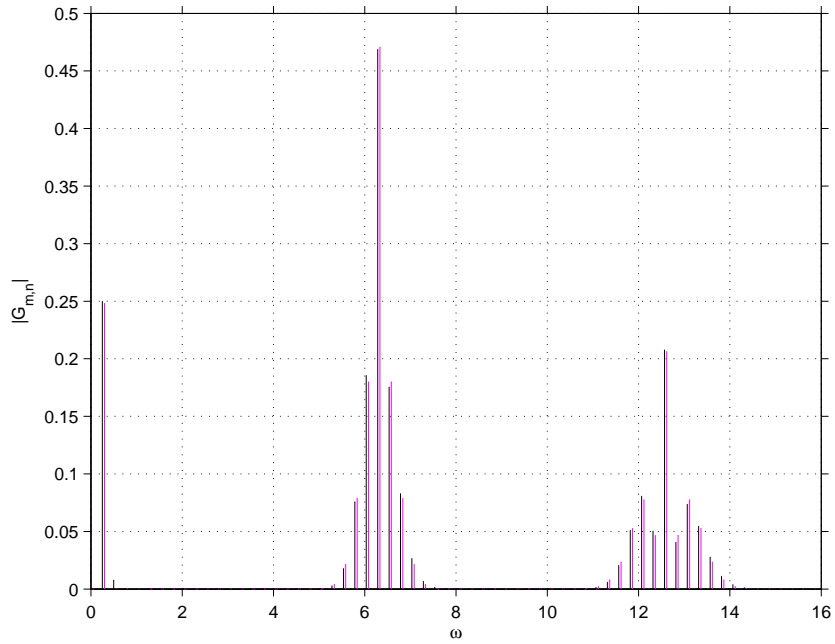
Figure 2.11: Regular sampling spectrum (in black) and averaged two-sample three-term Taylor series spectrum (in magenta, shifted to the right by 0.05) resulting from leading-edge modulation of a sinusoidal input signal, $0.5 \sin 0.25t$.

Immediately we can see that this scheme is an improvement on both regular sampling and the two-sample three-term Taylor series scheme: the second harmonic has here been reduced to $O(\omega_a^3)$, compared with $O(\omega_a)$ and $O(\omega_a^2)$ respectively. The other harmonics are of the same order as those for both regular sampling and the two-sample three-term Taylor series scheme, but we notice the same odd/even pattern in the series expansions here as when the averaged two-sample scheme was used. These characteristics are evident in figures 2.11 and 2.12

As in the previous section, we can see how the reduction in amplitude of the second harmonic arises if we look at $G_{2,0}$ in more detail. Here, the second harmonic is

$$G_{2,0} = \sum_{p=-\infty}^{\infty} \mathcal{G}_p,$$

where

$$\mathcal{G}_p = \frac{(-1)^p J_{2-2p}\left(\zeta_{2,0}\right) J_p\left(\iota_{2,0}\right)}{i\omega_a}.$$

Using the same series expansions as for the two-sample three-term Taylor series scheme, we find that the orders of magnitude of the terms in the sum $G_{2,0}$ follow the same pattern as for the two-sample three-term Taylor series scheme, and thus we find again that
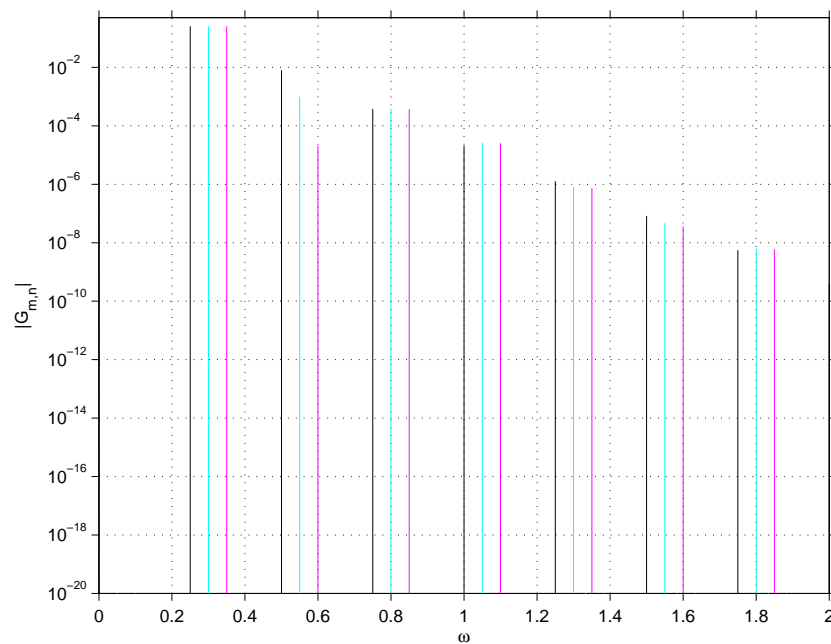
Figure 2.12: Regular sampling (in black), two-sample three-term Taylor series (in cyan, shifted to the right by 0.05) and averaged two-sample three-term Taylor series (in magenta, shifted to the right by 0.1) spectra resulting from leading-edge modulation of a sinusoidal input signal, $0.5 \sin 0.25t$. Only the low-frequency parts of the spectra are plotted here, and with a logarithmic scale on the vertical axis.

46

$p = 0$ and $p = 1$ contribute the largest terms to $G_{2,0}$. If we look at series expansions for these two values of p separately we obtain

$$\mathcal{G}_0 = -\frac{i}{8}s_0^2\omega_a + \frac{i}{96}s_0^2(s_0^2 + 3)\omega_a^3 + O(\omega_a^5),$$
$$\mathcal{G}_1 = \frac{i}{8}s_0^2\omega_a - \frac{i}{96}s_0^2(3s_0^2 + 2)\omega_a^3 + O(\omega_a^5),$$

and we see that the $O(\omega_a)$ terms cancel as in the previous section. But in contrast to the two-sample three-term Taylor series scheme, since there are no $O(\omega_a^2)$ terms from $p = 1$, the largest terms contributing to the sum $G_{2,0}$ are now only $O(\omega_a^3)$. The absence of any $O(\omega_a^2)$ terms from $p = 1$ arises here because the exponential term $e^{i\eta_{2,0,1}}$, which appears in the corresponding two-sample three-term Taylor series scheme term, is missing here.

Equivalence to Δ-compensation uniform sampling. A sampling process equivalent to the averaged two-sample three-term Taylor series scheme has been implemented before and is called Δ-Compensation uniform sampling [14]. Rather than the leading-edge modulation we have used above, Δ-compensation uniform sampling is defined for trailing-edge modulation, and so some manipulation is required to establish that the schemes are equivalent.

The trailing-edge switching times are derived in [14] using similar triangles and approximating one of the lengths involved. For a signal $S(t)$ the trailing-edge switching times are defined by

$$\alpha_n = S(n) + \frac{1}{2}[S(n+1) + S(n)][S(n+1) - S(n)], \tag{2.4.5}$$

from equation (3) of [14]. The period T is taken to be 1 and both the signal and the carrier wave have been scaled to vary only between 0 and 1. In the averaged two-sample three-term Taylor series scheme above, the dimensionless signal and carrier wave vary between -1 and $+1$. Thus we substitute $S = \frac{1}{2}(1 + s)$ into (2.4.5) to obtain

$$\alpha_n = \frac{1}{2}\left[1 + \frac{s(n+1) + s(n)}{2} + \frac{s(n) + s(n+1)}{2}\frac{s(n+1) - s(n)}{2}\right]. \tag{2.4.6}$$

To show that these trailing-edge switching times are equivalent to the leading-edge switching times (2.4.3) for the averaged two-sample three-term Taylor series scheme, we first consider how leading-edge and trailing-edge modulation are related.

The switching times for leading-edge modulation are determined by the intersection of the input signal $s(t)$ with minus the carrier wave, $-v(t)$, defined by (2.3.6). The switching times for trailing-edge modulation are determined by the intersection of $s(t)$
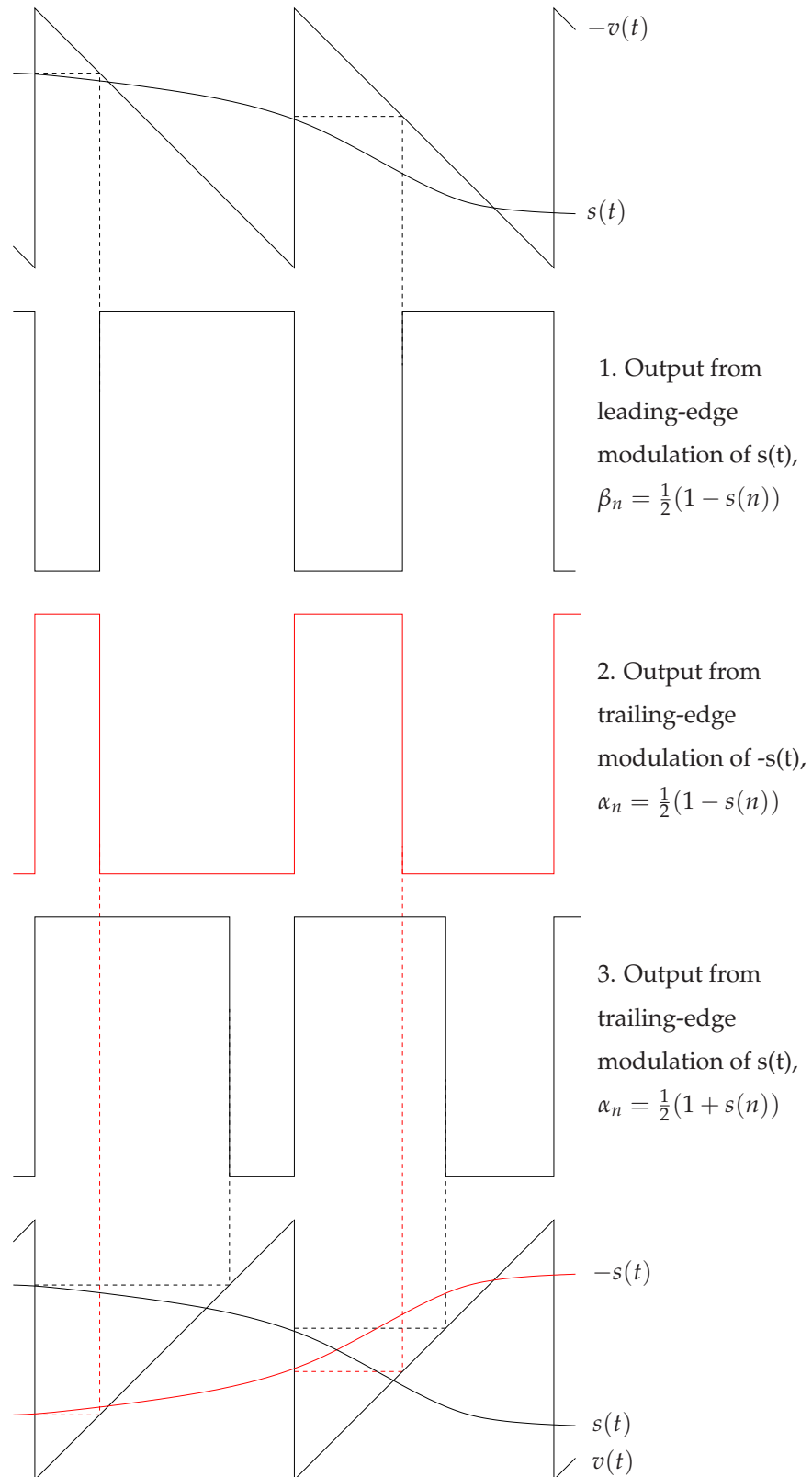
Figure 2.13: Diagram showing how trailing-edge modulation is related to leading-edge modulation for regular sampling.

with the carrier wave, $v(t)$. The outputs resulting from these two modulation processes are depicted in figure 2.13 by outputs 1 and 3, and the corresponding switching times are also given. Output 2 in figure 2.13 illustrates the output resulting from trailing-edge modulation of $-s(t)$, i.e. a modulation scheme where the switching times are determined by the intersection of $-s(t)$ with $v(t)$. It is clear that output 2 is exactly minus output 1. Therefore, to find leading-edge switching times equivalent to trailing-edge switching times, we must merely replace $s(t)$ by $-s(t)$. Note that we have used regular sampling in figure 2.13 as a simple example, but this rule is true for any sampling scheme.

To find the leading-edge switching times equivalent to (2.4.6) we must therefore replace $s(t)$ in (2.4.6) by $-s(t)$. Doing so we obtain (2.4.3), the switching times for the averaged two-sample three-term Taylor series scheme. Hence it is clear that Δ-compensation uniform sampling is equivalent to the averaged two-sample three-term Taylor series scheme investigated above.

From a simulation of a class-D amplifier implementing these switching times, the authors of [14] note that the sampling scheme produces low distortion, low enough to be used in a digital hearing aid. However, the authors do not calculate the output analytically, as we have here. Our calculation reveals it is the reduction in amplitude of the second harmonic that provides such improved distortion performance compared with regular sampling.

2.4.1.4 Discussion

We have discussed and compared three sampling schemes, the last of which was equivalent to Δ-compensation uniform sampling. Our aim was to find a scheme with less distortion than regular sampling, but that still could be easily implemented digitally.

The output created by the averaged two-sample scheme is almost identical to the regular sampling output, and so is not an improvement. However, the symmetry introduced to this scheme by using samples of the input signal at the beginning and end of the carrier wave period, instead of just one sample at the beginning of the period, results in an odd/even pattern in the series expansions for the harmonics, which we made use of later. The output produced by the two-sample three-term Taylor series scheme is similar to that for regular sampling, except that the amplitude of the second harmonic is one order of magnitude smaller than that for regular sampling, and as such is an improvement on regular sampling. To create the switching times for the third scheme, the averaged two-sample three-term Taylor series scheme, we further

symmetrised the switching times for the two-sample three-term Taylor series scheme. We found that this scheme is an improvement on both regular sampling and the two-sample three-term Taylor series scheme, since the amplitude of the second harmonic is reduced by another order of magnitude, so two orders of magnitude smaller than that for regular sampling.

We demonstrated in §2.4.1.3 that the averaged two-sample three-term Taylor series scheme is equivalent to the Δ-compensation uniform sampling scheme [14]. The advantages of our analysis are that we calculated the output analytically, via the Fourier transform/Poisson resummation method, and also that we derived the switching times more systematically. From our analysis of the harmonics, we saw that while the amplitude of the second harmonic is reduced considerably, the other harmonics remain of the same order. It would be desirable to obtain a scheme that reduces the amplitude of the second harmonic further, as well as to reduce the amplitudes of the next harmonics, thus reducing the distortion heard in the final amplifier output.

One possible improvement to the averaged two-sample three-term Taylor series scheme, which we can see from our derivation of the switching times, is to create a scheme by incorporating an additional term in the Taylor series. However, as we use only two samples of the input signal per carrier wave period, only limited improvement upon the schemes we have considered so far is possible. Another possibility for improvement is to convert the averaged two-sample three-term Taylor series scheme, which is defined for leading-edge modulation, to an asymmetric double-edged modulation scheme. Regular asymmetric double-edged modulation results in an output with fewer harmonics (and of lower amplitude) than regular single-edged modulation [4, 16], and it therefore seems possible that applying the same adaptation to the averaged two-sample three-term Taylor series scheme would result in reduced distortion.

Note that the switching times we defined for the three schemes above all use samples of the input signal at the beginning and end of the carrier wave period to determine the switching time during that carrier wave period, i.e. $s(n)$ and $s(n + 1)$ are used to determine the switching time $t = n + \beta_n$, which is between $t = n$ and $t = n + 1$. This would involve the future knowledge of $s(n + 1)$ and so is obviously not possible practically. In practice, samples from the previous period would be used to determine the switching time in any given period, i.e. $s(n - 1)$ and $s(n)$ would be used to determine β_n. This would introduce a delay of one carrier wave period into the output, but because the carrier wave period is so short (typically approximately 10 microseconds) it would not be detected by the human ear. We have not included this effect in our model so that it can be seen more easily that the averaged two-sample three-term Taylor series

scheme is equivalent to the Δ-compensation uniform sampling scheme.

We used the Fourier transform/Poisson resummation method here to examine the outputs from the three sampling schemes. The switching times of these schemes have increasing complexity, and so to analyse the outputs via the double Fourier series method would require increasingly lengthy calculations, whereas using the Fourier transform/Poisson resummation method the analysis is relatively simple.

Although we focus on class-D amplifiers in this thesis, it should be noted that the benefits of the Fourier transform/Poisson resummation method also can be realised in the analysis of other applications of PWM. For example, PWM technology is used in electronic circuits called inverters, which convert direct current to alternating current. Inverters have many applications. These include uninterruptible power supplies, which provide stored electrical power when mains power is unavailable. In this case, the inverter is used to provide AC power from the batteries. Another application is in battery electric vehicles and hybrid electric vehicles such as the Toyota Prius, where the inverter is used to power the traction motor. The double Fourier series method is traditionally used to investigate inverters (see for example [20], [27]) but more recently the Fourier transform/Poisson resummation method discussed here has been applied successfully [28].

One type of modulation used in inverters is hysteresis modulation [29–34], which is different to the sampling-based PWM we have investigated here. As we have seen, when sampling-based PWM is used, an input signal is compared with a carrier wave of fixed period to produce a pulse width modulated square wave output. In contrast, when hysteresis modulation is implemented, a carrier wave is not used, and so not only does the duty cycle of the square wave output vary with the input signal, but also the period of the output varies according to the input signal.

We have used the Fourier transform/Poisson resummation method to investigate hysteresis modulation. In our analysis we obtained recurrence relations for the switching times of the output. These are nonlinear, and they cannot be solved exactly analytically. By constructing a linear approximation to the switching period we were able to analytically solve the recurrence relations approximately, and so calculate the output analytically via the Fourier transform/Poisson resummation method. Finally we compared our results with those obtained by solving the exact equations numerically, and found that there was good agreement. We found that our results agree with those of Bowes, Grewel and Holliday [35], who constructed a linear approximation making the same assumptions that we did, though using the Fourier transform/Poisson resummation method here made the analysis much simpler, and again shows the adaptability of

the method.

2.5 Conclusions

We have considered in detail the PWM process and investigated the methods by which pulse width modulated square waves can be analysed.

In §2.3 we discussed in detail two different approaches to analysing the pulse width modulated output created by a classical class-D amplifier. The double Fourier series method, which is the conventional technique, was shown to be unnecessarily complex. We demonstrated that the Fourier transform/Poisson resummation method is simpler and quicker to implement, as well as being easier to adapt to different sampling schemes, which we illustrated further in §2.4.

In our analysis of the classical class-D amplifier, we determined that, if natural sampling is used, the low-frequency part of the output is exactly the input signal. However, the classical design is susceptible to noise, and negative feedback is often included in the circuit to counter this problem. We devote the rest of the thesis to the investigation of negative feedback designs, and incorporate the Fourier transform/Poisson resummation method into the later part of the analysis of each model.

First-order negative feedback amplifier

3.1 Introduction

IT is possible for a classical class-D amplifier to reproduce the input signal exactly in the low-frequency components of the output with no distortion, as was shown in §2.3. However, the analysis does not take into account non-ideal components, or that the carrier wave may not be exactly a triangular or sawtooth wave. When a classical class-D amplifier is used in practice, these factors result in noise in the output, in addition to the reproduced input signal. To rectify this problem, negative feedback is often implemented.

Negative feedback allows the output to be fed back into the input of the circuit. The components of the circuit then work to change the output to ensure that the difference between the two input voltages is as close to zero as possible. This creates an amplifier that is self-correcting, meaning that the final output is closer to the input signal, and thus negative feedback reduces noise in the output.

The idea of introducing negative feedback to an amplifier to decrease noise was put forward by Black [36], and negative feedback is now commonly used in class-D amplifiers. Although negative feedback reduces the output noise, it unfortunately also introduces distortion into the output, and so more recently research has investigated modifying negative feedback amplifiers to reduce this inherent distortion.

Most research into negative feedback class-D amplifiers focuses on experiment and simulation, and while it has been shown that the introduction of negative feedback reduces the output noise that is present in a classical class-D amplifier (see, for example [37]), these methods do not provide much insight into how the inherent distortion is

created, or how it could be reduced. Modelling the design analytically is therefore desirable, though not straightforward, because the equations governing the design are nonlinear and cannot be solved exactly analytically. However, Cox and Candy [7] presented an analytical method for modelling the design, and by implementing the method were able to propose a new design with negative feedback that reduces the inherent distortion.

Here we implement a more formalised version of the analysis used in [7] to model a first-order negative feedback class-D amplifier. We thereby significantly extend the results of [7], in particular providing expressions for additional components of the distortion beyond those reported in [7]. As discussed in chapter 1, the input signal is amplified before being input to a class-D amplifier. Therefore we are considering the output stage only, where the input is converted to a pulse-width modulated square wave, and so the aim here is to reproduce the input signal as accurately as possible. As in the analysis of a classical class-D amplifier, once we have found the switching times of the square wave output, we use the Fourier transform/Poisson resummation method to calculate the leading audio-frequency components of the output. However, in contrast to the classical design, the switching times of the square wave output for a negative feedback amplifier are not easily obtained, and so more work is required in this step.

We first model the amplifier design in dimensional terms in §3.2, and then nondimensionalise in §3.3 to simplify the model. Before analysing the dimensionless model for a general (time-varying) input signal, we consider a constant input signal in §3.4. This is useful because the audio input signal varies slowly compared with the carrier wave frequency, and so the results for a constant input signal will give us the limiting case for a general input signal. We therefore use results from the constant signal analysis to make important decisions in the general signal analysis, and to check the results for a general signal later. In §3.5 we investigate the design for a general input signal. We are able to obtain a system of nonlinear difference equations for the switching times, which is composed of considerably fewer equations than that in [7]. We then use perturbation expansions to solve the system, thus finding the switching times. Finally, we implement the Fourier transform/Poisson resummation method to determine the amplifier output for a general input signal, and see that our improved formulation of the system of difference equations enables us to find additional components of the distortion compared with [7]. We verify that our analytical solutions agree with numerical simulations of the problem, for both a constant input, in §3.4.2, and a general input, in §3.5.2. Concluding remarks are in §3.6.
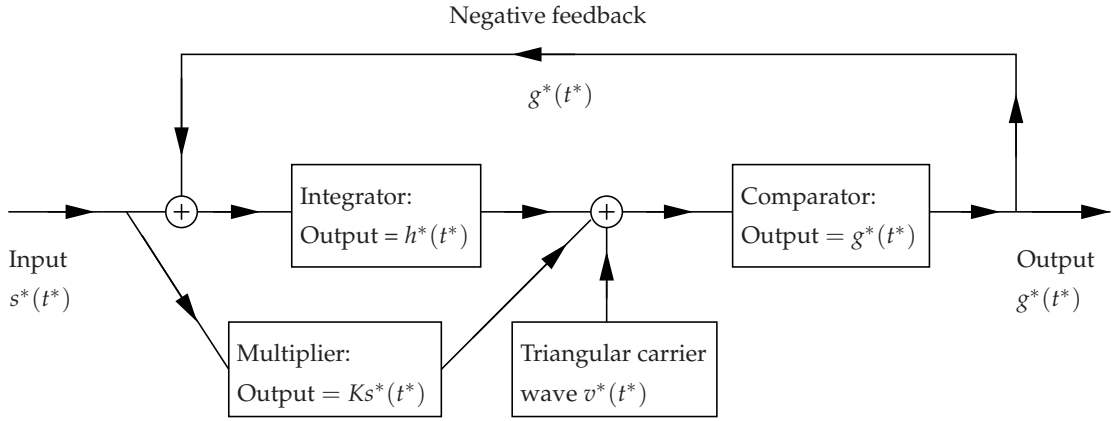
Figure 3.1: Schematic diagram representing the design of a first-order negative feedback class-D amplifier.

3.2 Dimensional model for the amplifier design

The first-order negative feedback amplifier design is represented by the diagram in figure 3.1. Here we discuss how this type of class-D amplifier operates, and present the dimensional equations that govern it. We use the superscript $*$ to denote dimensional variables.

The input signal is $s^*(t^*)$ and the output is $g^*(t^*)$, a pulse width modulated square wave. The input signal is first fed into an integrator that has output $h^*(t^*)$, defined by

$$\frac{d}{dt^*}h^*(t^*) = -c_1\left[g^*(t^*) + s^*(t^*)\right],$$ (3.2.1)

where

$$[h^*(t^*)] = \text{volts},$$
$$[g^*(t^*)] = \text{volts},$$
$$[s^*(t^*)] = \text{volts}.$$

The integrator circuit contains a resistor and a capacitor, and it is the reciprocal of the product of the resistance and the capacitance that determines the constant c_1. The product "resistance x capacitance" has units of time, and thus c_1 is a positive constant with dimension $1/\text{time}$. We will need to integrate the above equation to find $h^*(t^*)$ later on, and so we define $r^*(t^*)$ to be the integral of $s^*(t^*)$,

$$\frac{d}{dt^*}r^*(t^*) = s^*(t^*),$$ (3.2.2)

and thus

$$[r^*(t^*)] = \text{volts x time}.$$

Therefore (3.2.1) becomes

$$\frac{d}{dt^*}h^*(t^*) = -c_1 \left[g^*(t^*) + \frac{d}{dt^*}r^*(t^*) \right].$$

(3.2.3)

The input signal is also fed into a multiplier, whose output is $Ks^*(t^*)$, where K is an $O(1)$ dimensionless positive constant we are free to choose. By choosing the value of K appropriately later, we will be able to eliminate some of the inherent distortion of the amplifier.

The integrator output $h^*(t^*)$, multiplier output $Ks^*(t^*)$, and a periodic triangular carrier wave $v^*(t^*)$ are added together and fed into a comparator. The carrier wave is given by

$$v^*(t^*) = \begin{cases} \left(1 - \frac{4}{T}(t^* - nT)\right)V & \text{for } nT \le t^* < \left(n + \frac{1}{2}\right)T \\ \left(-3 + \frac{4}{T}(t^* - nT)\right)V & \text{for } \left(n + \frac{1}{2}\right)T \le t^* < (n+1)T, \end{cases}$$

(3.2.4)

where V is a constant with dimension volts. The carrier wave thus has period T, (angular) frequency $\omega_c = \frac{2\pi}{T}$, and dimension given by

$$[v^*(t^*)] = \text{volts}.$$

The output from the comparator is the pulse width modulated square wave $g^*(t^*)$, which is defined by

$$g^*(t^*) = \begin{cases} -V & \text{for } h^*(t^*) + Ks^*(t^*) + v^*(t^*) < 0 \\ +V & \text{for } h^*(t^*) + Ks^*(t^*) + v^*(t^*) > 0, \end{cases}$$

(3.2.5)

and $s^*(t^*)$ is constrained by

$$|s^*(t^*)| < V.$$

We define two regions within each carrier wave period, according to the sign of $g^*(t^*)$, as depicted in figure 3.2. In region I, the comparator output $g^*(t^*)$ is $-V$, and in region II, $g^*(t^*) = +V$. Therefore these regions are bounded by the switching times of the comparator output: at the times $t^* = nT + \alpha_n^*$, the comparator output switches from $+V$ to $-V$; at the times $t^* = nT + \beta_n^*$, the comparator output switches from $-V$ to $+V$. Thus

$$g^*(t^*) = \begin{cases} -V & \text{for } nT + \alpha_n^* < t^* < nT + \beta_n^* \\ +V & \text{for } nT + \beta_n^* < t^* < (n+1)T + \alpha_{n+1}^*. \end{cases}$$

(3.2.6)

Note that as in chapter 2, we have presented two expressions for $g^*(t^*)$: (3.2.5) gives the conditions for $g^*(t^*)$ to switch in terms of $h^*(t^*)$, $s^*(t^*)$ and $v^*(t^*)$, while (3.2.6) then defines the switching times α_n^* and β_n^*.

56
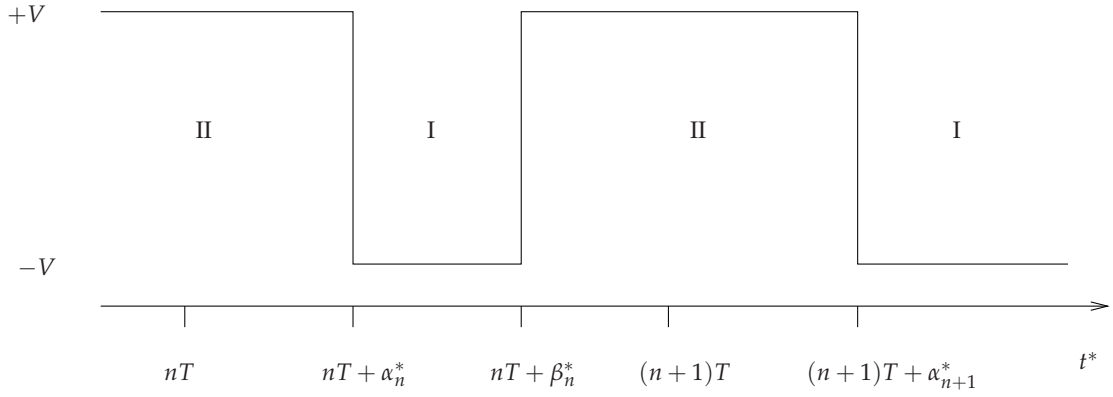
Figure 3.2: The dimensional square wave $g^*(t^*)$ showing the regions I and II.

We observe that the corresponding analysis in [7] involves three regions within each carrier wave period, $nT < t^* < nT + \alpha_n^*$, $nT + \alpha_n^* < t^* < nT + \beta_n^*$ and $nT + \beta_n^* < t^* < (n+1)T$. This results in an unnecessarily unwieldy formulation of the governing equations for the design, whereas here the governing equations are much simpler.

We assume that $h^*(t^*) + Ks^*(t^*) = -v^*(t^*)$ at two instants t^* in each carrier wave period, once at $t^* = nT + \alpha_n^*$ and once at $t^* = nT + \beta_n^*$. Hence

$$0 < \alpha_n^* < \frac{T}{2},$$
$$\frac{T}{2} < \beta_n^* < T.$$

This results in double-edge asymmetric modulation, as introduced in §2.2.

The square wave $g^*(t^*)$ is fed back into the integrator, as shown in (3.2.3), and it is this feature that provides the negative feedback in the amplifier.

Equations (3.2.3)-(3.2.6) constitute the dimensional model for the amplifier. We now nondimensionalise to simplify the model.

3.3 Nondimensionalisation

We now nondimensionalise the model, and use unstarred symbols to denote the dimensionless equivalents of the starred dimensional variables.

We scale dimensional times with the period of the carrier wave, and thus define the dimensionless time

$$t = \frac{t^*}{T},$$

and dimensionless switching times

$$\alpha_n = \frac{\alpha_n^*}{T},$$
$$\beta_n = \frac{\beta_n^*}{T}.$$

We scale voltages with V, and thus define the dimensionless input signal, integrator output, carrier wave and comparator output as respectively

$$s(t) = \frac{s^*(t^*)}{V},$$
$$h(t) = \frac{h^*(t^*)}{V},$$
$$v(t) = \frac{v^*(t^*)}{V},$$
$$g(t) = \frac{g^*(t^*)}{V}.$$

By considering our definitions of $s(t)$ and dimensionless time, and the definition (3.2.2) of $r^*(t^*)$ we define

$$r(t) = \frac{r^*(t^*)}{TV},$$

which ensures that

$$\frac{d}{dt}r(t) = s(t). \tag{3.3.1}$$

Noting that the positive constant c_1 has dimension $1/\text{time}$, we define the dimensionless $O(1)$ parameter

$$k_1 = c_1 T > 0.$$

We now nondimensionalise the equations governing the model using the above definitions of the dimensionless variables and parameters. Thus equations (3.2.3)-(3.2.6) defining the integrator output, carrier wave, comparator output and switching times become

$$\frac{d}{dt}h(t) = -k_1 \left[g(t) + \frac{d}{dt}r(t) \right], \tag{3.3.2}$$

$$v(t) = \begin{cases} 1 - 4(t-n) & \text{for } n \leq t < n + \frac{1}{2} \\ -3 + 4(t-n) & \text{for } n + \frac{1}{2} \leq t < n+1, \end{cases} \tag{3.3.3}$$

$$g(t) = \begin{cases} -1 & \text{for } h(t) + Ks(t) + v(t) < 0 \\ +1 & \text{for } h(t) + Ks(t) + v(t) > 0, \end{cases} \tag{3.3.4}$$

$$g(t) = \begin{cases} -1 & \text{for } n + \alpha_n < t < n + \beta_n \\ +1 & \text{for } n + \beta_n < t < n+1+\alpha_{n+1}. \end{cases} \tag{3.3.5}$$
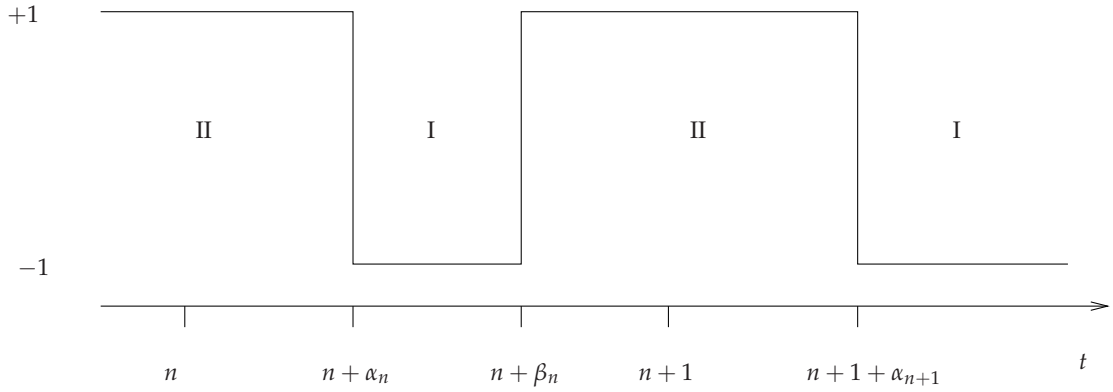
Figure 3.3: The dimensionless square wave $g(t)$ showing the regions I and II.

Figure 3.3 is the dimensionless equivalent of figure 3.2, depicting the dimensionless comparator output $g(t)$, and the dimensionless switching times bounding regions I and II.

We also nondimensionalise the restriction on the input signal, obtaining

$$|s(t)| < 1, \tag{3.3.6}$$

and the constraints on the switching times, giving

$$0 < \alpha_n < \frac{1}{2}, \tag{3.3.7}$$

$$\frac{1}{2} < \beta_n < 1. \tag{3.3.8}$$

We now proceed to solve the dimensionless model for a constant input signal, in §3.4, and then for a general input signal, in §3.5. The input signal varies slowly compared with the carrier wave frequency, and so the constant input signal analysis is valuable because it provides the limiting case for a general input signal.

3.4 Dimensionless model for a constant input signal

We now consider the dimensionless equations governing the amplifier, (3.3.2)-(3.3.5), for a constant input signal. We let $s(t) = s_0$, where $-1 < s_0 < 1$ is a constant, and thus from (3.3.1), $r(t) = s_0 t$. By analysing the model for a constant input, before investigating the model for a general input in §3.5, we hope to understand how the amplifier behaves for a constant input. In addition, this will provide us with an important insight into how to tackle the general input problem, because a constant input signal is the limiting case of a slowly-varying input signal.

We first calculate the integrator output, $h(t)$, by integrating (3.3.2) separately over the regions I and II defined in figure 3.3,

$$h(t) - h(t_0) = \begin{cases} k_1(1 - s_0)(t - t_0) & \text{in region I} \\ -k_1(1 + s_0)(t - t_0) & \text{in region II}, \end{cases} \tag{3.4.1}$$

where t_0 is the time at the beginning of the region ($t_0 = n + \alpha_n$ and $t_0 = n + \beta_n$ respectively). Therefore in region I, for $n + \alpha_n < t < n + \beta_n$, we obtain

$$h(t) = h(n + \alpha_n) + k_1(1 - s_0)(t - n - \alpha_n), \tag{3.4.2}$$

and because $h(t)$ is continuous, we can find $h(t)$ at the end of this particular region from (3.4.2),

$$h(n + \beta_n) = h(n + \alpha_n) + k_1(1 - s_0)(\beta_n - \alpha_n). \tag{3.4.3}$$

Similarly, from (3.4.1), in region II, for $n + \beta_n < t < n + 1 + \alpha_{n+1}$ we obtain

$$h(t) = h(n + \beta_n) - k_1(1 + s_0)(t - n - \beta_n). \tag{3.4.4}$$

Since $h(t)$ is continuous, we can now find $h(t)$ at the end of this particular region using (3.4.4),

$$h(n + 1 + \alpha_{n+1}) = h(n + \beta_n) - k_1(1 + s_0)(1 + \alpha_{n+1} - \beta_n). \tag{3.4.5}$$

Recall that the configuration of regions we use here, in comparison to the three regions used in [7], is much simpler. The above equations for the integrator output $h(t)$ are therefore considerably algebraically simpler than those in [7].

We now turn our attention to the switching times. These are defined to be the times at which $h(t) + Ks(t) + v(t) = 0$, from (3.3.4). By considering the restrictions imposed upon α_n and β_n, (3.3.7) and (3.3.8), we find $v(n + \alpha_n)$ and $v(n + \beta_n)$ from (3.3.3). Hence the switching times are defined by

$$h(n + \alpha_n) + Ks_0 + 1 - 4\alpha_n = 0, \tag{3.4.6}$$

$$h(n + \beta_n) + Ks_0 - 3 + 4\beta_n = 0. \tag{3.4.7}$$

The four exact equations (3.4.3), (3.4.5)-(3.4.7) constitute the model for the amplifier when a constant signal is input. If we know α_n we can iterate these exact equations (using also (3.4.6) for α_{n+1}) to obtain $h(n + \alpha_n)$, β_n, $h(n + \beta_n)$, and thus α_{n+1} and $h(n + 1 + \alpha_{n+1})$. Therefore if we know the initial conditions of the amplifier (those when the amplifier is first switched on), we can determine exactly the switching times and thus the output $g(t)$, because the switching times define $g(t)$. However, we would need to

iterate numerically for particular parameter values to proceed in this way, and would learn little about the amplifier behaviour. Instead therefore, we assume that after a transient state, the system reaches a stable steady state. We find these steady-state solutions analytically in §3.4.1. In §3.4.2 we verify the analytical steady-state solutions by iterating the exact equations numerically.

3.4.1 Exact steady-state solution for a constant input signal

We here look for steady-state solutions to the exact equations (3.4.3), (3.4.5)-(3.4.7), which govern the model for a constant input signal.

We therefore set

$$\alpha_{n+1} = \alpha_n,$$
$$h(n+1+\alpha_{n+1}) = h(n+\alpha_n),$$

in (3.4.3), (3.4.5)-(3.4.7), and find that the only change is to (3.4.5), which becomes

$$h(n+\alpha_n) = h(n+\beta_n) - k_1(1+s_0)(1+\alpha_n-\beta_n). \tag{3.4.8}$$

The exact steady-state equations are therefore (3.4.3), (3.4.6), (3.4.7) and (3.4.8).

Note that by manipulating (3.4.3) and (3.4.8) we find

$$\beta_n - \alpha_n = \frac{1}{2}(1+s_0). \tag{3.4.9}$$

From this equation for the difference between the switching times we see that the restriction $|s_0| < 1$ means that

$$0 < \beta_n - \alpha_n < 1,$$

ensuring that the amplifier will operate correctly, with $g(t)$ switching from $+1$ to -1 and back to $+1$ within one carrier wave period. From (3.4.9) we also see that in each carrier wave period, the square wave output $g(t)$ is $+1$ for the duration $1 - (\beta_n - \alpha_n) = \frac{1}{2}(1-s_0)$, and -1 for the remaining duration, $\beta_n - \alpha_n = \frac{1}{2}(1+s_0)$. The short-time average of $g(t)$ (defined by (2.3.10)) is therefore given by

$$\langle g(t) \rangle = -s_0. \tag{3.4.10}$$

Because the input signal $s(t)$ is s_0 we should expect this. The minus sign arises because the carrier wave is added to the noninverting input of the comparator, rather than the inverting input. If it is added to the inverting input instead (so that $g(t)$ switches at times $h(t) + Ks(t) - v(t) = 0$ rather than $h(t) + Ks(t) + v(t) = 0$) the short-time

average of $g(t)$ would be simply s_0. However, the minus sign is not perceived by the user of the amplifier, and so this change is not necessary.

We now solve the exact steady-state equations and find the steady-state solutions to be

$$\alpha_n = \frac{1}{16}(1-s_0)[4-k_1(1+s_0)], \tag{3.4.11}$$

$$\beta_n = \frac{1}{2} + \frac{1}{16}(1+s_0)[4-k_1(1-s_0)], \tag{3.4.12}$$

$$h(n+\alpha_n) = -s_0(1+K) + \frac{k_1}{4}\left(s_0^2-1\right), \tag{3.4.13}$$

$$h(n+\beta_n) = -s_0(1+K) - \frac{k_1}{4}\left(s_0^2-1\right). \tag{3.4.14}$$

Comparing the solutions for the switching times with the leading-order switching times for a general input signal, calculated in [7] for the same first-order negative feedback amplifier design as here, we see that they agree. We therefore see that it is possible to determine the leading-order switching times for a general input signal merely by computing the steady-state switching times for a constant input signal, which is a much shorter calculation.

By considering the restrictions on the input signal and switching times, (3.3.6)-(3.3.8) we can find a condition on k_1 for the amplifier to operate correctly, where we already know $k_1 > 0$. From the solution for α_n, (3.4.11), and the restrictions on α_n and s_0 we find $k_1 < \frac{4}{1+s_0}$. Correspondingly, from the solution for β_n, (3.4.12), and the restrictions on β_n and s_0 we find $k_1 < \frac{4}{1-s_0}$. Thus the appropriate range for k_1, as can be seen in figure 3.4, is

$$0 < k_1 < \frac{4}{1+|s_0|}.$$

To ensure this condition is valid for all $|s_0| < 1$, the parameter k_1 must satisfy

$$0 < k_1 < 2. \tag{3.4.15}$$

The steady-state solution for the integrator output $h(t)$ is given by (3.4.2) for $n + \alpha_n < t < n + \beta_n$ and (3.4.4) for $n + \beta_n < t < n + 1 + \alpha_{n+1}$, where the constants $h(n+\alpha_n)$ and $h(n+\beta_n)$ are given by (3.4.13) and (3.4.14). In the next section we plot $h(t)$, $Ks(t)$ and $v(t)$ to show how $h(t)$ behaves for different parameter values, and also to show how the switching times are determined by these three voltages.

3.4.1.1   Graphs of integrator output, multiplier output and carrier wave

Figure 3.5 plots the integrator output added to the multiplier output, $h(t) + Ks(t)$, and minus the carrier wave, $-v(t)$, over one carrier wave period, for a constant input signal.
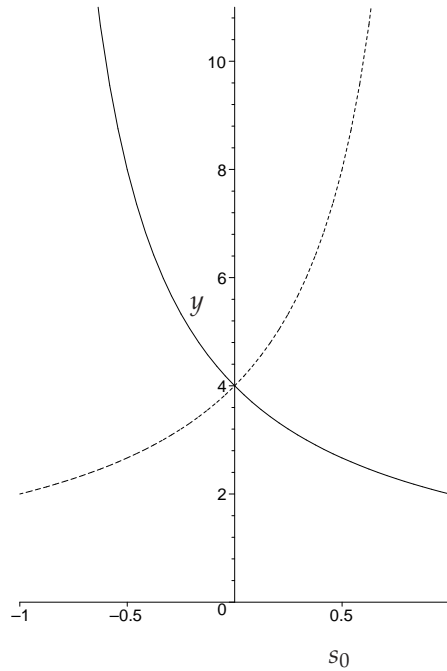
Figure 3.4: The upper limits on k_1: the solid and dotted lines are the curves $y = \frac{4}{1+s_0}$ and $y = \frac{4}{1-s_0}$ respectively, which are the upper limits on k_1 as determined by the restrictions on α_n and β_n respectively.

We choose the parameter values $k_1 = 0.5$ and $k_1 = 1.5$, which lie within the range given by (3.4.15), and $K = 1$ and $K = 2$ so that $K = O(1)$, though as we will discuss below, the value of K is unimportant for a constant input.

The switching times of $g(t)$ are defined to be the times at which $h(t) + Ks(t) + v(t) = 0$. Thus the intersections of $h(t) + Ks_0$ with $-v(t)$ in figure 3.5 are the switching times for a constant input signal. For $k_1 = 0.5$ in figure 3.5(a), $\alpha_n = \frac{145}{512}$ and $\beta_n = \frac{337}{512}$. For $k_1 = 1.5$ in figure 3.5(b), $\alpha_n = \frac{115}{512}$ and $\beta_n = \frac{307}{512}$. In both cases, it is clear that $\beta_n - \alpha_n = \frac{3}{8} = \frac{1}{2}\left(1 - \frac{1}{4}\right)$ as predicted by (3.4.9). The switching times are independent of K, as can be seen from the solutions (3.4.11) and (3.4.12).

For a constant input signal the integrator output $h(t)$, given by (3.4.2) and (3.4.4), is piecewise linear, with gradient determined by k_1. This can be observed by comparing the two graphs in figure 3.5. Note that the restriction on k_1, given by (3.4.15), ensures that the gradient of $h(t)$ is such that $h(t) + Ks_0$ intersects with $-v(t)$ twice in each carrier wave period, allowing correct operation of the amplifier. The dependence of $h(t)$ on the parameter K is only through the constants $h(n + \alpha_n)$ and $h(n + \beta_n)$, given by (3.4.13) and (3.4.14), where $-Ks_0$ appears in both solutions. Thus the only effect on $h(t)$ of changing K is to shift $h(t)$ up or down, and since we plot $h(t) + Ks_0$ in figure 3.5 this effect cannot be observed here. Because the switching times are independent of K as well, and the output $g(t)$ is dependent on only the switching times, the parameter

63
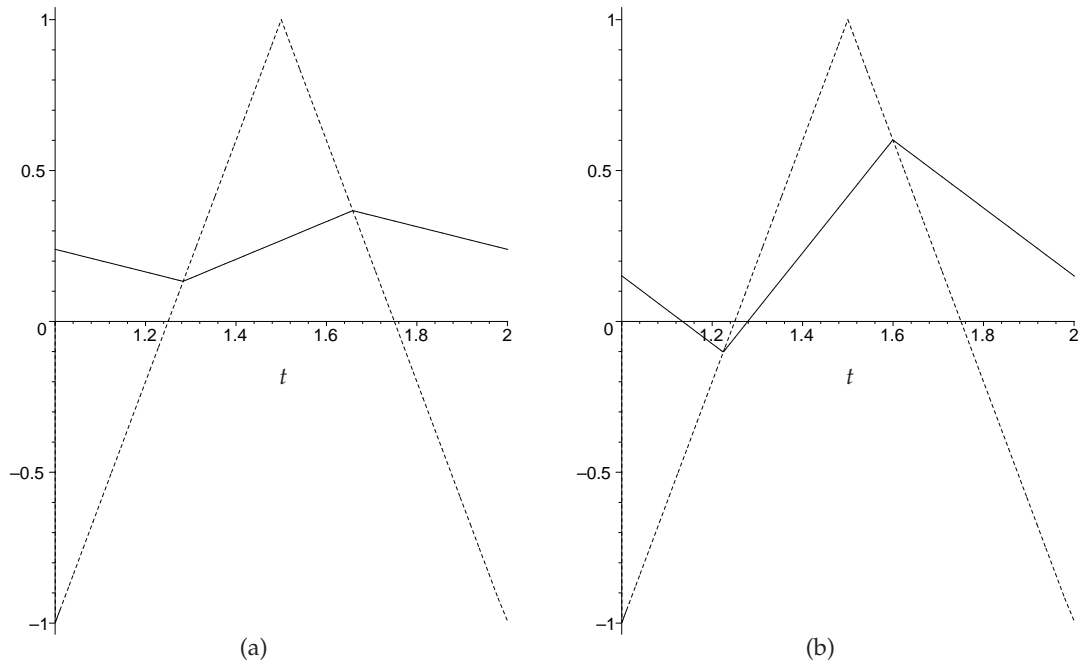
Figure 3.5: For a constant input signal, $s(t) = s_0$ where $s_0 = -0.25$: the integrator output added to the multiplier output, $h(t) + Ks_0$, (solid line) and minus the carrier wave, $-v(t)$, (dotted line) for (a) $k_1 = 0.5$, $K = 1$ and (b) $k_1 = 1.5$, $K = 2$.

K has no impact on the amplifier when a constant signal is input. The importance of the value of K (and therefore the importance of including a multiplier in the amplifier circuit) will be seen later when we consider a general input signal.

3.4.2 Numerical simulation of switching times

We have determined the steady-state solution to the four exact nonlinear difference equations (3.4.3), (3.4.5)-(3.4.7) governing the amplifier for a constant input signal. In order to confirm our results, we now numerically solve the four equations in Maple.

Because the initial conditions of the amplifier are unknown, we choose $\alpha_0 = 0$ arbitrarily, and then iterate the four equations numerically in Maple. We compare the numerical switching times with the analytical steady-state solutions for the switching times, (3.4.11) and (3.4.12). Using Maple we find that the numerical switching times converge to the steady-state solutions, after an initial transient state, which occurs because we choose the initial conditions of the amplifier arbitrarily. For example, for $s_0 = -0.25$, $k_1 = 0.5$ and $K = 1$, after approximately 100 carrier wave periods the numerical switching times converge to $\alpha_n = 0.283203125$ and $\beta_n = 0.658203125$, in agreement with our steady-state solutions. For a typical carrier wave frequency of between

80kHz and 250kHz, the transient state lasts for approximately only a millisecond, and so will not appreciably affect the amplifier output.

For the amplifier when a constant signal is input, we have analytically determined the steady-state solutions, and confirmed our results numerically via a simulation of the exact equations governing the amplifier. Noting that the steady-state solutions are the same as the leading-order solutions for a general input signal, as given in [7], we see that the route used here is much more succinct. We now proceed to model the amplifier when a general signal is input, making use of several of the results obtained for a constant input signal.

3.5 Dimensionless model for a general input signal

We now analyse the amplifier when a general signal is input. For a constant input signal we were able to simplify the governing equations because the system quickly moves into a steady state. This will obviously not be the case for a general input signal, so we need to use a different method to solve the equations, although the governing equations we will start from are the same, equations (3.3.2)-(3.3.5).

We first outline the method we use to establish the amplifier output, $g(t)$. We begin by solving the governing equation for $h(t)$, the integrator output, (3.3.2). Using the definition of the carrier wave, (3.3.3), and the switching times, (3.3.4), we then eliminate $h(t)$ to determine two exact nonlinear difference equations relating the switching times to the input, $s(t)$, and the integral of the input, $r(t)$, both evaluated at the switching times. Because the output $g(t)$ that we aim to calculate is defined in terms of the switching times, as given by (3.3.5), eliminating $h(t)$ greatly reduces the amount of algebraic manipulation required. We then use perturbation expansions to solve the two exact equations to find the switching times. Finally we implement the Fourier transform/Poisson resummation method to determine the leading audio-frequency components of the output from the amplifier.

Thus we start by solving the governing equation for the integrator output, $h(t)$. For a general input signal, integrating (3.3.2) over regions I and II (defined by figure 3.3) separately we obtain

$$h(t) - h(t_0) + k_1[r(t) - r(t_0)] = \begin{cases} k_1(t - t_0) & \text{in region I} \\ -k_1(t - t_0) & \text{in region II,} \end{cases} \tag{3.5.1}$$

where t_0 is the time at the beginning of each region. Thus in region I, for $n + \alpha_n < t <$

$n + \beta_n$, we find

$$h(t) - h(n + \alpha_n) + k_1[r(t) - r(n + \alpha_n)] = k_1(t - n - \alpha_n),$$

and because $h(t)$ is continuous we can evaluate this at $t = n + \beta_n$ to give

$$h(n + \beta_n) - h(n + \alpha_n) + k_1[r(n + \beta_n) - r(n + \alpha_n)] = k_1(\beta_n - \alpha_n). \qquad (3.5.2)$$

Similarly, in region II, for $n + \beta_n < t < n + 1 + \alpha_{n+1}$, from (3.5.1) we obtain

$$h(t) - h(n + \beta_n) - k_1[r(t) - r(n + \beta_n)] = -k_1(t - n - \beta_n),$$

and evaluating this at $t = n + 1 + \alpha_{n+1}$ we find

$$h(n + 1 + \alpha_{n+1}) - h(n + \beta_n) - k_1[r(n + 1 + \alpha_{n+1}) - r(n + \beta_n)] =$$
$$-k_1(1 + \alpha_{n+1} - \beta_n). \qquad (3.5.3)$$

In (3.5.2) and (3.5.3) we have two equations relating $h(t)$ and $r(t)$, both evaluated at the switching times, to the switching times themselves. We now use the definition of the switching times, (3.3.4), and the carrier wave, (3.3.3), to determine three equations relating $h(t)$ and $s(t)$, evaluated at the switching times, to the switching times themselves.

The switching times are defined to be the times at which $h(t) + Ks(t) + v(t) = 0$. From the restrictions on the switching times, (3.3.7) and (3.3.8), and the definition of the carrier wave $v(t)$, (3.3.3), we can determine $v(n + \alpha_n)$, $v(n + \beta_n)$ and $v(n + 1 + \alpha_{n+1})$. We are then able to establish three equations, defining each of the switching times α_n, β_n and α_{n+1},

$$\begin{aligned}
h(n + \alpha_n) + Ks(n + \alpha_n) + 1 - 4\alpha_n &= 0, \\
h(n + \beta_n) + Ks(n + \beta_n) - 3 + 4\beta_n &= 0, \\
h(n + 1 + \alpha_{n+1}) + Ks(n + 1 + \alpha_{n+1}) + 1 - 4\alpha_{n+1} &= 0.
\end{aligned}$$

Using these three equations to eliminate $h(t)$ from (3.5.2) and (3.5.3) we are thus left with two exact nonlinear difference equations relating the switching times to $s(t)$ and $r(t)$ at those switching times,

$$(4 - k_1)\alpha_n - 4 + (4 + k_1)\beta_n =$$
$$k_1[r(n + \beta_n) - r(n + \alpha_n)] - K[s(n + \beta_n) - s(n + \alpha_n)], \qquad (3.5.4)$$
$$(4 + k_1)\alpha_{n+1} - 4 + k_1 + (4 - k_1)\beta_n =$$
$$-k_1[r(n + 1 + \alpha_{n+1}) - r(n + \beta_n)] + K[s(n + 1 + \alpha_{n+1}) - s(n + \beta_n)]. \quad (3.5.5)$$

The two equations (3.5.4) and (3.5.5) are equivalent to equations (3.6), (3.9) and (3.11) in [7] for a first-order negative feedback amplifier. They appear superficially quite different, but this is only because the authors of [7] split the carrier wave period into three regions whereas we have used two regions for simplicity, and here we eliminate $h(t)$, further simplifying the model. Because our formulation is more concise, we are able to calculate additional information about the distortion in the output compared with [7].

If we know α_n we can use (3.5.4) to find β_n, and then (3.5.5) to obtain α_{n+1}. Thus, if we know the initial conditions of the amplifier we can solve these equations iteratively to find the switching times of the output. However, we would need to specify the input signal and values of the parameters to do this, and would learn about that one case only.

A more fruitful approach is to solve this system for a general input signal, and thus derive expressions for the distortion in the output for a general input signal. In order to achieve this we convert this discrete system into continuous one that we can then solve analytically.

3.5.1 Continuous model

We here translate the discrete system arrived at above into a continuous one, in order to determine the switching times of the amplifier output, which will then allow us to establish the output itself.

We are interested in the input signal $s(t)$ being slowly varying compared with the other voltages in the circuit, $g(t)$, $h(t)$ and $v(t)$, which vary on the timescale of the carrier wave. Thus we introduce

$$s(t) = S(\epsilon t),$$

where $\epsilon = \omega_a T$, where ω_a is a typical audio frequency, and we assume $\epsilon \ll 1$. We define a new dimensionless slow time, $\sigma = \epsilon t$ and thus

$$s(t) = S(\sigma).$$

We also define a new function $R(\sigma)$, which relates to $r(t)$ via

$$R(\sigma) = \epsilon r(t), \tag{3.5.6}$$

so that we have a simple relationship between $R(\sigma)$ and $S(\sigma)$,

$$\frac{d}{d\sigma} R(\sigma) = S(\sigma).$$

We now introduce two $O(1)$ functions $A(\sigma)$ and $B(\sigma)$. We define them by their values at discrete points,

$$A(\epsilon n) = \alpha_n, \tag{3.5.7}$$

$$B(\epsilon n) = \beta_n. \tag{3.5.8}$$

Note that with these definitions we can also write α_{n+1} in terms of the slowly-varying function A, thus

$$\alpha_{n+1} = A(\epsilon(n+1)).$$

To define fully the two functions $A(\sigma)$ and $B(\sigma)$ we then interpolate smoothly between these discrete points ensuring that each function is continuous and smooth. We then write the two nonlinear difference equations for the switching times, (3.5.4) and (3.5.5), in terms of the functions $A(\sigma)$ and $B(\sigma)$. Thus, in (3.5.4) and (3.5.5) we replace

$$\begin{aligned} \alpha_n &\quad \text{by} \quad A(\sigma), \\ \beta_n &\quad \text{by} \quad B(\sigma), \\ \alpha_{n+1} &\quad \text{by} \quad A(\sigma + \epsilon). \end{aligned}$$

Thus the new functions $A(\sigma)$ and $B(\sigma)$ at times $t = n$, i.e. $\sigma = \epsilon n$, take the values of α_n and β_n respectively, and both functions are slowly-varying with respect to time t.

There are two important points to note in the definitions of $A(\sigma)$ and $B(\sigma)$. The first is that we have made a choice in the time at which to assign the sampled values of α_n and β_n to the functions $A(\sigma)$ and $B(\sigma)$ in (3.5.7) and (3.5.8). For example, we could have chosen $A(\epsilon(n + \alpha_n)) = \alpha_n$, or in fact any other times for $A(\sigma)$ and α_n to coincide. However, choosing $A(\epsilon n) = \alpha_n$ simplifies the algebra later on without affecting the solution.

The second point to note is the orders of magnitude of α_n and β_n. Consideration of the steady-state solutions for the switching times when a constant signal is input, (3.4.11) and (3.4.12), suggests that α_n and β_n are $O(1)$. Therefore we choose both switching times to be $O(1)$, as defined by (3.5.7) and (3.5.8), and find the resulting equations are consistent.

Using the above definitions of $A(\sigma)$ and $B(\sigma)$, (3.5.7) and (3.5.8), and our definition (3.5.6) of $R(\sigma)$ we write $r(t)$ at the switching times in terms of R, σ, A and B. For example,

$$r(n + \alpha_n) = r(n + A(\epsilon n)),$$

which we replace by $r(t + A(\epsilon t))$ in our continuous model. Then

$$
\begin{aligned}
r(t + A(\epsilon t)) &= \frac{1}{\epsilon}R(\epsilon t + \epsilon A(\epsilon t)) \\
&= \frac{1}{\epsilon}R(\sigma + \epsilon A(\sigma)).
\end{aligned}
$$

We now write the nonlinear difference equations (3.5.4) and (3.5.5) in terms of our new functions. These become

$$
\begin{aligned}
(4 - k_1)A(\sigma) - 4 + &(4 + k_1)B(\sigma) = \\
&+ k_1 \left[\frac{R(\sigma + \epsilon B(\sigma)) - R(\sigma + \epsilon A(\sigma))}{\epsilon} \right] \\
&- K \left[S(\sigma + \epsilon B(\sigma)) - S(\sigma + \epsilon A(\sigma)) \right],
\end{aligned}
\tag{3.5.9}
$$

$$
\begin{aligned}
(4 + k_1)A(\sigma + \epsilon) - 4 + &k_1 + (4 - k_1)B(\sigma) = \\
&- k_1 \left[\frac{R(\sigma + \epsilon(1 + A(\sigma + \epsilon))) - R(\sigma + \epsilon B(\sigma))}{\epsilon} \right] \\
&+ K \left[S(\sigma + \epsilon(1 + A(\sigma + \epsilon))) - S(\sigma + \epsilon B(\sigma)) \right].
\end{aligned}
\tag{3.5.10}
$$

It is clear that these equations are too complicated to be solved exactly, so in order to find a perturbation solution to these equations we expand $A(\sigma)$ and $B(\sigma)$ as series in ϵ, where

$$
\begin{aligned}
A(\sigma) &= \sum_{m=0}^{\infty} \epsilon^m A_m(\sigma), \\
B(\sigma) &= \sum_{m=0}^{\infty} \epsilon^m B_m(\sigma),
\end{aligned}
$$

and solve the resulting equations at successive orders in ϵ. Note that to do this we must expand the remaining functions in (3.5.9) and (3.5.10) as Taylor series in ϵ. For

example,

$$
\begin{aligned}
S(\sigma + \epsilon A(\sigma)) &= S(\sigma) + \epsilon A(\sigma)\frac{d}{d\sigma}S(\sigma) + \frac{\epsilon^2}{2}A(\sigma)^2\frac{d^2}{d\sigma^2}S(\sigma) + O(\epsilon^3) \\
&= S(\sigma) + \epsilon A_0(\sigma)\frac{d}{d\sigma}S(\sigma) \\
&\quad + \epsilon^2\left(A_1(\sigma)\frac{d}{d\sigma}S(\sigma) + \frac{1}{2}A_0(\sigma)^2\frac{d^2}{d\sigma^2}S(\sigma)\right) + O(\epsilon^3), \\
R(\sigma + \epsilon A(\sigma)) &= R(\sigma) + \epsilon A(\sigma)\frac{d}{d\sigma}R(\sigma) + \frac{\epsilon^2}{2}A(\sigma)^2\frac{d^2}{d\sigma^2}R(\sigma) + O(\epsilon^3) \\
&= R(\sigma) + \epsilon A_0(\sigma)S(\sigma) \\
&\quad + \epsilon^2\left(A_1(\sigma)S(\sigma) + \frac{1}{2}A_0(\sigma)^2\frac{d}{d\sigma}S(\sigma)\right) + O(\epsilon^3), \\
R(\sigma + \epsilon(1 + A(\sigma + \epsilon))) &= R(\sigma) + \epsilon(1 + A(\sigma + \epsilon))\frac{d}{d\sigma}R(\sigma) \\
&\quad + \frac{\epsilon^2}{2}(1 + A(\sigma + \epsilon))^2\frac{d^2}{d\sigma^2}R(\sigma) + O(\epsilon^3) \\
&= R(\sigma) + \epsilon(1 + A_0(\sigma))S(\sigma) \\
&\quad + \epsilon^2\left(A_1(\sigma)S(\sigma) + \frac{d}{d\sigma}A_0(\sigma)S(\sigma) + \frac{1}{2}\frac{d}{d\sigma}S(\sigma)\right. \\
&\quad \left. + A_0(\sigma)\frac{d}{d\sigma}S(\sigma) + \frac{1}{2}A_0(\sigma)^2\frac{d}{d\sigma}S(\sigma)\right) + O(\epsilon^3),
\end{aligned}
$$

where we have used $\frac{d}{d\sigma}R(\sigma) = S(\sigma)$ in the expansions for R.

We now consider (3.5.9) and (3.5.10) at successive orders in ϵ. As can be deduced from the Taylor series expansions above, the equations become progressively longer for higher orders in ϵ. Therefore we present only the $O(1)$ and $O(\epsilon)$ equations here, though we will use the equations up to $O(\epsilon^4)$. We deliberately do not rearrange the following equations, in order that the origin of each term can be seen easily.

At $O(1)$ from (3.5.9) we obtain

$$(4 - k_1)A_0 - 4 + (4 + k_1)B_0 = k_1[B_0 - A_0]S, \tag{3.5.11}$$

and from (3.5.10) we find

$$(4 + k_1)A_0 - 4 + k_1 + (4 - k_1)B_0 = -k_1[1 + A_0 - B_0]S. \tag{3.5.12}$$

At $O(\epsilon)$, (3.5.9) gives

$$
\begin{aligned}
(4 - k_1)A_1 + (4 + k_1)B_1 &= \\
k_1\left[B_1S + \frac{1}{2}B_0^2\frac{dS}{d\sigma} - A_1S - \frac{1}{2}A_0^2\frac{dS}{d\sigma}\right] &- K[B_0 - A_0]\frac{dS}{d\sigma},
\end{aligned}
\tag{3.5.13}
$$

and (3.5.10) gives

$$(4 + k_1) \left(\frac{dA_0}{d\sigma} + A_1 \right) + (4 - k_1)B_1 =$$
$$- k_1 \left[A_1 S + \frac{dA_0}{d\sigma} S + \frac{1}{2} \frac{dS}{d\sigma} + A_0 \frac{dS}{d\sigma} + \frac{1}{2} A_0^2 \frac{dS}{d\sigma} - B_1 S - \frac{1}{2} B_0^2 \frac{dS}{d\sigma} \right]$$
$$+ K[1 + A_0 - B_0] \frac{dS}{d\sigma}. \tag{3.5.14}$$

As mentioned above, the equations at higher orders in ϵ are rather long and so we do not present them here. It suffices to note that the equations at $O(\epsilon^2)$ relate A_2 and B_2 to A_1, B_1, A_0, B_0, and S and its derivatives up the second derivative with respect to σ, and correspondingly, the equations at $O(\epsilon^3)$ relate A_3 and B_3 to A_2, B_2, A_1, B_1, A_0, B_0, and S and its derivatives up to the third derivative with respect to σ.

The dramatic increase in the number of terms in the equations at higher orders in ϵ means that it is more time-consuming to solve the equations at higher orders. Using the formulation in [7] this quickly becomes problematic, even using computer algebra. Therefore we see that it is our more concise formulation here that allows us to extend the results of [7].

From the $O(1)$ equations, (3.5.11) and (3.5.12), we determine

$$B_0 - A_0 = \frac{1}{2}(1 + S).$$

Using this we may now calculate the $O(1)$ short-time average of $g(t)$, which we find is $-S$. Comparing these results with the corresponding results for a constant input signal, i.e. the difference between the switching times, given by (3.4.9), and $\langle g(t) \rangle$, given by (3.4.10), we see that the results are equivalent. In fact, if we solve (3.5.11) and (3.5.12) simultaneously we obtain the $O(1)$ switching times for a general input signal,

$$A_0 = \frac{1}{16}(1 - S)\left[4 - k_1(1 + S)\right], \tag{3.5.15}$$
$$B_0 = \frac{1}{2} + \frac{1}{16}(1 + S)\left[4 - k_1(1 - S)\right], \tag{3.5.16}$$

and comparing these leading-order switching times with those for a constant input, (3.4.11) and (3.4.12), we see that they are equivalent. This should be expected because we have assumed that the input signal is slowly-varying, and therefore to leading-order it is constant. We also compare our leading-order switching time solutions with those in [7] and find that they agree, as expected.

Our aim is to determine the amplifier output $g(t)$, and since it is defined by its switching times, we need to determine only these switching times to reach our goal. In [7], Cox and Candy establish this amplifier output up to $O(\epsilon^3)$, but because of our more

streamlined formulation we are able to significantly extend this result to determine the next order terms in the output, and so calculate $g(t)$ up to $O(\epsilon^4)$. Therefore we must determine the switching times up to $O(\epsilon^4)$ as well. We use the more limited results of [7] to verify our solutions up to $O(\epsilon^3)$.

To find the $O(\epsilon)$ switching times, we solve the $O(\epsilon)$ equations (3.5.13) and (3.5.14), obtaining

$$
\begin{aligned}
A_1 &= \frac{1}{64k_1}\frac{dS}{d\sigma}\Big[16 - 4k_1 + k_1^2 + 16K + k_1 S\left(-4 + 2k_1 - 8K - k_1^2\right) \\
&\quad - 3k_1^2 S^2 + k_1^3 S^3\Big], \quad\quad\quad\quad\quad\quad\quad\quad\quad\quad\quad\quad (3.5.17) \\
B_1 &= \frac{1}{64k_1}\frac{dS}{d\sigma}\Big[-16 + 12k_1 - k_1^2 - 16K + k_1 S\left(-4 + 6k_1 - 8K - k_1^2\right) \\
&\quad + 3k_1^2 S^2 + k_1^3 S^3\Big]. \quad\quad\quad\quad\quad\quad\quad\quad\quad\quad\quad\quad (3.5.18)
\end{aligned}
$$

Similarly, though after much more algebraic manipulation, by solving (3.5.9) and (3.5.10) at order $O(\epsilon^2)$ simultaneously we find the $O(\epsilon^2)$ switching times, and then determine the $O(\epsilon^3)$ switching times by solving the corresponding $O(\epsilon^3)$ equations simultaneously. These higher order switching times contain many more terms than is useful to present here. However, it is worth noting that the solutions for A_2 and B_2 contain S, its derivatives up to the second with respect to σ, as well as nonlinear combinations of these terms. Correspondingly, the solutions for A_3 and B_3 contain S, its derivatives up to the third with respect to σ, as well as nonlinear combinations of these terms. Thus we see that the $O(\epsilon)$ and higher order switching times contain nonlinear terms. These nonlinear terms will appear in the amplifier output, so it is interesting to note from where they originate.

We have now determined the switching times up to $O(\epsilon^4)$, and so we proceed to calculate the amplifier output.

3.5.1.1 Calculation of the amplifier output

We now calculate the leading audio-frequency components of the amplifier output. We use the Fourier transform/Poisson resummation method to do this, and because we know the switching times explicitly, we use the method as adapted for regular sampling (demonstrated in §2.3.2.2). Therefore we first take the Fourier transform of the output, and then apply the Poisson resummation formula before inverting the Fourier transform to obtain the output in the desired form.

We start by writing $g(t)$ in the form

$$
g(t) = \sum_{n=-\infty}^{\infty} \chi(t; n + \beta_n, n + 1 + \alpha_{n+1}) - \sum_{n=-\infty}^{\infty} \chi(t; n + \alpha_n, n + \beta_n),
$$

where the "top hat" function $\chi(t; t_1, t_2)$ is defined by (2.3.33). We then take the Fourier transform, as defined by (2.3.44),

$$
\begin{aligned}
\hat{g}(\omega) &= \int_{-\infty}^{\infty} \sum_{n=-\infty}^{\infty} \chi(t; n + \beta_n, n + 1 + \alpha_{n+1}) e^{-i\omega t} \, dt \\
&\quad - \int_{-\infty}^{\infty} \sum_{n=-\infty}^{\infty} \chi(t; n + \alpha_n, n + \beta_n) e^{-i\omega t} \, dt \\
&= \sum_{n=-\infty}^{\infty} \left[\int_{n+\beta_n}^{n+1+\alpha_{n+1}} e^{-i\omega t} \, dt - \int_{n+\alpha_n}^{n+\beta_n} e^{-i\omega t} \, dt \right].
\end{aligned}
$$

We split this expression into two parts: the zero-frequency component of the output, which we will consider later; and the nonzero-frequency component,

$$
\hat{g}(\omega) = \sum_{n=-\infty}^{\infty} \frac{2e^{-i\omega n}}{i\omega} \left[e^{-i\omega \beta_n} - e^{-i\omega \alpha_n} \right],
$$

for $\omega \neq 0$. We write this nonzero-frequency component in terms of $A(\epsilon n)$ and $B(\epsilon n)$ using the definitions (3.5.7) and (3.5.8), and then apply the Poisson resummation formula (2.3.31) to obtain

$$
\hat{g}(\omega) = \sum_{n=-\infty}^{\infty} \int_{-\infty}^{\infty} \frac{2e^{i(2\pi n - \omega)\tau}}{i\omega} \left[e^{-i\omega B(\epsilon \tau)} - e^{-i\omega A(\epsilon \tau)} \right] d\tau. \tag{3.5.19}
$$

The integral in (3.5.19) is a Fourier transform, and each term in the sum corresponds to frequencies around the nth harmonic of the carrier wave frequency. We are primarily interested in the audio part of the output, as frequencies above this low-frequency range will be attenuated by a low-pass filter, and thus the audio part constitutes the amplifier output that is heard by the user. We will therefore consider only the terms $n = 0$ in (3.5.19). As we consider only frequencies in the audio range we assume ω is $O(\epsilon)$ and define

$$
\omega = \epsilon \tilde{\omega},
$$

where $\tilde{\omega}$ is dimensionless and $O(1)$, and also introduce a longer timescale for integration and so define

$$
\tilde{\tau} = \epsilon \tau.
$$

We denote the audio part of $\hat{g}(\omega)$ by $\hat{g}_a(\omega)$, and with the above definitions find

$$
\hat{g}_a(\epsilon \tilde{\omega}) = \frac{1}{\epsilon} \int_{-\infty}^{\infty} \frac{2e^{-i\tilde{\omega}\tilde{\tau}}}{i\epsilon\tilde{\omega}} \left[e^{-i\epsilon\tilde{\omega}B(\tilde{\tau})} - e^{-i\epsilon\tilde{\omega}A(\tilde{\tau})} \right] d\tilde{\tau}.
$$

Expanding the integrand in powers of ϵ we obtain

$$
\begin{aligned}
\hat{g}_a(\epsilon \tilde{\omega}) &= \frac{1}{\epsilon} \int_{-\infty}^{\infty} 2e^{-i\tilde{\omega}\tilde{\tau}} \sum_{n=1}^{\infty} \frac{(-i\epsilon\tilde{\omega})^{n-1}}{n!} \left[A(\tilde{\tau})^n - B(\tilde{\tau})^n \right] d\tilde{\tau} \\
&= \frac{1}{\epsilon} \int_{-\infty}^{\infty} 2e^{-i\tilde{\omega}\tilde{\tau}} \sum_{n=1}^{\infty} \frac{(-1)^{n-1}}{n!} \epsilon^{n-1} \frac{d^{n-1}}{d\tilde{\tau}^{n-1}} \left[A(\tilde{\tau})^n - B(\tilde{\tau})^n \right] d\tilde{\tau},
\end{aligned}
$$

via integration by parts. Reverting to the original variables ω and τ the nonzero-frequency component becomes

$$\hat{g}_a(\omega) = \int_{-\infty}^{\infty} 2e^{-i\omega\tau} \sum_{n=1}^{\infty} \frac{(-1)^{n-1}}{n!} \epsilon^{n-1} \frac{d^{n-1}}{d(\epsilon\tau)^{n-1}} \left[A(\epsilon\tau)^n - B(\epsilon\tau)^n \right] d\tau, \quad (3.5.20)$$

for $\omega \neq 0$. This is now written directly as a Fourier transform, and so can be inverted simply. From the $O(1)$ short-time average of $g(t)$, which we found above to be $-S$, we can deduce that for a typical audio input signal, which has a long-time average of zero, the long-time average of $g(t)$ is zero. Therefore $g(t)$ has no zero-frequency component. Noting that (3.5.20) does in fact contain a zero-frequency term at $O(1)$ (since $A_0 - B_0 = -\frac{1}{2}(1+S)$), to obtain the audio part of the output, $g_a(t)$, we therefore invert (3.5.20) and add 1 to the result. We find

$$g_a(t) = 1 + 2 \sum_{n=1}^{\infty} \frac{(-1)^{n-1}}{n!} \epsilon^{n-1} \frac{d^{n-1}}{d\sigma^{n-1}} \left[A^n(\sigma) - B^n(\sigma) \right]. \quad (3.5.21)$$

This formula is valid for any amplifier whose switching times are described by the functions $A(\sigma)$ and $B(\sigma)$, and so we will use it to determine the audio part of the amplifier output here as well as for other negative feedback designs in chapters 4 and 5.

Expanding (3.5.21) we obtain

$$\begin{aligned}
g_a(t) &= 1 + 2(A(\sigma) - B(\sigma)) - \epsilon \frac{d}{d\sigma} \left[A(\sigma)^2 - B(\sigma)^2 \right] \\
&\quad + \frac{\epsilon^2}{3} \frac{d^2}{d\sigma^2} \left[A(\sigma)^3 - B(\sigma)^3 \right] - \frac{\epsilon^3}{12} \frac{d^2}{d\sigma^3} \left[A(\sigma)^4 - B(\sigma)^4 \right] + O\left(\epsilon^4\right) \\
&= 1 + 2[A_0 - B_0] + \epsilon \left[2(A_1 - B_1) - \frac{d}{d\sigma} \left(A_0^2 - B_0^2 \right) \right] \\
&\quad + \epsilon^2 \left[2(A_2 - B_2) + 2\frac{d}{d\sigma}(A_0 A_1 - B_0 B_1) + \frac{1}{3} \frac{d^2}{d\sigma^2} \left(A_0^3 - B_0^3 \right) \right] \\
&\quad + \epsilon^3 \left[2(A_3 - B_3) - \frac{d}{d\sigma}(A_1^2 + 2A_0 A_2 - B_1^2 - 2B_0 B_2) \right. \\
&\quad \left. + \frac{d^2}{d\sigma^2}(A_0^2 A_1 - B_0^2 B_1) - \frac{1}{12} \frac{d^3}{d\sigma^3}(A_0^4 - B_0^4) \right] + O\left(\epsilon^4\right),
\end{aligned}$$

and then inserting the switching time solutions at $O(1)$ and $O(\epsilon)$, (3.5.15)-(3.5.18), and the solutions at $O(\epsilon^2)$ and $O(\epsilon^3)$, which we have not displayed, we thus find the lead-

ing audio-frequency components of the output for a general input signal,

$$
\begin{aligned}
g_a(t) &= -S(\sigma) + \epsilon \frac{1+K}{k_1} \frac{d}{d\sigma} S(\sigma) + \frac{\epsilon^2}{48 k_1^2} \frac{d^2}{d\sigma^2} \left[\left(k_1^2 - 48(1+K) \right) S(\sigma) + k_1^2 S(\sigma)^3 \right] \\
&\quad + \frac{\epsilon^3}{192 k_1^3} \frac{d}{d\sigma} \left[4k_1^2 (k_1^2 S(\sigma)^2 - 12 - 6K) S(\sigma) \left(\frac{d}{d\sigma} S(\sigma) \right)^2 + \left(192(1+K) \right. \right. \\
&\quad \left. - 4k_1^2(2+K) - k_1^2 S(\sigma)^2(24+12K+k_1^2) + k_1^4 S(\sigma)^4 \right) \frac{d^2}{d\sigma^2} S(\sigma) \Big] \\
&\quad + O\left(\epsilon^4 \right).
\end{aligned}
\tag{3.5.22}
$$

This result is one of the major achievements of this analysis; it significantly extends (3.29) of [7], and that more limited result allows us to verify the audio part of the output up to $O(\epsilon^3)$. Here we have computed $g_a(t)$ up to $O(\epsilon^4)$ for a general input signal, giving more insight into the nonlinear distortion inherent in the negative feedback design. As the authors of [7] discuss, if we let

$$
K^2 = 1 - \frac{1}{24} k_1^2,
\tag{3.5.23}
$$

then the linear terms up to $O(\epsilon^3)$ in (3.5.22) form the start of a Taylor series for a delayed signal $-S\left(\sigma - \epsilon \frac{1+K}{k_1} \right)$. Thus we may write (3.5.22) in the form

$$
\begin{aligned}
g_a(t) &= -S\left(\sigma - \epsilon \frac{1+K}{k_1} \right) + \frac{\epsilon^2}{48} \frac{d^2}{d\sigma^2} S(\sigma)^3 \\
&\quad + \frac{\epsilon^3}{10368} \frac{d}{d\sigma} \left[108 k_1^2 \left(2k_1^2 S(\sigma)^2 - 24 - (144 - 6k_1^2)^{\frac{1}{2}} \right) S(\sigma) \left(\frac{d}{d\sigma} S(\sigma) \right)^2 \right. \\
&\quad + \left(3456 + 432(144 - 6k_1^2)^{\frac{1}{2}} - (144 - 6k_1^2)^{\frac{3}{2}} - 216 k_1^2 - 18 k_1^2 (144 - 6k_1^2)^{\frac{1}{2}} \right. \\
&\quad \left. \left. - 54 k_1^2 S(\sigma)^2 \left(24 + (144 - 6k_1^2)^{\frac{1}{2}} + k_1^2 \right) + 54 k_1^4 S(\sigma)^4 \right) \frac{d^2}{d\sigma^2} S(\sigma) \right] + O\left(\epsilon^4 \right).
\end{aligned}
$$

By writing $g_a(t)$ in this form it is evident that the output is dominated by a slightly delayed version of the input signal. If we revert to dimensional terms, we observe that the delay is on the timescale of the carrier wave and so is imperceptible to the human ear. Writing $g_a(t)$ in this delayed form, and choosing the value of K as above, removes the $O(\epsilon)$ and $O(\epsilon^2)$ linear terms in (3.5.22), though the nonlinear term at $O(\epsilon^2)$ and both linear and nonlinear terms at $O(\epsilon^3)$ persist. The cubic nonlinear term at $O(\epsilon^2)$ is independent of the parameter k_1 so cannot be removed by choosing k_1 carefully. Although the $O(\epsilon^3)$ terms are dependent on k_1, they also cannot be removed by a particular choice of this parameter.

We can now understand the importance of including a multiplier in the amplifier design. Recall that the output from the multiplier is $Ks(t)$. The effect of the multiplier was not apparent from the analysis for a constant input signal, because the switching

times (and hence the output) are independent of K. However, from the above analysis for a general input signal, we see that by making the appropriate choice of K (as given by (3.5.23)) we can eliminate some of the inherent distortion in the amplifier.

If we specify that the input signal is sinusoidal, $S(\sigma) = s_0 \sin \sigma$, (3.5.22) becomes

$$
\begin{aligned}
g_a(t) \quad = \quad & -s_0 \sin \sigma + \epsilon \frac{s_0(1+K)}{k_1} \cos \sigma \\
& + \epsilon^2 \frac{s_0}{192 k_1^2} \left[\left(192(1+K) - k_1^2(4+3s_0^2)\right) \sin \sigma + 9 k_1^2 s_0^2 \sin 3\sigma \right] \\
& + \epsilon^3 \frac{s_0}{3072 k_1^3} \left[\left(-3072(1+K) + 16 k_1^2(2+K)(4+3s_0^2) + 2 k_1^4 s_0^2(6-s_0^2)\right) \cos \sigma \right. \\
& \left. - 3 k_1^2 s_0^2 \left(144(2+K) + k_1^2(4-9s_0^2)\right) \cos 3\sigma - 25 k_1^4 s_0^4 \cos 5\sigma \right] + O\left(\epsilon^4\right).
\end{aligned}
$$

Writing this in dimensional terms,

$$
\begin{aligned}
g_a^*(t^*) \quad = \quad & -s_0 V \sin \omega_a t^* + \omega_a \frac{s_0 V(1+K)}{c_1} \cos \omega_a t^* \\
& + \omega_a^2 \frac{s_0 V}{192 c_1^2} \left[\left(192(1+K) - c_1^2 T^2(4+3s_0^2)\right) \sin \omega_a t^* + 9 c_1^2 s_0^2 T^2 \sin 3\omega_a t^* \right] \\
& + \omega_a^3 \frac{s_0 V}{3072 c_1^3} \left[\left(-3072(1+K) + 16 c_1^2 T^2(2+K)(4+3s_0^2) \right. \right. \\
& \left. + 2 c_1^4 s_0^2 T^4(6-s_0^2)\right) \cos \omega_a t^* \\
& - 3 c_1^2 s_0^2 T^2 \left(144(2+K) + c_1^2 T^2(4-9s_0^2)\right) \cos 3\omega_a t^* \\
& \left. - 25 c_1^4 s_0^4 T^4 \cos 5\omega_a t^* \right] + O\left((\omega_a T)^4\right),
\end{aligned}
$$

we can see clearly that the distortion terms in (3.5.22) affect the amplitude of the signal at frequency ω_a, and that this effect is nonlinear. The distortion terms also result in third- and fifth-harmonic terms. The third harmonics have amplitude $O\left((\omega_a T)^2\right)$, and fifth harmonics have amplitude $O\left((\omega_a T)^3\right)$. Thus we see that calculating the $O\left((\omega_a T)^3\right)$ terms, which are in addition to previous work [7], give the first term with fifth-harmonic distortion.

We have determined that the audio output from this first-order negative feedback design contains inherent nonlinear distortion. Before concluding in §3.6 we carry out a numerical simulation to confirm the analytical results we found above.

3.5.2 Numerical simulation of switching times

In order to verify the analytical solutions we have found above for a general input signal, we perform a numerical simulation. We numerically simulate the switching times of the output, and then compare them with the switching times we found analytically up to $O(\epsilon^4)$ above.

To simulate the switching times numerically, we iterate in Maple the two exact non-linear difference equations governing the switching times, (3.5.4) and (3.5.5). We choose the input signal to be sinusoidal, of the form $s(t) = s_0 \sin \epsilon t$. We take the parameter values $s_0 = -0.25$, $k_1 = 1$, $K = 0.5$, the initial value $\alpha_0 = 0$ arbitrarily, and solve the system for ϵ ranging from 0.064 to 0.001. We then compare the switching times found numerically with those we found analytically.

As when we simulated the switching times numerically for a constant input signal, in §3.4.2, there are transients in the numerical simulations of the switching times for a general input signal. These do not appear in our analytical switching times because the transients decay on a short timescale compared with the input signal, and the continuous model we implement assumes that $A(\sigma)$ and $B(\sigma)$ vary only on the timescale of the input signal. Transients arise in the numerical simulation because we choose the initial value α_0 arbitrarily, and they decay because negative feedback is included in the circuit.

The absolute error between the simulated and analytical switching times varies over the period of the input signal. Therefore to compare the switching times sensibly we need to calculate the absolute difference between the simulated and analytical switching times at any point in time, and then take the maximum of these values over one whole period of the input signal. Thus we define the error in the analytical switching times $A(\sigma)$ and $B(\sigma)$ as

$$E_A(\epsilon) = \max |\alpha_n - A(\epsilon n)|, \tag{3.5.24}$$

$$E_B(\epsilon) = \max |\beta_n - B(\epsilon n)|, \tag{3.5.25}$$

respectively, where α_n and β_n are the numerically simulated switching times, and the maximum is taken over n over one period of the input signal. As discussed above, there are transients in our numerical simulations, which do not appear in the analytically found switching times, and so for a sensible comparison we must compare the switching times only after the transients have decayed.

We calculated the switching times analytically up to $O(\epsilon^4)$ and therefore we expect the error between the numerically simulated and analytical switching times to be $O(\epsilon^4)$. Tables 3.1 and 3.2 show the ratios of $E_A(\epsilon)$ and $E_B(\epsilon)$ respectively for different values of ϵ. It is clear that when ϵ is halved, the error is approximately divided by 16, and for smaller ϵ this ratio gets closer to 16. Hence the analytical switching times agree up to $O(\epsilon^4)$ with those simulated numerically.

Note that because the errors are smaller for smaller ϵ, we must be careful to use adequate precision in these calculations. To show that the ratio of the errors con-

Comparison	Result
$E_A(0.128)/E_A(0.064)$	15.974431
$E_A(0.064)/E_A(0.032)$	15.995355
$E_A(0.032)/E_A(0.016)$	15.998980
$E_A(0.016)/E_A(0.008)$	15.999788
$E_A(0.008)/E_A(0.004)$	15.999947
$E_A(0.004)/E_A(0.002)$	15.999985
$E_A(0.002)/E_A(0.001)$	15.999996

Table 3.1: Table comparing values of $E_A(\epsilon)$ with $s_0 = -0.25$, $k_1 = 1$ and $K = 0.5$, with results given to 6 decimal places.

Comparison	Result
$E_B(0.128)/E_B(0.064)$	15.976203
$E_B(0.064)/E_B(0.032)$	15.995697
$E_B(0.032)/E_B(0.016)$	15.999065
$E_B(0.016)/E_B(0.008)$	15.999778
$E_B(0.008)/E_B(0.004)$	15.999939
$E_B(0.004)/E_B(0.002)$	15.999993
$E_B(0.002)/E_B(0.001)$	15.999996

Table 3.2: Table comparing values of $E_B(\epsilon)$ with $s_0 = -0.25$, $k_1 = 1$ and $K = 0.5$, with results given to 6 decimal places.

verges to 16, it is sufficient to use 20 digits of precision for ϵ ranging from 0.064 to 0.004, but not for $\epsilon = 0.002$ and smaller. For example, with 20 digits of precision $E_A(0.004)/E_A(0.002) = 15.999900$ and $E_A(0.002)/E_A(0.001) = 15.995286$, and so we use 25 digits of precision to determine the results in table 3.1.

We have verified that the analytical switching times we found in §3.5.1 agree with a numerical simulation.

3.6 Conclusions

We have significantly extended the analysis of [7] to investigate a first-order negative feedback amplifier. Our results for a constant input gave us an insight into how to solve the model for a general input, as well as a means of verifying the leading-order results we obtained for a general input signal. For a general input signal we derived

the leading audio-frequency components of the amplifier output via a superior concise analytical formulation, showing that whilst the input signal is reproduced in this output, it also contains inherent nonlinear distortion. By specifying the parameter K, where the multiplier output is $Ks(t)$, we were able to remove some of the distortion. The remaining nonlinear distortion terms cannot be removed by any choice of the parameter k_1, the integrator constant, though a range for k_1 ensuring correct operation of the amplifier was derived through our constant input analysis. For a sinusoidal input signal we found that the nonlinear distortion terms affect the signal appearing in the output at the frequency of the input signal, and result in third- and fifth-harmonics of the input signal.

The analysis we have presented here is useful in itself since we have calculated the next order terms in the output compared with [7], giving further insight into the nonlinear distortion, and also verified the results via a numerical simulation. Furthermore, it forms a basis for the work that follows in the next two chapters, where we will consider more complex amplifier designs with negative feedback. These more complex designs attempt to reduce the distortion introduced by negative feedback, which we have investigated above. Here we have formalised and streamlined a method for analysing the first-order negative feedback amplifier, presented in [7], which will allow us to extend the analysis more easily to investigate the designs that follow. Recall that the formula giving the audio-frequency components of the output of the amplifier in terms of its switching times, (3.5.21), derived here via the Fourier transform/Poisson resummation method, is valid for any amplifier design. Therefore, having obtained the nonlinear difference equations for the switching times for the other amplifier designs, we will determine the switching times by employing a continuous model and perturbation expansions as we have done here, and then use (3.5.21) to establish the audio output. This will enable us to ascertain whether these amplifier designs offer reduced distortion compared with the first-order negative feedback design.

79

Second-order negative feedback amplifier

4.1 Introduction

N EGATIVE feedback is commonly used to reduce noise in the output of class-D amplifiers, but unfortunately it also introduces nonlinear distortion, as was discussed in chapter 3. Correspondingly, many more complex amplifier designs have been developed that include negative feedback, as well as other features that attempt to reduce distortion. One such design is a second-order negative feedback amplifier, which we analyse here.

A first-order negative feedback amplifier consists of an integrator, multiplier, comparator and a negative feedback loop, as we saw in chapter 3. The design of the second-order negative feedback amplifier considered here is similar, except for two important differences. Firstly, instead of a single integrator, there are two integrators, implemented through a second-order loop filter. Secondly, to simplify matters, the design does not include a multiplier.

Previous work [38] has shown that second-order negative feedback amplifiers show reduced distortion compared with the first-order negative feedback amplifier, but this analysis was based only on numerical simulation. A limited analytical investigation of the particular design we investigate here [39] has been performed, where the leading-order behaviour of the amplifier was determined for a sinusoidal input, but this tells us nothing about the distortion in the output. By investigating the design analytically here, we aim to derive the leading audio-frequency components of the amplifier output, and determine whether the distortion can be reduced. As for previous designs in this thesis, the input signal is amplified before being input to this amplifier, and so

we analyse the output stage only, where the aim is to reproduce the input signal as accurately as possible. Despite the differences in design compared with the first-order negative feedback amplifier, we are able to extend the method of analysis as detailed in chapter 3 to investigate this design. Due to the increased complexity of the design here, using the streamlined formulation we introduced in chapter 3 enables us to determine the leading audio-frequency components of the amplifier output for a general input signal, which otherwise would be impossible.

The structure of the chapter is as follows. In §4.2 we establish a dimensional model for the amplifier, before nondimensionalising in §4.3 to simplify our analysis. As in chapter 3, we then investigate the model for a constant input signal in §4.4. Because the audio input signal is slowly-varying compared with the carrier wave frequency, the slowly-varying input signal is constant to leading order. Thus the constant input signal analysis allows us to obtain the leading-order solutions for a general (time-varying) input, which assists us in solving the model for a general input, as well as giving us a means for checking our results.

In §4.5 we analyse the design for a general input, extending the method of analysis introduced in chapter 3. We determine a system of nonlinear difference equations for the switching times of the output, and then use perturbation expansions to obtain the switching times. To derive the leading audio-frequency components of the amplifier output we utilise the formula (3.5.21) that we obtained in chapter 3 giving the audio-frequency components of the output in terms of its switching times. We confirm, for both a constant input in §4.4.2 and a general input in §4.5.2, that our analytical solutions agree with numerical simulations. We conclude in §4.6.

4.2   Dimensional model for the amplifier design

We start by creating a dimensional model for the amplifier, the design of which is as appears in figure 3 of [39], represented by the diagram in figure 4.1 below. Dimensional variables are denoted by the superscript $*$.

The input signal $s^*(t^*)$ is added to the comparator output $g^*(t^*)$ and then both voltages are fed into the second-order loop filter. We look in more detail at the operation of the second-order loop filter in §4.2.1. The output from the second-order loop filter is $H^*(t^*)$. This output $H^*(t^*)$ is in turn added to a periodic triangular carrier wave $v^*(t^*)$ and fed into a comparator. The carrier wave has period T and is defined by

$$v^*(t^*) = \begin{cases} \left(1 - \frac{4}{T}(t^* - nT)\right) V & \text{for } nT \leq t^* < \left(n + \frac{1}{2}\right) T \\ \left(-3 + \frac{4}{T}(t^* - nT)\right) V & \text{for } \left(n + \frac{1}{2}\right) T \leq t^* < (n+1)T, \end{cases} \tag{4.2.1}$$
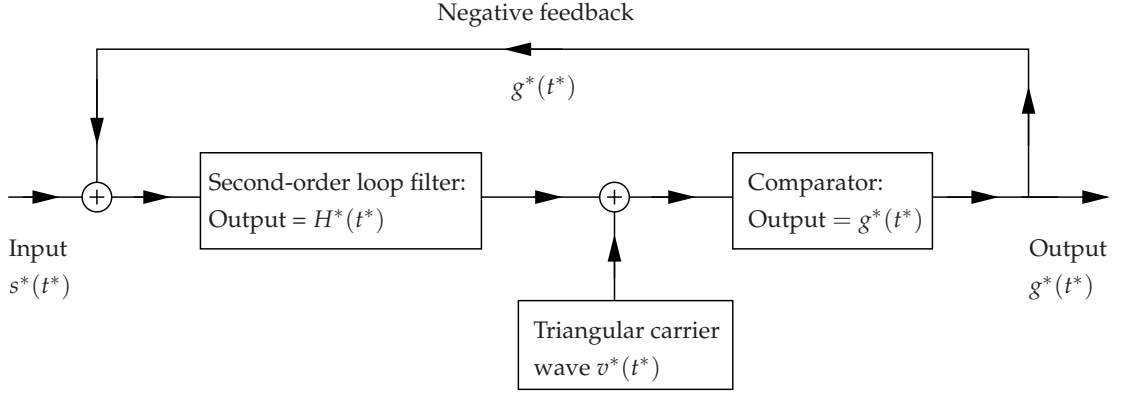
Figure 4.1: Schematic diagram representing the design of a negative feedback amplifier with a second-order loop filter.

where V is a constant with dimension volts. The comparator compares $H^*(t^*)$ with $v^*(t^*)$ and outputs a square wave, $g^*(t^*)$, which is defined by

$$g^*(t^*) = \begin{cases} -V & \text{for } H^*(t^*) + v^*(t^*) < 0 \\ +V & \text{for } H^*(t^*) + v^*(t^*) > 0. \end{cases} \tag{4.2.2}$$

Therefore we define two regions as shown in figure 4.2, as we did in chapter 3. In region I, $g^*(t^*) = -V$, and in region II, $g^*(t^*) = +V$. The switching times are defined to be the times at which $g^*(t^*)$ switches between $\pm V$: at the times $t^* = nT + \alpha_n^*$, the square wave $g^*(t)$ switches from $+V$ to $-V$; at the times $t^* = nT + \beta_n^*$, the square wave $g^*(t^*)$ switches from $-V$ to $+V$. Thus

$$g^*(t^*) = \begin{cases} -V & \text{for } nT + \alpha_n^* < t^* < nT + \beta_n^* \\ +V & \text{for } nT + \beta_n^* < t^* < (n+1)T + \alpha_{n+1}^*. \end{cases} \tag{4.2.3}$$

As in previous chapters, note that we have given two expressions for $g^*(t^*)$: (4.2.2) defines the conditions for $g^*(t^*)$ to switch in terms of $H^*(t^*)$ and $v^*(t^*)$, whilst (4.2.3) defines the switching times α_n^* and β_n^*.

We will assume that $H^*(t^*) = -v^*(t^*)$ at two instants t^* in each carrier wave period, first at the time $t^* = nT + \alpha_n^*$ and then at the time $t^* = nT + \beta_n^*$. Therefore α_n^* and β_n^* are constrained by

$$0 < \alpha_n^* < \frac{T}{2},$$
$$\frac{T}{2} < \beta_n^* < T.$$

Note that for correct operation the input signal must satisfy

$$|s^*(t^*)| < V.$$
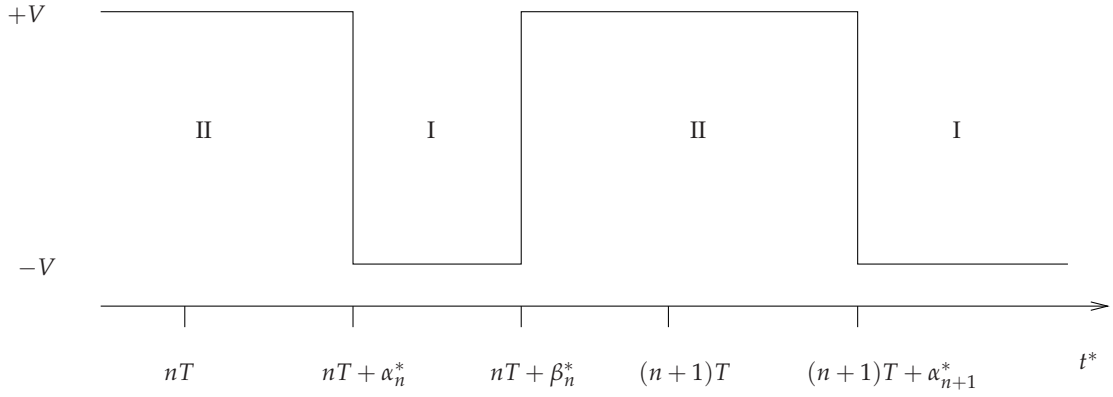
Figure 4.2: The dimensional square wave $g^*(t^*)$ showing the regions I and II.

The comparator output $g^*(t^*)$ is then fed back into the second-order loop filter via a negative feedback loop.

The variables $s^*(t^*)$, $g^*(t^*)$, $H^*(t^*)$ and $v^*(t^*)$ have dimension volts, whilst the variables α_n^* and β_n^* have dimension time. Before nondimensionalising the model in §4.3, we first consider the operation of the second-order loop filter.

4.2.1 Second-order loop filter

We now look at circuit for the second-order loop filter in isolation to work out how its output relates to its input, i.e. to determine how $H^*(t^*)$ is related to $s^*(t^*)$ and $g^*(t^*)$.

The circuit diagram in figure 4.3 represents the second-order loop filter used in this amplifier. For simplicity we first look at this isolated circuit rather than at the circuit for the whole amplifier. We define the input voltage to be $V_{in}^*(t^*)$ and the output voltage to be $V_{out}^*(t^*)$. We aim to find $V_{out}^*(t^*)$ purely in terms of $V_{in}^*(t^*)$. All of the voltage and current laws we use here, as well as the governing equations for the components in this circuit can be found in [40].

The resistor with resistance R_1 is connected in series with an operational amplifier, which we assume to be ideal. The noninverting input (marked with a $+$) of the operational amplifier is grounded so the inverting input (marked with a $-$) is also at zero volts. Therefore the current $I_1^*(t^*)$ through the resistor with resistance R_1 is related to $V_{in}^*(t^*)$ via

$$V_{in}^*(t^*) = R_1 I_1^*(t^*). \tag{4.2.4}$$

We define the voltage across the resistor with resistance R_2 to be $V_2^*(t^*)$. $V_2^*(t^*)$ is
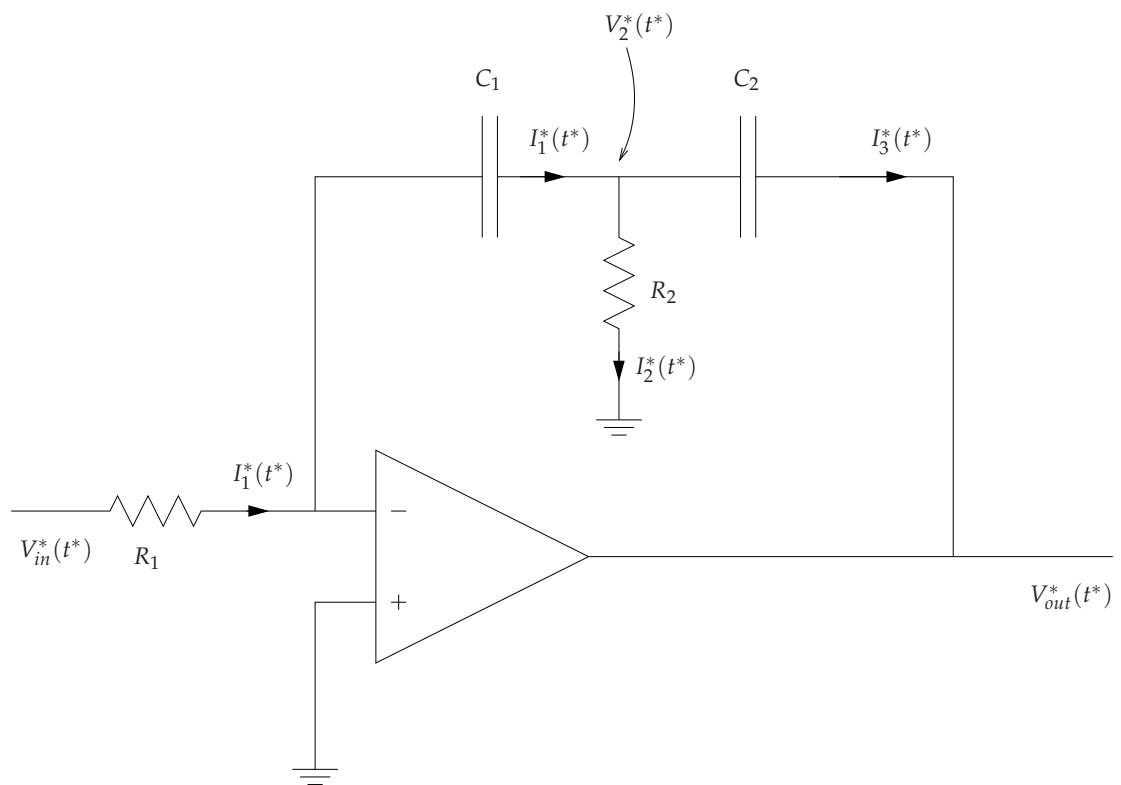
Figure 4.3: Circuit diagram of the second-order loop filter. The arrows represent the direction of current flow when $I_1^*(t^*)$, $I_2^*(t^*)$ and $I_3^*(t^*)$ are positive.

related to the current $I_2^*(t^*)$ flowing through it via

$$V_2^*(t^*) = R_2 I_2^*(t^*).$$ (4.2.5)

The current $I_1^*(t^*)$ flows through the capacitor with capacitance C_1. The voltage across this capacitor is that of the inverting input of the operational amplifier minus $V_2^*(t^*)$, and so

$$I_1^*(t^*) = -C_1 \frac{d}{dt^*} V_2^*(t^*).$$ (4.2.6)

From (4.2.4) and (4.2.6) we find the relationship between the input voltage and $V_2^*(t^*)$ to be

$$\frac{d}{dt^*} V_2^*(t^*) = -\frac{1}{C_1 R_1} V_{in}^*(t^*).$$ (4.2.7)

Applying Kirchhoff's current law to the loop filter circuit gives the following relationship between the currents in the circuit,

$$I_1^*(t^*) = I_2^*(t^*) + I_3^*(t^*),$$ (4.2.8)

where $I_3^*(t^*)$ is the current through the capacitor with capacitance C_2. The voltage across this second capacitor is $V_2^*(t^*) - V_{out}^*(t^*)$, and thus

$$I_3^*(t^*) = C_2 \frac{d}{dt^*} (V_2^*(t^*) - V_{out}^*(t^*)).$$ (4.2.9)

We eliminate $I_3^*(t^*)$ from (4.2.8) using (4.2.9), and also substitute for $I_1^*(t^*)$ and $I_2^*(t^*)$ using (4.2.4) and (4.2.5) to find an equation relating the voltages in the circuit,

$$\frac{1}{C_2 R_2} V_2^*(t^*) = \left(\frac{1}{C_1 R_1} + \frac{1}{C_2 R_1} \right) V_{in}^*(t^*) + \frac{d}{dt^*} V_{out}^*(t^*).$$ (4.2.10)

Since the voltage across each capacitor is a continuous function of time, $V_2^*(t^*)$ and $V_2^*(t^*) - V_{out}^*(t^*)$ must be continuous. Thus $V_{out}^*(t^*)$ is continuous, and from (4.2.10),

$$\left(\frac{1}{C_1 R_1} + \frac{1}{C_2 R_1} \right) V_{in}^*(t^*) + \frac{d}{dt^*} V_{out}^*(t^*)$$ (4.2.11)

is continuous. Differentiating (4.2.10) and using (4.2.7) to eliminate $V_2^*(t^*)$ we find the equation we require relating $V_{in}^*(t^*)$ to $V_{out}^*(t^*)$,

$$\frac{d^2}{dt^{*2}} V_{out}^*(t^*) = - \left(\frac{1}{C_1 R_1} + \frac{1}{C_2 R_1} \right) \frac{d}{dt^*} V_{in}^*(t^*) - \frac{1}{C_1 C_2 R_1 R_2} V_{in}^*(t^*).$$ (4.2.12)

If we now consider the second-order loop filter as connected to the rest of the amplifier we can determine the relationship between $s^*(t^*)$, $g^*(t^*)$ and $H^*(t^*)$. In the

amplifier, the voltage corresponding to $V_{in}^*(t^*)$ is $s^*(t^*) + g^*(t^*)$, and the voltage corresponding to $V_{out}^*(t^*)$ is $H^*(t^*)$. Thus from (4.2.12) we find

$$
\frac{d^2}{dt^{*2}} H^*(t^*) = -\left(\frac{1}{C_1 R_1} + \frac{1}{C_2 R_1} \right) \frac{d}{dt^*} (s^*(t^*) + g^*(t^*))
$$
$$
- \frac{1}{C_1 C_2 R_1 R_2} (s^*(t^*) + g^*(t^*)). \tag{4.2.13}
$$

Note that $\frac{d}{dt^*} g^*(t^*) = 0$ at all times except at the switching times, when the derivative does not exist. Thus (4.2.13) is valid everywhere except at the switching times. From continuity of both $V_{out}^*(t^*)$ and (4.2.11) we find two continuity conditions:

Continuity condition 1: $\quad H^*(t^*)$ is continuous; $\tag{4.2.14}$

Continuity condition 2: $\quad \left(\dfrac{1}{C_1 R_1} + \dfrac{1}{C_2 R_1} \right) (s^*(t^*) + g^*(t^*)) + \dfrac{d}{dt^*} H^*(t^*)$

is continuous. $\tag{4.2.15}$

Since later we will integrate (4.2.13) to find $H^*(t^*)$ it makes sense to define $r^*(t^*)$ as the integral of the input signal, and $q^*(t^*)$ as the double integral of the input signal, so

$$
\frac{d}{dt^*} r^*(t^*) = s^*(t^*), \tag{4.2.16}
$$
$$
\frac{d}{dt^*} q^*(t^*) = r^*(t^*), \tag{4.2.17}
$$

where $r^*(t^*)$ has dimension volts x time and $q^*(t^*)$ has dimension volts x time^2. With these definitions, (4.2.13) becomes

$$
\frac{d^2}{dt^{*2}} H^*(t^*) = -\left(\frac{1}{C_1 R_1} + \frac{1}{C_2 R_1} \right) \left(\frac{d^2}{dt^{*2}} r^*(t^*) + \frac{d}{dt^*} g^*(t^*) \right)
$$
$$
- \frac{1}{C_1 C_2 R_1 R_2} \left(\frac{d^2}{dt^{*2}} q^*(t^*) + g^*(t^*) \right), \tag{4.2.18}
$$

valid at all times except at the switching times.

We now have the dimensional equations we require to find the square wave output $g^*(t^*)$. These are (4.2.1)-(4.2.3) and (4.2.18) with the two derived continuity conditions above, (4.2.14) and (4.2.15). In the following section we nondimensionalise these equations in order to solve them.

4.3 Nondimensionalisation

We now nondimensionalise the equations governing the amplifier. We represent dimensionless variables by unstarred symbols.

The nondimensionalisation here is similar to that in chapter 3. Thus we scale the dimensional times t^*, α_n^* and β_n^* with the period of the carrier wave, T, to obtain the

dimensionless times t, α_n and β_n. We scale the dimensional voltages $g^*(t^*)$, $H^*(t^*)$, $s^*(t^*)$ and $v^*(t^*)$ with V to obtain the dimensionless voltages $g(t)$, $H(t)$, $s(t)$ and $v(t)$. Using our definition of $s(t)$, dimensionless time, and the definitions (4.2.16) and (4.2.17) of $r^*(t^*)$ and $q^*(t^*)$ we define

$$r(t) = \frac{r^*(t^*)}{TV},$$
$$q(t) = \frac{q^*(t^*)}{T^2V},$$

which ensure that

$$\frac{d}{dt}r(t) = s(t), \tag{4.3.1}$$

$$\frac{d}{dt}q(t) = r(t). \tag{4.3.2}$$

Noting that the product "resistance x capacitance" has dimensions of time, we define two dimensionless $O(1)$ parameters

$$k_2 = T\left(\frac{1}{C_1R_1} + \frac{1}{C_2R_1}\right) > 0,$$

$$k_3 = \frac{T^2}{C_1C_2R_1R_2} > 0.$$

With the above definitions of dimensionless variables and parameters we now nondimensionalise the governing equations for the amplifier. Equations (4.2.1)-(4.2.3) defining the carrier wave, square wave output and the switching times become, in dimensionless terms,

$$v(t) = \begin{cases} 1 - 4(t - n) & \text{for } n \le t < n + \frac{1}{2} \\ -3 + 4(t - n) & \text{for } n + \frac{1}{2} \le t < n + 1, \end{cases} \tag{4.3.3}$$

$$g(t) = \begin{cases} -1 & \text{for } H(t) + v(t) < 0 \\ +1 & \text{for } H(t) + v(t) > 0, \end{cases} \tag{4.3.4}$$

$$g(t) = \begin{cases} -1 & \text{for } n + \alpha_n < t < n + \beta_n \\ +1 & \text{for } n + \beta_n < t < n + 1 + \alpha_{n+1}. \end{cases} \tag{4.3.5}$$

Figure 4.4 shows the dimensionless square wave $g(t)$ and the dimensionless switching times which bound regions I and II. We nondimensionalise the restrictions on the dimensionless switching times α_n and β_n and find

$$0 < \alpha_n < \frac{1}{2}, \tag{4.3.6}$$

$$\frac{1}{2} < \beta_n < 1. \tag{4.3.7}$$
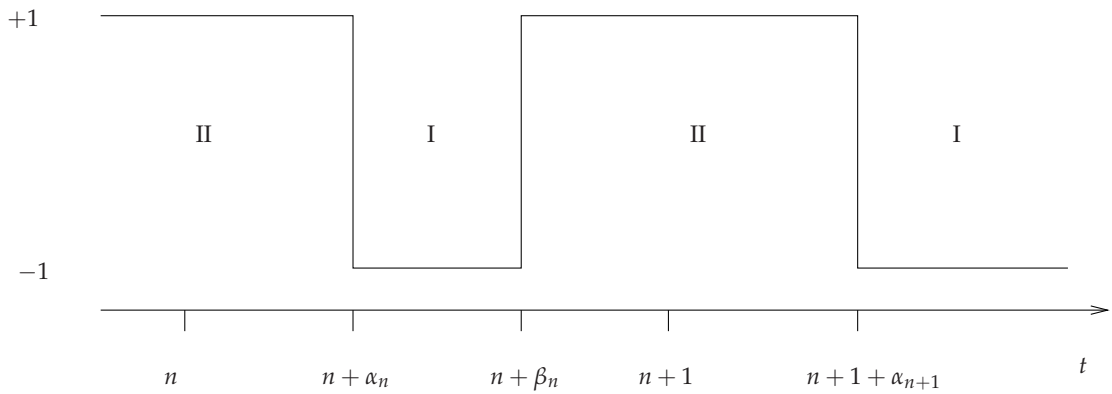
Figure 4.4: The dimensionless square wave $g(t)$ showing the regions I and II.

We also nondimensionalise the restriction on the input signal and find that the dimensionless input signal must satisfy

$$|s(t)| < 1. \tag{4.3.8}$$

The dimensionless equivalent of (4.2.18) is

$$\ddot{H}(t) = -k_2\left(\ddot{r}(t) + \dot{g}(t)\right) - k_3\left(\ddot{q}(t) + g(t)\right), \tag{4.3.9}$$

where we now use the notation $\dot{H}(t) = \frac{d}{dt}H(t)$ and $\ddot{H}(t) = \frac{d^2}{dt^2}H(t)$. Note again that this equation defining the loop filter output $H(t)$ is valid everywhere except at the switching times. Finally, we nondimensionalise the two continuity conditions relating to the loop filter, (4.2.14) and (4.2.15) and thus find two dimensionless continuity conditions:

Continuity condition 1: $H(t)$ is continuous; $\tag{4.3.10}$

Continuity condition 2: $k_2(s(t) + g(t)) + \dot{H}(t)$ is continuous. $\tag{4.3.11}$

Recall that in our analysis of the first-order negative feedback amplifier, in chapter 3, we investigated the dimensionless equations governing the amplifier first for a constant input signal, before considering a general (time-varying) input signal. This was useful because the amplifier's input is slowly varying compared with the carrier wave frequency, and so the constant input signal analysis provides the limiting case for a general input signal. This is also true of the second-order negative feedback amplifier we analyse here, and thus we proceed by analysing the dimensionless governing equations (4.3.3)-(4.3.5) and (4.3.9) first for a constant input signal in §4.4, before considering a general input signal in §4.5.

4.4 Dimensionless model for a constant input signal

We now look in more detail at the dimensionless equations governing the amplifier for a constant input signal. Therefore in this section we define $s(t) = s_0$, where $-1 < s_0 < 1$ is a constant, and thus from (4.3.1), $r(t) = s_0 t$, and from (4.3.2), $q(t) = s_0 t^2$. As when we carried out constant signal analysis for the first-order negative feedback amplifier in chapter 3, by considering a constant input signal here we aim to understand how the second-order negative feedback amplifier behaves, and also to help us to solve the model for a general input signal. We use the notation $\dot{H}(t) = \frac{d}{dt} H(t)$ throughout.

We start by looking at the second-order loop filter output, $H(t)$. We integrate (4.3.9) over regions I and II separately and find

$$H(t) = \begin{cases} H(t_0) + \dot{H}(t_0^+)(t - t_0) + \frac{k_3}{2}(1 - s_0)(t - t_0)^2 & \text{in region I} \\ H(t_0) + \dot{H}(t_0^+)(t - t_0) - \frac{k_3}{2}(1 + s_0)(t - t_0)^2 & \text{in region II} \end{cases} \tag{4.4.1}$$

where t_0 is the time at the beginning of the region (respectively, $t_0 = n + \alpha_n$ and $t_0 = n + \beta_n$). We use the notation $\dot{H}(t_0^+)$ to denote $\dot{H}(t)$ evaluated at a time just after the beginning of the region. This is necessary because $\dot{H}(t)$ is not continuous. Evaluating (4.4.1) in region I, for $n + \alpha_n < t < n + \beta_n$, we obtain

$$H(t) = H(n + \alpha_n) + \dot{H}(n + \alpha_n^+)(t - n - \alpha_n) + \frac{k_3}{2}(1 - s_0)(t - n - \alpha_n)^2. \tag{4.4.2}$$

From (4.3.10) we know that $H(t)$ is continuous so we may use (4.4.2) to find $H(t)$ at the end of the region,

$$H(n + \beta_n) = H(n + \alpha_n) + \dot{H}(n + \alpha_n^+)(\beta_n - \alpha_n) + \frac{k_3}{2}(1 - s_0)(\beta_n - \alpha_n)^2. \tag{4.4.3}$$

Evaluating (4.4.1) in region II, for $n + \beta_n < t < n + 1 + \alpha_{n+1}$, we obtain

$$H(t) = H(n + \beta_n) + \dot{H}(n + \beta_n^+)(t - n - \beta_n) - \frac{k_3}{2}(1 + s_0)(t - n - \beta_n)^2. \tag{4.4.4}$$

Again, since $H(t)$ is continuous we may use (4.4.4) to find $H(t)$ at the end of the region,

$$\begin{aligned} H(n + 1 + \alpha_{n+1}) &= H(n + \beta_n) + \dot{H}(n + \beta_n^+)(1 + \alpha_{n+1} - \beta_n) \\ &\quad - \frac{k_3}{2}(1 + s_0)(1 + \alpha_{n+1} - \beta_n)^2. \end{aligned} \tag{4.4.5}$$

We now use the second continuity condition, (4.3.11), to find the relationship between $\dot{H}(t)$ at the different switching times. Applying the continuity condition at the time $t = n + \beta_n$, using (4.4.2) to determine $\dot{H}(n + \beta_n^-)$, we obtain

$$\dot{H}(n + \beta_n^+) = \dot{H}(n + \alpha_n^+) - 2k_2 + k_3(1 - s_0)(\beta_n - \alpha_n). \tag{4.4.6}$$

Similarly, applying the continuity condition at the time $t = n + 1 + \alpha_{n+1}$, using (4.4.4) to determine $\dot{H}(n + 1 + \alpha_n^-)$, we obtain

$$\dot{H}(n + 1 + \alpha_{n+1}^+) = \dot{H}(n + \beta_n^+) + 2k_2 - k_3(1 + s_0)(1 + \alpha_{n+1} - \beta_n). \qquad (4.4.7)$$

Finally we consider the definitions of the switching times to find equations directly relating the switching times to $H(t)$ at those switching times. From (4.3.4) we know that the switching times are the times that satisfy $H(t) + v(t) = 0$. Using the restrictions imposed on α_n and β_n, (4.3.6) and (4.3.7), we determine $v(n + \alpha_n)$ and $v(n + \beta_n)$ from (4.3.3), and therefore

$$H(n + \alpha_n) + 1 - 4\alpha_n = 0, \qquad (4.4.8)$$
$$H(n + \beta_n) - 3 + 4\beta_n = 0. \qquad (4.4.9)$$

The six exact nonlinear difference equations (4.4.3), (4.4.5), and (4.4.6)-(4.4.9) govern the operation of the amplifier when a constant signal is input. Recall that for the first-order negative feedback amplifier we investigated in chapter 3, the model was governed by only four equations. The additional two equations arise here because the integrator in the first-order negative feedback amplifier is replaced in the second-order amplifier by a second-order loop filter. We saw that the integrator output was defined by a first-order differential equation with one continuity condition, whereas here the second-order loop filter output, $H(t)$, is defined by a second-order differential equation with two continuity conditions. Therefore solving to find $H(t)$ results in two additional equations here. Because of this increased complexity, using the streamlined formulation introduced in chapter 3 is even more advantageous here.

As discussed in chapter 3, we could in principle numerically iterate the governing equations for particular parameter values, obtaining the switching times, and thus the output $g(t)$. However, by doing this we would learn little about the behaviour of the amplifier. Therefore, as in chapter 3, we proceed by assuming that after a transient state, the system reaches a steady state. We obtain the steady-state solutions analytically in §4.4.1, and then in §4.4.2 verify those solutions by numerically iterating the exact governing equations.

4.4.1 Exact steady-state solution for a constant input signal

We now look for exact steady-state solutions to the six dimensionless equations (4.4.3), (4.4.5), (4.4.6)-(4.4.9) governing the operation of the amplifier for a constant input signal.

Setting

$$\begin{aligned}
\alpha_{n+1} &= \alpha_n, \\
H(n+1+\alpha_{n+1}) &= H(n+\alpha_n), \\
\dot{H}(n+1+\alpha_{n+1}^+) &= \dot{H}(n+\alpha_n^+),
\end{aligned}$$

in the governing equations the only changes are to (4.4.5) and (4.4.7), which become respectively

$$\begin{aligned}
H(n+\alpha_n) &= H(n+\beta_n) + \dot{H}(n+\beta_n^+)(1+\alpha_n-\beta_n) \\
&\quad - \frac{k_3}{2}(1+s_0)(1+\alpha_n-\beta_n)^2, \qquad (4.4.10) \\
\dot{H}(n+\alpha_n^+) &= \dot{H}(n+\beta_n^+) + 2k_2 - k_3(1+s_0)(1+\alpha_n-\beta_n). \qquad (4.4.11)
\end{aligned}$$

Thus the steady-state equations are (4.4.3), (4.4.6), (4.4.8)-(4.4.11).

Eliminating $\dot{H}(n+\alpha_n^+)$ and $\dot{H}(n+\beta_n^+)$ from (4.4.6) and (4.4.11) we can immediately find an equation relating the switching times,

$$\beta_n - \alpha_n = \frac{1}{2}(1+s_0), \qquad (4.4.12)$$

and the short-time average of $g(t)$, defined by (2.3.10),

$$\langle g(t) \rangle = -s_0. \qquad (4.4.13)$$

These two results are the same as those for a first-order negative feedback amplifier, and as before we see that the restriction $s_0 < 1$ ensures that $0 < \beta_n - \alpha_n < 1$ for correct operation of the amplifier. Therefore we see that the second-order loop filter in this design has not altered these important results.

Solving the exact steady-state equations we now find

$$\begin{aligned}
\alpha_n &= \frac{1}{16}(1-s_0)[4-k_2(1+s_0)], \qquad &(4.4.14) \\
\beta_n &= \frac{1}{2} + \frac{1}{16}(1+s_0)[4-k_2(1-s_0)], \qquad &(4.4.15) \\
H(n+\alpha_n) &= -s_0 + \frac{k_2}{4}\left(s_0^2-1\right), \qquad &(4.4.16) \\
H(n+\beta_n) &= -s_0 - \frac{k_2}{4}\left(s_0^2-1\right), \qquad &(4.4.17) \\
\dot{H}(n+\alpha_n^+) &= \frac{1}{4}(1-s_0)(4k_2-k_3(1+s_0)), \qquad &(4.4.18) \\
\dot{H}(n+\beta_n^+) &= \frac{1}{4}(1+s_0)(k_3(1-s_0)-4k_2). \qquad &(4.4.19)
\end{aligned}$$

Comparing the switching times (4.4.14) and (4.4.15) with those for a first-order negative feedback amplifier, (3.4.11) and (3.4.12), we see that they are the same, except that the

integrator constant k_1 is replaced by the second-order loop filter constant k_2. Recalling that the integrator in the first-order design is replaced in this second-order design by the second-order loop filter, it is evident that k_1 and k_2 are comparable. Since a constant input signal is the limiting case of a slowly-varying general input signal, we therefore also expect the leading-order switching times for a general input signal for the first-order negative feedback design to be equivalent to those for the second-order amplifier.

As the switching times are the same for the first-order negative feedback amplifier as here (except for the difference in parameters) and the same restrictions (4.3.6)-(4.3.8) apply for both designs, we find that for correct operation, k_2 must satisfy the same condition here as k_1 for the first-order negative feedback amplifier, namely

$$0 < k_2 < 2. \tag{4.4.20}$$

The solution for $H(t)$ is given by (4.4.2) for $n + \alpha_n < t < n + \beta_n$, and (4.4.4) for $n + \beta_n < t < n + 1 + \alpha_{n+1}$. The constants $H(n + \alpha_n)$, $H(n + \beta_n)$, $\dot{H}(n + \alpha_n^+)$ and $\dot{H}(n + \beta_n^+)$ are given by (4.4.16)-(4.4.19). In the next section we plot $H(t)$ to see more clearly how it behaves for different parameter values.

4.4.1.1 Graphs of second-order loop filter output and carrier wave

In figure 4.5 we plot the second-order loop filter output $H(t)$ and minus the carrier wave $v(t)$ over one carrier wave period, for a constant input signal $s(t) = -0.25$. We choose the parameter values $k_2 = 0.5$ and 1.5 which satisfy (4.4.20), and $k_3 = 0.5$ and 5 so that $k_3 = O(1)$.

The switching times of $g(t)$ are defined to be the times at which $H(t) + v(t) = 0$. Therefore the times at which $H(t)$ and $-v(t)$ intersect in figure 4.5 are the switching times for a constant input signal. The switching times are independent of k_3 but dependent on k_2. For $k_2 = 0.5$ in figures 4.5(a) and (c), $\alpha_n = \frac{145}{512}$ and $\beta_n = \frac{337}{512}$. For $k_2 = 1.5$ in figures 4.5(b) and (d), $\alpha_n = \frac{115}{512}$ and $\beta_n = \frac{307}{512}$. Therefore as predicted by (4.4.12), we see that $\beta_n - \alpha_n = \frac{3}{8}$ in both cases.

Comparing the four graphs in figure 4.5 we observe that as we increase k_2, $H(t)$ becomes more piecewise linear, but as we increase k_3, $H(t)$ becomes more piecewise quadratic. This is justified by the solutions for $H(t)$ (given by (4.4.2) for $n + \alpha_n < t < n + \beta_n$, and (4.4.4) for $n + \beta_n < t < n + 1 + \alpha_{n+1}$), where terms linear in time contain a factor of k_2, but the term quadratic in time is independent of k_2 but dependent on k_3.
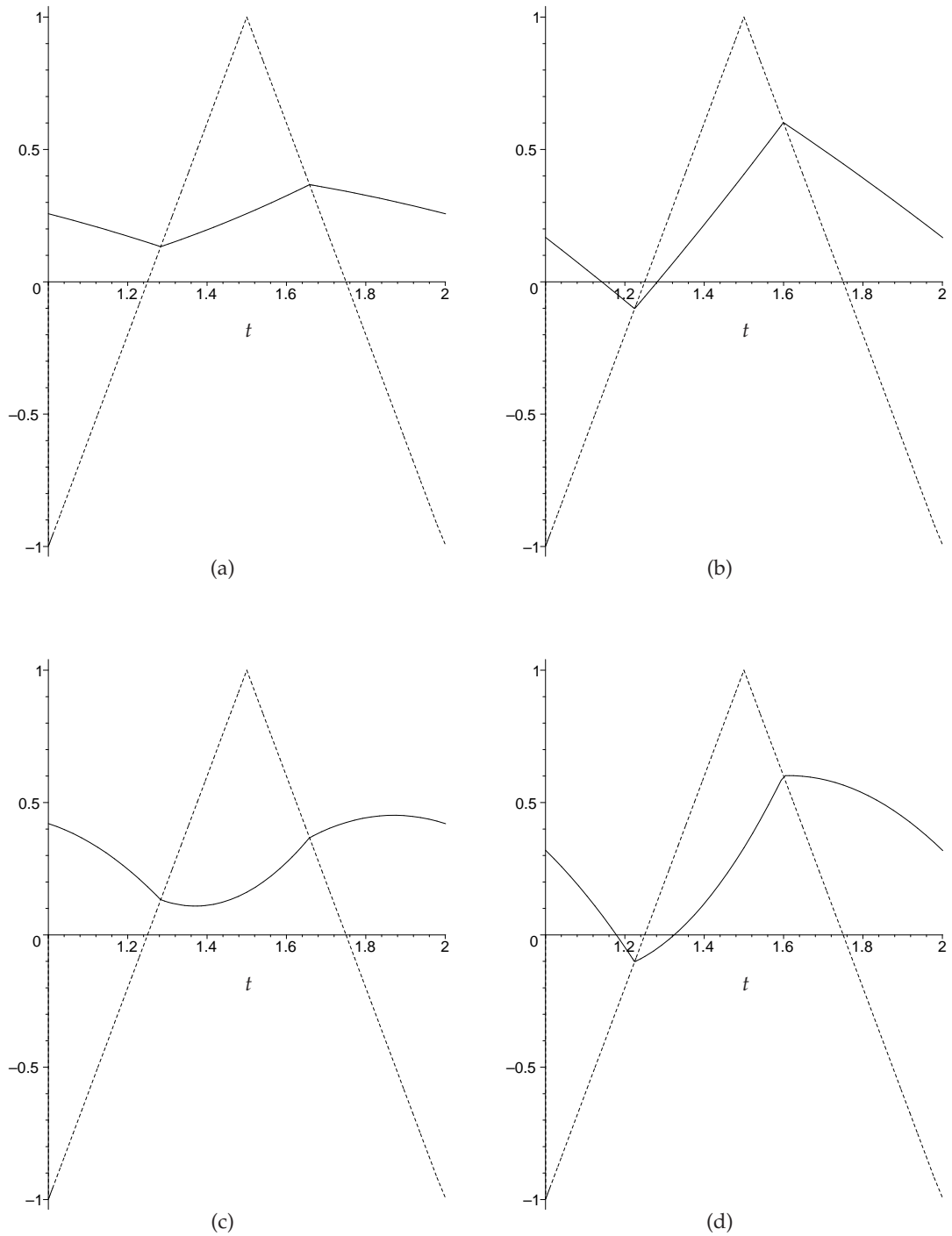
Figure 4.5: For $s_0 = -0.25$. The second-order loop filter output $H(t)$ (solid line) and minus the carrier wave $-v(t)$ (dotted line) for (a) $k_2 = 0.5$, $k_3 = 0.5$, (b) $k_2 = 1.5$, $k_3 = 0.5$, (c) $k_2 = 0.5$, $k_3 = 5$, and (d) $k_2 = 1.5$, $k_3 = 5$.

4.4.2 Numerical simulation of switching times

In the previous section we established the steady-state solutions to the six exact nonlinear difference equations (4.4.3), (4.4.5), and (4.4.6)-(4.4.9), which govern the amplifier when a constant signal is input. We now verify these results by comparing them with numerical simulations of the six equations in Maple.

We take $\alpha_0 = 0$ and $\dot{H}(0) = 0$ arbitrarily, since the initial conditions of the amplifier are unknown, and numerically iterate the six difference equations. We thus obtain the numerical switching times, which we compare with the analytical steady-state switching times, (4.4.14) and (4.4.15). After an initial transient state, which occurs because we choose the initial conditions of the amplifier arbitrarily, we find that the numerical switching times converge to our analytical steady-state solutions. For example, for $s_0 = -0.25$, $k_2 = 0.5$ and $k_3 = 0.5$, after approximately 100 carrier wave periods, the numerical switching times converge to $\alpha_n = 0.283203125$ and $\beta_n = 0.658203125$, as predicted by our analytical steady-state solutions. Therefore we see that, as for first-order negative feedback in chapter 3, because a typical carrier wave frequency is high, the transient state lasts for such a short time that it is not perceived by the amplifier user.

For this second-order negative feedback amplifier, we have found the analytical steady-state solutions for a constant input signal via a concise analysis, and verified these by comparison with a numerical simulation of the exact equations. Notably, the steady-state solutions for a constant input signal are the same as the leading-order solutions for a general input signal, which will help us considerably in our aim to solve the model for a general input signal in the following section.

4.5 Dimensionless model for a general input signal

Having found the steady state solution for a constant input signal, we now investigate the amplifier when a general signal is input. We use the method of analysis introduced in chapter 3. Thus we start by determining the nonlinear difference equations governing the amplifier for a general input signal, then convert the discrete model to a continuous one and solve using perturbation expansions to find the switching times of the output. Finally, we use the formula giving the audio output of the amplifier in terms of its switching times, (3.5.21), obtained in chapter 3, to establish the audio-frequency components of the amplifier output.

We therefore begin by considering the governing equations for the amplifier, (4.3.3)-(4.3.5) and (4.3.9), and the continuity conditions (4.3.10) and (4.3.11). We first integrate

the second-order differential equation for $H(t)$, (4.3.9), separately over the two regions defined by figure 4.4 to obtain

$$
H(t) - H(t_0) - \dot{H}(t_0^+)(t - t_0) + k_2[r(t) - r(t_0) - s(t_0)(t - t_0)]
$$
$$
+k_3[q(t) - q(t_0) - r(t_0)(t - t_0)] = \begin{cases} \frac{k_3}{2}(t - t_0)^2 & \text{in region I} \\ -\frac{k_3}{2}(t - t_0)^2 & \text{in region II,} \end{cases} \tag{4.5.1}
$$

where t_0 is the time at the beginning of the region, and $r(t)$ and $q(t)$ are defined respectively as the integral and double integral of the input signal $s(t)$. Since $H(t)$ is continuous by (4.3.10), evaluating (4.5.1) at the end of region I, for $n + \alpha_n < t < n + \beta_n$, we obtain

$$
\begin{aligned}
H(n + \beta_n) &= H(n + \alpha_n) + \dot{H}(n + \alpha_n^+)(\beta_n - \alpha_n) \\
&\quad - k_2 \left[r(n + \beta_n) - r(n + \alpha_n) - s(n + \alpha_n)(\beta_n - \alpha_n) \right] \\
&\quad - k_3 \bigg[q(n + \beta_n) - q(n + \alpha_n) - r(n + \alpha_n)(\beta_n - \alpha_n) \\
&\quad - \frac{1}{2}(\beta_n - \alpha_n)^2 \bigg].
\end{aligned} \tag{4.5.2}
$$

Similarly, evaluating (4.5.1) at the end of region II, for $n + \beta_n < t < n + 1 + \alpha_{n+1}$, we obtain

$$
\begin{aligned}
H(n + 1 + \alpha_{n+1}) &= H(n + \beta_n) + \dot{H}(n + \beta_n^+)(1 + \alpha_{n+1} - \beta_n) \\
&\quad - k_2 \left[r(n + 1 + \alpha_{n+1}) - r(n + \beta_n) - s(n + \beta_n)(1 + \alpha_{n+1} - \beta_n) \right] \\
&\quad - k_3 \bigg[q(n + 1 + \alpha_{n+1}) - q(n + \beta_n) - r(n + \beta_n)(1 + \alpha_{n+1} - \beta_n) \\
&\quad + \frac{1}{2}(1 + \alpha_{n+1} - \beta_n)^2 \bigg].
\end{aligned} \tag{4.5.3}
$$

Applying the second continuity condition (4.3.11) at $t = n + \beta_n$ we find

$$
\begin{aligned}
\dot{H}(n + \beta_n^+) &= \dot{H}(n + \alpha_n^+) - 2k_2 - k_2[s(n + \beta_n) - s(n + \alpha_n)] \\
&\quad - k_3[r(n + \beta_n) - r(n + \alpha_n) + \alpha_n - \beta_n],
\end{aligned} \tag{4.5.4}
$$

and applying the same at $t = n + 1 + \alpha_{n+1}$ gives

$$
\begin{aligned}
\dot{H}(n + 1 + \alpha_{n+1}^+) &= \dot{H}(n + \beta_n^+) + 2k_2 - k_2[s(n + 1 + \alpha_{n+1}) - s(n + \beta_n)] \\
&\quad - k_3[r(n + 1 + \alpha_{n+1}) - r(n + \beta_n) + 1 + \alpha_{n+1} - \beta_n]. \tag{4.5.5}
\end{aligned}
$$

The four equations (4.5.2)-(4.5.5) relate $H(t)$, $q(t)$, $r(t)$ and $s(t)$, evaluated at the switching times, to the switching times themselves. By considering the definition of the switching times, (4.3.5), we now determine three equations directly relating $H(t)$ evaluated at the switching times to the switching times themselves.

The switching times for this design are the times at which $H(t) + v(t) = 0$. By considering the restrictions on the switching times, (4.3.6) and (4.3.7), we find $v(t)$ at the switching times from (4.3.3), and thus obtain

$$H(n + \alpha_n) + 1 - 4\alpha_n = 0, \tag{4.5.6}$$

$$H(n + \beta_n) - 3 + 4\beta_n = 0, \tag{4.5.7}$$

$$H(n + 1 + \alpha_{n+1}) + 1 - 4\alpha_{n+1} = 0. \tag{4.5.8}$$

Our aim is to determine the audio part of the amplifier output, where the amplifier output is defined only by its switching times. Therefore, since we will not need to calculate $H(t)$, to simplify our model we now eliminate as many terms in $H(t)$ as possible. We use (4.5.2), (4.5.4), (4.5.6) and (4.5.8) to eliminate $H(n + \beta_n)$, $\dot{H}(n + \beta_n^+)$, $H(n + \alpha_n)$ and $H(n + 1 + \alpha_{n+1})$ respectively, and after some effort we are left with just three equations,

$$
\begin{aligned}
4(1 - \alpha_n - \beta_n) = {} & \dot{H}(n + \alpha_n^+)(\beta_n - \alpha_n) \\
& - k_2 \left[r(n + \beta_n) - r(n + \alpha_n) - s(n + \alpha_n)(\beta_n - \alpha_n) \right] \\
& - k_3 \Big[q(n + \beta_n) - q(n + \alpha_n) - r(n + \alpha_n)(\beta_n - \alpha_n) \\
& \quad - \frac{1}{2}(\beta_n - \alpha_n)^2 \Big],
\end{aligned}
\tag{4.5.9}
$$

$$
\begin{aligned}
4(\alpha_{n+1} + \beta_n - 1) = {} & \dot{H}(n + \alpha_n^+)(1 + \alpha_{n+1} - \beta_n) - k_2 [r(n + 1 + \alpha_{n+1}) - r(n + \beta_n) \\
& + [2 - s(n + \alpha_n)](1 + \alpha_{n+1} - \beta_n)] \\
& - k_3 \Big[q(n + 1 + \alpha_{n+1}) - q(n + \beta_n) - r(n + \alpha_n)(1 + \alpha_{n+1} - \beta_n) \\
& \quad + \frac{1}{2}(1 + \alpha_{n+1} - \beta_n)(1 + \alpha_{n+1} + 2\alpha_n - 3\beta_n) \Big],
\end{aligned}
\tag{4.5.10}
$$

$$
\begin{aligned}
\dot{H}(n + 1 + \alpha_{n+1}^+) = {} & \dot{H}(n + \alpha_n^+) - k_2 [s(n + 1 + \alpha_{n+1}) - s(n + \alpha_n)] \\
& - k_3 [r(n + 1 + \alpha_{n+1}) - r(n + \alpha_n) \\
& + 1 + \alpha_{n+1} + \alpha_n - 2\beta_n].
\end{aligned}
\tag{4.5.11}
$$

These three equations are the nonlinear difference equations governing the amplifier for a general input signal. By implementing the streamlined formulation introduced in chapter 3 we have derived as concise a system as possible. This will enable us to solve the model, which is clearly more complex than that for the first-order negative feedback amplifier, and thus to establish the switching times and the audio-frequency components of the amplifier output.

As discussed in chapter 3, we can specify the input signal and parameter values and then iterate the system of difference equations numerically to obtain the switching

times, but would learn only about a particular case via this method. Therefore, as in chapter 3, we seek an analytical solution to the system for a general input signal, and so proceed by converting the discrete system into a continuous one that we will be able to solve analytically.

4.5.1 Continuous model

We now transform the discrete system of governing equations (4.5.9)-(4.5.11) into a continuous one, in order to solve it analytically. Thus we will derive the switching times of the output, which will allow us to determine the audio-frequency components of the amplifier output.

The configuration of the continuous model is the same as that for first-order negative feedback, except that some extensions are required here to manage the increased complexity of the model for the second-order negative feedback design. Thus we start by defining

$$s(t) = S(\sigma),$$

where σ is the dimensionless slow time, $\sigma = \epsilon t$, and $\epsilon = \omega_a T \ll 1$, where ω_a is a typical audio frequency. We define a function $R(\sigma)$, as in chapter 3, as well as a new function $Q(\sigma)$,

$$R(\sigma) = \epsilon r(t), \tag{4.5.12}$$
$$Q(\sigma) = \epsilon^2 q(t), \tag{4.5.13}$$

so that $R(\sigma)$ and $Q(\sigma)$ are related simply to $S(\sigma)$,

$$\frac{d}{d\sigma}R(\sigma) = S(\sigma),$$
$$\frac{d^2}{d\sigma^2}Q(\sigma) = S(\sigma).$$

We use the same two $O(1)$ functions $A(\sigma)$ and $B(\sigma)$ as in chapter 3, but also introduce a new $O(1)$ function $\nu(\sigma)$. The three functions are defined by their values at discrete points,

$$A(\epsilon n) = \alpha_n, \tag{4.5.14}$$
$$B(\epsilon n) = \beta_n, \tag{4.5.15}$$
$$\nu(\epsilon n) = \dot{H}(n + \alpha_n^+). \tag{4.5.16}$$

Thus $A(\epsilon n)$ and $B(\epsilon n)$ are the respectively the trailing- and leading-edge switching times in the nth period, whilst $\nu(\epsilon n)$ is a sample of the derivative of the loop filter

output. As in chapter 3 with these definitions we write α_{n+1} in terms of the slowly-varying function A, but here also write $\dot{H}(n+1+\alpha_{n+1}^+)$ in terms of the slowly-varying function ν, thus

$$
\begin{aligned}
\alpha_{n+1} &= A(\epsilon(n+1)), \\
\dot{H}(n+1+\alpha_{n+1}^+) &= \nu(\epsilon(n+1)).
\end{aligned}
$$

To complete the definitions of the three functions $A(\sigma)$, $B(\sigma)$ and $\nu(\sigma)$ we now interpolate smoothly between these discrete points ensuring that each function is continuous and smooth. This allows us to write the three nonlinear difference equations, (4.5.9)-(4.5.11), in terms of the functions $A(\sigma)$, $B(\sigma)$ and $\nu(\sigma)$. In (4.5.9)-(4.5.11) we therefore replace

$$
\begin{aligned}
\alpha_n &\quad\text{by}\quad A(\sigma), \\
\alpha_{n+1} &\quad\text{by}\quad A(\sigma+\epsilon), \\
\beta_n &\quad\text{by}\quad B(\sigma), \\
\dot{H}(n+\alpha_n^+) &\quad\text{by}\quad \nu(\sigma), \\
\dot{H}(n+1+\alpha_{n+1}^+) &\quad\text{by}\quad \nu(\sigma+\epsilon).
\end{aligned}
$$

Hence we see that the functions $A(\sigma)$, $B(\sigma)$ and $\nu(\sigma)$ at times $t = n$, i.e. $\sigma = \epsilon n$, take the values of α_n, β_n and $\dot{H}(n+\alpha_n^+)$ respectively, and all three functions are slowly-varying with respect to time t.

We can now appreciate more fully why eliminating $H(n+\alpha_n)$ (and $H(n+1+\alpha_{n+1})$), $H(n+\beta_n)$ and $\dot{H}(n+\beta_n^+)$ from the difference equations simplifies the model so drastically. If we had not eliminated these terms, we would have to introduce three additional slowly-varying functions, unnecessarily complicating the model. One function would be required to accommodate the samples $H(n+\alpha_n)$, one for $H(n+\beta_n)$, and one for $\dot{H}(n+\beta_n^+)$. The argument for needing to define separate functions for the samples $H(n+\alpha_n)$ and $H(n+\beta_n)$ is simply that the values of $H(n+\alpha_n)$ and $H(n+\beta_n)$ differ from each other by up to an $O(1)$ amount in each period, and so no slowly-varying function of time can simultaneously interpolate both functions. The necessity of defining one function for the samples $\dot{H}(n+\beta_n^+)$ follows from the corresponding argument for the samples $\dot{H}(n+\alpha_n^+)$ and $\dot{H}(n+\beta_n^+)$.

Eliminating $H(n+\alpha_n)$ (and $H(n+1+\alpha_{n+1})$), $H(n+\beta_n)$ and $\dot{H}(n+\beta_n^+)$ from the difference equations therefore results in a more streamlined formulation of the continuous model: we need to define only the three slowly-varying functions $A(\sigma)$, $B(\sigma)$ and $\nu(\sigma)$ as above. In addition to the factors taken into account when defining $A(\sigma)$ and $B(\sigma)$, discussed in chapter 3, there is another point of significance in the definitions here. Namely, we have established that $\dot{H}(n+\alpha_n^+) = O(1)$ by referring to the

steady-state solution for $\dot{H}(n + \alpha_n^+)$ for a constant input signal, (4.4.11), and hence the definition of $\nu(\sigma)$, (4.5.16).

As discussed in chapter 3, we write $r(t)$ at the switching times in terms of R, σ, A and B, so that, for example, $r(n + \alpha_n)$ is replaced by $\frac{1}{\epsilon}R(\sigma + \epsilon A(\sigma))$. Our model here also includes $q(t)$ at the switching times, and so we must also convert these terms to continuous ones. We use the definitions of $R(\sigma)$, $Q(\sigma)$, $A(\sigma)$ and $B(\sigma)$, (4.5.12)-(4.5.15), to do this. For example,

$$q(n + \alpha_n) = q(n + A(\epsilon n)),$$

which, in our continuous model, we replace by $q(t + A(\epsilon t))$. We then write

$$q(t + A(\epsilon t)) = \frac{1}{\epsilon^2}Q(\epsilon t + \epsilon A(\epsilon t))$$
$$= \frac{1}{\epsilon^2}Q(\sigma + \epsilon A(\sigma)).$$

We may now convert the discrete system of three nonlinear difference equations (4.5.9)-(4.5.11) into a continuous one. Writing each in terms of our new functions, (4.5.9) becomes

$$
4(1 - A(\sigma) - B(\sigma)) = \nu(\sigma)(B(\sigma) - A(\sigma))
$$
$$
- k_2\left[\frac{1}{\epsilon}R(\sigma + \epsilon B(\sigma)) - \frac{1}{\epsilon}R(\sigma + \epsilon A(\sigma)) - S(\sigma + \epsilon A(\sigma))(B(\sigma) - A(\sigma))\right]
$$
$$
- k_3\left[\frac{1}{\epsilon^2}Q(\sigma + \epsilon B(\sigma)) - \frac{1}{\epsilon^2}Q(\sigma + \epsilon A(\sigma)) - \frac{1}{\epsilon}R(\sigma + \epsilon A(\sigma))(B(\sigma) - A(\sigma))\right.
$$
$$
\left. - \frac{1}{2}(B(\sigma) - A(\sigma))^2\right], \tag{4.5.17}
$$

and then (4.5.10) becomes

$$
4(A(\sigma + \epsilon) + B(\sigma) - 1) = \nu(\sigma)(1 + A(\sigma + \epsilon) - B(\sigma))
$$
$$
- k_2\left[\frac{1}{\epsilon}R(\sigma + \epsilon + \epsilon A(\sigma + \epsilon)) - \frac{1}{\epsilon}R(\sigma + \epsilon B(\sigma))\right.
$$
$$
+ \left[2 - S(\sigma + \epsilon A(\sigma))\right](1 + A(\sigma + \epsilon) - B(\sigma))\right] - k_3\left[\frac{1}{\epsilon^2}Q(\sigma + \epsilon + \epsilon A(\sigma + \epsilon))\right.
$$
$$
- \frac{1}{\epsilon^2}Q(\sigma + \epsilon B(\sigma)) - \frac{1}{\epsilon}R(\sigma + \epsilon A(\sigma))(1 + A(\sigma + \epsilon) - B(\sigma))
$$
$$
\left. + \frac{1}{2}(1 + A(\sigma + \epsilon) - B(\sigma))(1 + A(\sigma + \epsilon) + 2A(\sigma) - 3B(\sigma))\right], \tag{4.5.18}
$$

and finally, (4.5.11) becomes

$$
\nu(\sigma + \epsilon) = \nu(\sigma) - k_2[S(\sigma + \epsilon + \epsilon A(\sigma + \epsilon)) - S(\sigma + \epsilon A(\sigma))]
$$
$$
- k_3\left[\frac{1}{\epsilon}R(\sigma + \epsilon + \epsilon A(\sigma + \epsilon)) - \frac{1}{\epsilon}R(\sigma + \epsilon A(\sigma))\right.
$$
$$
\left. + 1 + A(\sigma + \epsilon) + A(\sigma) - 2B(\sigma)\right]. \tag{4.5.19}
$$

In spite of our streamlined formulation, these three equations are obviously too complicated to allow an exact solution, and so, as in chapter 3, we now seek a perturbation solution to these equations. We expand $A(\sigma)$, $B(\sigma)$ and $\nu(\sigma)$ as series in ϵ, where

$$
\begin{aligned}
A(\sigma) &= \sum_{m=0}^{\infty} \epsilon^m A_m(\sigma), \\
B(\sigma) &= \sum_{m=0}^{\infty} \epsilon^m B_m(\sigma), \\
\nu(\sigma) &= \sum_{m=0}^{\infty} \epsilon^m \nu_m(\sigma).
\end{aligned}
$$

As detailed in chapter 3, we expand the remaining functions in (4.5.17)-(4.5.19) as Taylor series in ϵ, for example

$$
\begin{aligned}
Q(\sigma + \epsilon A(\sigma)) &= Q(\sigma) + \epsilon A(\sigma)\frac{d}{d\sigma}Q(\sigma) + \frac{\epsilon^2}{2}A(\sigma)^2\frac{d^2}{d\sigma^2}Q(\sigma) \\
&\quad + \frac{\epsilon^3}{6}A(\sigma)^3\frac{d}{d\sigma}S(\sigma) + O\left(\epsilon^4\right) \\
&= Q(\sigma) + \epsilon A_0(\sigma)R(\sigma) + \epsilon^2\left(A_1(\sigma)R(\sigma) + \frac{1}{2}A_0(\sigma)^2 S(\sigma)\right) \\
&\quad + \epsilon^3\left(A_0(\sigma)A_1(\sigma)S(\sigma) + A_2(\sigma)R(\sigma) + \frac{1}{6}A_0(\sigma)^3\frac{d}{d\sigma}S(\sigma)\right) \\
&\quad + O\left(\epsilon^4\right),
\end{aligned}
$$

where we have used $\frac{d}{d\sigma}Q(\sigma) = R(\sigma)$ and $\frac{d^2}{d\sigma^2}Q(\sigma) = S(\sigma)$. We then consider the three equations at successive orders in ϵ. Note that we do not rearrange the following equations, so that the source of each term can be seen more easily.

At $O(1)$, from (4.5.17) we find

$$
\begin{aligned}
4(1 - A_0 - B_0) &= \nu_0(B_0 - A_0) \\
&\quad - k_3\left[\frac{1}{2}A_0^2 S + \frac{1}{2}B_0^2 S - A_0 B_0 S - \frac{1}{2}(B_0 - A_0)^2\right],
\end{aligned} \tag{4.5.20}
$$

from (4.5.18) we find

$$
\begin{aligned}
4(A_0 + B_0 - 1) &= \nu_0(1 + A_0 - B_0) - 2k_2[1 + A_0 - B_0] - k_3\left[-\frac{1}{2}A_0^2 S - \frac{1}{2}B_0^2 S\right. \\
&\quad \left. + A_0 B_0 S + \frac{1}{2} + 2A_0 - 2B_0 + \frac{3}{2}A_0^2 - 3A_0 B_0 + \frac{3}{2}B_0^2\right],
\end{aligned} \tag{4.5.21}
$$

and from (4.5.19) we obtain

$$
0 = -k_3[S + 2A_0 - 2B_0 + 1]. \tag{4.5.22}
$$

Immediately from (4.5.22) we see that

$$
B_0 - A_0 = \frac{1}{2}(1 + S),
$$

and therefore find that the $O(1)$ short-time average of $g(t)$ is $-S$. If we compare these results with their equivalents for a constant input signal, (4.4.12) and (4.4.13), we see that they agree. This should be anticipated because we have assumed that the general input signal is slowly-varying, and so to leading order the signal is constant. Thus, the leading-order switching times for a general input signal should correspond with those for a constant input signal, (4.4.14) and (4.4.15). Solving our three $O(1)$ equations (4.5.20)-(4.5.22) simultaneously we find this is the case, and so

$$A_0 = \frac{1}{16}(1 - S)\left[4 - k_2(1 + S)\right], \tag{4.5.23}$$

$$B_0 = \frac{1}{2} + \frac{1}{16}(1 + S)\left[4 - k_2(1 - S)\right]. \tag{4.5.24}$$

It is interesting to note that these are the same as the leading-order switching times for the first-order negative feedback amplifier we investigated in chapter 3, equations (3.5.15) and (3.5.15), except that the integrator constant k_1 is replaced here by the second-order loop filter constant k_2. Thus we see that the only effect to leading order of the differences in the design of the second-order amplifier we examine here, compared with the first-order negative feedback amplifier (the use of a second-order loop filter instead of an integrator, and the removal of the multiplier), is a change of constant, and thus we expect the leading-order component of the amplifier output to be the same as for the first-order negative feedback amplifier, namely $-S(\sigma)$.

We also note that from our $O(1)$ switching times we can obtain an $O(1)$ duty cycle (the ratio between the length of time the wave is at $+1$ and the period of the carrier wave) in agreement with equation (8) of [39]. The authors of [39] do not present the switching times themselves though, and their result is determined only for a sinusoidal input signal, unlike ours here which is valid for a general input signal. In addition, the results of [39] are further limited because the authors do not calculate the distortion terms in the amplifier output, as is our aim here.

To determine the audio-frequency components of the amplifier output we will use the formula (3.5.21) derived in chapter 3, which gives the output we desire in terms of its switching times. Thus to reach our goal we need to compute only the switching times. We wish to find the audio part of the output up to $O(\epsilon^3)$, which will give the first nonlinear term, and so we must find switching times up to $O(\epsilon^3)$ also.

To obtain the $O(\epsilon)$ switching times we first establish (4.5.17)-(4.5.19) at $O(\epsilon)$. (4.5.17)

gives

$$-4(A_1 + B_1) = \nu_0(B_1 - A_1) + \nu_1(B_0 - A_0) - k_2\left[\frac{1}{2}A_0^2\frac{dS}{d\sigma} + \frac{1}{2}B_0^2\frac{dS}{d\sigma} - A_0B_0\frac{dS}{d\sigma}\right]$$
$$- k_3\left[A_0A_1S + B_0B_1S - A_0B_1S - A_1B_0S + \frac{1}{3}A_0^3\frac{dS}{d\sigma} - \frac{1}{2}A_0^2B_0\frac{dS}{d\sigma} + \frac{1}{6}B_0^3\frac{dS}{d\sigma}\right.$$
$$\left. - A_0A_1 - B_0B_1 + A_0B_1 + A_1B_0\right], \tag{4.5.25}$$

while (4.5.18) gives

$$4\left(A_1 + \frac{dA_0}{d\sigma} - B_1\right) = \nu_0\left(A_1 + \frac{dA_0}{d\sigma} + B_1\right) + \nu_1(1 + A_0 - B_0)$$
$$- k_2\left[\frac{1}{2}\frac{dS}{d\sigma} - \frac{1}{2}A_0^2\frac{dS}{d\sigma} - \frac{1}{2}B_0^2\frac{dS}{d\sigma} + 2A_1 + 2\frac{dA_0}{d\sigma} - 2B_1 + A_0B_0\frac{dS}{d\sigma}\right]$$
$$- k_3\left[\frac{1}{6}\frac{dS}{d\sigma} + \frac{1}{2}A_0\frac{dS}{d\sigma} - \frac{1}{3}A_0^3\frac{dS}{d\sigma} + \frac{1}{2}A_0^2B_0\frac{dS}{d\sigma} - \frac{1}{6}B_0^3\frac{dS}{d\sigma} - A_0A_1S + A_0B_1S\right.$$
$$+ A_1B_0S + \frac{dA_0}{d\sigma}S + 2A_1 + \frac{dA_0}{d\sigma} - 2B_1 + 2A_0\frac{dA_0}{d\sigma} - 2B_0\frac{dA_0}{d\sigma} + 3A_0A_1 + 3B_0B_1$$
$$\left. - 3A_0B_1 - 3A_1B_0\right], \tag{4.5.26}$$

and (4.5.19) yields

$$\frac{d\nu_0}{d\sigma} = -k_2\frac{dS}{d\sigma} - k_3\left[\frac{1}{2}\frac{dS}{d\sigma} + A_0\frac{dS}{d\sigma} + \frac{dA_0}{d\sigma}S + 2A_1 + \frac{dA_0}{d\sigma} - 2B_1\right]. \tag{4.5.27}$$

Solving the three equations (4.5.25)-(4.5.27) simultaneously, and substituting in our $O(1)$ solutions, we obtain the $O(\epsilon)$ switching times

$$A_1 = \frac{1}{192}\frac{dS}{d\sigma}(S-1)\left[12 - 3k_2 + (3k_2^2 - 9k_2 - k_3)S + (3k_2^2 - k_3)S^2\right], \tag{4.5.28}$$
$$B_1 = \frac{1}{192}\frac{dS}{d\sigma}\left[36 - 3k_2 + (12 + 18k_2 - 3k_2^2 + k_3)S + 9k_2S^2\right.$$
$$\left. + (3k_2^2 - k_3)S^3\right]. \tag{4.5.29}$$

Similarly, to determine the $O(\epsilon^2)$ switching times, we consider each of the three equations (4.5.17)-(4.5.19) at $O(\epsilon^2)$, and then solve the resulting equations simultaneously to find A_2 and B_2. As can be seen from the analysis so far, the equations and solutions for higher orders of ϵ become progressively algebraically long, and so we do not display the $O(\epsilon^2)$ equations and solutions here. We do note however, that the solutions for A_2 and B_2 contain S, its derivatives up to the second with respect to σ, as well as nonlinear combinations of these terms.

Having derived the switching times up to $O(\epsilon^3)$, we are now able to find the amplifier output.

4.5.1.1 Calculation of $g(t)$, the amplifier output

The formula (3.5.21) we established for the audio-frequency components of the amplifier output in chapter 3 is valid for any amplifier. This formula gives $g_a(t)$, the audio part of the amplifier output, in terms of only the switching times of $g(t)$, and thus to find the output for the second-order negative feedback amplifier here, all that remains to do is to insert our switching time solutions.

We aim to find the audio-frequency components of the amplifier output up to $O(\epsilon^3)$, and so substituting our switching time solutions (4.5.23), (4.5.24), (4.5.28), (4.5.29), and the lengthy $O(\epsilon^2)$ solutions into (3.5.21) we obtain

$$g_a(t) = -S(\sigma) + \frac{\epsilon^2}{24k_3}\frac{d^2}{d\sigma^2}\left[(24 + k_3)S(\sigma) - k_3 S(\sigma)^3\right] + O(\epsilon^3). \qquad (4.5.30)$$

This result gives the leading audio-frequency components of the amplifier output for a general input signal, and as such is a considerable achievement made possible through our concise formulation of the problem. As anticipated, the leading-order component is exactly minus the input signal. It is noteworthy that there is no $O(\epsilon)$ distortion, but there is nonlinear distortion at $O(\epsilon^2)$, which cannot be removed by any choice of parameter $k_3 > 0$.

Specifying the input signal to be sinusoidal, $S(\sigma) = s_0 \sin\sigma$, (4.5.30) becomes

$$g_a(t) = -s_0 \sin\sigma + \frac{\epsilon^2}{96k_3}\left[(-(96 + 4k_3)s_0 + 3k_3 s_0^3)\sin\sigma - 9k_3 s_0^3 \sin 3\sigma\right] + O(\epsilon^3),$$

and if we revert to dimensional terms we find

$$\begin{aligned}
g_a^*(t^*) &= -s_0 V \sin\omega_a t^* \\
&\quad + \frac{\omega_a^2 V}{96}C_1 C_2 R_1 R_2\left[\left(-\left(96 + \frac{4T^2}{C_1 C_2 R_1 R_2}\right)s_0 + \frac{3T^2}{C_1 C_2 R_1 R_2}s_0^3\right)\sin\omega_a t^* \right.\\
&\quad \left. - \frac{9T^2}{C_1 C_2 R_1 R_2}s_0^3 \sin 3\omega_a t^*\right] + O\left((\omega_a T)^3\right).
\end{aligned}$$

From this result it is evident that the $O(\epsilon^2)$ distortion affects the amplitude of the signal at frequency ω_a, and also creates a third-harmonic with amplitude $O\left((\omega_a T)^2\right)$.

We compare these results with the corresponding results in chapter 3 for a first-order negative feedback amplifier. The slight delay to the input signal for the first-order negative feedback design has been removed by this second-order design, though the $O\left((\omega_a T)^2\right)$ third-harmonic remains. Thus we see that this second-order design may be argued to be an improvement on the previous design, if slight.

For a general input signal we have derived the leading audio-frequency components of the amplifier output, including the first nonlinear distortion terms. We now verify these analytical results via a numerical simulation, before concluding in §4.6.
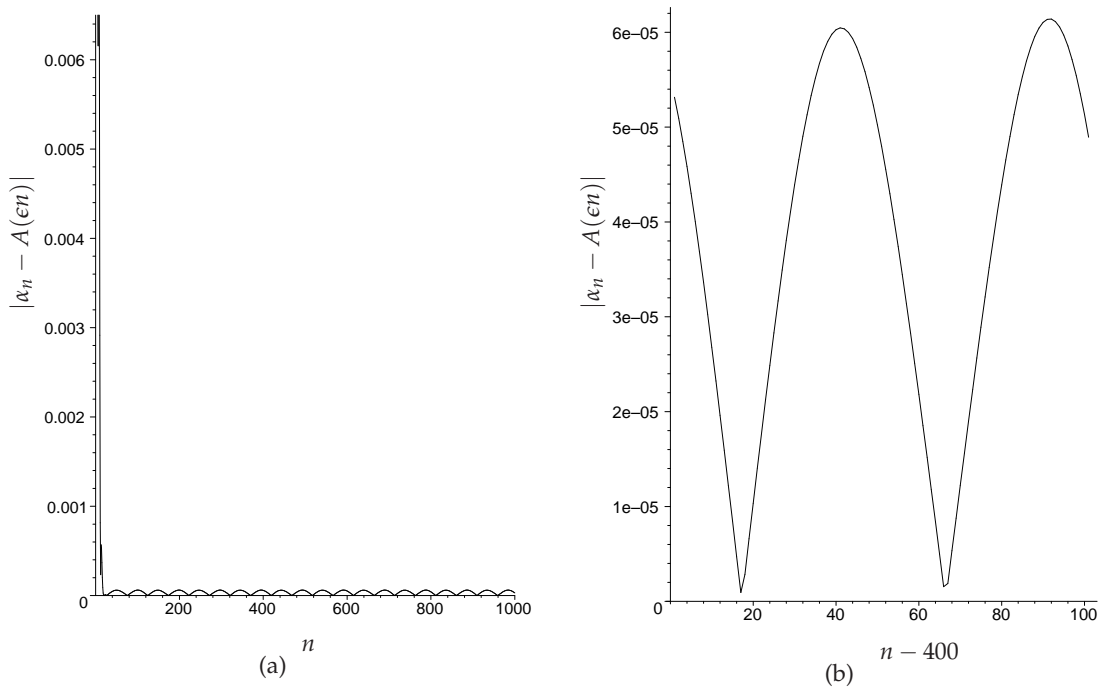
Figure 4.6: Graphs of $|\alpha_n - A(\epsilon n)|$ for $\epsilon = 0.064$.

4.5.2 Numerical simulation of switching times

To check our analytical solution, we now compare the analytical switching times found above with a numerical simulation.

The method we use to carry out this verification is the same as for first-order negative feedback, detailed in §3.5.2, and so we will outline the method only briefly here. In Maple we iterate the three exact nonlinear difference equations, (4.5.9)-(4.5.11), and thus determine the switching times numerically. We specify that the input signal is sinusoidal, $s(t) = s_0 \sin \epsilon t$, and choose the parameter values $s_0 = -0.25$, $k_2 = 1$, $k_3 = 0.5$, the initial values $\alpha_0 = 0$ and $\dot{H}(0) = 0$ arbitrarily, and solve the system for values of ϵ between 0.064 and 0.001.

Because the absolute error between the simulated and analytical switching times varies over the period of the input signal, we compare the switching times by computing $E_A(\epsilon)$ and $E_B(\epsilon)$, defined by (3.5.24) and (3.5.25). These are the maxima, taken over one period of the input signal, of the absolute values of the differences between the numerically simulated and analytical switching times, for the trailing- and leading-edge switching times respectively. As for first-order negative feedback, there are transients in the numerical simulations, which are not present in our analytical solutions, and therefore we compute $E_A(\epsilon)$ and $E_B(\epsilon)$ only after these transients have decayed. As an example, figure 4.6 shows two graphs of $|\alpha_n - A(\epsilon n)|$ for $\epsilon = 0.064$, where α_n denotes

Comparison	Result
$E_A(0.128)/E_A(0.064)$	8.11643
$E_A(0.064)/E_A(0.032)$	8.04935
$E_A(0.032)/E_A(0.016)$	8.02012
$E_A(0.016)/E_A(0.008)$	8.00893
$E_A(0.008)/E_A(0.004)$	8.00417
$E_A(0.004)/E_A(0.002)$	8.00200
$E_A(0.002)/E_A(0.001)$	8.00081

Table 4.1: Table comparing values of $E_A(\epsilon)$ for $s_0 = -0.25$, $k_2 = 1$ and $k_3 = 0.5$, with results given to 5 decimal places.

Comparison	Result
$E_B(0.128)/E_B(0.064)$	8.15041
$E_B(0.064)/E_B(0.032)$	8.05827
$E_B(0.032)/E_B(0.016)$	8.02206
$E_B(0.016)/E_B(0.008)$	8.00942
$E_B(0.008)/E_B(0.004)$	8.00428
$E_B(0.004)/E_B(0.002)$	8.00201
$E_B(0.002)/E_B(0.001)$	8.00030

Table 4.2: Table comparing values of $E_B(\epsilon)$ for $s_0 = -0.25$, $k_2 = 1$ and $k_3 = 0.5$, with results given to 5 decimal places.

the numerically simulated trailing-edge switching times. The transients can be seen in figure 4.6(a), since we have deliberately plotted $|\alpha_n - A(\epsilon n)|$ for $n = 0$ to 1000. In figure 4.6(b) we plot $|\alpha_n - A(\epsilon n)|$ for values of n after the transients have decayed and only over one period of the input signal. Therefore, to calculate $E_A(0.064)$ we take the maximum of the values of $|\alpha_n - A(\epsilon n)|$ in figure 4.6(b).

Tables 4.1 and 4.2 give the ratios of $E_A(\epsilon)$ and $E_B(\epsilon)$ respectively for different values of ϵ. We derived the analytical switching times up to $O(\epsilon^3)$, and so the error between the numerically simulated and analytical switching times should be $O(\epsilon^3)$. This is indeed what we find, as evident in tables 4.1 and 4.2. When ϵ is halved, the error is approximately divided by 8, and as ϵ decreases the ratio gets closer to 8. Thus we see that the analytical switching times agree up to $O(\epsilon^3)$ with the numerically simulated ones. Note that since the errors are smaller for smaller values of ϵ, we must be careful to use sufficient precision in these calculations. We find that 20 digits of precision is adequate here.

We have confirmed here that the switching times we found analytically in 4.5.1 agree with those found via a numerical simulation.

4.6   Conclusions

We have developed the analysis introduced for first-order negative feedback in chapter 3 to investigate a more sophisticated design, a second-order negative feedback amplifier. We first analysed the amplifier design for a constant input signal, which as well as establishing solutions that we used to solve and check our results for a general input signal later, enabled us to determine a sensible operating range for k_2, one of the second-order loop filter constants.

We then carried out a thorough investigation of the design for a general input signal. By adapting the streamlined approach we presented in chapter 3 to this more complex design, we were able to derive the leading audio-frequency components of the amplifier output for a general input signal, which to our knowledge has not been achieved for this design before (a related topology having been analysed mathematically in [41]). The leading-order audio-frequency output is exactly minus the input signal, but at higher order nonlinear distortion appears, which cannot be removed by any choice of parameters. Comparing our results with those for first-order negative feedback, we saw that although there is arguably a slight reduction in distortion, there remain nonlinear distortion terms. For a sinusoidal input signal these terms alter the amplitude of the signal in the output at the frequency of the input signal, and result in third-harmonics of the input signal. We verified our analytical results for both a constant and general input signal via numerical simulations.

Although this second-order negative feedback design reduces the distortion in the output slightly compared to the first-order negative feedback design, nonlinear distortion persists. There is, therefore, still scope for improvement, and so in the following chapter we investigate another negative feedback amplifier that aims to reduce output distortion.

Derivative negative feedback amplifier

5.1 Introduction

W HEN negative feedback is incorporated in a class-D amplifier, undesirable non-linear distortion is created in the output, as discussed in chapter 3. The second-order negative feedback design analysed in the previous chapter attempted to reduce this distortion, with limited success. Here we investigate another negative feedback design, aiming to determine whether it offers any advantages over the first- or second-order designs considered above.

The amplifier design we examine here, which we will refer to as a derivative negative feedback amplifier, comprises an integrator, comparator, low-pass filter and two negative feedback loops [42]. The main body of the amplifier circuit operates in the same way as the first-order design discussed in chapter 3, except that this design does not include a multiplier. Thus the input signal feeds into the integrator, the output of which is compared with a carrier wave in the comparator, before the first negative feedback loop adds the comparator output back into the circuit. The comparator output is also input to the low-pass filter, whose output is the final amplifier output. This filter output is also differentiated and inserted back into the amplifier circuit via the second negative feedback loop.

To our knowledge this derivative negative feedback design has not been analysed mathematically. We therefore investigate the design, aiming to derive the leading audio-frequency components of the filtered output, determine whether distortion in the output can be reduced, and identify optimum operating conditions. To do this we implement the method introduced in chapter 3 and developed in chapter 4, though
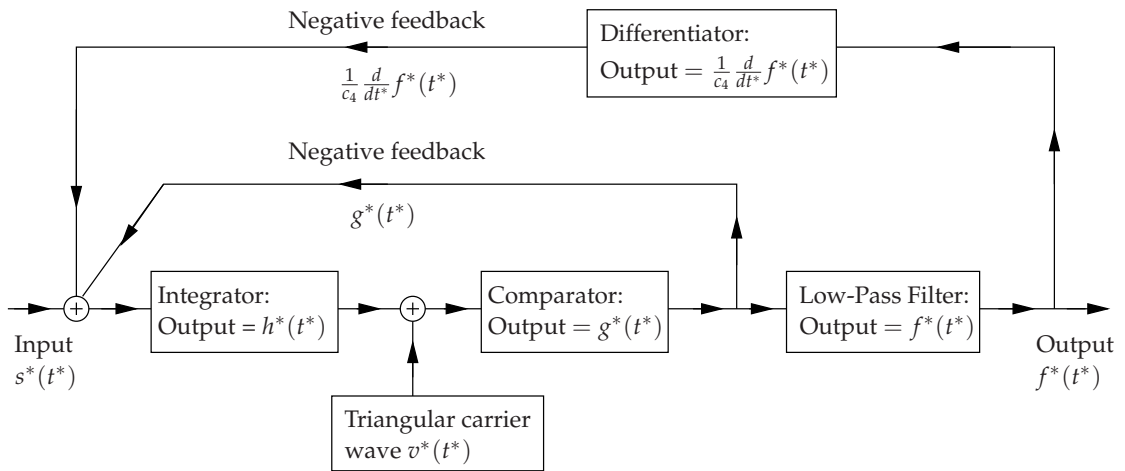
Figure 5.1: Schematic diagram representing the design of a derivative negative feedback class-D amplifier.

modelling this design presents an increased challenge because the filtered output is incorporated into the circuit, unlike the previous negative feedback designs we have examined. The added complexity of the design means that using the streamlined mathematical formulation we have developed is vital here.

In §5.2 we generate a dimensional model for the design, which we nondimensionalise in §5.3 in order to clarify the separation between the timescale of the input signal and the timescale of the carrier wave. As we have done in previous chapters, we examine the dimensionless model for a constant input signal in §5.4, and in §5.4.3 verify our results numerically. The constant input signal solutions provide crucial guidance in solving the model for a general (time-varying) input signal, since to leading order the slowly-varying input signal is constant. In §5.5 we then investigate the dimensionless model for a general input signal, which, as we have hinted above, involves considerably more work than for the other negative feedback designs above. In the latter stages of the calculations we are, however, able to use the formula (3.5.21), which gives the audio-frequency components of the comparator output in terms of its switching times, and which substantially shortens the computations. The results for a general input signal are discussed in §5.5.4 and confirmed numerically in §5.5.5. We conclude in §5.6.

5.2 Dimensional model for the amplifier design

The amplifier design, depicted in figure 5 of [42], is represented here by the diagram in figure 5.1. We use the superscript * to denote dimensional variables. The input signal

$s^*(t^*)$ is first fed into an integrator. The integrator has output $h^*(t^*)$, given by

$$\frac{d}{dt^*}h^*(t^*) = -c_1\left[g^*(t^*) + s^*(t^*) + \frac{1}{c_4}\frac{d}{dt^*}f^*(t^*)\right],\tag{5.2.1}$$

where $h^*(t^*)$, $f^*(t^*)$, $g^*(t^*)$ and $s^*(t^*)$ have dimension volts, and where c_1 is the integrator constant and c_4 is the differentiator constant. Both the integrator and the differentiator circuits contain a resistor and a capacitor, and it is the reciprocal of the product of the resistance and the capacitance that determines the constants c_1 and c_4. The product "resistance x capacitance" has units of time and thus c_1 and c_4 are positive constants with dimension 1/time. As for first-order negative feedback (see chapter 3), we will need to integrate the above equation to find the integrator output $h^*(t^*)$ later, and so it is sensible to define $r^*(t^*)$ as the integral of $s^*(t^*)$,

$$\frac{d}{dt^*}r^*(t^*) = s^*(t^*),$$

so that $r^*(t^*)$ has dimension volts x time. With this definition, (5.2.1) becomes

$$\frac{d}{dt^*}\left[h^*(t^*) + \frac{c_1}{c_4}f^*(t^*)\right] = -c_1\left[g^*(t^*) + \frac{d}{dt^*}r^*(t^*)\right].\tag{5.2.2}$$

The output from the integrator is added to a periodic triangular carrier wave $v^*(t^*)$ and fed into a comparator. The carrier wave has period T and is defined by

$$v^*(t^*) = \begin{cases} \left(1 - \frac{4}{T}(t^* - nT)\right)V & \text{for } nT \leq t^* < \left(n + \frac{1}{2}\right)T \\ \left(-3 + \frac{4}{T}(t^* - nT)\right)V & \text{for } \left(n + \frac{1}{2}\right)T \leq t^* < (n+1)T, \end{cases}\tag{5.2.3}$$

where $v^*(t^*)$ has dimension volts, and V is a constant with dimension volts. The output $g^*(t^*)$ from the comparator is defined by

$$g^*(t^*) = \begin{cases} -V & \text{for } h^*(t^*) + v^*(t^*) < 0 \\ +V & \text{for } h^*(t^*) + v^*(t^*) > 0, \end{cases}\tag{5.2.4}$$

and $s^*(t^*)$ is restricted by

$$|s^*(t^*)| < V.$$

As for the other negative feedback designs we have investigated in chapters 3 and 4, we now define two regions as shown in figure 5.2: in region I, the comparator output $g^*(t^*)$ is $-V$, and in region II, $g^*(t^*) = +V$. Again, these regions are bounded by the switching times: at the times $t^* = nT + \alpha_n^*$, the comparator output $g^*(t^*)$ switches from $+V$ to $-V$; at the times $t^* = nT + \beta_n^*$, the comparator output switches from $-V$ to $+V$. Therefore

$$g^*(t^*) = \begin{cases} -V & \text{for } nT + \alpha_n^* < t^* < nT + \beta_n^* \\ +V & \text{for } nT + \beta_n^* < t^* < (n+1)T + \alpha_{n+1}^*. \end{cases}\tag{5.2.5}$$
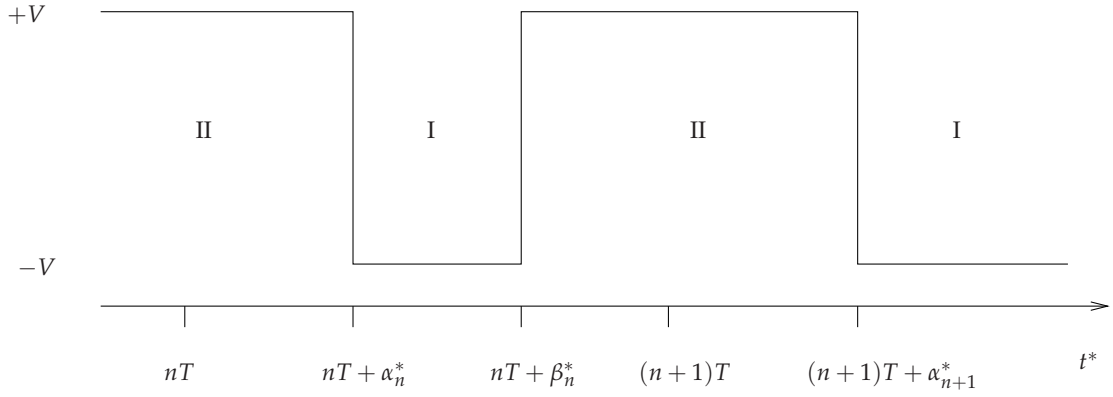
Figure 5.2: The dimensional square wave $g^*(t^*)$ showing the regions I and II.

As we have done throughout this thesis, we have obtained two expressions for $g^*(t^*)$: (5.2.4) defines the conditions under which $g^*(t^*)$ switches in terms of $h^*(t^*)$ and $v^*(t^*)$, whereas (5.2.5) defines the switching times α_n^* and β_n^*.

For correct operation of the amplifier, we assume that $h^*(t^*) = -v^*(t^*)$ at two instants t^* in each carrier wave period, once at $t^* = nT + \alpha_n^*$ and once at $t^* = nT + \beta_n^*$. Thus

$$0 < \alpha_n^* < \frac{T}{2},$$
$$\frac{T}{2} < \beta_n^* < T.$$

The square wave $g^*(t^*)$ is in turn fed back into the integrator, as shown in (5.2.2), via one of the negative feedback loops. The output $g^*(t^*)$ also feeds into the low-pass filter, which is discussed in more detail in §5.2.1. The low-pass filter output $f^*(t^*)$ is the final output from the amplifier. This filtered output is also used in the second negative feedback loop, where it is first fed into a differentiator (whose output voltage is proportional to the rate of change of the input voltage, i.e. $\frac{d}{dt^*}f^*(t^*)$) and then input to the integrator, as shown in (5.2.2).

We nondimensionalise the model in §5.3, but first examine the operation of the low-pass filter.

5.2.1 Low-pass filter

We now look in more detail at the low-pass filter included in this amplifier design. The low-pass filter is used to reduce the amplitude of any unwanted high-frequency oscillations in the comparator output $g^*(t^*)$. It operates, roughly speaking, by attenuating oscillations with frequencies above a set frequency, and letting through oscillations

with frequencies below the set frequency.

The low-pass filter used in this design consists of an inductor with inductance L in series with a capacitor with capacitance C, shown in figure 5.3. The voltage input to the filter is the square wave $g^*(t^*)$ and the voltage output from the filter is $f^*(t^*)$. The voltage across the inductor is $v_L^*(t^*)$, and the voltage across the capacitor is $f^*(t^*)$. The currents through the inductor and capacitor are respectively $i_L^*(t^*)$ and $i_C^*(t^*)$. The voltage and current laws, as well as the equations governing the operation of the components in this circuit can all be found in [40].

Since the inductor and capacitor are in series, the total voltage across the two components, $g^*(t^*)$, and the voltages across the individual components are related via

$$v_L^*(t^*) + f^*(t^*) = g^*(t^*). \tag{5.2.6}$$

The voltage across the inductor with inductance L and the current $i_L^*(t^*)$ passing through it are related by

$$v_L^*(t^*) = L\frac{d}{dt^*}i_L^*(t^*).$$

Since the two components are in series, and we assume that no further current is drawn from this filter circuit, $i_L^*(t^*) = i_C^*(t^*)$. The relationship between the current through a capacitor with capacitance C and the voltage $f^*(t^*)$ across it is

$$i_C^*(t^*) = C\frac{d}{dt^*}f^*(t^*).$$

Thus $v_L^*(t^*) = LC\frac{d^2}{dt^{*2}}f^*(t^*)$ and in view of (5.2.6) the voltages are related by the second order differential equation

$$LC\frac{d^2}{dt^{*2}}f^*(t^*) + f^*(t^*) = g^*(t^*).$$

From this equation we note that the filter output will not depend on L and C individually, but as the product LC. The product "inductance x capacitance" has units of time squared. Thus we define a frequency associated with the filter,

$$\omega_f = \frac{1}{\sqrt{LC}},$$

which has dimension 1/time, and the differential equation becomes

$$\frac{d^2}{dt^{*2}}f^*(t^*) + \omega_f^2 f^*(t^*) = \omega_f^2 g^*(t^*). \tag{5.2.7}$$

We now define two more frequencies associated with the amplifier: a typical audio input frequency ω_a, and the carrier wave (angular) frequency, $\omega_c = \frac{2\pi}{T}$, where both

111

Inductor, inductance L

$g^*(t^*)$ — [inductor] — $f^*(t^*)$

Capacitor, capacitance C
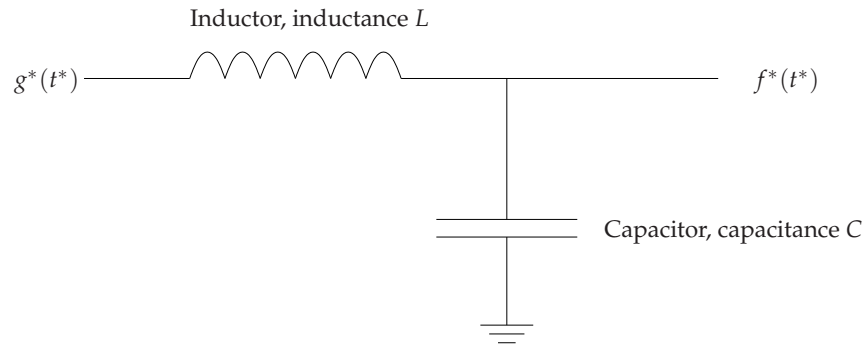
Figure 5.3: The low-pass filter circuit.

have dimension 1/time. For the filtering process to operate correctly, the relative sizes of ω_a, ω_f and ω_c are very important. The aim is for the output from the filter to be a faithful reproduction of the input signal, thus containing only frequencies close to ω_a. To achieve this, the filter frequency must be sufficiently high to allow the audio frequencies through, but sufficiently low to attenuate the oscillations at the carrier wave frequency. Thus we must have

$$\omega_a < \omega_f < \omega_c.$$

The relative sizes of ω_a, ω_f and ω_c will be discussed further in §5.5.

We now look at how the filter proposed in this design operates, by comparing the input to the filter with the associated output. For a periodic audio input signal, the comparator output is quasiperiodic and, if we ignore any transients, the filter output is also quasiperiodic. We therefore assume that the comparator output and the filter output take the general forms

$$g^*(t^*) = \sum_{m=-\infty}^{\infty} g_m^* e^{i\omega_m t^*}, \qquad f^*(t^*) = \sum_{m=-\infty}^{\infty} f_m^* e^{i\omega_m t^*},$$

where ω_m is the frequency of each component, and g_m^* and f_m^* are the amplitudes of the respective components. Thus from the differential equation (5.2.7) we find the relationship between the coefficients of $g^*(t^*)$ and $f^*(t^*)$ to be

$$f_m^* = G_1 g_m^*,$$

where

$$G_1 = \frac{1}{1 - \frac{\omega_m^2}{\omega_f^2}}.$$

Thus the effect of the filter is to multiply the amplitude of each component with frequency ω_m by the factor G_1, which is dependent on ω_m. The modulus of the multiplying factor G_1 is plotted in figure 5.4, where we can see that unbounded resonance

112
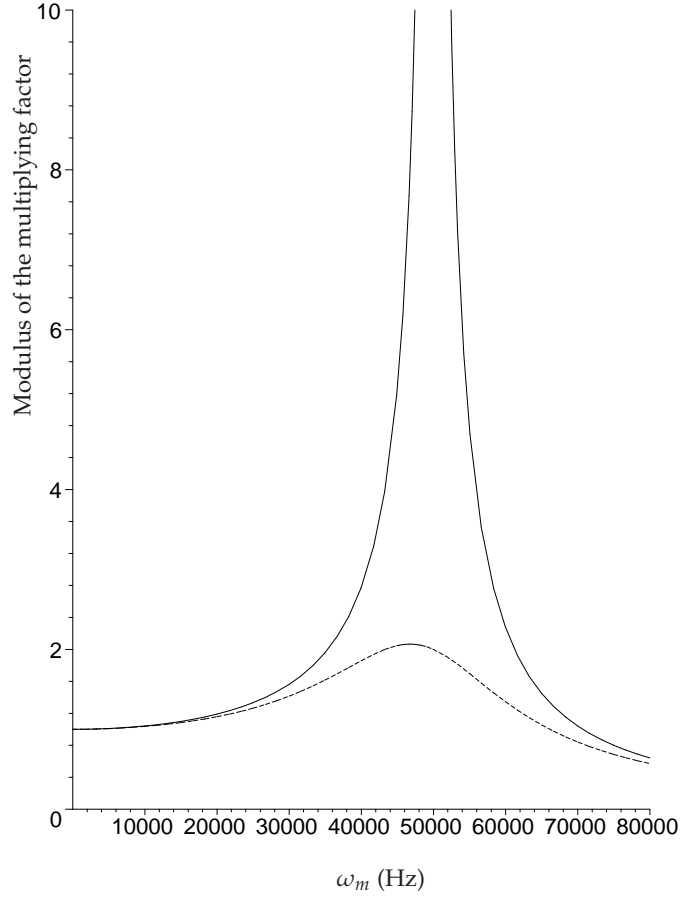
Figure 5.4: Moduli of the multiplying factors G_1 (solid line) and G_2 (dashed line) plotted against frequency of the component, ω_m, for the typical parameter values $\omega_d =$ 25kHz, $\omega_f =$ 50kHz.

occurs at frequency ω_f. This is undesirable practically as components with frequencies close to the resonant frequency will be greatly amplified.

One way to remove unbounded resonance from the filter is to include a resistor in the filter circuit, in series with the inductor and capacitor, which damps the system. In this case, the differential equation for the filter output is

$$\frac{d^2}{dt^{*2}}f^*(t^*) + \omega_d \frac{d}{dt^*}f^*(t^*) + \omega_f^2 f^*(t^*) = \omega_f^2 g^*(t^*), \tag{5.2.8}$$

where $\omega_d = \frac{R}{L}$, and R is the resistance of the resistor. If we proceed as above by assuming a general form for $f^*(t^*)$ and $g^*(t^*)$ we obtain a similar relationship between the coefficients of $g^*(t^*)$ and $f^*(t^*)$,

$$f_m^* = G_2 g_m^*,$$

where

$$G_2 = \frac{1}{1 + i\frac{\omega_d \omega_m}{\omega_f^2} - \frac{\omega_m^2}{\omega_f^2}}.$$

113

Because G_2 is complex, both the amplitude and the phase of each component are altered by this damped filter. Here, the amplitude of each component is multiplied by the factor $|G_2|$, compared to the factor G_1 for the undamped filter. The moduli of the multiplying factors G_1 and G_2 are compared in figure 5.4. We see that if a resistor is included in the filter circuit resonance occurs, but it is not unbounded. The maximum amplitude of $|G_2|$ occurs when $\omega_m = \sqrt{\omega_f^2 - \frac{\omega_d^2}{2}}$, so the resonant frequency for the damped filter circuit is lower than the resonant frequency of the undamped filter circuit. (Note that neither of the filter designs in this comparison are especially good low-pass filters, but we consider only these two here for simplicity.)

Although a resistor would in practice be used in the filter circuit in order to avoid unbounded resonance, one is not included in the design we investigate here [42], presumably because only the novel components need to be included in the patent. We therefore model the design as it appears in [42], without a resistor in the filter circuit, which keeps the model relatively simple. However, in our final solutions we will use the fact that in practice, damping is essential, and will discuss this again in §5.4.1, §5.4.2, §5.5.1 and §5.5.4.

5.3   Nondimensionalisation

Here we nondimensionalise the model created above, using unstarred symbols to denote the dimensionless versions of the starred dimensional variables.

This nondimensionalisation is the same as that in chapter 3, except that here we must also define a dimensionless version of the filter output, $f^*(t^*)$, and we use the additional constant c_4 so must define an additional corresponding dimensionless parameter. Therefore we define the dimensionless times t, α_n and β_n by scaling the dimensionless times t^*, α_n^* and β_n^* with the period of the carrier wave, T. To obtain the dimensionless voltages $g(t)$, $f(t)$, $h(t)$, $s(t)$ and $v(t)$ we scale the dimensional voltages $g^*(t^*)$, $f^*(t^*)$, $h^*(t^*)$, $s^*(t^*)$ and $v^*(t^*)$ with V. Correspondingly, we define a dimensionless version of $r^*(t^*)$, the integral of the input signal, by

$$r(t) = \frac{r^*(t^*)}{TV},$$

so that

$$\frac{d}{dt}r(t) = s(t). \tag{5.3.1}$$

Recalling that the integrator constant c_1 and the differentiator constant c_4 are both pos-

itive and have dimension 1/time, we establish two dimensionless $O(1)$ parameters,

$$k_1 = c_1 T > 0,$$
$$k_4 = c_4 T > 0.$$

Finally, we define λ to be the dimensionless combination of the filter frequency and the period of the carrier wave,

$$\lambda = \omega_f T.$$

We now use the definitions of our dimensionless variables and parameters to nondimensionalise (5.2.2)-(5.2.7). From (5.2.2) we obtain the dimensionless differential equation describing the operation of the integrator,

$$\frac{d}{dt}\left[h(t) + \frac{k_1}{k_4}f(t)\right] = -k_1\left[g(t) + \frac{d}{dt}r(t)\right], \tag{5.3.2}$$

and from (5.2.3)-(5.2.5) we obtain

$$v(t) = \begin{cases} 1 - 4(t-n) & \text{for } n \le t < n + \frac{1}{2} \\ -3 + 4(t-n) & \text{for } n + \frac{1}{2} \le t < n+1, \end{cases} \tag{5.3.3}$$

$$g(t) = \begin{cases} -1 & \text{for } h(t) + v(t) < 0 \\ +1 & \text{for } h(t) + v(t) > 0, \end{cases} \tag{5.3.4}$$

$$g(t) = \begin{cases} -1 & \text{for } n + \alpha_n < t < n + \beta_n \\ +1 & \text{for } n + \beta_n < t < n + 1 + \alpha_{n+1}, \end{cases} \tag{5.3.5}$$

The comparator output $g(t)$, as well as the switching times bounding regions I and II are depicted in figure 5.5. Nondimensionalising the restriction on the input signal we obtain

$$|s(t)| < 1, \tag{5.3.6}$$

and nondimensionalising the restrictions imposed on the switching times we find

$$0 < \alpha_n < \frac{1}{2}, \tag{5.3.7}$$

$$\frac{1}{2} < \beta_n < 1. \tag{5.3.8}$$

Lastly, from (5.2.7) we obtain

$$\ddot{f}(t) + \lambda^2 f(t) = \lambda^2 g(t), \tag{5.3.9}$$

where we use the notation $\ddot{f}(t) = \frac{d^2}{dt^2}f(t)$.

115
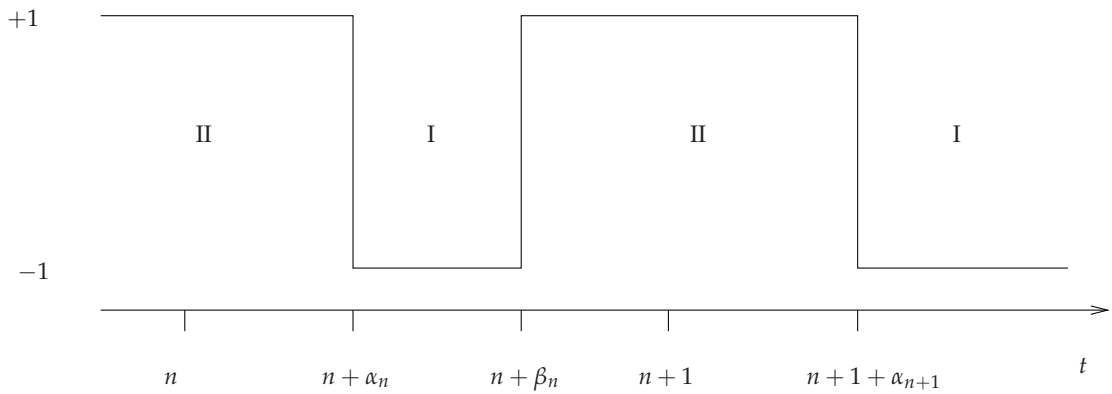
Figure 5.5: The dimensionless square wave $g(t)$ showing the regions I and II.

Recall from our previous analysis of negative feedback amplifiers in chapters 3 and 4 that examining the dimensionless governing equations for a constant input signal helped us to investigate the behaviour of the amplifier for a general (time-varying) input signal later. This is because the input to the amplifier varies slowly compared with the carrier wave frequency, and so the solutions for a constant input signal give the limiting case for a general input signal. We therefore proceed in the same manner here, by first considering the operation of the amplifier for a constant input signal, in §5.4, before tackling a general input signal in §5.5.

5.4 Dimensionless model for a constant input signal

We here investigate the amplifier when a constant signal is input. This will give us an insight into how the amplifier behaves when a constant signal is input, as well as helping us to solve the model for a general input signal. We choose $s(t) = s_0$, where $-1 < s_0 < 1$ is a constant, and therefore $r(t) = s_0 t$ from (5.3.1).

We now start to solve the dimensionless equations governing the amplifier, (5.3.2)-(5.3.5) and (5.3.9). We first solve (5.3.9), the differential equation defining the filter output $f(t)$, separately in regions I and II to find $f(t)$, which we split into the solution in region I, $f^I(t)$, and the solution in region II, $f^{II}(t)$. We consider $f(t)$ over one period of $g(t)$, $n + \alpha_n < t < n + 1 + \alpha_{n+1}$. We use the notation $\dot{f}(t) = \frac{d}{dt} f(t)$.

We first solve (5.3.9) for $n + \alpha_n < t < n + \beta_n$. In solving the second-order differential equation we obtain two constants of integration, which we then write in terms of

116

$f(t)$ and $\dot{f}(t)$ at $t = n + \alpha_n$, the starting time for this region. We obtain

$$\begin{aligned} f^I(t) &= [f^I(n + \alpha_n) + 1] \cos(\lambda(t - n - \alpha_n)) \\ &\quad + \frac{1}{\lambda} \dot{f}^I(n + \alpha_n) \sin(\lambda(t - n - \alpha_n)) - 1. \end{aligned}$$

Next we solve (5.3.9) for $n + \beta_n < t < n + 1 + \alpha_{n+1}$ and again write the resulting constants of integration in terms of $f(t)$ and $\dot{f}(t)$ at the starting time for the region, which in this case is $t = n + \beta_n$,

$$\begin{aligned} f^{II}(t) &= [f^{II}(n + \beta_n) - 1] \cos(\lambda(t - n - \beta_n)) \\ &\quad + \frac{1}{\lambda} \dot{f}^{II}(n + \beta_n) \sin(\lambda(t - n - \beta_n)) + 1. \end{aligned}$$

We impose continuity of both $f(t)$ and $\dot{f}(t)$ at the switching times $t = n + \alpha_n$ and $t = n + \beta_n$ and thus we drop the superscripts for $f^I(n + \alpha_n)$, $\dot{f}^I(n + \alpha_n)$, $f^{II}(n + \beta_n)$ and $\dot{f}^{II}(n + \beta_n)$. Hence the filtered output is given by

$$\begin{aligned} f^I(t) &= [f(n + \alpha_n) + 1] \cos(\lambda(t - n - \alpha_n)) \\ &\quad + \frac{1}{\lambda} \dot{f}(n + \alpha_n) \sin(\lambda(t - n - \alpha_n)) - 1, \qquad (5.4.1) \\ f^{II}(t) &= [f(n + \beta_n) - 1] \cos(\lambda(t - n - \beta_n)) \\ &\quad + \frac{1}{\lambda} \dot{f}(n + \beta_n) \sin(\lambda(t - n - \beta_n)) + 1, \qquad (5.4.2) \end{aligned}$$

where $f^I(t)$ is valid for $n + \alpha_n < t < n + \beta_n$ and $f^{II}(t)$ is valid for $n + \beta_n < t < n + 1 + \alpha_{n+1}$.

From (5.4.1) we find that the equations for $f(t)$ and $\dot{f}(t)$ at $t = n + \beta_n$ in terms of these functions at the previous switching time, $t = n + \alpha_n$, are

$$\begin{aligned} f(n + \beta_n) &= [f(n + \alpha_n) + 1] \cos(\lambda(\beta_n - \alpha_n)) \\ &\quad + \frac{1}{\lambda} \dot{f}(n + \alpha_n) \sin(\lambda(\beta_n - \alpha_n)) - 1, \qquad (5.4.3) \\ \dot{f}(n + \beta_n) &= \dot{f}(n + \alpha_n) \cos(\lambda(\beta_n - \alpha_n)) \\ &\quad - \lambda[f(n + \alpha_n) + 1] \sin(\lambda(\beta_n - \alpha_n)), \qquad (5.4.4) \end{aligned}$$

and from (5.4.2) we find that the equations for $f(t)$ and $\dot{f}(t)$ at $t = n + 1 + \alpha_{n+1}$ in terms of these functions at the previous switching time, $t = n + \beta_n$, are

$$\begin{aligned} f(n + 1 + \alpha_{n+1}) &= [f(n + \beta_n) - 1] \cos(\lambda(1 - \beta_n + \alpha_{n+1})) \\ &\quad + \frac{1}{\lambda} \dot{f}(n + \beta_n) \sin(\lambda(1 - \beta_n + \alpha_{n+1})) + 1, \qquad (5.4.5) \\ \dot{f}(n + 1 + \alpha_{n+1}) &= \dot{f}(n + \beta_n) \cos(\lambda(1 - \beta_n + \alpha_{n+1})) \\ &\quad + \lambda[1 - f(n + \beta_n)] \sin(\lambda(1 - \beta_n + \alpha_{n+1})). \qquad (5.4.6) \end{aligned}$$

The four equations (5.4.3)-(5.4.6) relate the filter output and its derivative at a switching time to those quantities at a previous switching time. (5.4.3) and (5.4.4) determine $f(t)$

and $\dot{f}(t)$ at $t = n + \beta_n$ in terms of $f(t)$ and $\dot{f}(t)$ at $t = n + \alpha_n$. Similarly (5.4.5) and (5.4.6) determine $f(t)$ and $\dot{f}(t)$ at $t = n + 1 + \alpha_{n+1}$ in terms of $f(t)$ and $\dot{f}(t)$ at $t = n + \beta_n$. These equations are valid for any input signal $s(t)$ and consequently we will also use these equations later to analyse the amplifier for a general input signal, in §5.5.

We now turn our attention to the output from the integrator, $h(t)$, and the switching times. We use (5.3.2)-(5.3.5) to find equations relating $h(t)$ at different times in the period to the switching times. From (5.3.2) we have

$$h(t) - h(t_0) + \frac{k_1}{k_4}(f(t) - f(t_0)) = \begin{cases} k_1(1 - s_0)(t - t_0) & \text{in region I} \\ -k_1(1 + s_0)(t - t_0) & \text{in region II} \end{cases} \quad (5.4.7)$$

where t_0 is the time at the beginning of the region (respectively, $t_0 = n + \alpha_n$ and $t_0 = n + \beta_n$). In region I, for $n + \alpha_n < t < n + \beta_n$, we therefore find

$$h(t) = h(n + \alpha_n) - \frac{k_1}{k_4}\left[f^I(t) - f(n + \alpha_n)\right] + k_1(1 - s_0)(t - n - \alpha_n). \quad (5.4.8)$$

Since $h(t)$ is continuous, we can obtain $h(t)$ at the end of this particular region from (5.4.8),

$$\begin{aligned} h(n + \beta_n) &= h(n + \alpha_n) - \frac{k_1}{k_4}\left[f(n + \beta_n) - f(n + \alpha_n)\right] \\ &\quad + k_1(1 - s_0)(\beta_n - \alpha_n). \end{aligned} \quad (5.4.9)$$

Similarly, in region II, for $n + \beta_n < t < n + 1 + \alpha_{n+1}$, we find from (5.4.7)

$$h(t) = h(n + \beta_n) - \frac{k_1}{k_4}\left[f^{II}(t) - f(nT + \beta_n)\right] - k_1(1 + s_0)(t - n - \beta_n), \quad (5.4.10)$$

and again, because $h(t)$ is continuous we can now determine $h(t)$ at the end of this region from (5.4.10),

$$\begin{aligned} h(n + 1 + \alpha_{n+1}) &= h(n + \beta_n) - \frac{k_1}{k_4}\left[f(n + 1 + \alpha_{n+1}) - f(n + \beta_n)\right] \\ &\quad - k_1(1 + s_0)(1 + \alpha_{n+1} - \beta_n). \end{aligned} \quad (5.4.11)$$

Using the definitions of the switching times we now establish equations relating $h(t)$ at the switching times to the switching times themselves. The switching times are the times that satisfy $h(t) + v(t) = 0$, from (5.3.4). We determine $v(n + \alpha_n)$ and $v(n + \beta_n)$ from (5.3.3) and by observing the restrictions on α_n and β_n, (5.3.7) and (5.3.8), we therefore obtain

$$h(n + \alpha_n) + 1 - 4\alpha_n = 0, \quad (5.4.12)$$
$$h(n + \beta_n) - 3 + 4\beta_n = 0. \quad (5.4.13)$$

We have now derived the eight exact nonlinear equations that determine the output for a constant input signal. The equations comprising the model are: (5.4.3)-(5.4.6) for $f(t)$ and $\dot{f}(t)$; (5.4.9) and (5.4.11) for $h(t)$; and (5.4.13) and (5.4.13) for the switching times. Recall that our analysis of the first-order negative feedback amplifier in chapter 3 required only four equations. Here, we have two equations for the integrator output and two for the switching times, as for the first-order negative feedback amplifier, but in addition have four equations for the filter output. It is necessary to include the filtering process in the model here because the filter output is fed back into the amplifier circuit via the second negative feedback loop. The added complexity of modelling the filter output means that implementing the streamlined formulation introduced in chapter 3 is even more important here, to keep the model as simple as possible.

As discussed in chapters 3 and 4, it would be possible to iterate the exact governing equations for specific parameter values. We would obtain the switching times, and hence the comparator output $g(t)$, and then find the filter output $f(t)$. By proceeding in this way we would however understand little about the operation of the amplifier, and so we seek an analytical solution here. We assume that after a transient state, the system reaches a stable steady state, and we discuss this assumption in the following section. We obtain these steady-state solutions analytically in §5.4.2. Then in §5.4.3 we verify the analytical steady-state solutions by iterating the exact equations numerically.

5.4.1 Discussion of damping

General solutions to the exact equations (5.4.3)-(5.4.6), (5.4.9), (5.4.11), (5.4.13) and (5.4.13) will include an initial transient state. We expect these transients to arise from two causes. Firstly, when the circuit is initially switched on, the initial currents and voltages in the amplifier circuit are not what they need to be for the steady-state response, and so transients appear in the currents and voltages in the amplifier circuit. Secondly, after the circuit is initially switched on, the initial currents and voltages in the filter circuit are not what they need to be for the steady-state response, resulting in transients in the filter output. We expect the first type of transients to decay as the currents and voltages in the amplifier circuit are "corrected" by the negative feedback loops. If the filter in this model included damping (discussed in §5.2.1), because the input signal is constant, we would also expect the second type of transients to die away leaving the system in a steady state. We will assume that damping has a negligible effect on the steady-state solution, i.e. that the steady state reached by the damped system is almost identical to that reached by the undamped system. We justify this assumption with the following example.

We solve (5.2.8), the dimensional differential equation for the filter output with a resistor included in the filter circuit to provide damping. We choose $g^*(t^*) = s_0 V \sin \omega_a t^*$, and thus find the general solution,

$$
\begin{aligned}
f^*(t^*) &= D_1 e^{-\frac{\omega_d}{2} t^*} \sin \left(\sqrt{\omega_f^2 - \frac{\omega_d^2}{4}} t^* + D_2 \right) \\
&\quad + \Omega(\omega_a, \omega_d, \omega_f) \sin(\omega_a t^* - \theta(\omega_a, \omega_d, \omega_f)),
\end{aligned} \tag{5.4.14}
$$

where D_1 and D_2 are undetermined constants, and

$$
\Omega(\omega_a, \omega_d, \omega_f) = \frac{s_0 V}{\left(\frac{\omega_a^2 \omega_d^2}{\omega_f^4} + \left(1 - \frac{\omega_a^2}{\omega_f^2} \right)^2 \right)^{\frac{1}{2}}},
$$

$$
\theta(\omega_a, \omega_d, \omega_f) = \arctan \frac{\omega_a \omega_d}{\omega_f^2 - \omega_a^2}.
$$

We see that the complementary function is in fact a transient solution, and the particular integral is the steady-state solution, where $\Omega(\omega_a, \omega_d, \omega_f)$ and $\theta(\omega_a, \omega_d, \omega_f)$ are respectively the amplitude of and the delay to the steady-state solution. The transient solution will decay quickly (within a few seconds) provided that $\omega_d \gg 1$Hz, since the transient solution will decrease by a factor e^m after a time $\frac{2m}{\omega_d}$ seconds. Note that setting $\omega_d = 0$ in (5.4.14) provides the general solution to (5.2.7), the differential equation for the filter output when a resistor is not included in the circuit. Therefore we see that including damping in the filter introduces a delay to the steady-state solution. This delay is given by $\theta(\omega_a, \omega_d, \omega_f)$, which is zero in the filter output without damping.

We compare the constants $\Omega(\omega_a, \omega_d, \omega_f)$ and $\theta(\omega_a, \omega_d, \omega_f)$ for a filter that includes damping with those for a filter without damping. Using the typical parameter values $\omega_a = 8$kHz, $\omega_d = 25$kHz, $\omega_f = 50$kHz we find to 3s.f.

$$
\begin{aligned}
\Omega(8000, 0, 50000) &= 0.513, \\
\theta(8000, 0, 50000) &= 0, \\
\Omega(8000, 25000, 50000) &= 0.511, \\
\theta(8000, 25000, 50000) &= 0.0819.
\end{aligned}
$$

The change in $\Omega(\omega_a, \omega_d, \omega_f)$ is approximately 0.3% and the change in $\theta(\omega_a, \omega_d, \omega_f)$ is also very small. Therefore the effect of damping on the steady-state solution is small. If we seek a steady-state solution to our model without damping, and ignore oscillations with frequency ω_f, we will therefore obtain approximately the same steady-state solution as if we had included damping in the model. Thus we proceed to calculate the steady-state solution for the undamped system, ignoring the transient state.

5.4.2 Exact steady-state solution for a constant input signal

We seek the steady-state solutions to the eight exact nonlinear equations (5.4.3)-(5.4.6), (5.4.9), and (5.4.11)-(5.4.13), which describe the operation of the amplifier when a constant signal is input.

We therefore set

$$
\begin{aligned}
f(n+1+\alpha_{n+1}) &= f(n+\alpha_n), \\
\dot{f}(n+1+\alpha_{n+1}) &= \dot{f}(n+\alpha_n), \\
h(n+1+\alpha_{n+1}) &= h(n+\alpha_n), \\
\alpha_{n+1} &= \alpha_n,
\end{aligned}
$$

in (5.4.3)-(5.4.6), (5.4.9) and (5.4.11)-(5.4.13). We find that only (5.4.5),(5.4.6) and (5.4.11) are altered by these changes, and these equations become, respectively

$$
\begin{aligned}
f(n+\alpha_n) &= [f(n+\beta_n)-1]\cos(\lambda(1-\beta_n+\alpha_n)) \\
&\quad + \frac{1}{\lambda}\dot{f}(n+\beta_n)\sin(\lambda(1-\beta_n+\alpha_n))+1, \\
\end{aligned}
\tag{5.4.15}
$$

$$
\begin{aligned}
\dot{f}(n+\alpha_n) &= \dot{f}(n+\beta_n)\cos(\lambda(1-\beta_n+\alpha_n)) \\
&\quad + \lambda[1-f(n+\beta_n)]\sin(\lambda(1-\beta_n+\alpha_n)), \\
\end{aligned}
\tag{5.4.16}
$$

$$
\begin{aligned}
h(n+\alpha_n) &= h(n+\beta_n) - \frac{k_1}{k_4}[f(n+\alpha_n)-f(nT+\beta_n)] \\
&\quad - k_1(1+s_0)(1+\alpha_n-\beta_n).
\end{aligned}
\tag{5.4.17}
$$

Therefore the steady-state equations are (5.4.3), (5.4.4), (5.4.15) and (5.4.16) for $f(t)$, (5.4.9) and (5.4.17) for $h(t)$, and (5.4.13) and (5.4.13) for the switching times.

From (5.4.9) and (5.4.17) we find the simple relation

$$
\beta_n - \alpha_n = \frac{1}{2}(1+s_0),
\tag{5.4.18}
$$

and therefore the short-time average of $g(t)$, defined by (2.3.10), is given by

$$
\langle g(t) \rangle = -s_0.
\tag{5.4.19}
$$

These two results are in agreement with those for both the first-order negative feedback amplifier and the second-order negative feedback amplifier. Hence, as discussed for those amplifier designs, the restriction $|s_0| < 1$ forces $0 < \beta_n - \alpha_n < 1$ for correct operation of this derivative negative feedback amplifier, and we observe that the second feedback loop in this design has not altered this important restriction.

By calculating the short-time average of the differential equation (5.3.9) we can now calculate the short-time average of $f(t)$. Taking the average of (5.3.9) and using (5.4.19)

we obtain

$$\left[\dot{f}(t)\right]_n^{n+1} + \lambda^2 \langle f(t) \rangle = -\lambda^2 s_0.$$

Since we are looking for steady-state solutions, this simplifies to

$$\langle f(t) \rangle = -s_0. \tag{5.4.20}$$

Thus, for a constant input signal the short-time average of the filtered output is minus the input signal. The comparator output and the filter output therefore have the same short-time average, and so we see that the filtering process does not alter this characteristic.

We now determine the solutions to the steady-state equations. Solving (5.4.3), (5.4.4), (5.4.15) and (5.4.16) with (5.4.18) we find the steady-state solutions for $f(t)$,

$$f(n + \alpha_n) = \frac{-\sin\left(\frac{\lambda}{2}(s_0 + 1)\right) - \sin\left(\frac{\lambda}{2}(s_0 - 1)\right)}{\sin \lambda}, \tag{5.4.21}$$

$$\dot{f}(n + \alpha_n) = \lambda \left[\frac{\cos\left(\frac{\lambda}{2}(s_0 + 1)\right) + \cos\left(\frac{\lambda}{2}(s_0 - 1)\right) - \cos \lambda - 1}{\sin \lambda}\right], \tag{5.4.22}$$

$$f(n + \beta_n) = f(n + \alpha_n), \tag{5.4.23}$$

$$\dot{f}(n + \beta_n) = -\dot{f}(n + \alpha_n). \tag{5.4.24}$$

These are the four constants in (5.4.1) and (5.4.2) which determine the steady-state filter output. We confirm that these four constants are correct by integrating the solution we have now found for $f(t)$ to obtain the short-time average of $f(t)$,

$$\begin{aligned}
\langle f(t) \rangle &= \int_n^{n+1} f(t)\, dt \\
&= -s_0.
\end{aligned}$$

This agrees with the short-time average we found above, (5.4.20), using a different method.

The steady-state solution for the filter output is thus given by (5.4.1) in region I and (5.4.2) in region II, where (5.4.21)-(5.4.24) determine the constants in these equations. Expanding these solutions as series for small λ we find

$$f^I(t) = -s_0 + O(\lambda^2), \tag{5.4.25}$$

$$f^{II}(t) = -s_0 + O(\lambda^2). \tag{5.4.26}$$

Therefore, for a constant input signal s_0, the filter output oscillates around $-s_0$. (In particular, note that if the input signal is zero, then $f(n + \alpha_n) = f(n + \beta_n) = 0$ but $\dot{f}(n + \alpha_n)$ and $\dot{f}(n + \beta_n)$ are nonzero, and so $f(t)$ will oscillate around zero.) From (5.4.1) and

(5.4.2) it is clear that in dimensional terms the oscillations have frequency ω_f. Recall from §5.4.1 that if a resistor were included in the filter circuit, these oscillations would be damped, and so the filter output would in fact be constant, and so equal $-s_0$.

Now that we know $f(n + \alpha_n)$, $\dot{f}(n + \alpha_n)$, $f(n + \beta_n)$ and $\dot{f}(n + \beta_n)$, the remaining steady-state equations are greatly simplified, and we are able to find the steady-state solutions for $h(t)$,

$$h(n + \alpha_n) = \frac{k_1}{4} \left(s_0^2 - 1 \right) - s_0, \tag{5.4.27}$$

$$h(n + \beta_n) = -\frac{k_1}{4} \left(s_0^2 - 1 \right) - s_0, \tag{5.4.28}$$

as well as the switching times,

$$\alpha_n = \frac{1}{16} \left[4 - 4s_0 + k_1 \left(s_0^2 - 1 \right) \right], \tag{5.4.29}$$

$$\beta_n = \frac{1}{16} \left[12 + 4s_0 + k_1 \left(s_0^2 - 1 \right) \right]. \tag{5.4.30}$$

If we compare these switching times with the corresponding results for the first-order negative feedback design, (3.4.11) and (3.4.12), we see that they are the same. As we have discussed in previous chapters, because a constant signal is the limiting case of a slowly-varying general signal, we also anticipate that the leading-order switching times for a general input signal for this derivative negative feedback design will agree with those for the first-order design.

Because the switching times for this design are the same as those for the first-order negative feedback design, and the restrictions on s_0 and the switching times, (5.3.6)-(5.3.8) are also the same, the range for k_1 ensuring correct operation, which we obtained in chapter 3, also applies here. Thus

$$0 < k_1 < 2. \tag{5.4.31}$$

We have found the steady-state solutions for $f(t), h(t), \alpha_n$ and β_n in terms of the parameters k_1, k_4, and λ. The filter output $f(t)$ is given by (5.4.1) in region I and (5.4.2) in region II. The integrator output $h(t)$ is given by (5.4.8) in region I and (5.4.10) in region II. The constants in these four equations are given by (5.4.21)-(5.4.28). The switching times α_n and β_n are given by (5.4.29) and (5.4.30) respectively. In the next section we plot our solutions to understand how they behave for different parameter values.

5.4.2.1   Graphs of integrator output, carrier wave and filter output

We now plot the integrator output, $h(t)$, carrier wave, $v(t)$, and filter output, $f(t)$, for different parameter values. We plot the integrator output and the carrier wave on the
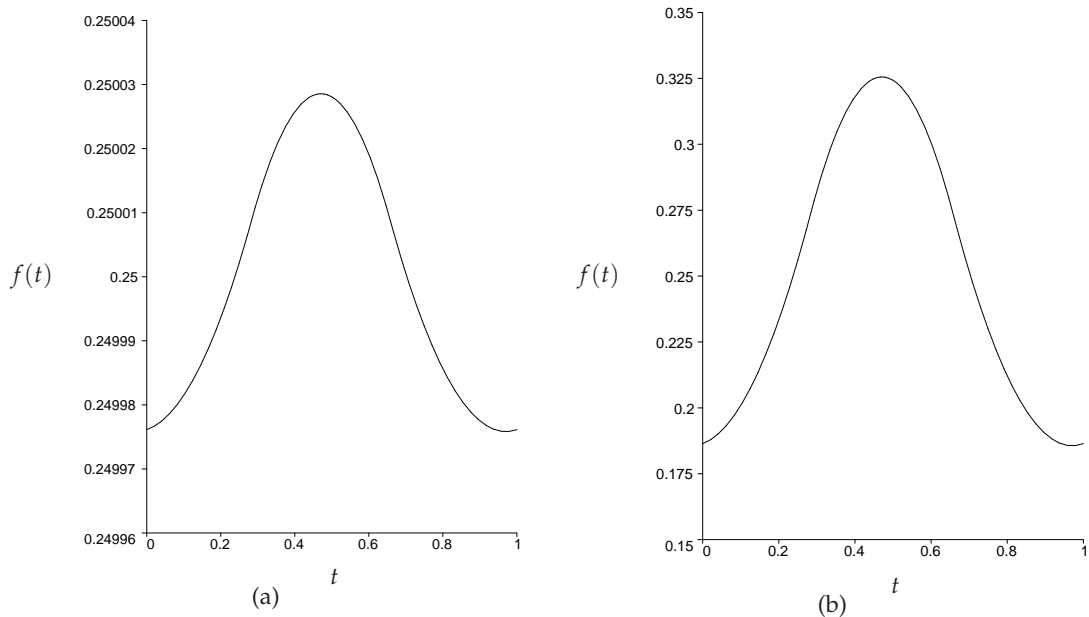
Figure 5.6: The filter output $f(t)$ when the input signal is $s_0 = -0.25$ for (a) $\lambda = 0.03$ and (b) $\lambda = 1.5$.

same graph to show the switching times. These graphs give us more of an insight into how the amplifier behaves for different parameter values.

For the graphs that follow we compare two values for the dimensionless combination $\lambda = \omega_f T$: $\lambda =$0.03 and 1.5. For typical audio and carrier wave frequencies these values span the range $\omega_a T < \lambda < \omega_c T$, a requirement discussed in §5.2.1. We choose $k_1 =$0.5 and 1.5, values that fall within the range specified by (5.4.31), and choose $k_4 =$0.5 and 1.5 to ensure $k_4 = O(1)$. We arbitrarily choose the input signal to be $s_0 = -0.25$. Figures 5.6-5.8 show $f(t)$, $h(t)$ and $-v(t)$ for these different values of λ, k_1 and k_4.

Comparing the graphs in figure 5.6 we see that the shape of $f(t)$ is unaffected by the change in λ. It is only the amplitude of the oscillations that increases by a factor of 2500 when λ increases from 0.03 to 1.5 (notice the change in scale on the y-axis). In both cases $f(t)$ oscillates around 0.25, as expected since the input signal is $s_0 = -0.25$. These observations can be explained by looking at the solution for $f(t)$, (5.4.1) in region I and (5.4.2) in region II, where the constants $f(n + \alpha_n)$, $f(n + \beta_n)$, $\dot{f}(n + \alpha_n)$ and $\dot{f}(n + \beta_n)$ are given by (5.4.21)-(5.4.24). The amplitude of $f(t)$ is determined by the constants $f(n + \alpha_n)$, $f(n + \beta_n)$, $\dot{f}(n + \alpha_n)$ and $\dot{f}(n + \beta_n)$, which are dependent on λ. From the series expansions of $f(t)$ for small λ in regions I and II, which are given by (5.4.25) and (5.4.26) respectively, it is clear that a factor of 50 change in λ should result in a factor of 2500 change in the amplitude of $f(t)$, as observed. Note that $f(t)$ is independent of k_1
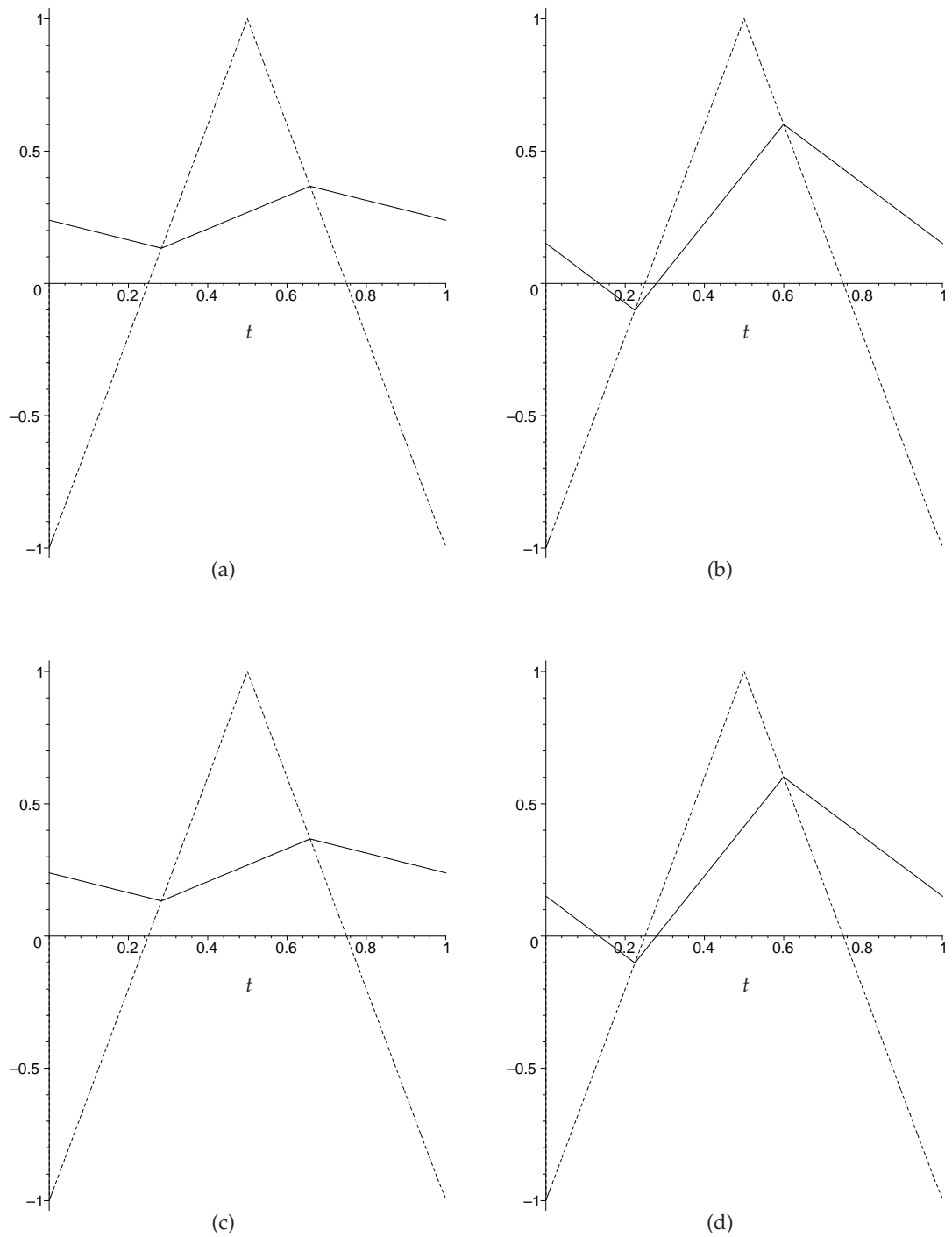
Figure 5.7: For $\lambda = 0.03$. The integrator output $h(t)$ (solid line) and $-v(t)$ (dotted line) for (a) $k_1 = 0.5$, $k_4 = 0.5$, (b) $k_1 = 1.5$, $k_4 = 0.5$, (c) $k_1 = 0.5$, $k_4 = 1.5$, and (d) $k_1 = 1.5$, $k_4 = 1.5$.
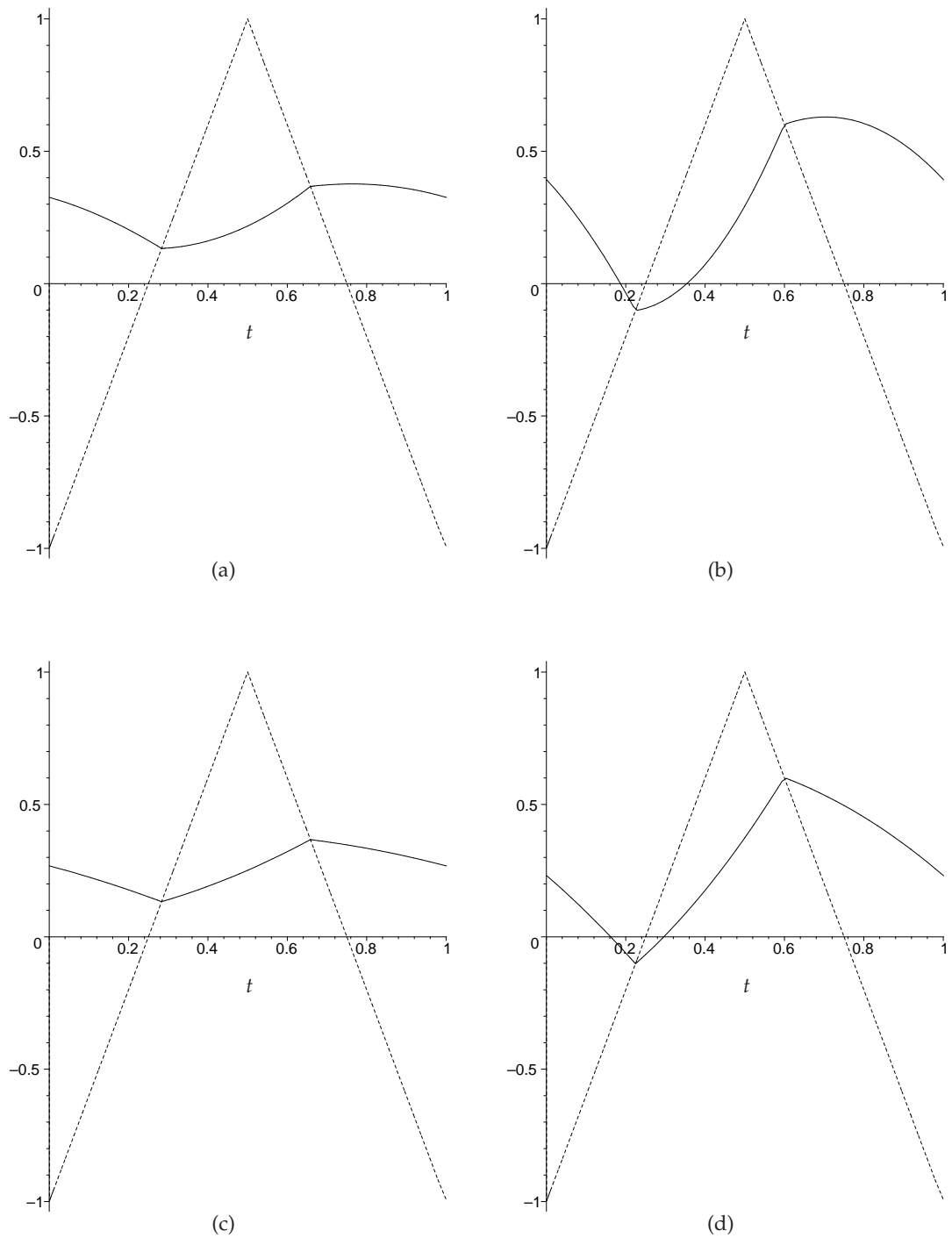
Figure 5.8: For $\lambda = 1.5$. The integrator output $h(t)$ (solid line) and $-v(t)$ (dotted line) for (a) $k_1 = 0.5$, $k_4 = 0.5$, (b) $k_1 = 1.5$, $k_4 = 0.5$, (c) $k_1 = 0.5$, $k_4 = 1.5$, and (d) $k_1 = 1.5$, $k_4 = 1.5$.

and k_4 so we have not plotted $f(t)$ for different values of these two parameters.

Subfigures (a)-(d) in figures 5.7 and 5.8 each show a plot of $h(t)$ and $-v(t)$. The times at which the curves intersect are the switching times, α_n and β_n. From (5.4.29) and (5.4.30) we can calculate the switching times, which are independent of k_4. For $k_1 = 0.5$, as in subfigures (a) and (c) of figures 5.7 and 5.8, $\alpha_n = \frac{145}{512}$ and $\beta_n = \frac{337}{512}$. For $k_1 = 1.5$, as in subfigures (b) and (d) of figures 5.7 and 5.8, $\alpha_n = \frac{115}{512}$ and $\beta_n = \frac{307}{512}$. For both of these sets of switching times $\beta_n - \alpha_n = \frac{3}{8}$, in agreement with (5.4.18).

If we compare figures 5.7 and 5.8 we can see how changing λ, k_1 and k_4 affects $h(t)$. When λ is small $f(t)$ has a small amplitude and so over the short switching timescale $f(t)$ is approximately linear, and thus $h(t)$, which depends on $f(t)$, is approximately piecewise linear. As we see in the general equation for $h(t)$, (5.4.7), $f(t)$ is multiplied by $\frac{k_1}{k_4}$. Because $f(t)$ has a small amplitude for small λ, changing k_1 and k_4 has little effect on the shape of $h(t)$, as can be observed in figure 5.7. For larger λ, $f(t)$ is approximately piecewise sinusoidal on the short switching timescale. Hence, as $\frac{k_1}{k_4}$ increases, $h(t)$ is influenced more strongly by $f(t)$, and so changes from approximately piecewise linear to approximately piecewise sinusoidal. These effects can be seen in figure 5.8, where $\frac{k_1}{k_4}$ is smallest in subfigure (c) and largest in subfigure (b).

We have plotted and compared our steady-state solutions for a constant input signal. We now confirm these analytical solutions by comparing them with a numerical simulation.

5.4.3 Numerical simulation of switching times

In order to verify our results we use Maple to numerically iterate in time the eight exact equations that determine the output for a constant input signal, (5.4.3)-(5.4.6), (5.4.9), and (5.4.11)-(5.4.13).

We arbitrarily choose $\alpha_0 = 0$, $f(0) = 0$ and $\dot{f}(0) = 0$, and then solve the eight exact equations iteratively. We compare the switching times found numerically with the exact steady-state solutions for the switching times, (5.4.29) and (5.4.30). We find that after an initial transient state, which occurs because we choose the initial values α_0, $f(0)$ and $\dot{f}(0)$ arbitrarily, the numerical switching times converge to our exact steady-state switching times. For example, for $s_0 = -0.25$, $\lambda = 0.2$, $k_1 = 1$ and $k_4 = 1$, after approximately 1000 carrier wave periods the switching times appear to converge to $\alpha_n = 0.25390625$ and $\beta_n = 0.62890625$, as predicted by (5.4.29) and (5.4.30). Thus, for a typical carrier wave frequency of 80-250kHz, the transients decay in such a short time that they are not noticed by the amplifier user.

We have concisely determined the analytical steady-state solutions for this amplifier when a constant signal is input, and confirmed these solutions by comparison with a numerical simulation. Crucially, the steady-state solutions are the same as the leading-order solutions for a general input signal, and so we use these results in the next section, where we model the amplifier for a general input signal.

5.5   Dimensionless model for a general input signal

We now investigate the amplifier when a general signal is input. We implement the now familiar method of analysis introduced and extended in chapters 3 and 4, though find that additional work is required here to incorporate the filtering process into the model.

The method is therefore as follows. We begin by solving the dimensionless governing equations (5.3.2)-(5.3.5) and (5.3.9) to determine the nonlinear difference equations describing the operation of the amplifier for a general input signal. Converting this discrete model into a continuous model, we are able to solve the system using perturbation expansions to find the switching times of the comparator output, $g(t)$. Using (3.5.21), the formula giving the audio-frequency components of $g(t)$ in terms of its switching times, we then find the leading audio-frequency components of $g(t)$ itself. Finally, from (5.3.9), the differential equation relating the filter output $f(t)$ to $g(t)$, we obtain the leading audio-frequency components of $f(t)$.

Recall that for a constant input signal we were able to find an exact steady-state solution without specifying the relative sizes of the dimensionless combinations $\omega_a T$, $\lambda = \omega_f T$ and $\omega_c T$, where ω_a, ω_f and ω_c are typical audio, filter and carrier wave frequencies, and T is the period of the carrier wave. However, for a general input signal the relative sizes of $\omega_a T$, λ and $\omega_c T$ are significant in how we solve the model. We mentioned briefly in §5.2.1, in dimensional terms, that $\omega_a < \omega_f < \omega_c$. We now formalise this in dimensionless terms. Remembering that $\omega_c T = 2\pi = O(1)$, we choose $\epsilon = \omega_a T$ and define λ relative to ϵ. There are three sensible choices, each with $\epsilon \ll \omega_c T$, and therefore we here analyse three separate regimes:

Regime 1: $\lambda = \epsilon \lambda_2$, so that $O(\epsilon) = \lambda \ll \omega_c T$,
Regime 2: $\lambda = \epsilon^{\frac{1}{2}} \lambda_1$, so that $\epsilon \ll \lambda \ll \omega_c T$,
Regime 3: $\lambda = \lambda_0$, so that $\epsilon \ll \lambda = O(\omega_c T)$,

where λ_i is an $O(1)$ constant in each case. Note that for the second regime we have chosen $\lambda = O\left(\epsilon^{\frac{1}{2}}\right)$ in favour of any other intermediate scaling. This is because it results in a particular balance of terms that does not occur for any other intermediate scaling. We investigate these three regimes separately in §5.5.1-§5.5.3, following the method outlined in the preceding paragraph to determine the leading audio-frequency components of the filter output for each regime, aiming to establish the effect of the different scalings, and then discuss and compare our results in §5.5.4. We continue to use the notation $\dot{f}(t) = \frac{d}{dt}f(t)$ throughout.

5.5.1 Regime 1: $\lambda = \epsilon\lambda_2$

We here analyse the amplifier when a general signal is input, and the amplifier operates in regime 1, where $\lambda = \epsilon\lambda_2$. With this scaling λ is the same order as $\epsilon = \omega_a T$. The dimensionless governing equations for the amplifier are (5.3.2)-(5.3.5) and (5.3.9). Because λ appears explicitly only in (5.3.9), the differential equation for the filter output, the only adaptation needed to model the amplifier for this regime is to replace λ by $\epsilon\lambda_2$ in this equation. Thus

$$\ddot{f}(t) + \epsilon^2\lambda_2^2 f(t) = \epsilon^2\lambda_2^2 g(t), \tag{5.5.1}$$

and so the dimensionless governing equations for the amplifier for this regime are (5.3.2)-(5.3.5) and (5.5.1).

We first solve (5.5.1) to find equations for the filter output, $f(t)$, relating the values of $f(t)$ and $\dot{f}(t)$ at the switching times to the switching times themselves. Recall that the equations (5.4.3)-(5.4.6) for the filter output from our analysis for a constant input signal are valid for any input signal. Thus replacing λ by $\epsilon\lambda_2$ and using (5.4.3) and (5.4.4) to eliminate $f(n + \beta_n)$ and $\dot{f}(n + \beta_n)$ we find equations for $f(n + 1 + \alpha_{n+1})$ and $\dot{f}(n + 1 + \alpha_{n+1})$,

$$
\begin{aligned}
f(n + 1 + \alpha_{n+1}) &= [f(n + \alpha_n) + 1]\cos(\epsilon\lambda_2(1 + \alpha_{n+1} - \alpha_n)) \\
&\quad + \frac{1}{\epsilon\lambda_2}\dot{f}(n + \alpha_n)\sin(\epsilon\lambda_2(1 + \alpha_{n+1} - \alpha_n)) \\
&\quad - 2\cos(\epsilon\lambda_2(1 - \beta_n + \alpha_{n+1})) + 1, \tag{5.5.2}
\end{aligned}
$$

$$
\begin{aligned}
\dot{f}(n + 1 + \alpha_{n+1}) &= \dot{f}(n + \alpha_n)\cos(\epsilon\lambda_2(1 + \alpha_{n+1} - \alpha_n)) \\
&\quad - \epsilon\lambda_2[f(n + \alpha_n) + 1]\sin(\epsilon\lambda_2(1 + \alpha_{n+1} - \alpha_n)) \\
&\quad + 2\epsilon\lambda_2\sin(\epsilon\lambda_2(1 - \beta_n + \alpha_{n+1})). \tag{5.5.3}
\end{aligned}
$$

Next we solve the remaining four governing equations, (5.3.2)-(5.3.5), to find equations relating the values of $h(t)$, $f(t)$ and $\dot{f}(t)$ at the switching times, $r(t)$ (which we

defined as the integral of $s(t)$), and the switching times. We start by solving the differential equation for $h(t)$, (5.3.2), separately in regions I and II. Integrating (5.3.2) we obtain

$$h(t) - h(t_0) + \frac{k_1}{k_4}[f(t) - f(t_0)] + k_1[r(t) - r(t_0)]$$
$$= \begin{cases} +k_1(t - t_0) & \text{in region I} \\ -k_1(t - t_0) & \text{in region II,} \end{cases} \tag{5.5.4}$$

where t_0 is the time at the beginning of each region. Because $h(t)$ is continuous, we may evaluate (5.5.4) at the end of region I, for $n + \alpha_n < t < n + \beta_n$, to obtain an equation for $h(n + \beta_n)$. We find

$$\begin{aligned} h(n + \beta_n) &= h(n + \alpha_n) - \frac{k_1}{k_4}[f(n + \beta_n) - f(n + \alpha_n)] \\ &\quad - k_1[r(n + \beta_n) - r(n + \alpha_n)] + k_1(\beta_n - \alpha_n). \end{aligned} \tag{5.5.5}$$

Similarly, we evaluate (5.5.4) at the end of region II, for $n + \beta_n < t < n + 1 + \alpha_{n+1}$, finding an equation for $h(n + 1 + \alpha_{n+1})$,

$$\begin{aligned} h(n + 1 + \alpha_{n+1}) &= h(n + \beta_n) - \frac{k_1}{k_4}[f(n + 1 + \alpha_{n+1}) - f(n + \beta_n)] \\ &\quad - k_1[r(n + 1 + \alpha_{n+1}) - r(n + \beta_n)] \\ &\quad - k_1[1 + \alpha_{n+1} - \beta_n]. \end{aligned} \tag{5.5.6}$$

Turning our attention to the definitions of the switching times we now establish three equations relating $h(t)$ at the switching times to the switching times themselves. The comparator output $g(t)$ switches at the times satisfying $h(t) + v(t) = 0$, as defined by (5.3.4). Taking into consideration the restrictions on the switching times, (5.3.7) and (5.3.8), and then determining $v(t)$ at the switching times from (5.3.3) we obtain

$$\begin{aligned} h(n + \alpha_n) + 1 - 4\alpha_n &= 0, \\ h(n + \beta_n) - 3 + 4\beta_n &= 0, \\ h(n + 1 + \alpha_{n+1}) + 1 - 4\alpha_{n+1} &= 0. \end{aligned}$$

We use these three equations for the switching times to eliminate $h(t)$ from (5.5.5) and (5.5.6), resulting in the two equations

$$\begin{aligned} (4 - k_1)\alpha_n &- 4 + (4 + k_1)\beta_n = \\ &\frac{k_1}{k_4}[f(n + \beta_n) - f(n + \alpha_n)] + k_1[r(n + \beta_n) - r(n + \alpha_n)], \end{aligned} \tag{5.5.7}$$

$$\begin{aligned} (4 + k_1)\alpha_{n+1} &- 4 + k_1 + (4 - k_1)\beta_n = \\ &- \frac{k_1}{k_4}[f(n + 1 + \alpha_{n+1}) - f(n + \alpha_n)] \\ &- k_1[r(n + 1 + \alpha_{n+1}) - r(n + \beta_n)]. \end{aligned} \tag{5.5.8}$$

We then use (5.4.3) with $\lambda = \epsilon\lambda_2$ to eliminate $f(n + \beta_n)$ from these equations to obtain

$$
\begin{aligned}
(4 - k_1)\alpha_n - 4 + (4 + k_1)\beta_n = \\
\frac{k_1}{k_4}\bigg[-1 - f(n + \alpha_n) + [f(n + \alpha_n) + 1]\cos(\epsilon\lambda_2(\beta_n - \alpha_n)) \\
+ \frac{1}{\epsilon\lambda_2}\dot{f}(n + \alpha_n)\sin(\epsilon\lambda_2(\beta_n - \alpha_n))\bigg] + k_1[r(n + \beta_n) - r(n + \alpha_n)], \quad (5.5.9)
\end{aligned}
$$

$$
\begin{aligned}
(4 + k_1)\alpha_{n+1} - 4 + k_1 + (4 - k_1)\beta_n = \\
- \frac{k_1}{k_4}\bigg[f(n + 1 + \alpha_{n+1}) + 1 - [f(n + \alpha_n) + 1]\cos(\epsilon\lambda_2(\beta_n - \alpha_n)) \\
- \frac{1}{\epsilon\lambda_2}\dot{f}(n + \alpha_n)\sin(\epsilon\lambda_2(\beta_n - \alpha_n))\bigg] \\
- k_1[r(n + 1 + \alpha_{n+1}) - r(n + \beta_n)]. \quad (5.5.10)
\end{aligned}
$$

We have now derived the four exact nonlinear difference equations (5.5.2), (5.5.3), (5.5.9) and (5.5.10) governing this amplifier when a general signal is input. If we compare them to the two equations governing the first-order negative feedback amplifier, (3.5.4) and (3.5.5), we can immediately see the added complexity inserting the filter output back into the circuit via the second negative feedback loop brings. (5.5.9) and (5.5.10) are the same as (3.5.4) and (3.5.5) except that there is no multiplier in this design so $K = 0$, and here there is a second negative feedback loop so we have introduced the term $\frac{k_1}{k_4}[f(t) - f(t_0)]$. (5.5.2) and (5.5.3) are additional equations required to model the filter output. The increased complexity of this amplifier compared with the previous designs we modelled in chapters 3 and 4 means that deriving as succinct a system as possible, via the streamlined formulation demonstrated in chapter 3, is crucial in enabling us to solve the model.

As in chapters 3 and 4, rather than numerically iterating the system of difference equations to obtain the switching times, we now transform this discrete system into a continuous one and seek an analytical solution.

5.5.1.1 Continuous model

We proceed by converting the discrete system of equations, (5.5.2), (5.5.3), (5.5.9) and (5.5.10), which govern the amplifier for a general input signal, into a continuous one. We aim to solve the resulting system analytically to determine the switching times of the comparator output, which will enable us to find the leading audio-frequency components of the comparator output, which in turn will allow us to obtain the leading audio-frequency components of the filter output.

We construct the continuous model in the same way as introduced in chapter 3

for the first-order negative feedback amplifier, but also extend our definitions here to incorporate the filter output, which is included in this more complex model for the derivative negative feedback design. Therefore we begin by defining a dimensionless slow time, $\sigma = \epsilon t$, where $\epsilon = \omega_a T$ as defined above, and we now assume $\epsilon \ll 1$. As in chapter 3 we introduce

$$
\begin{aligned}
S(\sigma) &= s(t), \\
R(\sigma) &= \epsilon r(t),
\end{aligned}
\tag{5.5.11}
$$

where the definition of $R(\sigma)$ ensures $\frac{d}{d\sigma} R(\sigma) = S(\sigma)$.

We use the same two $O(1)$ functions $A(\sigma)$ and $B(\sigma)$ as in chapter 3, and in addition introduce two new $O(1)$ functions $\phi(\sigma)$ and $\psi(\sigma)$. We define all of these functions by their values at discrete points,

$$
\begin{aligned}
A(\epsilon n) &= \alpha_n, \tag{5.5.12} \\
B(\epsilon n) &= \beta_n, \tag{5.5.13} \\
\phi(\epsilon n) &= f(n + \alpha_n), \tag{5.5.14} \\
\epsilon\psi(\epsilon n) &= \dot{f}(n + \alpha_n). \tag{5.5.15}
\end{aligned}
$$

Therefore $A(\epsilon n)$ and $B(\epsilon n)$ are respectively the trailing- and leading-edge switching times in the nth period, $\phi(\epsilon n)$ is a sample of the filter output and $\psi(\epsilon n)$ is a sample of the derivative of the filter output. With these definitions we may also write α_{n+1}, $f(n+1+\alpha_{n+1})$ and $\dot{f}(n+1+\alpha_n)$ in terms of the slowly-varying functions, thus

$$
\begin{aligned}
\alpha_{n+1} &= A(\epsilon(n+1)), \\
f(n+1+\alpha_{n+1}) &= \phi(\epsilon(n+1)), \\
\dot{f}(n+1+\alpha_n) &= \epsilon\psi(\epsilon(n+1)).
\end{aligned}
$$

We then interpolate smoothly between the discrete points ensuring that each function is continuous and smooth, thus completing the definitions of the four functions $A(\sigma)$, $B(\sigma)$, $\phi(\sigma)$ and $\psi(\sigma)$. This enables us to convert the discrete system of four nonlinear difference equations, (5.5.2), (5.5.3), (5.5.9) and (5.5.10), into a continuous one, since we can now replace

$$
\begin{aligned}
\alpha_n & \quad \text{by} \quad A(\sigma), \\
\beta_n & \quad \text{by} \quad B(\sigma), \\
f(n + \alpha_n) & \quad \text{by} \quad \phi(\sigma), \\
\dot{f}(n + \alpha_n) & \quad \text{by} \quad \epsilon\psi(\sigma).
\end{aligned}
$$
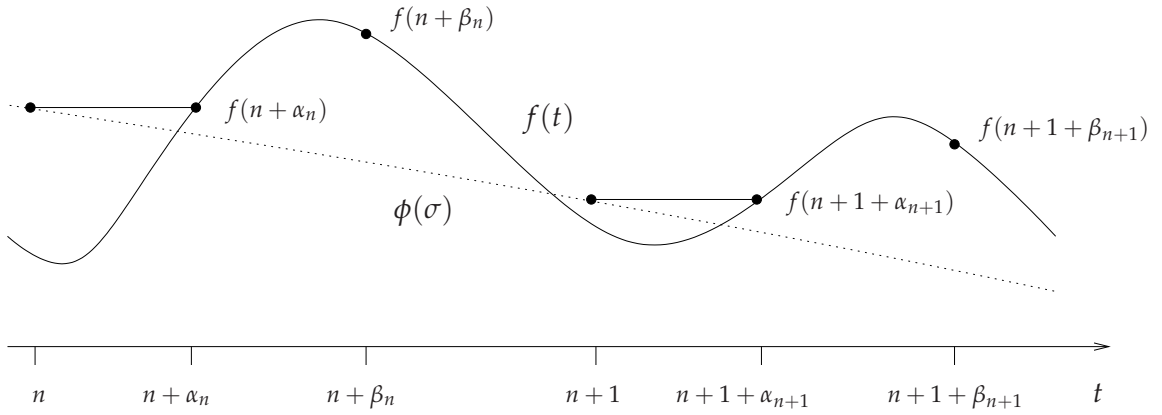
Figure 5.9: Diagram showing $f(t)$ (solid curve) and $\phi(\sigma)$ (dotted curve) for a typical input signal. The dots correspond to the values of $f(n + \alpha_n)$ and $f(n + \beta_n)$ and the horizontal lines correspond to the values of $f(n + \alpha_n)$.

Similarly, we can replace

$$\alpha_{n+1} \quad \text{by} \quad A(\sigma + \epsilon),$$
$$f(n + 1 + \alpha_{n+1}) \quad \text{by} \quad \phi(\sigma + \epsilon),$$
$$\dot{f}(n + 1 + \alpha_{n+1}) \quad \text{by} \quad \epsilon\psi(\sigma + \epsilon).$$

As we saw in previous chapters, the functions $A(\sigma)$ and $B(\sigma)$ at times $t = n$, i.e. $\sigma = \epsilon n$, take the values of α_n and β_n respectively. Additionally, the new functions $\phi(\sigma)$ and $\psi(\sigma)$ at times $t = n$ take the values of $f(n + \alpha_n)$ and $\dot{f}(n + \alpha_n)$ respectively. All four functions are slowly-varying with respect to time t.

The benefits of the streamlined analysis we have implemented can now be seen clearly. If we had retained all four of the samples $f(n + \alpha_n)$, $f(n + \beta_n)$, $\dot{f}(n + \alpha_n)$ and $\dot{f}(n + \beta_n)$, the continuous model here would be unnecessarily complicated. The values of $f(n + \alpha_n)$ and $f(n + \beta_n)$ differ from each other by up to an $O(1)$ amount in each period so we cannot define a function that is slowly-varying with respect to time t, but takes both of these samples into consideration (this is illustrated in figure 5.9, which shows the relationship between $\phi(\sigma)$ and $f(t)$). Therefore, rather than introduce two separate functions, one taking the values of the samples $f(n + \alpha_n)$ and the other taking the values of the samples $f(n + \beta_n)$, it is preferable to eliminate one set of samples, and we chose to eliminate $f(n + \beta_n)$. The same argument applies for $\dot{f}(n + \beta_n)$, which we also eliminated from the equations. Therefore this simplification results in the fewest new functions required here to formulate the continuous model.

Further to the factors considered in defining $A(\sigma)$ and $B(\sigma)$, discussed in chapter 3, there are two points of note in our definitions here. The first is that we introduce

133

a separate function $\psi(\sigma)$ as the slowly-varying version of $\dot{f}(n + \alpha_n)$ rather than using $\epsilon \frac{d}{d\sigma}\phi(\sigma)$. This is required as $\frac{d}{d\sigma}\phi(\epsilon(n + \alpha_n))$ is not necessarily related to $\dot{f}(n + \alpha_n)$, as can be seen in figure 5.9, where at $t = n + \alpha_n$ the derivative of $f(t)$ is not related to the derivative of $\phi(\sigma)$.

The second point to note is the orders of magnitude of $f(n + \alpha_n)$ and $\dot{f}(n + \alpha_n)$. To establish these we look at the solutions for $f(n + \alpha_n)$ and $\dot{f}(n + \alpha_n)$ for a constant signal, equations (5.4.21) and (5.4.23). Since $\lambda = \epsilon\lambda_2$ here, we replace λ by $\epsilon\lambda_2$ in these equations and expand for small ϵ,

$$
\begin{aligned}
f(n + \alpha_n) &= -s_0 + \frac{\epsilon^2\lambda_2^2 s_0(s_0^2 - 1)}{24} - \frac{\epsilon^4\lambda_2^4 s_0(3s_0^4 - 10s_0^2 + 7)}{5760} + O(\epsilon^6)\,, \\
\dot{f}(n + \alpha_n) &= \frac{\epsilon^2\lambda_2^2(1 - s_0^2)}{4} + \frac{\epsilon^4\lambda_2^4(s_0^4 - 2s_0^2 + 1)}{192} + O(\epsilon^6)\,.
\end{aligned}
$$

Thus, for an $O(1)$ general input signal we might expect $f(n + \alpha_n)$ to be $O(1)$ and $\dot{f}(n + \alpha_n)$ to be $O(\epsilon^2)$. This is certainly true for a constant signal, and is confirmed numerically: $f(n + \alpha_n)$ does not change significantly if λ is halved but $\dot{f}(n + \alpha_n)$ is approximately quartered if λ is halved. However, for a constant signal $\dot{s}(t) = 0$ so this expansion for $\dot{f}(n + \alpha_n)$ cannot tell us exactly how large $\dot{f}(n + \alpha_n)$ is for a general input signal. For a general input signal, because $s(t)$ varies and $s(t) = S(\sigma)$, there will be changes to $f(t)$ over the timescale σ, and so $\dot{f}(t) = O(\epsilon)$. Thus we choose $f(n + \alpha_n)$ to be $O(1)$ and $\dot{f}(n + \alpha_n)$ to be $O(\epsilon)$, hence the definitions (5.5.14) and (5.5.15), and find that the resulting equations are consistent.

We now write (5.5.2), (5.5.3), (5.5.9) and (5.5.10) in terms of our new functions, thereby transforming the discrete system into a continuous one. Thus, (5.5.2) and (5.5.3) become

$$
\begin{aligned}
\phi(\sigma + \epsilon) &= [\phi(\sigma) + 1]\cos(\epsilon\lambda_2(1 + A(\sigma + \epsilon) - A(\sigma))) \\
&\quad + \frac{1}{\lambda_2}\psi(\sigma)\sin(\epsilon\lambda_2(1 + A(\sigma + \epsilon) - A(\sigma))) \\
&\quad - 2\cos(\epsilon\lambda_2(1 - B(\sigma) + A(\sigma + \epsilon))) + 1, \quad\quad (5.5.16)
\end{aligned}
$$

$$
\begin{aligned}
\psi(\sigma + \epsilon) &= \psi(\sigma)\cos(\epsilon\lambda_2(1 + A(\sigma + \epsilon) - A(\sigma))) \\
&\quad - \lambda_2[\phi(\sigma) + 1]\sin(\epsilon\lambda_2(1 + A(\sigma + \epsilon) - A(\sigma))) \\
&\quad + 2\lambda_2\sin(\epsilon\lambda_2(1 - B(\sigma) + A(\sigma + \epsilon))). \quad\quad (5.5.17)
\end{aligned}
$$

To write (5.5.10) and (5.5.9) in terms of our new functions we must write $r(t)$ at the switching times in terms of R, σ, A and B, as discussed in chapter 3, where, for example,

we replace $r(n + \alpha_n)$ by $\frac{1}{\epsilon}R(\sigma + \epsilon A(\sigma))$. Thus (5.5.10) and (5.5.9) become

$$
\begin{aligned}
(4 - k_1)A(\sigma) - 4 + (4 + k_1)B(\sigma) = \\
\frac{k_1}{k_4}\Bigg[-1 - \phi(\sigma) + [\phi(\sigma) + 1]\cos(\epsilon\lambda_2(B(\sigma) - A(\sigma))) \\
+ \frac{1}{\lambda_2}\psi(\sigma)\sin(\epsilon\lambda_2(B(\sigma) - A(\sigma))) \Bigg] \\
+ k_1 \left[\frac{R(\sigma + \epsilon B(\sigma)) - R(\sigma + \epsilon A(\sigma))}{\epsilon} \right],
\end{aligned}
\tag{5.5.18}
$$

$$
\begin{aligned}
(4 + k_1)A(\sigma + \epsilon) - 4 + k_1 + (4 - k_1)B(\sigma) = \\
- \frac{k_1}{k_4}\Bigg[\phi(\sigma + \epsilon) + 1 - [\phi(\sigma) + 1]\cos(\epsilon\lambda_2(B(\sigma) - A(\sigma))) \\
- \frac{1}{\lambda_2}\psi(\sigma)\sin(\epsilon\lambda_2(B(\sigma) - A(\sigma))) \Bigg] \\
- k_1 \left[\frac{R(\sigma + \epsilon(1 + A(\sigma + \epsilon))) - R(\sigma + \epsilon B(\sigma))}{\epsilon} \right].
\end{aligned}
\tag{5.5.19}
$$

Despite deriving as concise a continuous model as possible, this involved system of four equations cannot be solved exactly, and therefore we pursue a perturbation solution, as in chapters 3 and 4. We thus expand $A(\sigma)$, $B(\sigma)$, $\phi(\sigma)$ and $\psi(\sigma)$ as series in ϵ, where

$$
A(\sigma) = \sum_{m=0}^{\infty} \epsilon^m A_m(\sigma),
\tag{5.5.20}
$$

$$
B(\sigma) = \sum_{m=0}^{\infty} \epsilon^m B_m(\sigma),
\tag{5.5.21}
$$

$$
\phi(\sigma) = \sum_{m=0}^{\infty} \epsilon^m \phi_m(\sigma),
\tag{5.5.22}
$$

$$
\psi(\sigma) = \sum_{m=0}^{\infty} \epsilon^m \psi_m(\sigma).
\tag{5.5.23}
$$

In addition, as discussed in chapter 3, we expand the remaining functions in (5.5.16)-(5.5.19) as Taylor series in ϵ. For example,

$$
\begin{aligned}
\phi(\sigma + \epsilon) &= \phi(\sigma) + \epsilon \frac{d}{d\sigma}\phi(\sigma) + \frac{\epsilon^2}{2}\frac{d^2}{d\sigma^2}\phi(\sigma) + O(\epsilon^3) \\
&= \phi_0(\sigma) + \epsilon \left(\phi_1(\sigma) + \frac{d}{d\sigma}\phi_0(\sigma) \right) \\
&\quad + \epsilon^2 \left(\phi_2(\sigma) + \frac{d}{d\sigma}\phi_1(\sigma) + \frac{1}{2}\frac{d^2}{d\sigma^2}\phi_0(\sigma) \right) + O(\epsilon^3), \\
\sin(\epsilon\lambda_2(1 - B(\sigma) + A(\sigma + \epsilon))) &= \epsilon\lambda_2(1 - B(\sigma) + A(\sigma + \epsilon)) + O(\epsilon^3) \\
&= \epsilon\lambda_2(1 - B_0(\sigma) + A_0(\sigma)) \\
&\quad + \epsilon^2 \left(-B_1(\sigma) + A_1(\sigma) + \frac{d}{d\sigma}A_0(\sigma) \right) + O(\epsilon^3),
\end{aligned}
$$

We then consider the four equations at successive orders in ϵ. We do not rearrange the following equations, so that the origin of each term can be seen more easily. At $O(1)$ all terms in both (5.5.16) and (5.5.17) cancel. At $O(\epsilon)$, (5.5.16) gives rise to

$$\frac{d\phi_0}{d\sigma} = \psi_0,$$ (5.5.24)

and at $O(\epsilon^2)$,

$$\frac{1}{2}\frac{d^2\phi_0}{d\sigma^2} + \frac{d\phi_1}{d\sigma} = -\frac{\lambda_2^2}{2}[\phi_0 + 1] + \psi_0\frac{dA_0}{d\sigma} + \psi_1 + \lambda_2^2(1 - B_0 + A_0)^2.$$ (5.5.25)

From (5.5.17), we find at $O(\epsilon)$,

$$\frac{d\psi_0}{d\sigma} = -\lambda_2^2(\phi_0 + 1) + 2\lambda_2^2(1 - B_0 + A_0),$$ (5.5.26)

and at $O(\epsilon^2)$,

$$\begin{aligned}
\frac{1}{2}\frac{d^2\psi_0}{d\sigma^2} + \frac{d\psi_1}{d\sigma} &= -\frac{\lambda_2^2}{2}\psi_0 - \lambda_2^2[\phi_0 + 1]\frac{dA_0}{d\sigma} - \lambda_2^2\phi_1 \\
&\quad + 2\lambda_2^2\left(-B_1 + A_1 + \frac{dA_0}{d\sigma}\right).
\end{aligned}$$ (5.5.27)

At $O(1)$, (5.5.18) gives

$$(4 - k_1)A_0 - 4 + (4 + k_1)B_0 = k_1[B_0 S - A_0 S],$$ (5.5.28)

at $O(\epsilon)$,

$$\begin{aligned}
(4 - k_1)A_1 + (4 + k_1)B_1 = \\
\frac{k_1}{k_4}\psi_0(B_0 - A_0) + k_1\left[B_1 S + \frac{1}{2}B_0^2\frac{dS}{d\sigma} - A_1 S - \frac{1}{2}A_0^2\frac{dS}{d\sigma}\right],
\end{aligned}$$ (5.5.29)

and at $O(\epsilon^2)$,

$$\begin{aligned}
(4 - k_1)A_2 + (4 + k_1)B_2 = \\
\frac{k_1}{k_4}\left[-\frac{\lambda_2^2}{2}[\phi_0 + 1](B_0 - A_0)^2 + \psi_0(B_1 - A_1) + \psi_1(B_0 - A_0)\right] \\
+ k_1\left[B_2 S + B_0 B_1\frac{dS}{d\sigma} + \frac{1}{6}B_0^3\frac{d^2 S}{d\sigma^2} - A_2 S - A_0 A_1\frac{dS}{d\sigma} - \frac{1}{6}A_0^3\frac{d^2 S}{d\sigma^2}\right].
\end{aligned}$$ (5.5.30)

Finally, from (5.5.19) we obtain, at $O(1)$,

$$(4 + k_1)A_0 - 4 + k_1 + (4 - k_1)B_0 = -k_1[(1 + A_0)S - B_0 S],$$ (5.5.31)

at $O(\epsilon)$,

$$\begin{aligned}
(4 + k_1)\left(A_1 + \frac{dA_0}{d\sigma}\right) + (4 - k_1)B_1 = \\
-\frac{k_1}{k_4}\left[\frac{d\phi_0}{d\sigma} - \psi_0(B_0 - A_0)\right] - k_1\left[\left(A_1 + \frac{dA_0}{d\sigma}\right)S \right. \\
\left. + \frac{1}{2}(1 + A_0)^2\frac{dS}{d\sigma} - B_1 S - \frac{1}{2}B_0^2\frac{dS}{d\sigma}\right],
\end{aligned}$$ (5.5.32)

and at $O(\epsilon^2)$,

$$
\begin{aligned}
(4 + k_1) &\left(\frac{1}{2} \frac{d^2 A_0}{d\sigma^2} + \frac{dA_1}{d\sigma} + A_2 \right) + (4 - k_1) B_2 = \\
&- \frac{k_1}{k_4} \left[\frac{1}{2} \frac{d^2 \phi_0}{d\sigma^2} + \frac{d\phi_1}{d\sigma} - \psi_0 (B_1 - A_1) - \psi_1 (B_0 - A_0) + \frac{\lambda_2^2}{2} [\phi_0 + 1](B_0 - A_0)^2 \right] \\
&- k_1 \left[\frac{dA_0}{d\sigma} \frac{dS}{d\sigma} + A_1 \frac{dS}{d\sigma} + A_0 \frac{dA_0}{d\sigma} \frac{dS}{d\sigma} + A_0 A_1 \frac{dS}{d\sigma} + \frac{1}{2} \frac{d^2 A_0}{d\sigma^2} S + \frac{dA_1}{d\sigma} S + A_2 S \right. \\
&+ \frac{1}{6} \frac{d^2 S}{d\sigma} + \frac{1}{2} A_0 \frac{d^2 S}{d\sigma^2} + \frac{1}{2} A_0^2 \frac{d^2 S}{d\sigma^2} + \frac{1}{6} A_0^3 \frac{d^2 S}{d\sigma^2} - B_2 S - B_0 B_1 \frac{dS}{d\sigma} - \frac{1}{6} B_0^3 \frac{d^2 S}{d\sigma^2} \left. \right]. \quad (5.5.33)
\end{aligned}
$$

Our aim is to find the leading audio-frequency components of the filter output. To do this we will need to determine the leading audio-frequency components of the comparator output, which, as discussed at the beginning of §5.5, we can obtain from the solutions for the switching times. We choose to find the audio-frequency components of the filter output only up to $O(\epsilon^3)$, which will show the first nonlinear terms, and therefore we must solve (5.5.24)-(5.5.33) to obtain the switching times only up to $O(\epsilon^3)$.

We begin by determining the $O(1)$ switching times. From (5.5.28) and (5.5.31) we find

$$
B_0 - A_0 = \frac{1}{2}(1 + S), \quad (5.5.34)
$$

and therefore the $O(1)$ short-time average of $g(t)$ is $-S$. We compare these results with the difference between the switching times for a constant signal, given by (5.4.18), and the short-time average of $g(t)$ for a constant input signal, (5.4.19), and find that the results are equivalent. Solving (5.5.28) and (5.5.31) simultaneously we find that the leading-order switching times for a general signal are

$$
A_0 = \frac{1}{16}(1 - S)\left[4 - k_1(1 + S)\right], \quad (5.5.35)
$$

$$
B_0 = \frac{1}{2} + \frac{1}{16}(1 + S)\left[4 - k_1(1 - S)\right], \quad (5.5.36)
$$

which are equivalent to those for a constant signal, given by (5.4.29) and (5.4.30). The equivalence of results at $O(1)$ for a general input signal and for a constant input signal is expected, because the slowly-varying general input signal we analyse here is constant to leading order. This is clearly the case for all three regimes we investigate for a general input signal, and so we anticipate that the leading-order switching times will be the same for all three regimes.

We now turn our attention to the higher-order switching times. Compared to the negative feedback designs we analysed in previous chapters, more work is required here to find these switching times. Namely, the configurations of (5.5.24) and (5.5.26)

result in a differential equation for $\phi_0(\sigma)$, which we must solve before we can obtain the $O(\epsilon)$ switching times. Similarly, (5.5.25) and (5.5.27) provide a differential equation for $\phi_1(\sigma)$, which we must solve to find the $O(\epsilon^2)$ switching times.

In order to obtain A_1 and B_1 we first solve (5.5.29) and (5.5.32) simultaneously, giving us the switching times at $O(\epsilon)$ in terms of ϕ_0 and ψ_0. Substituting for ϕ_0 using (5.5.24) it is straightforward to show that

$$
\begin{aligned}
A_1 & = \frac{1}{64 k_1 k_4}\left[k_4 \frac{dS}{d\sigma}\left(16 - 4k_1 + k_1^2 + k_1 S(-4 + 2k_1 - k_1^2) - 3k_1^2 S^2 + k_1^3 S^3\right)\right. \\
& \left. + 8 k_1 \psi_0(-2 + k_1 S)\right],
\end{aligned}
\tag{5.5.37}
$$

$$
\begin{aligned}
B_1 & = \frac{1}{64 k_1 k_4}\left[k_4 \frac{dS}{d\sigma}\left(-16 + 12k_1 - k_1^2 + k_1 S(-4 + 6k_1 - k_1^2) + 3k_1^2 S^2 + k_1^3 S^3\right)\right. \\
& \left. + 8 k_1 \psi_0(2 + k_1 S)\right].
\end{aligned}
\tag{5.5.38}
$$

We now compute ϕ_0, which will allow us to find ψ_0. Differentiating (5.5.24) we obtain an expression for $\frac{d\psi_0}{d\sigma}$. Substituting this, and $B_0 - A_0$ from (5.5.34), into (5.5.26) we obtain a second-order linear inhomogeneous differential equation for ϕ_0,

$$
\frac{d^2 \phi_0}{d\sigma^2} + \lambda_2^2 \phi_0 = -\lambda_2^2 S.
\tag{5.5.39}
$$

We compare this differential equation for $\phi_0(\sigma)$ with that for $f(t)$, (5.5.1). Recall that the function $\phi_0(\sigma)$ represents the leading-order component of a slowly-varying version of $f(t)$. If we write (5.5.1) in terms of the slow timescale $\sigma = \epsilon t$, and look at the equation at leading order, so that $g(t)$ becomes its $O(1)$ short-time average, $-S$, we obtain (5.5.39).

We now solve (5.5.39) using the method of variation of parameters (see, for example, [43]) and find the general solution for ϕ_0,

$$
\phi_0(\sigma) = \lambda_2 \int_0^\sigma S(t') \sin(\lambda_2(t' - \sigma))\, dt' + D \cos \lambda_2 \sigma + E \sin \lambda_2 \sigma,
$$

where D and E are constants. The oscillations at frequency λ_2 in this solution would in practice be damped by the inclusion of a resistor in the filter circuit (as discussed in §5.4.1) so we ignore them from now on. Thus at $O(1)$ the slowly varying function $\phi(\sigma)$ is given by

$$
\phi_0(\sigma) = \lambda_2 \int_0^\sigma S(t') \sin(\lambda_2(t' - \sigma))\, dt'.
\tag{5.5.40}
$$

Rather than continue our analysis for a general input signal, we now specify the input signal. This will simplify the subsequent calculations considerably as we will be able to compute the integral in (5.5.40), and thereby will enable us to determine the filter output in a form that clearly shows the distortion and harmonics.

We define the input signal to be sinusoidal, choosing in dimensional terms $s^*(t^*) = s_0 V \sin \omega_a t^*$ (where s_0 is a constant), which in dimensionless terms is $s(t) = s_0 \sin \epsilon t$. Transforming to the slow timescale σ, the input signal is now

$$S(\sigma) = s_0 \sin \sigma.$$

We may now simply integrate (5.5.40) to obtain the solution for $\phi_0(\sigma)$,

$$\phi_0(\sigma) = \frac{s_0 \lambda_2^2}{1 - \lambda_2^2} \sin \sigma.$$

This solution can also be obtained as a particular integral of (5.5.39). It is now straightforward to obtain ψ_0 from (5.5.24),

$$\psi_0(\sigma) = \frac{s_0 \lambda_2^2}{1 - \lambda_2^2} \cos \sigma.$$

Substituting this into (5.5.37) and (5.5.38) we find the solutions for the switching times at $O(\epsilon)$ for a sinusoidal input signal. Upon rearranging we find

$$A_1 = \gamma_1 \cos \sigma + \gamma_2 \sin 2\sigma + \gamma_3 \cos 3\sigma + \gamma_4 \sin 4\sigma, \qquad (5.5.41)$$

$$B_1 = \gamma_5 \cos \sigma + \gamma_6 \sin 2\sigma + \gamma_7 \cos 3\sigma + \gamma_4 \sin 4\sigma, \qquad (5.5.42)$$

where

$$\gamma_1 = \frac{s_0}{256 k_1} \left(64 - 16 k_1 + 4 k_1^2 - 3 k_1^2 s_0^2 \right) + \frac{s_0}{4 k_4 \left(1 - \frac{1}{\lambda_2^2} \right)},$$

$$\gamma_2 = \frac{s_0^2}{256} \left(-8 + 4 k_1 - 2 k_1^2 + k_1^2 s_0^2 \right) - \frac{k_1 s_0^2}{16 k_4 \left(1 - \frac{1}{\lambda_2^2} \right)},$$

$$\gamma_3 = \frac{3 k_1 s_0^3}{256},$$

$$\gamma_4 = -\frac{k_1^2 s_0^4}{512},$$

$$\gamma_5 = \frac{s_0}{256 k_1} \left(-64 + 48 k_1 - 4 k_1^2 + 3 k_1^2 s_0^2 \right) - \frac{s_0}{4 k_4 \left(1 - \frac{1}{\lambda_2^2} \right)},$$

$$\gamma_6 = \frac{s_0^2}{256} \left(-8 + 12 k_1 - 2 k_1^2 + k_1^2 s_0^2 \right) - \frac{k_1 s_0^2}{16 k_4 \left(1 - \frac{1}{\lambda_2^2} \right)},$$

$$\gamma_7 = -\gamma_3.$$

We must now find the switching times at $O(\epsilon^2)$. The method for determining A_2 and B_2 is equivalent to that for A_1 and B_1 but involves much more lengthy algebra, so we do not present the solutions here, although later we will use A_2 and B_2 to determine the leading audio-frequency components of the comparator output. We first differentiate (5.5.25) and obtain an expression for $\frac{d\psi_1}{d\sigma}$. We then substitute $\frac{d\psi_1}{d\sigma}$ into (5.5.27). This

results in a second-order differential equation for ϕ_1, which we solve using the method of variation of parameters, and ignoring oscillations at frequency λ_2. From the solution for ϕ_1 we can then find ψ_1 using (5.5.25). Using all of the solutions found above, and solving (5.5.30) and (5.5.33) simultaneously we determine A_2 and B_2, which we find contain all harmonics of the input signal up to and including the sixth.

We have now found $A(\sigma)$ and $B(\sigma)$ up to $O(\epsilon^3)$. As in previous chapters, we are primarily interested in the audio part of the amplifier output. The next step is therefore to calculate the leading audio-frequency components of the comparator output, which will then allow us to find the leading audio-frequency components of the filter output.

Calculation of $g(t)$, the comparator output. We now use the formula (3.5.21), which gives the audio-frequency components of the comparator output, $g_a(t)$, in terms of its switching times. This formula, derived in chapter 3, is valid for any amplifier design, and so we use it here to determine the leading audio-frequency components of the comparator output for this derivative negative feedback amplifier. Inserting our solutions for the $O(1)$ and $O(\epsilon)$ switching times for a sinusoidal input signal, using (5.5.35),(5.5.36),(5.5.41) and (5.5.42), and the solutions for A_2 and B_2 which we have not presented, we find $g_a(t)$ for a sinusoidal input signal,

$$g_a(t) = -s_0 \sin \sigma + \epsilon \gamma_8 \cos \sigma + \epsilon^2 (\gamma_9 \sin \sigma + \gamma_{10} \sin 3\sigma) + O(\epsilon^3),$$

where

$$\gamma_8 = \frac{s_0}{k_1} + \frac{s_0}{k_4 \left(1 - \frac{1}{\lambda_2^2}\right)}, \tag{5.5.43}$$

$$\gamma_9 = \frac{2s_0}{k_1 k_4 \left(1 - \frac{1}{\lambda_2^2}\right)} + \frac{s_0}{k_4^2 \left(1 - \frac{1}{\lambda_2^2}\right)^2} + \frac{s_0}{k_1^2} - \frac{s_0}{48} - \frac{s_0^3}{64}, \tag{5.5.44}$$

$$\gamma_{10} = \frac{3s_0^3}{64}. \tag{5.5.45}$$

In contrast to previous chapters, a little more work is required here to determine the amplifier output itself, which is the filter output $f(t)$. We did not compute the filter output in previous chapters because the filtering process was entirely separate in those designs, unlike here where the filter output is incorporated into the design.

Calculation of $f(t)$, the filter output. To calculate the audio part of the filter output we solve (5.5.1), the differential equation for the filter output, for frequencies in the audio range. Defining $f_a(t)$ to be the audio part of $f(t)$, (5.5.1) reduces to

$$\frac{d^2}{dt^2} f_a(t) + \epsilon^2 \lambda_2^2 f_a(t) = \epsilon^2 \lambda_2^2 g_a(t).$$

In terms of our slow time $\sigma = \epsilon t$ this becomes

$$\frac{d^2}{d\sigma^2} f_a(t) + \lambda_2^2 f_a(t) = \lambda_2^2 g_a(t). \tag{5.5.46}$$

To obtain $f_a(t)$ we define $f_{a,i}(t)$ to be the $O(\epsilon^i)$ component of $f_a(t)$, and $g_{a,i}(t)$ to be the $O(\epsilon^i)$ component of $g_a(t)$ and then solve (5.5.46) at successive orders in ϵ. Thus, at $O(1)$ we solve

$$
\begin{aligned}
\frac{d^2}{d\sigma^2} f_{a,0}(t) + \lambda_2^2 f_{a,0}(t) &= \lambda_2^2 g_{a,0}(t) \\
&= -s_0 \lambda_2^2 \sin \sigma,
\end{aligned}
$$

at $O(\epsilon)$ we solve

$$
\begin{aligned}
\frac{d^2}{d\sigma^2} f_{a,1}(t) + \lambda_2^2 f_{a,1}(t) &= \lambda_2^2 g_{a,1}(t) \\
&= \lambda_2^2 \gamma_8 \cos \sigma,
\end{aligned}
$$

and at $O(\epsilon^2)$ we solve

$$
\begin{aligned}
\frac{d^2}{d\sigma^2} f_{a,2}(t) + \lambda_2^2 f_{a,2}(t) &= \lambda_2^2 g_{a,2}(t) \\
&= \lambda_2^2 \left(\gamma_9 \sin \sigma + \gamma_{10} \sin 3\sigma \right).
\end{aligned}
$$

Ignoring the oscillations at frequency λ_2, which would be removed by damping in the filter, we obtain

$$
f_{a,0}(t) = -\frac{s_0}{1 - \frac{1}{\lambda_2^2}} \sin \sigma,
$$

$$
f_{a,1}(t) = \frac{\gamma_8}{1 - \frac{1}{\lambda_2^2}} \cos \sigma,
$$

$$
f_{a,2}(t) = \frac{\gamma_9}{1 - \frac{1}{\lambda_2^2}} \sin \sigma + \frac{\gamma_{10}}{1 - \frac{9}{\lambda_2^2}} \sin 3\sigma.
$$

Combining these terms we obtain

$$
\begin{aligned}
f_a(t) &= -\frac{s_0}{1 - \frac{1}{\lambda_2^2}} \sin \sigma + \epsilon \frac{\gamma_8}{1 - \frac{1}{\lambda_2^2}} \cos \sigma \\
&\quad + \epsilon^2 \left(\frac{\gamma_9}{1 - \frac{1}{\lambda_2^2}} \sin \sigma + \frac{\gamma_{10}}{1 - \frac{9}{\lambda_2^2}} \sin 3\sigma \right) + O(\epsilon^3), \tag{5.5.47}
\end{aligned}
$$

where γ_8-γ_{10} are given by (5.5.43)-(5.5.45). (5.5.47) gives the leading audio-frequency components of the filter output when the amplifier operates in regime 1 and a sinusoidal signal is input. The lengthy calculations required to achieve this result were facilitated by extending the streamlined analysis, introduced in chapter 3, to the more

complex design of this derivative negative feedback amplifier. The leading audio-frequency component of this amplifier output is proportional to the input signal. This is expected, as we know that the output of the filter is proportional to its input (as discussed in §5.2.1), and that the audio part of the input to the filter is $g_a(t)$, whose leading audio-frequency component is exactly minus the input signal. The terms at higher order in (5.5.47) represent distortion, and in particular the presence of the third-harmonic of the input signal reveals that there is nonlinear distortion, which cannot be removed by any choice of the constant s_0. If we revert to dimensional variables and parameters (5.5.47) becomes

$$
f_a^*(t^*) = -\frac{s_0 V \omega_f^2}{\omega_f^2 - \omega_a^2} \sin \omega_a t^* + \omega_a T \frac{V \omega_f^2 \gamma_8^*}{\omega_f^2 - \omega_a^2} \cos \omega_a t^*
$$
$$
+ (\omega_a T)^2 \left(\frac{V \omega_f^2 \gamma_9^*}{\omega_f^2 - \omega_a^2} \sin \omega_a t^* + (\omega_a T)^2 \frac{V \omega_f^2 \gamma_{10}^*}{\omega_f^2 - 9\omega_a^2} \sin 3\omega_a t^* \right) + O\big((\omega_a T)^3\big),
$$

where γ_i^* are the same as γ_i previously, except now written in terms of dimensional parameters,

$$
\gamma_8^* = \frac{s_0}{c_4 T \left(1 - \frac{1}{(\omega_f T)^2}\right)} + \frac{s_0}{c_1 T},
$$
$$
\gamma_9^* = \frac{2s_0}{c_1 c_4 T^2 \left(1 - \frac{1}{(\omega_f T)^2}\right)} + \frac{s_0}{(c_4 T)^2 \left(1 - \frac{1}{(\omega_f T)^2}\right)^2} + \frac{s_0}{(c_1 T)^2} - \frac{s_0}{48} - \frac{s_0^3}{64},
$$
$$
\gamma_{10}^* = \frac{3s_0^3}{64}.
$$

From this we can see clearly that the distortion terms affect the amplitude of the signal at frequency ω_a and that the third-harmonic introduced has amplitude $O\big((\omega_a T)^2\big)$.

Recall that we wish to analyse the operation of this amplifier in three separate regimes, each differing in the scaling of $\lambda = \omega_f T$ relative to $\epsilon = \omega_a T$ and $\omega_c T$. Here, for regime 1, we have taken $\lambda = \epsilon \lambda_2$, so that $O(\epsilon) = \lambda \ll \omega_c T$. We will discuss the results for this regime again later, in §5.5.4, in the context of the three different regimes. In the following section we analyse the second scaling for λ, aiming to determine the filter output in the same way as we have here.

5.5.2   Regime 2: $\lambda = \epsilon^{\frac{1}{2}} \lambda_1$

We now analyse the amplifier when it operates in regime 2, for a general input signal. In this regime, $\lambda = \epsilon^{\frac{1}{2}} \lambda_1$, where $\epsilon = \omega_a T$, which ensures that $\epsilon \ll \lambda \ll \omega_c T$, as discussed at the beginning of §5.5. The dimensionless equations governing the amplifier under these conditions are the same as those in regime 1, except that we impose

$\lambda = \epsilon^{\frac{1}{2}}\lambda_1$ in (5.3.9), the differential equation for the filter output, $f(t)$. Thus the governing equations are (5.3.2)-(5.3.5) and

$$\frac{d^2}{dt^2}f(t) + \epsilon\lambda_1^2 f(t) = \epsilon\lambda_1^2 g(t). \tag{5.5.48}$$

We solve these equations following the same steps as in regime 1. Because the only change we have made in this regime compared to the first regime is to the scaling for λ, the only difference in the solutions is that $\epsilon\lambda_2$ is replaced by $\epsilon^{\frac{1}{2}}\lambda_1$. Therefore, solving (5.5.48) we find two equations relating the filter output and its derivative, both evaluated at the switching times, to the switching times themselves,

$$
\begin{aligned}
f(n+1+\alpha_{n+1}) &= [f(n+\alpha_n)+1]\cos(\epsilon^{\frac{1}{2}}\lambda_1(1+\alpha_{n+1}-\alpha_n)) \\
&\quad + \frac{1}{\epsilon^{\frac{1}{2}}\lambda_1}\dot{f}(n+\alpha_n)\sin(\epsilon^{\frac{1}{2}}\lambda_1(1+\alpha_{n+1}-\alpha_n)) \\
&\quad - 2\cos(\epsilon^{\frac{1}{2}}\lambda_1(1-\beta_n+\alpha_{n+1})) + 1, \tag{5.5.49} \\
\dot{f}(n+1+\alpha_{n+1}) &= \dot{f}(n+\alpha_n)\cos(\epsilon^{\frac{1}{2}}\lambda_1(1+\alpha_{n+1}-\alpha_n)) \\
&\quad - \epsilon^{\frac{1}{2}}\lambda_1[f(n+\alpha_n)+1]\sin(\epsilon^{\frac{1}{2}}\lambda_1(1+\alpha_{n+1}-\alpha_n)) \\
&\quad + 2\epsilon^{\frac{1}{2}}\lambda_1\sin(\epsilon^{\frac{1}{2}}\lambda_1(1-\beta_n+\alpha_{n+1})). \tag{5.5.50}
\end{aligned}
$$

Similarly, solving (5.3.2)-(5.3.5), and after much algebraic manipulation, we obtain two equations relating $f(t)$, $\dot{f}(t)$, and the integral of the input signal $r(t)$, all evaluated at the switching times, to the switching times. These are

$$
\begin{aligned}
(4-k_1)\alpha_n &- 4 + (4+k_1)\beta_n = \\
&\frac{k_1}{k_4}\Big[-1 - f(n+\alpha_n) + [f(n+\alpha_n)+1]\cos(\epsilon^{\frac{1}{2}}\lambda_1(\beta_n-\alpha_n)) \\
&\quad + \frac{1}{\epsilon^{\frac{1}{2}}\lambda_1}\dot{f}(n+\alpha_n)\sin(\epsilon^{\frac{1}{2}}\lambda_1(\beta_n-\alpha_n))\Big] + k_1[r(n+\beta_n)-r(n+\alpha_n)], \tag{5.5.51} \\
(4+k_1)\alpha_{n+1} &- 4 + k_1 + (4-k_1)\beta_n = \\
&-\frac{k_1}{k_4}\Big[f(n+1+\alpha_{n+1}) + 1 - [f(n+\alpha_n)+1]\cos(\epsilon^{\frac{1}{2}}\lambda_1(\beta_n-\alpha_n)) \\
&\quad - \frac{1}{\epsilon^{\frac{1}{2}}\lambda_1}\dot{f}(n+\alpha_n)\sin(\epsilon^{\frac{1}{2}}\lambda_1(\beta_n-\alpha_n))\Big] \\
&\quad - k_1[r(n+1+\alpha_{n+1})-r(n+\beta_n)]. \tag{5.5.52}
\end{aligned}
$$

The four exact nonlinear difference equations (5.5.49)-(5.5.52) thus describe the operation of this amplifier in regime 2 when a general signal is input. They are equivalent to (5.5.2), (5.5.3), (5.5.9) and (5.5.10) for regime 1. We use the same method to solve the equations here as in §5.5.1 for regime 1, and therefore proceed by transforming the discrete system of equations into a continuous one.

5.5.2.1 Continuous model

We convert (5.5.49)-(5.5.52) into a continuous system by writing the equations in terms of the slowly-varying functions $R(\sigma)$, $A(\sigma)$, $B(\sigma)$, $\phi(\sigma)$ and $\psi(\sigma)$, which are defined by (5.5.11), (5.5.12)-(5.5.15) respectively.

We omit the details concerning the construction of the continuous model here, since they were discussed fully in §5.5.1.1. However, there is an important point to note in our using the same definitions of the slowly-varying functions as in the first regime, which would be easy to overlook. To establish the scalings for $f(n + \alpha_n)$ and $\dot{f}(n + \alpha_n)$ we proceed as before, by looking at the solutions for $f(n + \alpha_n)$ and $\dot{f}(n + \alpha_n)$ for a constant signal, equations (5.4.21) and (5.4.23). Here, we replace λ by $\epsilon^{\frac{1}{2}}\lambda_1$ in these solutions before expanding for small ϵ,

$$f(n + \alpha_n) = -s_0 + \frac{\epsilon\lambda_1^2 s_0(s_0^2 - 1)}{24} + O(\epsilon^2), \tag{5.5.53}$$

$$\dot{f}(n + \alpha_n) = \frac{\epsilon\lambda_1^2(1 - s_0^2)}{4} + O(\epsilon^2). \tag{5.5.54}$$

Thus for this regime, these expansions suggest that $f(n + \alpha_n)$ should be $O(1)$ and $\dot{f}(n + \alpha_n)$ should be $O(\epsilon)$. As discussed in §5.5.1.1, these expansions cannot necessarily tell us how large $\dot{f}(n + \alpha_n)$ is for a general input signal. By considering how $f(t)$ varies for a general input signal we expect $\dot{f}(t) = O(\epsilon)$. Therefore, here the expansions do predict the correct scalings for both $f(n + \alpha_n)$ and $\dot{f}(n + \alpha_n)$, and so we choose $f(n + \alpha_n)$ to be $O(1)$ and $\dot{f}(n + \alpha_n)$ to be $O(\epsilon)$.

In terms of the slowly-varying functions, (5.5.49) and (5.5.50) become

$$\begin{aligned}
\phi(\sigma + \epsilon) &= [\phi(\sigma) + 1]\cos(\epsilon^{\frac{1}{2}}\lambda_1(1 + A(\sigma + \epsilon) - A(\sigma))) \\
&\quad + \frac{\epsilon^{\frac{1}{2}}}{\lambda_1}\psi(\sigma)\sin(\epsilon^{\frac{1}{2}}\lambda_1(1 + A(\sigma + \epsilon) - A(\sigma))) \\
&\quad - 2\cos(\epsilon^{\frac{1}{2}}\lambda_1(1 - B(\sigma) + A(\sigma + \epsilon))) + 1, \tag{5.5.55} \\
\epsilon\psi(\sigma + \epsilon) &= \epsilon\psi(\sigma)\cos(\epsilon^{\frac{1}{2}}\lambda_1(1 + A(\sigma + \epsilon) - A(\sigma))) \\
&\quad - \epsilon^{\frac{1}{2}}\lambda_1[\phi(\sigma) + 1]\sin(\epsilon^{\frac{1}{2}}\lambda_1(1 + A(\sigma + \epsilon) - A(\sigma))) \\
&\quad + 2\epsilon^{\frac{1}{2}}\lambda_1\sin(\epsilon^{\frac{1}{2}}\lambda_1(1 - B(\sigma) + A(\sigma + \epsilon))), \tag{5.5.56}
\end{aligned}$$

144

while (5.5.52) and (5.5.51) become

$$
\begin{aligned}
(4 - k_1)A(\sigma) - 4 &+ (4 + k_1)B(\sigma) = \\
&\frac{k_1}{k_4}\left[-1 - \phi(\sigma) + [\phi(\sigma) + 1]\cos(\epsilon^{\frac{1}{2}}\lambda_1(B(\sigma) - A(\sigma))) \right. \\
&\left. + \frac{\epsilon^{\frac{1}{2}}}{\lambda_1}\psi(\sigma)\sin(\epsilon^{\frac{1}{2}}\lambda_1(B(\sigma) - A(\sigma))) \right] \\
&+ k_1\left[\frac{R(\sigma + \epsilon B(\sigma)) - R(\sigma + \epsilon A(\sigma))}{\epsilon} \right],
\end{aligned}
\tag{5.5.57}
$$

$$
\begin{aligned}
(4 + k_1)A(\sigma + \epsilon) - 4 &+ k_1 + (4 - k_1)B(\sigma) = \\
&-\frac{k_1}{k_4}\left[\phi(\sigma + \epsilon) + 1 - [\phi(\sigma) + 1]\cos(\epsilon^{\frac{1}{2}}\lambda_1(B(\sigma) - A(\sigma))) \right. \\
&\left. - \frac{\epsilon^{\frac{1}{2}}}{\lambda_1}\psi(\sigma)\sin(\epsilon^{\frac{1}{2}}\lambda_1(B(\sigma) - A(\sigma))) \right] \\
&- k_1\left[\frac{R(\sigma + \epsilon(1 + A(\sigma + \epsilon))) - R(\sigma + \epsilon B(\sigma))}{\epsilon} \right].
\end{aligned}
\tag{5.5.58}
$$

Although we use the same definitions of the slowly-varying functions as in regime 1, because we use a different scaling for λ inevitably there are differences in these equations compared with those for regime 1, (5.5.16)-(5.5.19). We now expand $A(\sigma)$, $B(\sigma)$, $\phi(\sigma)$ and $\psi(\sigma)$ as series in ϵ, as defined by (5.5.20)-(5.5.23), and expand the remaining functions in (5.5.55)-(5.5.58) as Taylor series in ϵ. After expanding the sine and cosine terms as Taylor series in ϵ, and because the sine terms are multiplied by $\epsilon^{\frac{1}{2}}$, there remain terms only in integer powers of ϵ in the equations. We therefore consider the four equations at successive integer orders in ϵ as we did for regime 1. At $O(1)$ all terms in both (5.5.55) and (5.5.56) cancel. From (5.5.55) we find, at $O(\epsilon)$,

$$
\frac{d\phi_0}{d\sigma} = -\frac{\lambda_1^2}{2}(\phi_0 + 1) + \psi_0 + \lambda_1^2(1 - B_0 + A_0)^2,
\tag{5.5.59}
$$

and at $O(\epsilon^2)$,

$$
\begin{aligned}
\frac{1}{2}\frac{d^2\phi_0}{d\sigma^2} + \frac{d\phi_1}{d\sigma} = \\
&[\phi_0 + 1]\left(\frac{\lambda_1^4}{24} - \lambda_1^2\frac{dA_0}{d\sigma} \right) - \frac{\lambda_1^2}{2}\phi_1 + \psi_0\left(\frac{dA_0}{d\sigma} - \frac{\lambda_1^2}{6} \right) + \psi_1 \\
&- \frac{\lambda_1^4}{12}(1 - B_0 + A_0)^4 + 2\lambda_1^2\left(-B_1 + \frac{dA_0}{d\sigma} + A_1 \right)(1 - B_0 + A_0).
\end{aligned}
\tag{5.5.60}
$$

At $O(\epsilon)$, (5.5.56) gives

$$
0 = -\lambda_1^2(\phi_0 + 1) + 2\lambda_1^2(1 - B_0 + A_0),
\tag{5.5.61}
$$

145

and at $O(\epsilon^2)$,

$$
\begin{aligned}
\frac{d\psi_0}{d\sigma} = {} & -\frac{\lambda_1^2}{2}\psi_0 - \lambda_1[\phi_0 + 1]\left(\lambda_1\frac{dA_0}{d\sigma} - \frac{\lambda_1^3}{6}\right) - \lambda_1^2\phi_1 \\
& + 2\lambda_1\left(\lambda_1\left(-B_1 + \frac{dA_0}{d\sigma} + A_1\right) - \frac{\lambda_1^3}{6}(1 - B_0 + A_0)^3\right).
\end{aligned}
\tag{5.5.62}
$$

At $O(1)$, (5.5.57) and (5.5.58) give

$$
\begin{aligned}
(4 - k_1)A_0 - 4 + (4 + k_1)B_0 &= k_1[B_0 S - A_0 S], \tag{5.5.63} \\
(4 + k_1)A_0 - 4 + k_1 + (4 - k_1)B_0 &= -k_1[(1 + A_0)S - B_0 S], \tag{5.5.64}
\end{aligned}
$$

respectively, which are the same as for regime 1. From (5.5.57) we obtain, at $O(\epsilon)$,

$$
\begin{aligned}
(4 - k_1)A_1 + (4 + k_1)B_1 = {} & \\
& \frac{k_1}{k_4}\left[-\frac{\lambda_1^2}{2}[\phi_0 + 1](B_0 - A_0)^2 + \psi_0(B_0 - A_0)\right] \\
& + k_1\left[B_1 S + \frac{1}{2}B_0^2\frac{dS}{d\sigma} - A_1 S - \frac{1}{2}A_0^2\frac{dS}{d\sigma}\right],
\end{aligned}
\tag{5.5.65}
$$

and at $O(\epsilon^2)$,

$$
\begin{aligned}
(4 - k_1)A_2 + (4 + k_1)B_2 = {} & \\
& \frac{k_1}{k_4}\left[[\phi_0 + 1]\left(\frac{\lambda_1^4}{24}(B_0 - A_0)^4 - \lambda_1^2(B_1 - A_1)(B_0 - A_0)\right)\right. \\
& \left. - \frac{\lambda_1^2}{2}\phi_1(B_0 - A_0)^2 + \psi_0\left(B_1 - A_1 - \frac{\lambda_1^2}{6}(B_0 - A_0)^3\right) + \psi_1(B_0 - A_0)\right] \\
& + k_1\left[-A_2 S - \frac{A_0^3}{6}\frac{d^2 S}{d\sigma^2} - A_0 A_1\frac{dS}{d\sigma} + B_2 S + \frac{B_0^3}{6}\frac{d^2 S}{d\sigma^2} + B_0 B_1\frac{dS}{d\sigma}\right].
\end{aligned}
\tag{5.5.66}
$$

Lastly, at $O(\epsilon)$, (5.5.58) gives

$$
\begin{aligned}
(4 + k_1)\left(A_1 + \frac{dA_0}{d\sigma}\right) + (4 - k_1)B_1 = {} & \\
& -\frac{k_1}{k_4}\left[\frac{d\phi_0}{d\sigma} + \frac{\lambda_1^2}{2}(\phi_0 + 1)(B_0 - A_0)^2 - \psi_0(B_0 - A_0)\right] \\
& - k_1\left[\left(A_1 + \frac{dA_0}{d\sigma}\right)S + \frac{1}{2}(1 + A_0)^2\frac{dS}{d\sigma} - B_1 S - \frac{1}{2}B_0^2\frac{dS}{d\sigma}\right],
\end{aligned}
\tag{5.5.67}
$$

and at $O(\epsilon^2)$,

$$
\begin{aligned}
(4 + k_1) & \left(\frac{1}{2} \frac{d^2 A_0}{d\sigma^2} + \frac{dA_1}{d\sigma} + A_2 \right) + (4 - k_1) B_2 = \\
& - \frac{k_1}{k_4} \left[\frac{d\phi_1}{d\sigma} + \frac{1}{2} \frac{d^2 \phi_0}{d\sigma^2} - [\phi_0 + 1] \left(\frac{\lambda_1^4}{24} (B_0 - A_0)^4 - \lambda_1^2 (B_1 - A_1)(B_0 - A_0) \right) \right. \\
& \left. + \frac{\lambda_1^2}{2} \phi_1 (B_0 - A_0)^2 - \psi_0 \left(B_1 - A_1 - \frac{\lambda_1^2}{6} (B_0 - A_0)^3 \right) - \psi_1 (B_0 - A_0) \right] \\
& - k_1 \left[-B_2 S - \frac{B_0^3}{6} \frac{d^2 S}{d\sigma^2} - B_0 B_1 \frac{dS}{d\sigma} + \frac{1}{2} \frac{d^2 A_0}{d\sigma^2} S + \frac{dA_1}{d\sigma} S + A_2 S + \frac{1}{6} \frac{d^2 S}{d\sigma^2} + \frac{A_0}{2} \frac{d^2 S}{d\sigma^2} \right. \\
& \left. + \frac{A_0^2}{2} \frac{d^2 S}{d\sigma^2} + \frac{A_0^3}{6} \frac{d^2 S}{d\sigma^2} + \frac{dA_0}{d\sigma} \frac{dS}{d\sigma} + A_1 \frac{dS}{d\sigma} + A_0 \frac{dA_0}{d\sigma} \frac{dS}{d\sigma} + A_0 A_1 \frac{dS}{d\sigma} \right]. \quad (5.5.68)
\end{aligned}
$$

As in the first regime our aim is to find the leading audio-frequency components of the filter output and to do this we will only need to find the switching times, from which we can obtain the leading audio-frequency components of the comparator output. We choose to find the audio-frequency components of the filter output only up to $O(\epsilon^3)$, and so we need to find the switching times only up to $O(\epsilon^3)$.

We start by establishing the leading-order switching times. Because (5.5.63) and (5.5.64) are the same as the corresponding equations for regime 1, we obtain the same equation for $B_0 - A_0$ as for regime 1,

$$
B_0 - A_0 = \frac{1}{2}(1 + S),
$$

and by solving (5.5.63) and (5.5.64) simultaneously we obtain the same leading-order switching times as for regime 1,

$$
A_0 = \frac{1}{16} \left[4 - 4S + k_1 (S^2 - 1) \right], \quad (5.5.69)
$$

$$
B_0 = \frac{1}{16} \left[12 + 4S + k_1 (S^2 - 1) \right]. \quad (5.5.70)
$$

We expected these switching times to be the same as those for regime 1, as we discussed in §5.5.1.

We now tackle the higher-order switching times. To establish these, we must find the components of $\phi(\sigma)$. This task is much simpler than for regime 1, where ϕ_0 and ϕ_1 were defined by second-order differential equations. These do not arise here due to the different scaling for λ. For example, the $O(\epsilon)$ equations (5.5.24) and (5.5.26) for regime 1 result in a second-order differential equation for ϕ_0, because the equations are linked by the $\frac{d\psi_0}{d\sigma}$ term in (5.5.26). However, this term does not appear in the corresponding $O(\epsilon)$ equation for regime 2, (5.5.61), as the different scaling for λ forces the term to appear in the $O(\epsilon^2)$ equation (5.5.62).

In order to find the $O(\epsilon)$ switching times we first determine ϕ_0 and ψ_0 by substituting the leading-order switching times into (5.5.61) and (5.5.59). We thus obtain

$$\phi_0 = -S, \tag{5.5.71}$$

$$\psi_0 = \frac{dS}{d\sigma} + \frac{\lambda_1^2}{2}(1 - S^2), \tag{5.5.72}$$

which are much simpler than the corresponding solutions in regime 1, (5.5.40) and (5.5.24). We compare the solutions for ϕ_0 and ψ_0 here with (5.5.53) and (5.5.54), the expansions of $f(n + \alpha_n)$ and $\dot{f}(n + \alpha_n)$ for a constant input signal where we set $\lambda = \epsilon^{\frac{1}{2}}\lambda_1$. Notice that ϕ_0 is equivalent to exactly the leading-order term of the expansion of $f(n + \alpha_n)$, and ψ_0 is composed of the equivalent leading-order terms in the expansion of $\dot{f}(n + \alpha_n)$ as well as the derivative of the input signal.

Solving (5.5.65) and (5.5.67) simultaneously and substituting our solutions for ϕ_0 and ψ_0 we can now obtain the $O(\epsilon)$ switching times,

$$\begin{aligned}
A_1 &= \frac{1}{64k_1k_4}\frac{dS}{d\sigma}\Big(16k_1 + 16k_4 + 8k_1^2 - 4k_1k_4 + k_1^2k_4 + 2k_1^2k_4S - 4k_1k_4S - k_1^3k_4S \\
&\quad - 3k_1^2k_4S^2 + k_1^3k_4S^3\Big), \tag{5.5.73}
\end{aligned}$$

$$\begin{aligned}
B_1 &= \frac{1}{64k_1k_4}\frac{dS}{d\sigma}\Big(-16k_1 - 16k_4 + 8k_1^2 + 12k_1k_4 - k_1^2k_4 - 4k_1k_4S + 6k_1^2k_4S \\
&\quad - k_1^3k_4S + 3k_1^2k_4S^2 + k_1^3k_4S^3\Big). \tag{5.5.74}
\end{aligned}$$

Correspondingly, to find the $O(\epsilon^2)$ switching times we first solve (5.5.60) and (5.5.62) to find ϕ_1 and ψ_1, and then solve (5.5.66) and (5.5.68) simultaneously. The solutions we obtain for A_2 and B_2 are, as for regime 1, quite lengthy so we do not present them here.

Notice that in contrast to the first regime, we have been able to find solutions for the switching times up to $O(\epsilon^3)$ for a general signal that do not involve integrals. This is due to $\phi(\sigma)$ and $\psi(\sigma)$ taking much simpler forms in this regime. We now proceed to calculate the leading audio-frequency components of the comparator output, before determining the leading audio-frequency components of the filter output.

Calculation of $g(t)$, the comparator output. The calculation of the leading audio-frequency components of the comparator output, $g_a(t)$, proceeds exactly as for the first regime, using the formula (3.5.21), which gives the audio-frequency components of $g(t)$ in terms of the switching times. Substituting our solutions for the $O(1)$ and $O(\epsilon)$ switching times, given by (5.5.69)-(5.5.74) as well as the lengthy $O(\epsilon^2)$ switching times

not displayed here, we find

$$
\begin{aligned}
g_a(t) \;=\; & -S(\sigma) + \epsilon \frac{k_1 + k_4}{k_1 k_4} \frac{d}{d\sigma} S(\sigma) \\
& - \frac{\epsilon^2}{48 k_1^2 k_4^2 \lambda_1^2} \left[k_1^2 k_4 \lambda_1^2 \frac{d}{d\sigma} S(\sigma) \left(6\lambda_1^2 S(\sigma)^2 - 6k_4 S(\sigma) \frac{d}{d\sigma} S(\sigma) - 2\lambda_1^2 \right) \right. \\
& + \lambda_1^2 \frac{d^2}{d\sigma^2} S(\sigma) \left(48 k_1^2 + 48 k_4^2 + 96 k_1 k_4 - k_1^2 k_4^2 - 3 k_1^2 k_4^2 S(\sigma)^2 \right) \\
& \left. + 48 k_1^2 k_4 \frac{d^3}{d\sigma^3} S(\sigma) \right] + O(\epsilon^3) \,.
\end{aligned}
$$

Calculation of $f(t)$, the filter output. Now that we have an expression for $g_a(t)$, all that remains is to find $f_a(t)$, the leading audio-frequency components of the filter output. Ignoring frequencies above the audio range, the differential equation for the filter output in this regime, (5.5.48), becomes in terms of our slow time $\sigma = \epsilon t$,

$$
\epsilon \frac{d^2}{d\sigma^2} f_a(t) + \lambda_1^2 f_a(t) = \lambda_1^2 g_a(t). \tag{5.5.75}
$$

Employing the notation for $f_{a,i}(t)$ and $g_{a,i}(t)$ defined in §5.5.1.1 we now solve (5.5.75) at successive orders in ϵ. This differential equation reduces at $O(1)$ to

$$
f_{a,0}(t) = g_{a,0}(t),
$$

at $O(\epsilon)$,

$$
\frac{d^2}{d\sigma^2} f_{a,0}(t) + \lambda_1^2 f_{a,1}(t) = \lambda_1^2 g_{a,1}(t),
$$

and at $O(\epsilon^2)$,

$$
\frac{d^2}{d\sigma^2} f_{a,1}(t) + \lambda_1^2 f_{a,2}(t) = \lambda_1^2 g_{a,2}(t),
$$

It is therefore straightforward to show that the leading audio-frequency components of the filter output are given by

$$
\begin{aligned}
f_a(t) \;=\; & -S(\sigma) + \epsilon \left[\frac{k_1 + k_4}{k_1 k_4} \frac{d}{d\sigma} S(\sigma) + \frac{1}{\lambda_1^2} \frac{d^2}{d\sigma^2} S(\sigma) \right] \\
& - \frac{\epsilon^2}{48 k_1^2 k_4^2 \lambda_1^4} \left[k_1^2 k_4 \lambda_1^4 \frac{d}{d\sigma} S(\sigma) \left(6\lambda_1^2 S(\sigma)^2 - 6k_4 S(\sigma) \frac{d}{d\sigma} S(\sigma) - 2\lambda_1^2 \right) \right. \\
& + \lambda_1^4 \frac{d^2}{d\sigma^2} S(\sigma) \left(48 k_1^2 + 48 k_4^2 + 96 k_1 k_4 - k_1^2 k_4^2 - 3 k_1^2 k_4^2 S(\sigma)^2 \right) \\
& \left. + 48 k_1 k_4 \lambda_1^2 (2k_1 + k_4) \frac{d^3}{d\sigma^3} S(\sigma) + 48 k_1^2 k_4^2 \frac{d^4}{d\sigma^4} S(\sigma) \right] + O(\epsilon^3) \,. \tag{5.5.76}
\end{aligned}
$$

It is clear that for this regime the leading-order component is exactly minus the input signal. At higher orders there is distortion in the output, which at $O(\epsilon)$ is linear in the

input signal, while at $O(\epsilon^2)$ there are terms linear and cubic in the input signal. These distortion terms cannot be removed by any choice of the positive parameters k_1, k_4 and λ_1. Notice that we have been able to obtain this output for a general input signal.

Choosing the input signal to be sinusoidal, $S(\sigma) = s_0 \sin \sigma$, (5.5.76) becomes

$$
\begin{aligned}
f_a(t) &= -s_0 \sin \sigma + \epsilon \left[\delta_1 \cos \sigma + \delta_2 \sin \sigma \right] \\
&\quad + \epsilon^2 \left[\delta_3 \sin \sigma + \delta_4 \cos \sigma + \delta_5 \sin 3\sigma + \delta_6 \cos 3\sigma \right] + O(\epsilon^3) , \quad (5.5.77)
\end{aligned}
$$

where δ_1-δ_6 are given by

$$
\begin{aligned}
\delta_1 &= \frac{s_0}{k_1} + \frac{s_0}{k_4}, \\
\delta_2 &= -\frac{s_0}{\lambda_1^2}, \\
\delta_3 &= \frac{2s_0}{k_1 k_4} + \frac{s_0}{k_4^2} + \frac{s_0}{k_1^2} - \frac{s_0}{48} - \frac{s_0^3}{64} - \frac{s_0}{\lambda_1^4}, \\
\delta_4 &= \frac{s_0}{k_1 \lambda_1^2} + \frac{2s_0}{k_4 \lambda_1^2} + \frac{s_0 \lambda_1^2}{24 k_4} - \frac{s_0^3 \lambda_1^2}{32 k_4}, \\
\delta_5 &= \frac{3 s_0^3}{64}, \\
\delta_6 &= \frac{s_0^3 \lambda_1^2}{32 k_4}.
\end{aligned}
$$

If we then revert to dimensional variables and parameters the audio part of the filter output is

$$
\begin{aligned}
f_a^*(t^*) &= -s_0 V \sin \omega_a t^* + \omega_a T V \left[\delta_1^* \cos \omega_a t^* \delta_2^* \sin \omega_a t^* \right] \\
&\quad + (\omega_a T)^2 V \left[\delta_3^* \sin \omega_a t^* + \delta_4^* \cos \omega_a t^* \right. \\
&\quad \left. + \delta_5^* \sin 3\omega_a t^* + \delta_6^* \cos 3\omega_a t^* \right] + O\left((\omega_a T)^3 \right),
\end{aligned}
$$

where δ_i^* are the same as δ_i previously, except now written in terms of dimensional

parameters,

$$\delta_1^* = \frac{s_0}{c_1 T} + \frac{s_0}{c_4 T}, \tag{5.5.78}$$

$$\delta_2^* = -\frac{s_0 \omega_a}{\omega_f^2 T}, \tag{5.5.79}$$

$$\delta_3^* = \frac{2s_0}{c_1 c_4 T^2} + \frac{s_0}{c_4^2 T^2} + \frac{s_0}{c_1^2 T^2} - \frac{s_0}{48} - \frac{s_0^3}{64} - \frac{s_0 \omega_a^2}{\omega_f^4 T^2}, \tag{5.5.80}$$

$$\delta_4^* = \frac{s_0 \omega_a}{c_1 \omega_f^2 T^2} + \frac{2s_0 \omega_a}{c_4 \omega_f^2 T^2} + \frac{s_0 \omega_f^2}{24 c_4 \omega_a} - \frac{s_0^3 \omega_f^2}{32 c_4 \omega_a}, \tag{5.5.81}$$

$$\delta_5^* = \frac{3s_0^3}{64}, \tag{5.5.82}$$

$$\delta_6^* = \frac{s_0^3 \omega_f^2}{32 c_4 \omega_a}. \tag{5.5.83}$$

It is clear from this result that the distortion affects the amplitude of the signal at frequency ω_a, and that the nonlinear distortion results in third-harmonics with amplitude $O\big((\omega_a T)^2\big)$.

Comparison of results with regime 1. Recall that in regime 1, $\lambda = \epsilon \lambda_2$, whilst here in regime 2, $\lambda = \epsilon^{\frac{1}{2}} \lambda_1$. We now discuss the differences and similarities between the solutions for $f_a(t)$ in either regime. We compare the solutions for a sinusoidal input signal, since the complexity of the results for regime 1 meant that specifying the input signal to be sinusoidal gave a result that was simple to analyse.

Comparing the regime 2 solution for $f_a(t)$, (5.5.77), with that for the first regime, (5.5.47), we see that there are several important differences. The $O(1)$ term for this regime is exactly minus the input signal, whereas for the first regime the factor $\frac{1}{1 - \frac{1}{\lambda_2^2}}$ multiplies $-s_0 \sin \sigma$. The only difference between the constants multiplying the $\epsilon \cos \sigma$, $\epsilon^2 \sin \sigma$ and $\epsilon^2 \sin 3\sigma$ terms is that these constants in regime 1 contain factors of $\frac{1}{1 - \frac{1}{\lambda_2^2}}$. At $O(\epsilon^2)$ for this second regime there are additional terms in $\epsilon \cos \sigma$ and $\epsilon^2 \cos 3\sigma$. These differences can be explained by the different scalings for λ used in the regimes. In regime 1, the filter frequency is of the same order as the audio frequency, and so the filtering process affects signals with audio frequencies, resulting in the multiplying factor $\frac{1}{1 - \frac{1}{\lambda_2^2}}$. Here in regime 2, the filter frequency is much higher than the audio frequency, so signals with audio frequencies are allowed to pass through the filter without being distorted, but also additional distortion terms appear in the filtered output.

Despite the differences between the results, if we let $\lambda_2 = \epsilon^{-\frac{1}{2}} \lambda_1$ in our regime 1 solution for $f_a(t)$ we expect to obtain the regime 2 solution for $f_a(t)$. This is indeed the case, and we can see this by expanding the resulting terms in the regime 1 solution for

$f_a(t)$ in powers of ϵ as follows,

$$\frac{1}{1 - \frac{\epsilon}{\lambda_1^2}} \left(-s_0 \sin \sigma + \epsilon \gamma_8 \cos \sigma + \epsilon^2 \gamma_9 \sin \sigma \right) + \epsilon^2 \frac{\gamma_{10}}{1 - \frac{9\epsilon}{\lambda_1^2}} \sin 3\sigma + O(\epsilon^3)$$

$$= -s_0 \left(1 + \frac{\epsilon}{\lambda_1^2} + \frac{\epsilon^2}{\lambda_1^4} \right) \sin \sigma + \epsilon \left(\frac{s_0}{k_1} + \frac{s_0}{k_4} \right) \cos \sigma + \epsilon^2 \left(\frac{2s_0}{k_4 \lambda_1^2} + \frac{s_0}{k_1 \lambda_1^2} \right) \cos \sigma$$

$$+ \epsilon^2 \left(\frac{2s_0}{k_1 k_4} + \frac{s_0}{k_4^2} + \frac{s_0}{k_1^2} - \frac{s_0}{48} - \frac{s_0^3}{64} \right) \sin \sigma + \epsilon^2 \frac{3s_0^3}{64} \sin 3\sigma + O(\epsilon^3).$$

Comparing this expansion with (5.5.77) we see that this expansion is the same as the solution for regime 2, except that the additional terms

$$\epsilon^2 \left[\frac{s_0 \lambda_1^2}{24 k_4} - \frac{s_0^3 \lambda_1^2}{32 k_4} \cos \sigma + \frac{s_0^3 \lambda_1^2}{32 k_4} \cos 3\sigma \right]$$

appear in the regime 2 solution. If we let $\lambda_1 = \epsilon^{\frac{1}{2}} \lambda_2$ we see that these terms, which appear at $O(\epsilon^2)$ in regime 2, are $O(\epsilon^3)$ in regime 1. We cannot expect the expansion of the solution for regime 1 to predict these terms, since we found the solution only up to $O(\epsilon^3)$. Therefore the audio part of the filtered output for regime 1 is consistent with that for regime 2.

We have seen that the scaling in this regime for λ ensures that the leading-order audio part of the filtered output is exactly minus the input signal, and as such is an improvement on the scaling we used in regime 1. However, the filtered output contains distortion, which cannot be removed by any careful choice of parameter values. In the next section we consider a third scaling for λ, again calculating the filtered output, and aiming to determine whether the resulting change to the filtering process offers an improvement in $f_a(t)$ over regime 2.

5.5.3 Regime 3: $\lambda = \lambda_0$

We now consider the operation of the amplifier for a general input signal for a third scaling of λ. Here we choose $\lambda = \lambda_0$, where λ_0 is an $O(1)$ constant, so that $\epsilon \ll \lambda = O(\omega_c T)$, where $\epsilon = \omega_a T$, as discussed at the beginning of §5.5. As for the previous two regimes, the amplifier is governed by the dimensionless equations (5.3.2)-(5.3.5) and the dimensionless differential equation for the filter output, $f(t)$. This we obtain by substituting $\lambda = \lambda_0$ into (5.3.9),

$$\frac{d^2}{dt^2} f(t) + \lambda_0^2 f(t) = \lambda_0^2 g(t). \tag{5.5.84}$$

To solve these equations we now follow the same method as in the previous two regimes, and so we omit many of the details here.

Solving (5.5.84) we determine two equations relating the $f(t)$ and $\dot{f}(t)$, both evaluated at the switching times, to the switching times themselves

$$
\begin{aligned}
f(n+1+\alpha_{n+1}) ={} & [f(n+\alpha_n)+1]\cos(\lambda_0(1+\alpha_{n+1}-\alpha_n)) \\
& + \frac{1}{\lambda_0}\dot{f}(n+\alpha_n)\sin(\lambda_0(1+\alpha_{n+1}-\alpha_n)) \\
& - 2\cos(\lambda_0(1-\beta_n+\alpha_{n+1}))+1, \tag{5.5.85}
\end{aligned}
$$

$$
\begin{aligned}
\dot{f}(n+1+\alpha_{n+1}) ={} & \dot{f}(n+\alpha_n)\cos(\lambda_0(1+\alpha_{n+1}-\alpha_n)) \\
& - \lambda_0[f(n+\alpha_n)+1]\sin(\lambda_0(1+\alpha_{n+1}-\alpha_n)) \\
& + 2\lambda_0\sin(\lambda_0(1-\beta_n+\alpha_{n+1})). \tag{5.5.86}
\end{aligned}
$$

Then, using (5.3.2)-(5.3.5), we find two equations linking $f(t)$, $\dot{f}(t)$, the integral of the input signal, $r(t)$, all evaluated at the switching times, to the switching times,

$$
\begin{aligned}
(4-k_1)\alpha_n &- 4 + (4+k_1)\beta_n = \\
& \frac{k_1}{k_4}\Bigg[-1 - f(n+\alpha_n) + [f(n+\alpha_n)+1]\cos(\lambda_0(\beta_n-\alpha_n)) \\
& + \frac{1}{\lambda_0}\dot{f}(n+\alpha_n)\sin(\lambda_0(\beta_n-\alpha_n))\Bigg] + k_1[r(n+\beta_n)-r(n+\alpha_n)], \tag{5.5.87}
\end{aligned}
$$

$$
\begin{aligned}
(4+k_1)\alpha_{n+1} &- 4 + k_1 + (4-k_1)\beta_n = \\
& -\frac{k_1}{k_4}\Bigg[f(n+1+\alpha_{n+1}) + 1 - [f(n+\alpha_n)+1]\cos(\lambda_0(\beta_n-\alpha_n)) \\
& - \frac{1}{\lambda_0}\dot{f}(n+\alpha_n)\sin(\lambda_0(\beta_n-\alpha_n))\Bigg] \\
& - k_1[r(n+1+\alpha_{n+1}) - r(n+\beta_n)]. \tag{5.5.88}
\end{aligned}
$$

These four exact nonlinear difference equations therefore control the amplifier in regime 3 for a general input signal. They are equivalent to (5.5.2), (5.3.3), (5.5.9) and (5.5.10) for regime 1, and to (5.5.49)-(5.5.52) for regime 2. Treating these discrete equations in the same way as in previous regimes, we now convert them into a continuous system of equations.

5.5.3.1 Continuous model

To transform (5.5.85)-(5.5.88) into a continuous model, we write the equations in terms of the slowly-varying functions $R(\sigma)$, $A(\sigma)$, $B(\sigma)$, $\phi(\sigma)$ and $\psi(\sigma)$, defined by (5.5.11)-(5.5.15) and

$$
\psi(\epsilon n) = \dot{f}(n+\alpha_n)
$$

respectively. Note that we use the same scaling for $f(n+\alpha_n)$ as in the first and second regimes, but a different scaling for $\dot{f}(n+\alpha_n)$. As in the first two regimes, to establish

these scalings for this regime we look at the solutions for $f(n + \alpha_n)$ and $\dot{f}(n + \alpha_n)$ for a constant signal, equations (5.4.21) and (5.4.23). For this regime, we replace λ by λ_0 in these solutions, and see that both $f(n + \alpha_n)$ and $\dot{f}(n + \alpha_n)$ appear to be $O(1)$. As discussed in both previous regimes, these solutions for a constant input signal cannot necessarily tell us how large $\dot{f}(n + \alpha_n)$ is for a general input signal. Consideration of how $f(t)$ varies for a general input signal tells us that $\dot{f}(t)$ is $O(\epsilon)$ or larger. Therefore, in this regime the solutions for a constant input signal do predict the correct scalings for $f(n + \alpha_n)$ and $\dot{f}(n + \alpha_n)$, and so we choose both $f(n + \alpha_n)$ and $\dot{f}(n + \alpha_n)$ to be $O(1)$.

Writing the discrete equations in terms of the slowly-varying functions, (5.5.85) and (5.5.86) become

$$
\begin{aligned}
\phi(\sigma + \epsilon) &= [\phi(\sigma) + 1]\cos(\lambda_0(1 + A(\sigma + \epsilon)) - A(\sigma)) \\
&\quad + \frac{1}{\lambda_0}\psi(\sigma)\sin(\lambda_0(1 + A(\sigma + \epsilon) - A(\sigma))) \\
&\quad - 2\cos(\lambda_0(1 - B(\sigma) + A(\sigma + \epsilon))) + 1,
\end{aligned}
\tag{5.5.89}
$$

$$
\begin{aligned}
\psi(\sigma + \epsilon) &= \psi(\sigma)\cos\lambda_0(1 + A(\sigma + \epsilon) - A(\sigma)) \\
&\quad - \lambda_0[\phi(\sigma) + 1]\sin(\lambda_0(1 + A(\sigma + \epsilon) - A(\sigma))) \\
&\quad + 2\lambda_0\sin(\lambda_0(1 - B(\sigma) + A(\sigma + \epsilon))),
\end{aligned}
\tag{5.5.90}
$$

and (5.5.87) and (5.5.88) become

$$
\begin{aligned}
(4 - k_1)A(\sigma) &- 4 + (4 + k_1)B(\sigma) = \\
&\frac{k_1}{k_4}\Bigg[-1 - \phi(\sigma) + [\phi(\sigma) + 1]\cos(\lambda_0(B(\sigma) - A(\sigma))) \\
&\quad + \frac{1}{\lambda_0}\psi(\sigma)\sin(\lambda_0(B(\sigma) - A(\sigma)))\Bigg] \\
&+ k_1\left[\frac{R(\sigma + \epsilon B(\sigma)) - R(\sigma + \epsilon A(\sigma))}{\epsilon}\right],
\end{aligned}
\tag{5.5.91}
$$

$$
\begin{aligned}
(4 + k_1)A(\sigma + \epsilon) &- 4 + k_1 + (4 - k_1)B(\sigma) = \\
&-\frac{k_1}{k_4}\Bigg[\phi(\sigma + \epsilon) + 1 - [\phi(\sigma) + 1]\cos(\lambda_0(B(\sigma) - A(\sigma))) \\
&\quad - \frac{1}{\lambda_0}\psi(\sigma)\sin(\lambda_0(B(\sigma) - A(\sigma)))\Bigg] \\
&- k_1\left[\frac{R(\sigma + \epsilon(1 + A(\sigma + \epsilon))) - R(\sigma + \epsilon B(\sigma))}{\epsilon}\right].
\end{aligned}
\tag{5.5.92}
$$

Seeking a perturbation solution to these equations, we now expand $A(\sigma)$, $B(\sigma)$, $\phi(\sigma)$ and $\psi(\sigma)$ as series in ϵ, as defined by (5.5.20)-(5.5.23), and expand the remaining functions in (5.5.89)-(5.5.92) as Taylor series in ϵ. Notice that as a result of the scaling used in this regime for λ, terms in $\sin\lambda_0$ and $\cos\lambda_0$ will remain in the expanded

equations. For example,

$$\cos(\lambda_0(1 - B(\sigma) + A(\sigma + \epsilon)))$$

$$= \cos\left(\lambda_0\left(1 - B_0 + A_0 + \epsilon\left(-B_1 + A_1 + \frac{dA_0}{d\sigma}\right) + O(\epsilon^2)\right)\right)$$

$$= \cos\left(\lambda_0\left(1 - B_0 + A_0\right)\right)$$

$$- \epsilon\left(-B_1 + A_1 + \frac{dA_0}{d\sigma}\right)\sin\left(\lambda_0\left(1 - B_0 + A_0\right)\right) + O(\epsilon^2). \tag{5.5.93}$$

We now examine the four equations at successive orders in ϵ.

In contrast to the previous two regimes, the $O(1)$ terms in (5.5.89) and (5.5.90) do not cancel with each other. Thus from (5.5.89) at $O(1)$ we obtain

$$\phi_0 = [\phi_0 + 1]\cos\lambda_0 + \frac{1}{\lambda_0}\psi_0\sin\lambda_0 - 2\cos(\lambda_0(1 - B_0 + A_0)) + 1, \tag{5.5.94}$$

and at $O(\epsilon)$,

$$\frac{d\phi_0}{d\sigma} + \phi_1 = \psi_0\frac{dA_0}{d\sigma}\cos\lambda_0 + \frac{1}{\lambda_0}\psi_1\cos\lambda_0 - \lambda_0[\phi_0 + 1]\frac{dA_0}{d\sigma}\sin\lambda_0 + \phi_1\cos\lambda_0$$

$$+ 2\lambda_0\left(-B_1 + A_1 + \frac{dA_0}{d\sigma}\right)\sin(\lambda_0(1 - B_0 + A_0)). \tag{5.5.95}$$

From (5.5.90) at $O(1)$ we obtain

$$\psi_0 = \psi_0\cos\lambda_0 - \lambda_0[\phi_0 + 1]\sin\lambda_0 + 2\lambda_0\sin(\lambda_0(1 - B_0 + A_0)), \tag{5.5.96}$$

and at $O(\epsilon)$,

$$\frac{d\psi_0}{d\sigma} + \psi_1 = -\lambda_0\psi_0\frac{dA_0}{d\sigma}\sin\lambda_0 + \psi_1\cos\lambda_0 - \lambda_0^2[\phi_0 + 1]\frac{dA_0}{d\sigma}\cos\lambda_0 - \lambda_0\phi_1\sin\lambda_0$$

$$+ 2\lambda_0^2\left(-B_1 + A_1 + \frac{dA_0}{d\sigma}\right)\cos(\lambda_0(1 - B_0 + A_0)). \tag{5.5.97}$$

Then (5.5.91) gives, at $O(1)$,

$$(4 - k_1)A_0 - 4 + (4 + k_1)B_0 =$$

$$\frac{k_1}{k_4}[-1 - \phi_0 + [\phi_0 + 1]\cos(\lambda_0(B_0 - A_0)) + \frac{1}{\lambda_0}\psi_0\sin(\lambda_0(B_0 - A_0))]$$

$$+ k_1[B_0 S - A_0 S], \tag{5.5.98}$$

and at $O(\epsilon)$,

$$(4 - k_1)A_1 + (4 + k_1)B_1 =$$

$$\frac{k_1}{k_4}\Bigg[-\phi_1 - \lambda_0[\phi_0 + 1](B_1 - A_1)\sin(\lambda_0(B_0 - A_0)) + \phi_1\cos(\lambda_0(B_0 - A_0))$$

$$+ \psi_0(B_1 - A_1)\cos(\lambda_0(B_0 - A_0)) + \frac{1}{\lambda_0}\psi_1\sin(\lambda_0(B_0 - A_0))\Bigg]$$

$$+ k_1\left[B_1 S + \frac{1}{2}B_0^2\frac{dS}{d\sigma} - A_1 S - \frac{1}{2}A_0^2\frac{dS}{d\sigma}\right]. \tag{5.5.99}$$

155

Finally, from (5.5.92) at $O(1)$ we obtain

$$
\begin{aligned}
(4 + k_1)A_0 - 4 &+ k_1 + (4 - k_1)B_0 = \\
&- \frac{k_1}{k_4}[\phi_0 + 1 - [\phi_0 + 1]\cos(\lambda_0(B_0 - A_0)) - \frac{1}{\lambda_0}\psi_0\sin(\lambda_0(B_0 - A_0))] \\
&- k_1[(1 + A_0)S - B_0 S],
\end{aligned} \tag{5.5.100}
$$

and at $O(\epsilon)$,

$$
\begin{aligned}
(4 + k_1)&\left(A_1 + \frac{dA_0}{d\sigma}\right) + (4 - k_1)B_1 = \\
&- \frac{k_1}{k_4}\left[\phi_1 + \frac{d\phi_0}{d\sigma} + \lambda_0[\phi_0 + 1](B_1 - A_1)\sin(\lambda_0(B_0 - A_0)) - \phi_1\cos(\lambda_0(B_0 - A_0))\right. \\
&\left. - \psi_0(B_1 - A_1)\cos(\lambda_0(B_0 - A_0)) - \frac{1}{\lambda_0}\psi_1\sin(\lambda_0(B_0 - A_0))\right] \\
&- k_1\left[\left(A_1 + \frac{dA_0}{d\sigma}\right)S + \left(1 + \frac{1}{2}A_0^2\right)\frac{dS}{d\sigma} - B_1 S - \frac{1}{2}B_0^2\frac{dS}{d\sigma}\right]. \tag{5.5.101}
\end{aligned}
$$

As we have discussed before, to establish the leading audio-frequency components of the filter output we must first find the leading audio-frequency components of the comparator output, which are determined only by the switching times. In this regime we choose to find the audio-frequency components of the filter output only up to $O(\epsilon^2)$, as this will produce the first nonlinear terms, and so we focus on finding the switching times only up to $O(\epsilon^2)$.

Despite (5.5.98) and (5.5.100) being quite different from the corresponding equations in regimes 1 and 2, by subtracting one from the other, we find that the same equation for $B_0 - A_0$ holds in this regime as in the two previous regimes,

$$
B_0 - A_0 = \frac{1}{2}(1 + S).
$$

In order to determine the leading-order switching times, we must first find the leading order components of $\phi(\sigma)$ and $\psi(\sigma)$. Using the above relationship between the leading-order switching times, we solve (5.5.94) and (5.5.96) simultaneously to find

$$
\begin{aligned}
\phi_0 &= \frac{-\sin\left(\frac{\lambda_0}{2}(S + 1)\right) - \sin\left(\frac{\lambda_0}{2}(S - 1)\right)}{\sin\lambda_0}, \\
\psi_0 &= \lambda_0\left[\frac{\cos\left(\frac{\lambda_0}{2}(S + 1)\right) + \cos\left(\frac{\lambda_0}{2}(S - 1)\right) - \cos\lambda_0 - 1}{\sin\lambda_0}\right].
\end{aligned}
$$

These solutions for ϕ_0 and ψ_0 involve sines and cosines of the input signal, and so are markedly different from the corresponding solutions in the two previous regimes. These terms arise only in this regime because, for $\lambda = \lambda_0$, the Taylor series expansions of the $\sin\lambda$ and $\cos\lambda$ terms in the governing equations result in trigonometric

terms involving $\sin \lambda_0$ and $\cos \lambda_0$, as shown in the example above, (5.5.93). In previous regimes, because λ is scaled to be $O(\epsilon)$ or $O\left(\epsilon^{\frac{1}{2}}\right)$, the Taylor series expansions of the corresponding sine and cosine terms result in purely algebraic terms. Note also that these solutions are equivalent to those for a constant input signal, (5.4.21) and (5.4.22), since unlike in previous regimes, we cannot expand the sines and cosines of λ here.

We can now find the leading-order switching times. Solving (5.5.98) and (5.5.100) simultaneously, and inserting the solutions for ϕ_0 and ψ_0 we find that the terms involving sines and cosines of the input signal cancel to give

$$A_0 = \frac{1}{16} \left[4 - 4S + k_1(S^2 - 1) \right], \tag{5.5.102}$$

$$B_0 = \frac{1}{16} \left[12 + 4S + k_1(S^2 - 1) \right]. \tag{5.5.103}$$

Thus the switching times for all three regimes are the same to leading order, as expected (discussed in §5.5.1.1).

Using our solutions for A_0, B_0, ϕ_0 and ψ_0, we now look for the $O(\epsilon)$ switching times. Subtracting (5.5.99) from (5.5.101) we obtain an expression for $B_1 - A_1$. We substitute this expression into (5.5.95) and (5.5.97) and solve the resulting equations simultaneously to find solutions for ϕ_1 and ψ_1. We now have all the information we need to solve (5.5.99) and (5.5.101) and thus we find A_1 and B_1. We write B_1 in terms of A_1 here for simplicity, and also because to find $g_a(t)$ up to $O(\epsilon)$ it is sufficient to know the difference $B_1 - A_1$. Thus

$$
\begin{aligned}
A_1 \;=\; & \frac{1}{64 k_1 k_4} \frac{dS}{d\sigma} \left(16 k_4 - 4 k_1 k_4 (1 + S) + k_1^2 k_4 (1 + 2S - 3S^2) - k_1^3 k_4 S (1 - S^2) \right. \\
& + \frac{2 k_1 \lambda_0}{\cos 2\lambda_0 - 1} \left(8 \cos \frac{\lambda_0 S}{2} \left[\sin \frac{3\lambda_0}{2} - \sin \frac{\lambda_0}{2} \right] + k_1 \sin \frac{\lambda_0 S}{2} \left[\cos \frac{3\lambda_0}{2} + 3 \cos \frac{\lambda_0}{2} \right] \right. \\
& \left. \left. + 2 k_1 S \cos \frac{\lambda_0 S}{2} \left[\sin \frac{3\lambda_0}{2} + \sin \frac{\lambda_0}{2} \right] \right) \right),
\end{aligned} \tag{5.5.104}
$$

$$
\begin{aligned}
B_1 \;=\; & A_1 + \frac{1}{32 k_1 k_4} \frac{dS}{d\sigma} \left(-16 k_4 + 8 k_1 k_4 + k_1^2 k_4 (-1 + 2S + 3S^2) \right. \\
& \left. - \frac{8 k_1 \lambda_0}{\sin \frac{\lambda_0}{2}} \cos \frac{\lambda_0 S}{2} \right).
\end{aligned} \tag{5.5.105}
$$

We note that these $O(\epsilon)$ switching times contain sines and cosines of the input signal, terms which first appear in the solutions for ϕ_0 and ψ_0, and do not appear in the solutions for regimes 1 and 2, as discussed above.

Now that we have determined the switching times up to $O(\epsilon^2)$, we proceed to calculate the audio-frequency components of the comparator output, which in turn will lead us to the audio-frequency components of the filter output.

Calculation of $g(t)$, the comparator output. The calculation here of $g_a(t)$, the audio-frequency components of $g(t)$, uses the same method as in previous regimes, where we substitute the switching times we have computed above into the formula (3.5.21). This formula gives $g_a(t)$ purely in terms of the switching times. Using the $O(1)$ and $O(\epsilon)$ switching times, (5.5.102)-(5.5.105), we therefore find

$$
\begin{aligned}
g_a(t) \;=\; & -S(\sigma) + \frac{\epsilon}{k_1 k_4 \sin \lambda_0} \frac{d}{d\sigma} S(\sigma) \left[k_4 \sin \lambda_0 + k_1 \lambda_0 \cos \left(\frac{\lambda_0}{2} \right) \cos \left(\frac{\lambda_0}{2} S(\sigma) \right) \right] \\
& + O(\epsilon^2) \,.
\end{aligned}
$$

Calculation of $f(t)$, the filter output. From our solution for $g_a(t)$ above we may now compute $f_a(t)$, the audio-frequency components of $f(t)$. Recall that (5.5.84), the differential equation for $f(t)$, links $f(t)$ to $g(t)$. Writing (5.5.84) in terms of our slow time $\sigma = \epsilon t$, and looking at frequencies only in the audio range, we obtain

$$
\epsilon^2 \frac{d^2}{d\sigma^2} f_a(t) + \lambda_0^2 f_a(t) = \lambda_0^2 g_a(t).
$$

As in previous regimes, we implement the notation defined in §5.5.1.1 for $f_{a,i}(t)$ and $g_{a,i}(t)$ and now solve this differential equation at successive orders in ϵ. In this regime the second derivative of $f_a(t)$ only contributes to the solution at $O(\epsilon^2)$ and above. Thus it is straightforward to show that

$$
\begin{aligned}
f_a(t) \;=\; & g_{a,0}(t) + \epsilon g_{a,1}(t) + O(\epsilon^2) \\
\;=\; & -S(\sigma) + \frac{\epsilon}{k_1 k_4 \sin \lambda_0} \frac{d}{d\sigma} S(\sigma) \left[k_4 \sin \lambda_0 + k_1 \lambda_0 \cos \left(\frac{\lambda_0}{2} \right) \cos \left(\frac{\lambda_0}{2} S(\sigma) \right) \right] \\
& + O(\epsilon^2) \,.
\end{aligned}
\tag{5.5.106}
$$

This result establishes the leading audio-frequency components of the filter output when the amplifier operates in regime 3. Note that as in regime 2, we have been able to obtain a relatively simple expression for $f_a(t)$ for a general input signal. The leading-order component of the output is equal to minus the input signal. The $O(\epsilon)$ distortion comprises terms linear and nonlinear in the input signal. We cannot eliminate the linear distortion term, and writing the nonlinear distortion term as $\frac{1}{k_4 \sin \frac{\lambda_0}{2}} \frac{d}{d\sigma} \sin \left(\frac{\lambda_0}{2} S(\sigma) \right)$, it is clear that we also cannot remove the nonlinear distortion.

If we choose the input signal to be sinusoidal, $S(\sigma) = s_0 \sin \sigma$, where s_0 is a constant, (5.5.106) gives

$$
f_a(t) = -s_0 \sin \sigma + \epsilon \left[\zeta_1 \cos \sigma + \zeta_2 \cos \sigma \cos \left(\frac{s_0 \lambda_0}{2} \sin \sigma \right) \right] + O(\epsilon^2) \,, \quad \text{(5.5.107)}
$$

where

$$\zeta_1 = \frac{s_0}{k_1(\sin\lambda_0)^4}\left[1-(\cos\lambda_0)^2\right]^2,$$

$$\zeta_2 = \frac{s_0}{16k_4(\sin\lambda_0)^5}\left[6\cos\frac{\lambda_0}{2} - 4\cos\frac{3\lambda_0}{2} - 4\cos\frac{5\lambda_0}{2}\right.$$
$$\left. + \cos\frac{7\lambda_0}{2} + \cos\frac{9\lambda_0}{2}\right].$$

Reverting to dimensional variables and parameters the audio part of the filter output for a sinusoidal input signal is

$$f_a^*(t^*) = -s_0 V \sin\omega_a t^* + \omega_a TV\left[\zeta_1^* \cos\omega_a t^* + \zeta_2^* \cos\omega_a t^* \cos\left(\frac{s_0\omega_f T}{2}\sin\omega_a t^*\right)\right]$$
$$+ O\left((\omega_a T)^2\right),$$

where ζ_i^* are the same as ζ_i previously, except now written in terms of dimensional constants,

$$\zeta_1^* = \frac{s_0}{c_1 T(\sin\omega_f T)^4}\left[1-(\cos\omega_f T)^2\right]^2,$$

$$\zeta_2^* = \frac{s_0}{16c_4 T(\sin\omega_f T)^5}\left[6\cos\frac{\omega_f T}{2} - 4\cos\frac{3\omega_f T}{2} - 4\cos\frac{5\omega_f T}{2}\right.$$
$$\left. + \cos\frac{7\omega_f T}{2} + \cos\frac{9\omega_f T}{2}\right].$$

From this it is evident that the distortion terms alter the amplitude of the signal at frequency ω_a and produce nonlinear distortion with amplitude $O(\omega_a T)$. Writing the nonlinear distortion term as $\frac{2V\zeta_2^*}{s_0\omega_f}\frac{d}{dt^*}\sin\left(\frac{s_0\omega_f T}{2}\sin\omega_a t^*\right)$, and noting that

$$\sin\left(\frac{s_0\omega_f T}{2}\sin\omega_a t^*\right) = 2\sum_{m=1}^{\infty}J_{2m-1}\left(\frac{s_0\omega_f T}{2}\right)\sin\left((2m-1)\omega_a t^*\right),$$

where we have used the Jacobi-Anger Bessel function identity (2.3.41), it is clear that the nonlinear distortion causes all odd harmonics of the input signal to appear in the output.

Comparison of results with regimes 1 and 2. Comparing the regime 3 solution for $f_a(t)$ with those for the other two regimes, we see that there are similarities: the leading-order term remains the same as that for the second regime; and at $O(\epsilon)$ there is linear distortion as in both previous regimes. However, there is a crucial difference between the regime 3 solution for $f_a(t)$ and those for the other two regimes: in this regime there is also nonlinear distortion at $O(\epsilon)$, whereas in the first and second regimes the lowest

order nonlinear distortion appears at $O(\epsilon^2)$. In addition, the nonlinear distortion term here involves the cosine of the input signal, whereas in the first and second regimes the nonlinear distortion terms are cubic in the input signal. For a sinusoidal input signal this difference in the nonlinear distortion corresponds to all odd harmonics of the input signal appearing in the output, as opposed to just the third harmonic.

These similarities and differences can be understood in the context of the scaling used for λ in this regime. We chose $\lambda = O(1)$ here, which means that the filter frequency is much higher than the audio frequency, but of the same order as the carrier wave frequency. This ensures that signals with audio frequencies pass through the filter without being distorted, as in regime 2, but also higher amplitude nonlinear distortion appears in the output compared with previous regimes.

In spite of the differences between the solutions for $f_a(t)$ in regimes 2 and 3, we expect the solutions to be consistent. If we let $\lambda_0 = \epsilon^{\frac{1}{2}}\lambda_1$ in our regime 3 solution, (5.5.106), and expand for small ϵ we obtain

$$-S(\sigma) + \frac{\epsilon}{k_1 k_4 \sin\left(\epsilon^{\frac{1}{2}}\lambda_1\right)} \frac{d}{d\sigma} S(\sigma) \left[k_4 \sin\left(\epsilon^{\frac{1}{2}}\lambda_1\right)\right.$$
$$\left. + k_1 \epsilon^{\frac{1}{2}} \lambda_1 \cos\left(\frac{\epsilon^{\frac{1}{2}}\lambda_1}{2}\right) \cos\left(\frac{\epsilon^{\frac{1}{2}}\lambda_1}{2} S(\sigma)\right)\right] + O(\epsilon^2)$$
$$= -S(\sigma) + \epsilon \left[\frac{k_1 + k_4}{k_1 k_4}\right] \frac{d}{d\sigma} S(\sigma) - \epsilon^2 \frac{\lambda_1^2}{24 k_4} \left[3S(\sigma)^2 - 1\right] \frac{d}{d\sigma} S(\sigma) + O(\epsilon^3) .$$

If we compare this expansion with $f_a(t)$ for regime 2, (5.5.76), we see that they are the same except that additional terms appear in the regime 2 solution. These additional terms have factors of either ϵ^2, $\frac{\epsilon^2}{\lambda_1^2}$ or $\frac{\epsilon^2}{\lambda_1^4}$ multiplying them, and so if we let $\lambda_1 = \epsilon^{-\frac{1}{2}}\lambda_0$ these terms are respectively $O(\epsilon^2)$, $O(\epsilon^3)$ or $O(\epsilon^4)$ in regime 3. For regime 3 we found the solution only up to $O(\epsilon^2)$ and so we should not expect the expansion of the solution to predict these terms. Therefore we see that the audio part of the filtered output for regime 3 is consistent with that for regime 2.

Analysing this third and final scaling for λ, we have seen that although the scaling ensures that the leading-order audio-frequency component of the output is exactly minus the input signal, as in regime 2, it also introduces higher amplitude nonlinear distortion compared with the previous scalings. We discuss and compare the results from all three regimes in the following section.

5.5.4 Discussion

For a general input signal we have carried out a thorough examination of the operation of this derivative negative feedback amplifier in three regimes, each with a different scaling for the dimensionless combination $\lambda = \omega_f T$. In all of the regimes, $\epsilon < \lambda < \omega_c T$, where $\epsilon = \omega_a T$ and $\omega_c T = O(1)$, but in the first regime $\lambda = \epsilon \lambda_2$, in the second $\lambda = \epsilon^{\frac{1}{2}} \lambda_1$, and in the third $\lambda = \lambda_0$, where $\lambda_i = O(1)$. These scalings significantly affect the final filtered output from the amplifier.

Despite the contrasting scalings, we find that the leading-order switching times are the same for all three regimes, as given by (5.5.35) and (5.5.36) in regime 1, (5.5.69) and (5.5.70) in regime 2, and (5.5.102) and (5.5.103) in regime 3. These switching times for a general input signal are equivalent to the steady-state switching times found for a constant input signal, (5.4.29) and (5.4.30), because to leading order the slowly-varying general input signal we analyse is constant.

As the leading-order switching times are the same in each regime, we find that the leading-order audio-frequency component of the filter output in each regime contains minus the input signal. However, the filtering process is sensitive to the different scalings for λ, and so there is an important difference across the regimes even in this leading-order component. In regime 1 the filter frequency is the same order as the audio frequency so filtering affects the $O(1)$ output. The leading-order audio-frequency filter output is therefore minus the input signal multiplied by the factor $\frac{1}{1 - \frac{1}{\lambda_2^2}}$, as given in (5.5.47). In regimes 2 and 3 the filter frequency is much higher than the audio frequency so audio frequencies are allowed to pass through the filter, incurring no distortion. Hence the leading-order audio-frequency component of the filter output, given by (5.5.76) in regime 2 and (5.5.106) in regime 3, is exactly minus the input signal.

In all three regimes, the audio part of the filter output contains distortion beyond leading order, but again there are disparities caused by the scalings for λ. In regimes 1 and 2 there is linear distortion at $O(\epsilon)$, as well as both linear and nonlinear distortion at $O(\epsilon^2)$, the nonlinear distortion being cubic in the input signal (i.e. for a sinusoidal input signal, the nonlinear distortion introduces a third harmonic). Contrastingly, we find in regime 3 that there is both linear and nonlinear distortion at $O(\epsilon)$. The nonlinear distortion in regime 3 differs from that in the first two regimes not only because it is of lower order, but also rather than being cubic, it involves the cosine of the input signal (i.e. for a sinusoidal input signal, the nonlinear distortion introduces all odd harmonics). These differences result from the scalings for λ: in the first two regimes the filter frequency is much lower than the carrier wave frequency, but in regime 3

161

the filter frequency is of the same order as the carrier wave frequency thus allowing additional distortion into the audio output.

There is another significant effect of the disparate scalings. Because in regime 1 the filter frequency is the same order as the audio frequency, oscillations with frequency ω_f appear in the intermediate solutions, although we ignore them to obtain our final audio output. These occur because our model does not include damping in the filter, and we ignore them as in practice they would be damped by the inclusion of a resistor in the filter circuit, as discussed in §5.4.1. We would expect to see oscillations of frequency ω_f in the outputs for the other regimes as well, but we have only calculated the audio parts, and since the filter frequency is much greater than the audio frequency in regimes 2 and 3, these oscillations would be outside the audio-frequency range.

It is clear that the amplifier operates best in regime 2. In this regime the input signal is reproduced exactly at leading order, and there is minimal distortion at higher orders. This is what we should expect, as the scaling of the filter frequency in this regime offers a balance between allowing the audio frequencies to pass through the filter with no distortion, whilst minimising distortion at higher orders.

Although there is consistency between the regimes, as we have seen at the ends of §5.5.2.1 and §5.5.3.1, the filtered output is markedly different in each regime. Therefore, if it is not clear which regime the amplifier is operating in, it is useful to know whether our solutions for the filtered output provide similar results. Figure 5.10 compares the audio part of the filter output for the three regimes when there is only a factor of three difference between the values of λ in each regime, and the input signal is sinusoidal. We see that our solutions for $f_a(t)$ for the three regimes result in similar waveforms, but those for regimes 1 and 3 have a larger amplitude than $f_a(t)$ for regime 2, and the regime 3 solution is slightly delayed compared with $f_a(t)$ for the other two regimes, which are approximately in phase. Therefore if it is not clear which regime the amplifier is operating in, our results can only give an approximate prediction of the output. Note that figure 5.10 supports our conclusion that regime 2 provides the best operating conditions, since we see that the output for regime 2 is the most similar to the input signal in terms of amplitude and phase.

Before concluding in §5.6 we first carry out a numerical simulation to check the analytical solutions found above in each of the regimes.
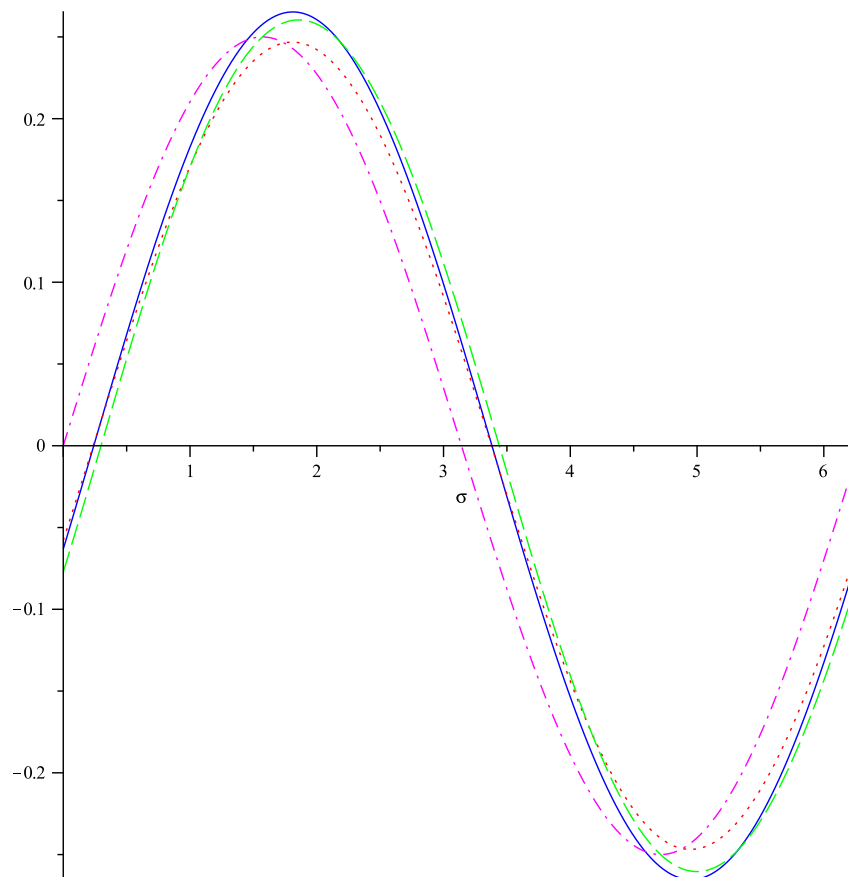
Figure 5.10: For a sinusoidal input signal, $S(\sigma) = s_0 \sin \sigma$, this graph shows $f_a(t)$ for regime 1 (blue solid curve), regime 2 (red dotted curve) and regime 3 (green dashed curve) for $s_0 = -0.25$, $k_1 = 1$, $k_4 = 1$, $\lambda_2 = \lambda_1 = \lambda_0 = 3.5$ and $\epsilon = \frac{1}{9}$. The magenta dash-dotted curve is the sinusoidal input signal, plotted as a comparison.
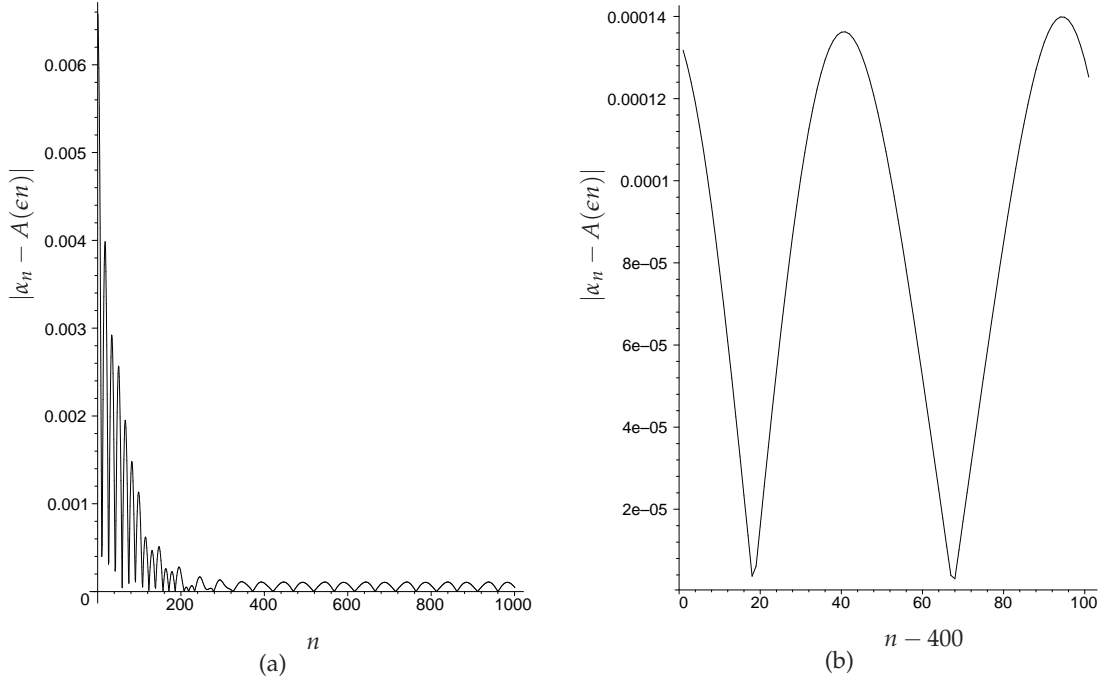
Figure 5.11: Graphs of $|\alpha_n - A(\epsilon n)|$ for regime 1 and $\epsilon = 0.064$.

5.5.5 Numerical simulation of switching times

Here we perform a check of our analytical solutions by comparing the analytical switching times found in each regime with numerical simulations. We use the same method of verification here as we used for the first- and second-order negative feedback amplifiers, the details of which were discussed thoroughly in §3.5.2. In each regime we begin by iterating the four exact nonlinear difference equations to determine the switching times. Thus for regime 1 we solve (5.5.2), (5.5.3), (5.5.9) and (5.5.10), for regime 2 we solve (5.5.49)-(5.5.52), and for regime 3 we solve (5.5.85)-(5.5.88). We choose the input signal to be sinusoidal, taking the form $s(t) = s_0 \sin \epsilon t$. We choose the parameter values $s_0 = -0.25$, $k_1 = 1$, $k_4 = 1$, and $\lambda_2 = \lambda_1 = \lambda_0 = 3$. We then solve the equations iteratively, taking the initial values $\alpha_0 = 0$, $f(0) = 0$ and $\dot{f}(0) = 0$ arbitrarily, and for ϵ ranging from 0.064 to 0.001. Then, for each regime, we compare the switching times we find numerically with those we found above analytically.

As we have seen in previous chapters, the absolute error between the numerically simulated and analytical switching times varies over the period of the input signal, and so for a sensible comparison of the switching times we calculate $E_A(\epsilon)$ and $E_B(\epsilon)$, defined by (3.5.24) and (3.5.25). These are the maxima, taken over one period of the input signal, of the absolute values of the differences between the simulated and analytical switching times, for respectively the trailing- and leading-edge switching times. As discussed in §5.4.3, there are transients in our numerical simulations of the switch-

164

Comparison	Regime 1	Regime 2	Regime 3
$E_A(0.128)/E_A(0.064)$	7.86478	7.80319	3.91091
$E_A(0.064)/E_A(0.032)$	7.96220	7.96021	3.98592
$E_A(0.032)/E_A(0.016)$	7.96576	7.99756	3.99771
$E_A(0.016)/E_A(0.008)$	7.97025	8.00308	3.99951
$E_A(0.008)/E_A(0.004)$	7.97380	8.00260	3.99988
$E_A(0.004)/E_A(0.002)$	7.97987	8.00143	3.99997
$E_A(0.002)/E_A(0.001)$	7.98065	8.00085	3.99999

Table 5.1: Table comparing values of $E_A(\epsilon)$ for each of the three regimes, with $s_0 = -0.25$, $k_1 = 1$, $k_4 = 1$, and $\lambda_2 = \lambda_1 = \lambda_0 = 3$, where results are given to 5 decimal places.

Comparison	Regime 1	Regime 2	Regime 3
$E_B(0.128)/E_B(0.064)$	7.88404	7.79761	3.91283
$E_B(0.064)/E_B(0.032)$	7.95760	7.95964	3.98622
$E_B(0.032)/E_B(0.016)$	7.95780	7.99662	3.99773
$E_B(0.016)/E_B(0.008)$	7.95850	8.00255	3.99951
$E_B(0.008)/E_B(0.004)$	7.96569	8.00220	3.99988
$E_B(0.004)/E_B(0.002)$	7.97002	7.99997	3.99997
$E_B(0.002)/E_B(0.001)$	7.97899	7.99998	3.99999

Table 5.2: Table comparing values of $E_B(\epsilon)$ for each of the three regimes, with $s_0 = -0.25$, $k_1 = 1$, $k_4 = 1$, and $\lambda_2 = \lambda_1 = \lambda_0 = 3$, where results are given to 5 decimal places.

ing times, which do not appear in the analytically found switching times. These occur because the initial values we have chosen are arbitrary, and they die away via the action of the negative feedback loops. We therefore calculate $E_A(\epsilon)$ and $E_B(\epsilon)$ only after these transients have decayed. Illustrating this, figure 5.11 presents two graphs of $|\alpha_n - A(\epsilon n)|$ for regime 1 and $\epsilon = 0.064$, where α_n represents the numerically simulated trailing-edge switching times. Figure 5.11(a) is plotted for $n = 0$ to 1000 showing the transients, whereas figure 5.11(b) is plotted for values of n after the transients have decayed and only over one period of the input signal. It is the maximum of the values of $|\alpha_n - A(\epsilon n)|$ in figure 5.11(b) that we take as $E_A(0.064)$ for regime 1.

In regimes 1 and 2 we calculated the switching times analytically up to $O(\epsilon^3)$, and in regime 3 we calculated the switching times analytically up to $O(\epsilon^2)$. Therefore we expect the error between the numerically simulated and analytical switching times to

be $O(\epsilon^3)$ in regimes 1 and 2, and $O(\epsilon^2)$ in regime 3. Tables 5.1 and 5.2 show the ratios of E_A and E_B respectively for different values of ϵ, and for all three regimes. As in previous chapters, we are careful to take adequate precision in the calculations presented in these tables, finding that 20 digits is sufficient. It is clear that for regimes 1 and 2 when ϵ is halved, the error is approximately divided by eight, and as ϵ gets smaller this ratio gets closer to eight. Correspondingly, we see that for regime 3 when ϵ is halved, the error is approximately quartered, and as ϵ decreases this ratio gets closer to four. Hence for regimes 1 and 2 the analytical switching times agree with the numerically simulated ones up to $O(\epsilon^3)$, and for regime 3 there is agreement up to $O(\epsilon^2)$.

We have determined that, for all three regimes, the analytical switching times agree with numerical simulations.

5.6 Conclusions

We have here analysed the derivative negative feedback amplifier proposed in [42] by further extending the method of analysis demonstrated and developed in chapters 3 and 4. Incorporating the low-pass filter output into the model via one of the negative feedback loops offered an additional complexity in this design. Investigating our model for a constant input signal we determined an optimum operating range for the integrator constant k_1, and also identified solutions that enabled us to understand the operation of the amplifier and to solve the model for a general input signal.

To tackle the general input signal case we found it was necessary to specify the size of the filter frequency, relative to the audio and carrier wave frequencies. We chose three separate scalings corresponding to three regimes, and analytically derived the leading audio-frequency filter outputs for each regime, confirming our solutions via numerical simulations. Comparing our analytical results we determined that choosing the filter frequency to be of order between that of the audio and carrier wave frequencies offered the best distortion performance. With this scaling, which corresponds to the second regime, the leading-order audio-frequency filter output is exactly minus the input signal, though at higher order linear and nonlinear distortion persists. This distortion can unfortunately not be removed by a choice in parameters. For this second regime, we found, for a sinusoidal input signal, that the distortion in the output has an effect on the amplitude of the signal at the frequency of the input signal and causes third-harmonics of the input signal. As this design has to our knowledge not been investigated analytically before, deriving the filter output for a general input signal represents a substantial achievement, made possible by our streamlined method of

analysis.

We compare this second regime solution with the outputs we found for the first-order negative feedback amplifier in chapter 3 and the second-order negative feedback amplifier in chapter 4. Notably, the first distortion term in the output here appears at lower order compared with the second-order negative feedback design. We saw in chapter 4 that the second-order design offered a slight improvement over the first-order design, and as such conclude that the second-order amplifier provides the best distortion performance, though admittedly the advantage is meager. All three negative feedback designs we have investigated produce nonlinear distortion at higher orders. Reducing or ideally eliminating this distortion would obviously be beneficial, and we discuss this in the following chapter, where we also conclude this thesis.

Conclusions and future work

HERE we give a summary of the achievements in this thesis, and highlight potential future work.

We began in chapter 1 by introducing class-D amplifiers, with particular emphasis on the advantage of the output being a square wave, created by pulse width modulation. Crucially, a signal input to a class-D amplifier can be reproduced from the square wave output with no distortion, and therefore these amplifiers are used in a highly-efficient output stage where the input signal is reproduced exactly in the audio-frequency components of the output with no distortion. We also discussed existing methods used to analyse the pulse width modulated square wave.

In chapter 2 we calculated the outputs from a classical class-D amplifier implementing either natural or regular sampling. We showed that the audio part of the output resulting from natural sampling is exactly the input signal, with no distortion, as desired. We utilised two separate methods to do so, and thus demonstrated the considerable advantages the Fourier transform/Poisson resummation method has over the double Fourier series method, which is the conventional method used. As further confirmation of the benefits of this method, we analysed several other sampling schemes at the end of chapter 2. Consequently we have employed the Fourier transform/Poisson resummation method throughout this thesis.

Because the classical class-D amplifier is susceptible to noise in the output, negative feedback is often incorporated into the design, as we investigated in chapter 3. Here, to examine the first-order negative feedback amplifier, we formalised and extended the analysis of [7]. By considering a constant input signal, we were able to identify a suitable operating range for k_1, the integrator constant. For a general input signal, we derived nonlinear difference equations governing the amplifier. We converted this discrete system of equations into a continuous one, and then found a per-

turbation solution, thus obtaining the switching times of the square wave output. We implemented the Fourier transform/Poisson resummation method to determine the formula (3.5.21), which gives the audio-frequency components of the square wave output purely in terms of its switching times. The use of the Fourier transform/Poisson resummation method was essential in deriving this formula for a general input signal. Inserting our switching time solutions, we established the leading audio-frequency components of the output, the leading-order component of which is exactly minus the input signal. Our most significant contribution in this chapter was the derivation of an additional distortion term in this output compared with those derived in [7], made possible through our concise formulation. The distortion introduced by negative feedback is clear in these results; it proves impossible to remove it entirely, despite choosing K, the multiplier constant, to minimise the distortion. We verified our analytical solutions for both a constant and a sinusoidal input signal via numerical simulations.

The increased distortion in the first-order negative feedback design compared with the classical design motivated us to consider other more complex negative feedback designs attempting to reduce this distortion. In chapter 4 we therefore examined a second-order negative feedback amplifier, and in chapter 5 a derivative negative feedback amplifier. In analysing these amplifiers of increasing complexity (as borne out by the number of equations governing each design) it became ever more important to derive as concise a model as possible for each design, thereby enabling us to determine solutions. Despite the differences in the designs, we were able to use the formula (3.5.21) in the latter stages of our calculations in both chapters, since the formula is valid for any amplifier design. As for the first-order design, we used numerical simulations to confirm our analytical solutions for these amplifiers.

To analyse the second-order negative feedback amplifier in chapter 4 we developed the method introduced for the first-order design, adapting our method to model the second-order loop filter in place of the integrator included in the first-order amplifier circuit. As in chapter 3 we were able to determine a sensible operating range for one of the parameters in the model, here for k_2, one of the loop filter constants, which is comparable to k_1 in the first-order design. For a general input signal we then computed the leading audio-frequency components of the output. We found that there is arguably a slight reduction in the output distortion compared with the first-order amplifier, but nonlinear distortion persists and thus we were prompted to consider another negative feedback design.

The derivative negative feedback amplifier we examined in chapter 5 presented an increased challenge. The main difference between this design and the other negative

feedback designs we investigated above is that the design incorporates the low-pass filter output into the circuit via a second negative feedback loop. Consequently, it is necessary to include the output filter in the model, in contrast to the first- and second-order negative feedback models where we ignored the output filter. To our knowledge this design has not been investigated analytically before, and so our analysis is a novel achievement. From our analysis for a constant input signal, we found that the same operating range for the parameter k_1 applies as for first-order negative feedback. To investigate the operation of the amplifier for a general input signal we further developed the method of analysis used in chapters 3 and 4 to include the filter output. Finding that the behaviour of the amplifier depended on the relative magnitudes of the typical audio, filter, and carrier wave frequencies, we derived the leading audio-frequency components of the outputs in three regimes, each differing in the scalings of the three aforementioned frequencies. We established that the amplifier output contains the least distortion when the order of the filter frequency is between that of the audio and carrier wave frequencies, although unfortunately this output still includes more distortion than we found in the second-order negative feedback output. We therefore concluded that of the three negative feedback amplifiers analysed in this thesis, the second-order design offers the best distortion performance, though the benefit is slight. Decreasing the distortion in any of these amplifiers therefore remains an active goal.

Our research has revealed several modifications that may result in reduced distortion. Recall that the first-order negative feedback design contains a multiplier, whereas the second-order and derivative negative feedback designs analysed here do not. As we saw in chapter 3, the inclusion of a multiplier in the first-order design provides a free parameter in the expression for the leading audio-frequency components of the output, and a careful choice of the value of this parameter removes some distortion. Incorporating a multiplier in either of the latter two designs therefore seems to offer potential. Analysis of a second-order design, whose topology is related to the one studied here, but includes a multiplier, has shown that distortion can be reduced but not eliminated by a choice in this free parameter [41].

A different adaptation to the second-order design is depicted in figure 5 of [39], where a second negative feedback loop and an additional second-order loop filter are added. The authors of [39] showed that this adapted second-order design offers advantages over the second-order design modelled here, though they did not carry out a thorough analytical study of the distortion in the resulting output. Analytical investigations of this design, and other modifications to negative feedback amplifiers, are now feasible for a general input signal via the formalised and streamlined analysis

presented in this thesis.

We now discuss other suggestions for extensions to our work. For the negative feedback designs examined here, we have focused on calculating the audio part of the outputs, as this is more pertinent to audio applications. It would be interesting to calculate the non-audio (i.e. high-frequency) part of the output as well, with a view to tailoring the filtering process to obtain the best possible filtered output (recall that frequencies above the audio range are attenuated by the filter, rather than eliminated completely).

For each of the amplifier topologies investigated here, we could perform a numerical simulation of the whole amplifier. These would further validate our results, as we could compare our analytical solutions for the outputs with numerical solutions. In addition, via these comparisons we could determine whether our analytical solutions are convergent series, or merely asymptotic series.

Another idea for future work relates to the derivative negative feedback model explored in chapter 5. We modelled the low-pass filter in this design without a resistor, as it appeared in the patent [42], but assumed that in practice a resistor would be included to provide damping. We thereby assumed that, by ignoring filter frequency oscillations, the solution we found for the undamped system is almost identical to that we would obtain for the damped system. To further verify this assumption it would be instructive to model the filter with a resistor, and confirm that there is a negligible difference between the solutions derived for the damped and undamped systems.

Pulse skipping is a phenomenon where, contrary to assumption, the square wave does not switch between ± 1 during the carrier wave period, i.e. one of the leading- or trailing-edge switchings is "missed". Its occurrence is unwelcome as it results in noise and harmonic distortion in the output, and although noise is filtered out, the lower-frequency harmonic distortion can remain. Pulse skipping was not observed in any of the analytical solutions for the designs in this thesis. However, we cannot expect our analysis to capture this behaviour because the continuous model we implement assumes that the functions involved are slowly varying, whereas pulse skipping results in high-frequency oscillations on the timescale of the carrier wave. Pulse skipping also did not appear in any of our numerical simulations of the difference equations to obtain the switching times. Incorporating an investigation of pulse skipping, as presented in [41], into the analysis for the negative feedback designs in this thesis offers potential for future work.

We have presented succinct analytical derivations of the outputs from both classical and negative feedback class-D amplifiers. In doing so we have demonstrated the

advantages of the Fourier transform/Poisson resummation method over the double Fourier series method, which is the traditional method used for such calculations. This superior method is crucial in determining the amplifier outputs for a general input signal, either explicitly for the classical class-D designs, or incorporated into the latter stages of our streamlined analysis for negative feedback designs. Whilst the selection of negative feedback amplifiers we have investigated do not dramatically improve upon the distortion performance of the first-order design, our analysis shows that the method demonstrated for the first-order design can be extended to model other negative feedback designs simply and effectively, thus establishing the great potential of this method of analysis in determining the outputs from negative feedback amplifiers. Reducing distortion is an area of ongoing research, and the work in this thesis will facilitate future investigation of more complex negative feedback topologies, whose analysis is now practicable.

References

[1] C. Pascual, Z. Song, P. T. Krein, D. V. Sarwate, P. Midya, and W. J. Roeckner. High-fidelity PWM inverter for digital audio amplification: spectral analysis, real-time DSP implementation, and results. *IEEE Transactions on Power Electronics*, 18(1): 473–485, 2003.

[2] M. Berkhout and L. Dooper. Class-D audio amplifiers in mobile applications. *IEEE Transactions on Circuits and Systems-I: Regular Papers*, 57(5):992–1002, 2010.

[3] H. S. Black. *Modulation Theory*. Van Nostrand, New York, 1953.

[4] Z. Song and D. V. Sarwate. The frequency spectrum of pulse width modulated signals. *Signal Processing*, 83:2227–2258, 2003.

[5] B. Putzeys. Digital audio's final frontier. *IEEE Spectrum*, 40(3):34–41, 2003.

[6] D. J. Benson. *Music: A Mathematical Offering*. Cambridge University Press, Cambridge, 2006.

[7] S. M. Cox and B. H. Candy. Class-D audio amplifiers with negative feedback. *SIAM Journal on Applied Mathematics*, 66(2):468–488, 2005.

[8] M. T. Tan, J. S. Chang, H. C. Chua, and B. H. Gwee. An investigation into the parameters affecting total harmonic distortion in low-voltage low-power class-D amplifiers. *IEEE Transactions on Circuits and Systems-I: Fundamental Theory and Applications*, 50(13):1304–1315, 2003.

[9] W. R. Bennett. New results in the calculation of modulation products. *Bell System Technical Journal*, 12:228–243, 1933.

[10] G. Fedele and D. Frascino. Spectral analysis of a class of DC-AC PWM inverters by Kapteyn series. *IEEE Transactions on Power Electronics*, 25(4):839–849, 2010.

[11] S. M. Cox and S. C. Creagh. Voltage and current spectra for matrix power converters. *SIAM Journal on Applied Mathematics*, 69(5):1415–1437, 2009.

[12] J. T. Boys and P. G. Handley. Harmonic analysis of space vector modulated PWM waveforms. *IEE Proceedings, Part B*, 137(4):197–204, 1990.

[13] D. G. Holmes. A general analytical method for determining the theoretical harmonic components of carrier based PWM strategies. In *Conf. Rec. IEEE-IAS Annual Meeting*, pages 1207–1214, 1998.

[14] H. Li, B. H. Gwee, and J. S. Chang. A digital class D amplifier design embodying a novel sampling process and pulse generator. In *Proceedings of the IEEE International Symposium on Circuits and Systems*, pages 826–829, 2001.

[15] R. A. Guinee and C. Lyden. A novel Fourier series time function for modeling and simulation of PWM. *IEEE Transactions on Circuits and Systems-I: Regular Papers*, 52 (11):2427–2435, 2005.

[16] D. G. Holmes and T. A. Lipo. *Pulse Width Modulation for Power Converters: Principles and Practice*. IEEE Press, Piscataway, NJ, 2003.

[17] R. A. Guinee and C. Lyden. A novel single Fourier series technique for the simulation and analysis of asynchronous pulse width modulation. In *Applied Power Electronics Conference proceedings*, pages 123–128, 1998.

[18] R. A. Guinee and C. Lyden. A single Fourier series technique for the simulation and analysis of asynchronous pulse width modulation in motor drive systems. In *Proceedings of the IEEE International Symposium on Circuits and Systems*, pages 653–656, 1998.

[19] R. A. Guinee and C. Lyden. A novel analytical technique for spectral analysis prediction in asynchronous pulse width modulated inverter systems. In *Proceedings of the IEEE International Conference on Electronics, Circuits and Systems*, pages 177–180, 1999.

[20] S. R. Bowes. New sinusoidal pulse width modulated inverter. *IEE Proceedings*, 122 (11):1279–1285, 1975.

[21] E. Jahnke and F. Emde. *Tables of Functions with Formulae and Curves*, page 149. Dover Press, New York, 4th edition, 1945.

[22] R. Courant and D. Hilbert. *Methods of Mathematical Physics*, volume 1. Interscience Publishers, New York, 1953.

[23] G. N. Watson. *A Treatise on the Theory of Bessel Functions*. Cambridge University Press, Cambridge, 2nd edition, 1944.

[24] Y. H. Kim and M. Ehsani. An algebraic algorithm for microcomputer-based (direct) inverter pulsewidth modulation. *IEEE Transactions on Industry Applications*, IA-23(4):654–660, 1987.

[25] S. R. Bowes. Discussion of "an algebraic algorithm for microcomputer-based (direct) inverter pulsewidth modulation". *IEEE Transactions on Industry Applications*, 24(6):998–1004, 1988.

[26] P. H. Mellor, S. P. Leigh, and B. M. G. Cheetham. Reduction of spectral distortion in class D amplifiers by an enhanced pulse width modulation sampling process. *IEEE Proceedings - G*, 138(4):441–448, 1991.

[27] D. G. Holmes B. P. McGrath. An analytical technique for the determination of spectral components of multilevel carrier-based PWM methods. *IEEE Transactions on Industrial Electronics*, 49(4):847–857, 2002.

[28] S. M. Cox. Voltage and current spectra for single-phase voltage source inverter. *IMA Journal of Applied Mathematics*, 74(5):782–805, 2009.

[29] M. P. Kazmierkowski and L. Malesani. Current control techniques for three-phase voltage-source PWM converters: a survey. *IEEE Transactions on Industrial Electronics*, 45(5):691–703, 1998.

[30] T. W. Chun and M. K. Choi. Development of adaptive hysteresis band current control strategy of PWM inverter with constant switching frequency. In *Proceedings of Applied Power Electronics Conference and Exposition*, pages 194–199, 1996.

[31] Y. Qin and S. Du. A novel adaptive hysteresis band current control using a DSP for a power factor corrected on-line UPS. In *Proceedings of IEE conference on Industrial Electronics, Control and Instrumentation*, pages 208–212, 1997.

[32] J. Dixon, S. Tepper, and L. Moran. Practical evaluation of different modulation techniques for current-controlled voltage source inverters. *IEE Proceedings - Electric Power Applications*, 143(4):301–306, 1996.

[33] K. M. Rahman, M. R. Khan, M. A. Choudhury, and M. A. Rahman. Variable-band hysteresis current controllers for PWM voltage-source inverters. *IEEE Transactions on Power Electronics*, 12(6):964–970, 1997.

[34] M. A. Rahman, T. S. Radwan, A. M. Osheiba, and A. E. Lashine. Analysis of current controllers for voltage-source inverter. *IEEE Transactions on Industrial Electronics*, 44(4):477–485, 1997.

[35] S. R. Bowes, S. Grewel, and D. Holliday. Novel adaptive hysteresis band modulation strategy for three-phase inverters. *IEE Proceedings - Electric Power Applications*, 148(1):51–61, 2001.

[36] H. S. Black. Stabilized feed-back amplifiers. *Electrical Engineering*, 53(1):114–120, 1934.

[37] C. Kao, P. Tsai, W. Lin, and Y. Chuang. A switching power amplifier with feed-back for improving total harmonic distortion. *Analog Integrated Circuits and Signal Processing*, 55(3):205–212, 2008.

[38] H. C. Foong and M. T. Tan. An analysis of THD in class D amplifiers. *IEEE Asia Pacific Conference on Circuits and Systems*, pages 724–727, 2006.

[39] W. Shu and J. S. Chang. Power supply noise in analog audio class D amplifiers. *IEEE Transactions on Circuits and Systems-I: Regular Papers*, 56(1):84–96, 2009.

[40] P. Horowitz and W. Hill. *The Art of Electronics*. Cambridge University Press, Cambridge, 2nd edition, 1989.

[41] S. M. Cox, M. T. Tan, and J. Yu. A second-order class-D audio amplifier. *SIAM Journal on Applied Mathematics*, 71(1):270–287, 2011.

[42] T. Maejima. Yamaha corporation (2007). *Class-D Amplifier*. U.S. Patent No.: 7,183,840 B2.

[43] C. M. Bender and S. A. Orszag. *Advanced Mathematical Methods for Scientists and Engineers I: Asymptotic Methods and Perturbation Theory*, page 15. Springer, New York, 1999.